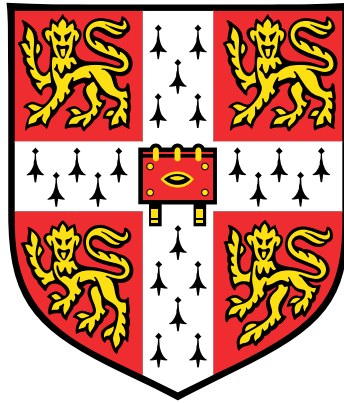


Development of human functional and structural brain networks in adolescence and its relevance to psychiatric disorders



Anna-Lena Dorfschmidt

Supervisors: Prof. Edward T. Bullmore &
Prof. Petra E. Vértes

Department of Psychiatry
University of Cambridge

This dissertation is submitted for the degree of
Doctor of Philosophy

Darwin College

March 2023

Declaration

I hereby declare that except where specific reference is made to the work of others, the contents of this dissertation are original and have not been submitted in whole or in part for consideration for any other degree or qualification in this, or any other university. This dissertation is my own work and contains nothing which is the outcome of work done in collaboration with others, except as specified in the text and Preamble. This dissertation contains fewer than 60,000 words excluding figures, tables, appendices and bibliography.

Annä-Lena Dorfschmidt

March 2023

Development of human functional and structural brain networks in adolescence and its relevance to psychiatric disorders

Anna-Lena Dorfschmidt

The human brain undergoes various phases of active development during the lifespan. While these neurodevelopmental processes are fundamental to the emergence of new cognitive and social capacities, they also coincide with a period of increased risk of neuropsychiatric disorders, which generally have their highest rates of clinical incidence in the first two decades. Since many neuropsychiatric disorders display sex differences in both prevalence or clinical presentation, this raises the question of whether there are underlying sex differences in processes of adolescent brain development. In this thesis, functional and structural magnetic resonance imaging (MRI) is used to map normative brain development, in adolescence and later life, which might differentially predispose men and women to different levels of risk for adolescent and adult mental illness.

First, **Chapter 1** reviews relevant research on understanding developmental changes in the brain during adolescence, focusing on prior studies of normative sexual differentiation of neurodevelopmental trajectories, and vulnerabilities associated with developmental changes.

Chapter 2 investigates whether there are sex differences in normative adolescent development of *functional* connectivity networks, using an accelerated longitudinal cohort of healthy adolescents aged 14-25 years (N=298), comprising 2 or 3 repeated scans on most participants. Sexually divergent development of functional connectivity was identified in the default mode network, limbic cortex, and subcortical structures. In these regions, females were shown to have a more “disruptive” pattern of development, whereby weak functional connectivity at age 14 became stronger during adolescence, specifically in a cortico-subcortical system including many areas of the default mode network. Using open data on whole genome transcription at multiple sites in adult post mortem brains (provided by the Allen Brain Institute), this fMRI-derived map of sexually divergent brain network development was found to be spatially co-located with brain regions where transcription was enriched for genes on the X chromosome and neurodevelopmentally relevant genes.

Chapter 3 starts from the hypothesis that the known sex difference in the prevalence of major depressive disorder (MDD), with increased rates of diagnosis in adolescent females compared to males, could be the psychological or clinical representation of underlying sex

differences in adolescent brain network development. To test this hypothesis, the sexually differentiated fMRI network identified in the previous chapter was further contextualized. The fMRI-derived map of sexually divergent brain network development was found to be co-located with prior loci of reward-related brain activation; a map of functional dysconnectivity in major depressive disorder derived from a prior, independent case-control study of adult MDD; and an adult brain gene transcriptional profile enriched for MDD risk genes, as defined by prior genome-wide association studies of MDD. These results collectively suggested that normative sexual divergence in adolescent development of a cortico-subcortical brain functional network was psychologically, anatomically and genetically relevant to depression.

Chapter 4 reviews literature on similarity-based structural brain networks. Subsequently, **Chapter 5** investigates adolescent changes in *structural* brain network development using morphometric similarity networks derived from the same accelerated longitudinal cohort of healthy adolescents previously used for analysis of functional network development. Morphometric similarity was found to increase during adolescence in insula and limbic regions and to decrease elsewhere in the brain. This profile of decreasing morphometric similarity, or increasing dissimilarity, was associated with the well-known adolescent process of cortical shrinkage, i.e., reduced macro-structural measures of cortical thickness, and with increased magnetization transfer, a micro-structural measure of intra-cortical myelination. Regional nodes of the morphometric similarity networks that became more dissimilar, putatively more differentiated in terms of their cyto- and myelo-architectonics during adolescence, were also found to de-couple from brain functional connectivity, suggesting that increasing morphometric dissimilarity may reflect adolescent development of functional independence.

In an effort to move from group level to subject-specific analyses, and acknowledging that brain development is not restricted to adolescence but is a continuous process throughout life, in **Chapter 6** a total of 41 prior studies, including a total of 90,000 structural MRI scans, were aggregated to estimate lifespan trajectories of normative subcortical development from 180 days post conception to 100 years of age. This analysis identified novel milestones of subcortical volume development; in particular a set of subcortical regions was defined that reached peak grey matter volume during adolescence. Furthermore, subject-specific deviations from normative, non-linear neurodevelopmental trajectories? were derived and used to estimate case-control differences in subcortical volume across the lifespan in multiple neuropsychiatric disorders, demonstrating the potential clinical applications of these normative subcortical growth charts.

In **Chapter 7**, these new experimental results on adolescent and life-span development of functional and structural brain networks, and subcortical grey matter volume were sum-

marised and drawn together, highlighting how these insights are aligned with each other and with the existing scientific literature on brain development, sexual differentiation and risk of psychiatric disorders.

Preamble

Work presented in **Chapter 2** and **Chapter 3** is adapted from material previously published in a peer-reviewed journal. Further, work presented in **Chapter 4 - 6** is being prepared for publication in peer reviewed journals, and has been presented or will be presented at scientific conferences. Analyses conducted within these studies, were principally designed and carried out by me. Contributions of all co-authors are listed below each reference.

Chapters 2-3

Dorfschmidt, L., Bethlehem, R. A., Seidlitz, J., Váša, F., White, S. R., Romero-García, R., Kitzbichler, M. G., Aruldass, A. R., Morgan, S. E., Goodyer, I. M., Fonagy, P., Jones, P. B., Dolan, R. J., NSPN Consortium, Harrison, N. A., Vértes, P. E., & Bullmore, E. T. (2022). Sexually divergent development of depression-related brain networks during healthy human adolescence. *Science advances*, 8(21), eabm7825. <https://doi.org/10.1126/sciadv.abm7825>

Data analysis: L.D. Research design: L.D., P.E.V., and E.T.B. NSPN MRI data preprocessing: F.V., R.R-G., M.G.K., P.E.V. COBRE data preprocessing: S.E.M. BioDep data preprocessing: A.R.A, M.G.K. Contribution of analytical tools: J.S., R.A.B., S.E.M., M.G.K., and A.R.A. Advice on statistical methods: S.R.W. NSPN study design: E.T.B., P.B.J., R.J.D., I.M.G., and P.F. BIODP study design: E.T.B. and N.A.H. Manuscript writing: L.D., E.T.B., and P.E.V.

Chapter 5

Dorfschmidt, L., R.A.I. Bethlehem, J. Seidlitz, F. Váša, S.R. White, R. Romero-García, P.E. Vértes, E.T. Bullmore. Adolescent morphometric similarity development. 2022. *Poster presentation at the Annual Meeting of the Organization for Human Brain Mapping*

Data analysis: L.D. MRI data preprocessing: F.V., R.R-G., P.E.V. Research design: L.D., R.A.B., J.S, P.E.V., and E.T.B. Advice on statistical methods: S.R.W. NSPN study design: E.T.B.

Chapter 6

Dorfschmidt, L., P.E. Vértes, E.T. Bullmore, A. Alexander-Bloch, R.A.I. Bethlehem, J. Seidlitz. Lifespan development of subcortical regions. 2023. *Annual Meeting of the Organization for Human Brain Mapping*

Data analysis: L.D. MRI data preprocessing: L.D., R.A.B., J.S. Code development: L.D., S.R.W., R.A.B. Research design: L.D., R.A.B., J.S, A.A.B, P.E.V., and E.T.B.

Due to these contributions, work presented in **Chapters 2-6** is presented in the plural form of a first-person narrative (“we”), while the Introduction and Summary are presented in the singular form (“I”). The above contributions do not affect the status of this thesis as being principally my own work.

Acknowledgements

This thesis would not have been possible without the support of many colleagues, friends and family.

First and foremost, the journey of this PhD had its start far from Cambridge: I would like to thank my parents, who, when 19-year-old-me told them that she wanted to move to Guatemala instead of going to med school, simply said: “If that is what your heart says, you need to do it.” You showed me an approach to decision making that was as wholesome as anyone could ever dream of.

Thank you also, to Johann Kruschwitz, Henrik Walter and Jon Clayden who showed me the ropes of science and encouraged me to embark into the adventure that doctoral research is – I would not have dared to take this path without your support.

I am immensely grateful to both my supervisors, Ed Bullmore and Petra Vértés, for their scientific guidance. Ed – thank you for mentorship, your scientific rigour and the clarity you can bring into a project. Petra – I am immensely grateful for the dedication with which you supervise not only scientifically, but also personally. It was a pleasure to work with such a power-woman who acts as a role-model for what science can look like. Thank you both.

My deepest gratitude goes to Richard Bethlehem, Jakob Seidlitz and František Váša – you showed me the beauty of collaborative science. I could not have been luckier than to have your scientific and moral guidance throughout this PhD, that simply would not have been finished without you.

To past and present BMU friends and colleagues – Rafa, Jordi, Sarah, Manfred, Ray, Isaac, Will, Sofia, Athina, Matt, Chats, Ricky, Elise – thank you for your support and your ideas. A particular thanks to Eva-Maria Stauffer – without you, the start of this PhD (and some middle bits) would have been incredibly lonely. To Saashi Bedford - colleague-housemate, for your delicious bread, but more importantly for your time and thoughts when things were not going well. And lastly to Simon White – for making sure every science catch-up started with a where-are-you-emotionally.

To the science friends I made along the way, in particular Jakub Vohryzek, Romy Lorenz, and Katja Schüler – I have such respect for you and am truly grateful for your friendship.

To my friends in Cambridge and beyond – thank you for being there when I needed some time off science. To the climbing crew, in particular Julia, Alex H., Jane Darby, Rob, Edo and Will – life outdoors is good with you.

An meine Freunde, nah und (oft) fern: danke für Telefonate, Umarmungen und Eure Nähe, die mich trägt.

Finally, to Alex – I cannot wait for the after.

Table of Contents

List of Figures	xix
List of Tables	xxiii
List of Abbreviations	xxv
1 Introduction	1
1.1 Brain networks in the context of maturation and disease	1
1.1.1 The brain as a complex network	1
1.1.2 Magnetic Resonance Imaging	2
1.1.3 MRI-derived subject-specific brain network construction	4
1.1.4 Brain network topology and analysis	7
1.2 Brain development throughout the lifespan	9
1.3 Adolescent brain development	10
1.3.1 Structural brain development	11
1.3.2 Functional brain development	12
1.4 Sex differences in brain development	13
1.4.1 Sex differences in structural MRI	14
1.4.2 Sex differences in resting state functional magnetic resonance imaging (rsfMRI)	16
1.5 Vulnerabilities during development	17
1.6 Thesis structure	20

2	Sex differences in adolescent development of functional connectivity	23
2.1	Introduction	23
2.2	Methods	26
2.2.1	Sample	26
2.2.2	Residual motion correction	31
2.2.3	Sex stratified analysis of developmental parameters	32
2.2.4	Age \times sex interaction model	36
2.2.5	Spatial auto-correlation (spin-tests)	37
2.2.6	Sensitivity analyses	39
2.2.7	Gene enrichment analyses	43
2.3	Results	46
2.3.1	Sex differences in parameters of adolescent development of global mean degree	46
2.3.2	Sex differences in maturational index	49
2.3.3	X-chromosome and developmental gene enrichment	52
2.3.4	Non-linear effects of age	54
2.3.5	Sensitivity to alternative modelling strategies	56
2.3.6	Sensitivity to alternative motion-correction strategies	57
2.3.7	Sensitivity of results to intra-cranial volume (ICV) and global functional connectivity (FC)	59
2.4	Discussion	61
3	Co-location of adolescent sex differences with major depression	65
3.1	Introduction	65
3.1.1	Adolescent depression	65
3.1.2	Summary and hypotheses	67
3.2	Methods	68
3.2.1	Adolescent functional connectivity sex difference	68

3.2.2	Psychological co-location with depression	68
3.2.3	Anatomical co-location with depression	69
3.2.4	Gene enrichment analysis	71
3.2.5	Diagnostic specificity	73
3.2.6	Robustness of results to alternative pre-processing strategies	75
3.3	Results	75
3.3.1	Anatomical and psychological co-location with depression	75
3.3.2	Celltype-specific and major depressive disorder (MDD) risk gene enrichment	77
3.3.3	Diagnostic specificity	80
3.3.4	Robustness of results to alternative processing strategies	82
3.4	Discussion	83
3.4.1	Limitations	85
4	A review of cortical similarity and connectivity networks	87
4.1	From histological stains to whole-brain connectomics	87
4.2	Approaches to structural brain network construction	88
4.2.1	Diffusion weighted imaging	88
4.2.2	Inter-subject structural covariation	88
4.2.3	Intra-subject structural similarity	91
4.3	Mapping to cytoarchitectonics and tractography	93
4.4	Predicting cognitive and behavioral outcomes	94
4.5	Bridging from micro to macro scales	94
4.6	Identifying neuroanatomical differences in health and disease	95
4.7	Clinical applications	96
4.8	Leveraging multimodal imaging	96
4.9	Tracking developmental changes in brain anatomy	98
4.10	Future directions	99

5	Adolescent morphometric similarity development	103
5.1	Introduction	103
5.1.1	Adolescent brain development	103
5.1.2	Structural network studies of adolescent development using MRI . .	104
5.1.3	Functional and metabolic correlates of structural network development	105
5.1.4	Summary and Hypotheses	106
5.2	Methods	106
5.2.1	Sample	106
5.2.2	Structural MRI acquisition and pre-processing	107
5.2.3	Functional magnetic resonance imaging (fMRI) acquisition and pre-processing	107
5.2.4	Morphometric feature estimation and quality control	108
5.2.5	Modeling of developmental change in morphometric features . . .	110
5.2.6	Adolescent changes in morphometric similarity	110
5.2.7	Co-location with adolescent changes in functional diversity	112
5.2.8	Adolescent changes in structure-function coupling	113
5.3	Results	114
5.3.1	Analyzable sample	114
5.3.2	Adolescent changes in global and regional MRI metrics	115
5.3.3	Adolescent change in morphometric similarity	119
5.3.4	Neurobiological and psychological context of adolescent changes in anatomical connectomes	124
5.3.5	Adolescent development of structure-function coupling	126
5.3.6	Exploratory analysis of lifespan changes in morphometric similarity	130
5.4	Discussion	132
6	Beyond human adolescence: lifespan trajectories	137
6.1	Introduction	137

6.1.1	Normative modelling	138
6.1.2	Lifespan development of subcortical regions	138
6.1.3	Subcortical volume differences in atypical development	139
6.2	Methods	140
6.2.1	Aggregated dataset	140
6.2.2	MRI pre-processing	141
6.2.3	Lifespan trajectories	142
6.2.4	GAMLSS models	143
6.2.5	Developmental milestones	145
6.2.6	Centile score estimation	146
6.2.7	Case-control differences in centile scores	146
6.2.8	Quality control	148
6.2.9	Leave-one-study-out	148
6.2.10	Bootstrap analyses	149
6.3	Results	149
6.3.1	Lifespan development of subcortical structures	149
6.3.2	Lifespan cerebellar and corpus callosum development	152
6.3.3	Sensitivity of results to image quality	154
6.3.4	Sensitivity of trajectories to specific studies	156
6.3.5	Bootstrapping studies of reliability and stability	158
6.3.6	Case-control differences in subcortical volumes	160
6.4	Discussion	162
7	Summary and concluding remarks	169
7.1	Summary of findings	169
7.2	Convergent themes	170
7.2.1	Brain development during adolescence - and beyond	170
7.2.2	Sex differences	171

7.2.3	Cortex vs subcortex	172
7.2.4	Vulnerabilities during development	173
7.3	A note on open science	174
7.4	Future directions	175
7.5	Conclusion	177
References		179
Appendix A Supplementary Tables		221
Appendix B Supplementary Figures		237
Appendix C Supplementary Text		239
C.1	Primary datasets	239
C.2	GAMLSS models	249
C.3	Data, code, and image availability	253

List of Figures

1.1	Complex networks	2
1.2	Brain network estimation	5
1.3	Basic graph metrics	9
1.4	Microscopic sex differences	15
1.5	Diagnosis of neuropsychiatric disorders	19
1.6	The value of longitudinal data	20
2.1	Two modes of adolescent FC development	24
2.2	Modes of adolescent development	26
2.3	Dropout regions	30
2.4	Sex differences in framewise displacement	31
2.5	Effect of head motion (FD) on functional connectivity (FC)	32
2.6	Distribution of random effects	36
2.7	FD regression of functional connectivity by sex sample	40
2.8	Simplified model of partial least squares analysis	44
2.9	All baseline connectivity FC_{14} plots	46
2.10	All baseline connectivity FC_{14} plots	47
2.11	Significance of sex difference in adolescent rate of change FC_{14-26}	48
2.12	Sex-specific maturational index	49
2.13	Trends in disruptive and conservative development of connectivity	50
2.14	Significance of sex difference in maturational index (MI)	51

2.16	Relationships between gene expression profiles and sexually divergent adolescent brain development	53
2.17	Enrichment for X-chromosome and developmental genes	54
2.18	Non-linear effects of age on FC	55
2.19	Age \times sex interaction model	56
2.20	Sensitivity of key findings to motion	58
2.21	Sensitivity of key findings to alternative modeling strategies	60
3.1	Anatomical and psychological co-location with depression	76
3.2	Neurosynth analysis of positive ΔMI regions	77
3.3	Sexually divergent, disruptive brain systems are co-located with brain tissue transcripts enriched for cell type-specific and MDD risk-related genes	79
3.4	Illustrative correlations between ΔMI and three genes (<i>somatostatin (SST)</i> , <i>neuropeptide Y (NPY)</i> and <i>cortistatin (CORT)</i>):	80
3.5	Diagnostic specificity	81
3.6	Robustness of MDD co-location results	83
4.1	Cortical similarity network estimation	90
4.2	Cytoarchitectonic similarity predicts projection density	92
4.3	Cortical depth profiles for magnetization transfer (MT)	93
5.1	Global morphometric outliers	109
5.2	Local morphometric outliers	110
5.3	Estimation of age effects on morphometric similarity	111
5.4	Structure-function coupling estimation	113
5.5	Adolescent changes in global macro-structural and micro-structural magnetic resonance imaging (MRI) metrics	116
5.6	Adolescent changes in regional macro-structural and micro-structural MRI metrics	118

5.7	Adolescent changes in macro-structural and micro-structural MRI metrics corrected for global effects	119
5.8	Adolescent changes in morphometric similarity	121
5.9	Cytoarchitectonic class-specific changes in morphometric similarity	122
5.10	Sex effects on adolescent changes in morphometric similarity	123
5.11	Divergent profile of morphometric similarity	124
5.12	Neurobiological relevance of adolescent changes in morphometric similarity network (MSN)	125
5.13	Psychological relevance of adolescent changes in MSN	126
5.14	Morphometric dissimilarity was associated with functional participation	127
5.15	Adolescent development of structure-function coupling	128
5.16	Structure-function coupling in relation to adolescent changes in MSN	129
5.17	Morphometric dissimilarity partially explains adolescent age-related changes in functional participation	130
5.18	Morphometric similarity network development over the life-cycle	132
6.1	Aggregated lifespan MRI dataset:	140
6.2	Dataset demographics	141
6.3	Normative modelling	143
6.4	Lifespan development of subcortical structures:	151
6.5	Lifespan development of cerebellum and corpus callosum:	153
6.6	Developmental milestones:	154
6.7	Age-related variation in image quality:	155
6.8	Associations between centile scores and MRI scan quality:	156
6.9	Leave-one-study-out sensitivity analysis:	157
6.10	Quality control - study offsets:	159
6.11	Case-control differences in centile scores of subcortical volumes for multiple neuropsychiatric disorders:	161
6.12	Psychopathology centile score differences by subcortical structure:	162

B.1 Effect of FD on FC in the motion-matched sample 238

List of Tables

2.1	Sample of healthy adolescent participants with fMRI data from the NSPN cohort	28
2.2	NSPN fMRI motion-matched sample overview	39
3.1	MDD case-control sample characteristics	71
4.1	Previously published studies using morphometric similarity networks. The studies were identified by a <i>pubmed</i> search in January 2022 using the search terms <i>morphometric similarity network</i> or <i>MSN</i>	101
5.1	Neuroscience in Psychiatry Network (NSPN) structural MRI data sample overview	115
5.2	Age and sex effects on individual morphometric features	117
6.1	Subject numbers for diagnostic groups of cases and controls	147
A.1	Sex differences in fMRI literature	225
A.3	ROIs with significantly different ΔMI	232
A.4	Significant regional effects of age on morphometric similarity	233
A.5	Processing pipelines by dataset	235
A.2	Human Connectome Project (HCP) parcellation regions	236

List of Abbreviations

ABCD adolescent brain cognitive development study

ACC anterior cingulate

AD Alzheimer's disease

ADHD attention deficit hyperactivity disorder

AFNI Analysis of Functional NeuroImages

AHBA Allen Human Brain Atlas

AIC Akaike information criterion

ANOVA analysis of variance

ANX anxiety and phobia

ASD autism spectrum disorder

Ast astrocytes

BIC Bayesian information criterion

BIDS Brain Imaging Data Format

BioDep Biomarkers in Depression study

BOLD blood-oxygen-level-dependent

CN healthy control

CNV copy number variation

CORT cortistatin

- CRP** C-reactive protein
- CSEA** cell-specific enrichment analysis
- CT** cortical thickness
- DF** degrees of freedom
- DK** Desikan-Killiany anatomical atlas
- DLPFC** dorsolateral prefrontal cortex
- DMN** default mode network
- DSM-5** Diagnostic and Statistical Manual of Mental Disorders fifth edition
- DTI** diffusion tensor imaging
- DWI** diffusion weighted imaging
- EI** Euler index
- End** endothelial cells
- EPI** echo-planar imaging
- Ex** excitatory neurons
- FA** fractional anisotropy
- FC** functional connectivity
- FD** framewise displacement
- FDA** U.S. Food and Drug Administration
- FDR** false discovery rate
- FI** folding index
- fMRI** functional magnetic resonance imaging
- GAMLSS** generalized additive models for location scale and shape
- FC_{global} global functional connectivity
- GM** grey matter volume

Gran cerebellar granule cells

GSR global signal regression

GWAS genome wide association study

HAM-D Hamilton Rating Scale for Depression

HARDI high-angular resolution diffusion-weighted image

HCP Human Connectome Project

IC intrinsic curvature

ICV intra-cranial volume

In inhibitory neurons

IQ intelligence quotient

LME linear mixed effects model

LOSO leave-one-study-out

MAD median absolute deviation

MC mean curvature

MCI mild cognitive impairment

MD mean diffusivity

MDD major depressive disorder

ME-ICA multi echo independent component analysis

MI maturational index

Mic microglia

MPM multi-parametric mapping

MRI magnetic resonance imaging

MSN morphometric similarity network

MT magnetization transfer

- NIH** U.S. National Institute of Health
- NODDI** neurite orientation dispersion and density imaging
- NPY** neuropeptide Y
- NSPN** Neuroscience in Psychiatry Network
- OCD** obsessive compulsive disorder
- Oli** oligodendrocytes
- OPC** oligodendrocyte precursor cells
- PCW** post conception week
- Per** pericytes
- PLS** partial least squares regression
- PLS1** first partial least squares regression component
- PMA** post menstrual age
- PRS** polygenic risk score
- Purk** purkinje cells
- RF** radio frequency
- ROI** region of interest
- rsfMRI** resting state functional magnetic resonance imaging
- SA** surface area
- SCID** structured clinical interview for DSM-V
- SCN** structural covariance network
- SCZ** schizophrenia
- SES** socio-economic status
- sMRI** structural magnetic resonance imaging
- SNIP** single nucleotid polymorphism

SST somatostatin

TE echo time

TR repetition time

tWM total white matter volume

UKB UK Biobank

VMPFC ventromedial prefrontal cortex

WHO World Health Organization

WM white matter volume

Chapter 1

Introduction

1.1 Brain networks in the context of maturation and disease

Over the course of the lifespan, the human brain undergoes various periods of increased plasticity, during which it changes in both structure and function. These maturational periods are often also a time of elevated incidence of a variety of neuropsychiatric disorders, which are increasingly understood to arise in the context of atypical brain development (Paus et al., 2008). One such period of neurodevelopmental activity is adolescence, a time of vast social and cognitive development, during which many psychiatric disorders are first diagnosed (Kessler et al., 2005; Paus et al., 2008). Many such disorders display sex differences, both in prevalence, as well as clinical expression. This thesis assesses maturational changes in brain structure and function during adolescence in particular, and during the lifespan more broadly, in relation to atypical development associated with mental health disorders. It further explores whether observed sex differences in psychiatric disorders may be the expression of underlying sex differences in brain maturation. A promising avenue for exploring brain changes in structure and function comes from the field of graph theory and network science, which has allowed researchers to derive “brain networks” from neuroimaging data and analyse changes in their topology during development and in disease.

1.1.1 The brain as a complex network

The brain can be thought of as a network, organized across multiple spatio-temporal scales, from genes and molecules, through microscopic neuronal and other cellular circuits, to macroscopic brain regions and whole-brain systems or connectomes (Betzel and Bassett,

2017; Bullmore and Sporns, 2009; Fornito et al., 2016). Networks have been used to represent complex interactions between relative features of a system in a multitude of fields, including psychology (Epskamp et al., 2018; Schueler et al., 2021), molecular biology (Szklarczyk et al., 2015), and genetics (Zhang and Horvath, 2005). In general, networks consist of multiple nodes that are connected via edges (**Fig. 1.1B**). Every network can be represented as a matrix A , the adjacency matrix, which in the context of brain networks is often called a “connectivity matrix” (**Fig. 1.1A**). Each of the entries, $A_{i,j}$, in the matrix describes a link or edge between two nodes i and j (**Fig. 1.1B**). A network can be unweighted, or binary, in which case each edge indicates the presence of a connection between two nodes (**Fig. 1.1B**); or weighted, in which case each edge has a continuous variable that describes the strength of connection between two nodes. As an example, in spatially embedded networks like the brain, edges can be weighted by the physical distance between nodes, which may act as a proxy measure of the “wiring cost” of the connection between them (**Fig. 1.1C**); equally, edges may be weighted by the strength of the co-fluctuation between two nodes’ functional activation, providing a measure of co-activation (see below for details). Lastly, networks can also be directed (**Fig. 1.1D**), meaning that edges (and their weights) have a direction, such that $A_{i,j}$ is not necessarily equal to $A_{j,i}$.

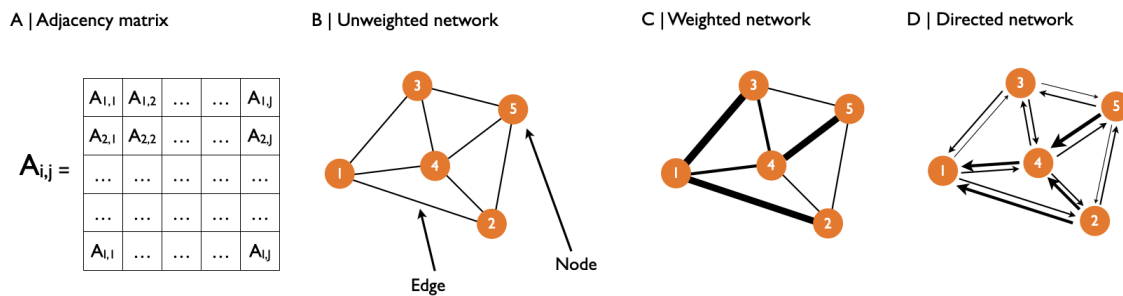


Fig. 1.1 Complex networks: Introduction to networks. (A) An adjacency matrix A describes the edge weights between a set of nodes, such that $A_{i,j}$ is the edge weight between node i and node j . (B) Networks consist of *nodes* which are connected to each other by *edges*. In an *unweighted* network, the edges indicate the presence of a connection between two nodes. (C) A network can be *weighted*, in which case edge weights indicate the strength of the connection between two nodes. (D) In *directed* networks, edges are directional, such that the edge weight $A_{i,j}$ is not necessarily the same as $A_{j,i}$.

1.1.2 Magnetic Resonance Imaging

So far, there is only one organism for which a brain network has been fully mapped on the neuronal level - the nematode worm *C. elegans* with its 302 neurons (White et al., 1986).

Fully mapping the vast complexity of the human brain, consisting of about 80 billion neurons, is currently not possible at equivalent microscopic scale, thus motivating research into mapping whole brain networks or connectomes, resolved at the macroscopic scale of cortical areas and subcortical nuclei, which can be resolved by non-invasive imaging techniques in humans (and other species). Magnetic resonance imaging (MRI) is a non-invasive approach to mapping brain structure and function that allows researchers to study complex network organization in the brain.

Multiple imaging modalities, so-called sequences, exist to capture different aspects of brain anatomy and function (Bernstein et al., 2004). In general, MRI images exploit the differing magnetic properties of different tissue types and states in the brain. Put simply, the scanner generates a large magnetic field which leads protons in the body to align with the magnetic field. During scanning, a radio frequency pulse is applied which throws protons out of alignment with the main magnetic field. It is possible to measure the time it takes them to re-align with the magnetic field.

Structural MRI images are typically derived using a T1-weighted or T2-weighted sequence, which measure the longitudinal relaxation time of tissue following a radio frequency pulse that aligns protons to the transverse plane (Bernstein et al., 2004). The time it takes protons to re-align is effected by the density of fat and water in the tissue, thus the signal strength can be exploited to differentiate between grey and white matter in the brain. Image processing pipelines rely on this difference in contrast to segment grey from white matter, and generate cortical surface meshes. Subsequently, pipelines derive cortical morphometric features, including for example cortical thickness (CT) (estimated as the distance between two corresponding points on the pial and grey/white surfaces), surface area (SA) (estimated as the local area of a triangle, or vertex, on the surface mesh), and grey matter volume (GM) (a combined estimate of thickness and area).

In recent years, functional MRI networks have evolved as a powerful tool to investigate intrinsic brain activity, that is spontaneous fluctuations in brain activity independent of a cognitive or sensory stimulus (van den Heuvel and Hulshoff Pol, 2010), in health and disease. The blood-oxygen-level-dependent (BOLD) contrast measured by resting state functional magnetic resonance imaging (rsfMRI) is reflective of local blood oxygenation changes coupled to neuronal activity (Logothetis and Wandell, 2004). Commonly, the BOLD signal is bandpass filtered and only low-frequency oscillations at between 0.01 Hz and 0.1 Hz are retained (Achard et al., 2006; Biswal et al., 1995), since (i) network fluctuation are thought to be maximally observed at low frequencies, thus filtering should increase statistical power; (ii) filtering may help to reduce the influence of noise on the retained signal, which is thought

to occur in higher-frequency oscillations; and lastly (iii) low-frequency drifts due to scanner noise are removed through the high-pass component of the filtering process. It is worth mentioning that a growing body of literature is investigating high-frequency contributions to functional connectivity measures, in particular providing evidence for relevant signal in higher frequencies during tasks (Craig et al., 2018). For the time being, in this thesis, which uses resting state fMRI, not task data, the traditional approach is employed.

1.1.3 MRI-derived subject-specific brain network construction

The nodes of MRI-derived brain networks are typically locations in the brain, and the edges are measures of connectivity between two distant locations. Different methods exist for defining nodes and edges. While diffusion weighted imaging (DWI) (Hagmann et al., 2006) and structural magnetic resonance imaging (sMRI) (Lerch et al., 2006) data can be used to derive networks of anatomically connected areas and nuclei, functional magnetic resonance imaging (fMRI) (Salvador et al., 2005) images can be used to estimate functional connectivity between nodes and thus the resulting adjacency matrix is often described as a functional connectivity matrix.

Here, I provide a brief overview of structural brain networks in the context of brain network analysis. **Chapter 4** will return to this topic again and introduce similarity-based structural brain networks, and in particular morphometric similarity networks, in more depth.

In general, the process of constructing a brain network involves (i) the acquisition of MRI data, (ii) the definition of network nodes, or region of interest (ROI) using a parcellation scheme, and (iii) the estimation of the strength and sign of anatomical or functional connectivity between those nodes, thus defining the values of the edges in the adjacency matrix.

First, the nodes of a brain network are typically defined by a parcellation template or atlas which is used to demarcate multiple macroscopic cortical areas and subcortical nuclei of the brain, as previously defined by cytoarchitecture (von Economo and Koskinas, 1925), anatomical boundaries (Desikan et al., 2006), functional activation (Yeo et al., 2011), or a combination thereof (Glasser et al., 2016b). Parcellation allows us to statistically compare anatomical or functional connectivity measures between individuals using a common reference atlas, but in doing so it trades off the ability to fully capture the individual variability in brain organization. A critical consideration in choosing a parcellation template is the number of nodes, often between 100 and 1000, to balance anatomical specificity with

computational feasibility and statistical power. The edges of the network are defined based on the imaging modality chosen, as follow below.

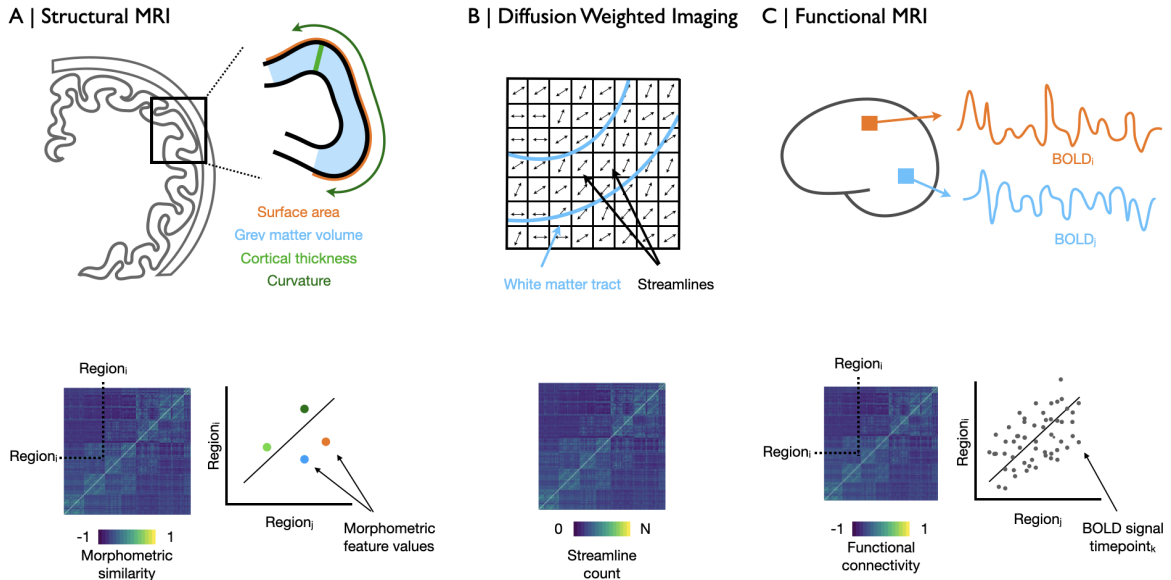


Fig. 1.2 Brain network estimation: Brain networks can be constructed using sMRI, or fMRI data, or DWI data. Typically, the nodes in these networks are regions of grey matter defined *a priori* by a parcellation template. (A) Structural brain networks can be constructed by estimating the pair-wise correlations between regional morphometric feature vectors to constitute a morphometric similarity matrix. (B) Computational tractography methods can be used to derive DTI networks, where the edges are weighted by the streamline count, indicative of the strength of white matter tracts connecting spatially distributed brain regions. (C) fMRI networks are typically derived by estimating the pairwise correlations between resting state fMRI time series averaged over all voxels in each of all possible pairs of two regions defined by the parcellation template.

Historically, *diffusion tensor imaging (DTI)* have been used to measure anatomical connectivity. These networks can be constructed from DWI data which generate contrast by exploiting the diffusion of water molecules through brain tissue. Computational tractography is used to identify large-scale white matter tracts mediating connections between pre-defined grey matter brain regions. This technique estimates the trajectories of white matter axonal pathways using estimates of diffusivity orientation. Brain networks are computed from these data by weighting the inter-regional connections by their streamline count (**Fig. 1.2B**, *bottom*).

Structural covariance network (SCN) were later proposed as an alternative to DTI networks (Alexander-Bloch et al., 2013). These networks are constructed on the basis of a group of scans from multiple subjects. SCN are estimated by correlating a single regional mor-

phometric feature, e.g., cortical thickness, over multiple subjects, resulting in a group-level network, where each edge describes the inter-regional correlation of a single morphometric feature across subjects. These networks suffer from a number of limitations: group level networks lack the ability to easily map changes over time, even though sliding-window approaches have been suggested as a mitigating measure (Váša et al., 2018); and they only make use of a single morphometric feature at a time, thus failing to leverage the growing capacity of multi-modal MRI to extract multiple morphometric features from different modalities of MRI data (Lerch et al., 2017). In response to these concerns, recent work has focused on the construction of subject-specific structural brain networks (Seidlitz et al., 2018), such as *morphometric similarity networks (MSNs)*, which consist of regions defined by a parcellation, and edges, estimated as the correlation between each possible regional pair of standardized MRI feature vectors (**Fig. 1.2A, bottom**). Morphometric similarity networks are based on the idea that similarity of regional MRI feature vectors is a proxy measure of the similarity of two regions in terms of their cytoarchitectonic and myeloarchitectonic organization; and axo-synaptic connectivity is known to be stronger between architectonically similar brain regions compared to cytoarchitectonically distinct or differentiated areas (Goulas et al., 2016, 2017).

MSNs can be estimated using vectors of morphometric feature values estimated at each region. Thus T1-weighted MRI scans can be used to extract multiple macro-structural features (**Fig. 1.2A, top**): for example, GM, the regional volume of each parcel; SA, the surface area of the “inflated” cortical sheet; CT, the depth of the cortical sheet; and several curvature measures can all be measured for each region and compiled in a feature vector used to estimate the morphometric similarity, a proxy for anatomical connectivity, between regions. Further, regional mean values of DWI-derived micro-structural MRI features can also be included as features in analysis of morphometric similarity, i.e. the degree of anisotropy, termed fractional anisotropy (FA), or the average diffusivity along the axonal tracts connecting two regions, termed mean diffusivity (MD), can be estimated at each voxel and averaged over voxels within each regional node. The estimation of MSNs is therefore possible for a single subject, either based only on a T1-weighted image or also including DWI data collected from the same subject.

Functional brain networks, are constructed from rsfMRI data. The nodes of these networks are anatomical brain regions, i.e. regions of interest defined by a parcellation template, whereas the edge weights are estimates of the functional connectivity (FC) between each pair of regional nodes, typically measured in terms of the correlation between each pair of regionally averaged rsfMRI time series (Biswal et al. (1995); **Fig. 1.2C, bottom**).

It is worth noting that while this thesis focuses on the analysis of MRI-derived brain networks, other imaging methods can be used to construct whole-brain networks, including electro-encephalography and magneto-encephalography (Van Diessen et al., 2015).

1.1.4 Brain network topology and analysis

Once a brain network has been constructed, its topology can be analysed using graph-theoretical methods (Bullmore and Sporns, 2009; Fornito et al., 2016). A wide range of network measures are available to characterise brain networks.

Possibly the simplest graph theoretical measure applied in brain network analysis is the nodal degree (**Fig. 1.3A**). In an unweighted network, or binary graph, for each node i the degree k_i is calculated simply as the sum of the non-zero edges $e_{i,j}$ connecting it to the rest of the brain:

$$k_i = \sum_{j=1; j \neq i}^N e_{i,j} \quad (1.1)$$

where k_i is the degree of node i , N is the number of nodes in the network, and $e_{i,j}$ indicates the presence of an edge between node i and an arbitrary node j . The sum is taken over all edges $e_{i,j}$ ($j \neq 1, 2, 3, \dots, N$).

In a weighted graph, it is likewise possible to estimate the mean weighted degree (**Fig. 1.3B**), or node strength, as the average of the weights of all edges connecting the index node to the rest of the brain network:

$$s_i = \sum_{j=1; j \neq i}^N w_{i,j} \quad (1.2)$$

where s_i is the mean weighted degree of node i , N is the number of nodes in the network, and $w_{i,j}$ is the weight of the edge between node i and an arbitrary node j . The sum is taken over all edges $w_{i,j}$ ($j \neq 1, 2, 3, \dots, N$).

Both the binary degree, as well as the weighted degree, are measures of how well connected a given node is to the rest of the network, providing one important measure of its topological centrality and likely its functional importance in the context of the connectome as a whole. To illustrate the concept with a real life example: even an observer that has never seen a map of the UK, would likely be able to pin point the largest cities in the

country by looking at a map of train lines. The observer will notice that a number of train stations appear to have large numbers of train lines connecting them to the rest of the train network. If we think of train stations as network nodes and train lines as edges, then train stations like London and Manchester have a large node degree, compared to the small train station at Iverness in northern Scotland. In fact, many real life networks have highly skewed distributions of node degree, such that a small number of nodes are highly connected to the rest of the network and function as a relay between different parts of the network while most other nodes are only directly connected to a small number of other nodes. These nodes highly connected nodes are often termed “hubs” and they serve the role of integrating information across the network, i.e. one may take a train from Southampton to London in order to travel on to Glasgow, illustrating the integrative role of the London station in transporting passengers from the south to the north of the country.

An array of other graph-theoretical properties can be used to characterise a network’s structure, for example: the shortest path length, a graph measure that describes the number of steps that have to be taken to connect any given node in a network to another (**Fig. 1.3C**); the clustering coefficient, a measure of the degree to which nodes in a graph tend to cluster together (**Fig. 1.3D**); the participation coefficient, which is a measure of the degree to which a node integrates between modules, measured as a nodes ratio of inter-modular to intra-modular connections (**Fig. 1.3E**); modules, which are subsets of regions that are more strongly connected to one another than to regions in other modules (**Fig. 1.3F**); and hubs which are particularly highly connected nodes (**Fig. 1.3F**).

Brain networks are thought to be constrained by two major driving forces which promote different network attributes: the minimization of cost (e.g. wiring volume, energy use), and the maximization of efficiency (e.g. speed of communication, information flow) (Bullmore and Sporns, 2012). It is believed that these constraints are balanced through a *modular* network organization: sets of nodes within the same module are densely intra-connected, but only sparsely inter-connected to nodes in other modules (Oldham and Fornito (2018); **Fig. 1.3F,G**). The segregation achieved by modularity is balanced by so-called connector hubs, which mediate integrative connections between regional nodes in different modules (Oldham and Fornito, 2018). The human brain network’s balance of topological segregation and integration is also evidenced by its core-periphery organization where a set of strongly inter-connected nodes, or hubs, act as intermediaries between modules, forming a so-called “rich club”. This topological organization allows for great robustness and adaptivity since in case of failure of individual nodes, distributive property of the core network is still retained.

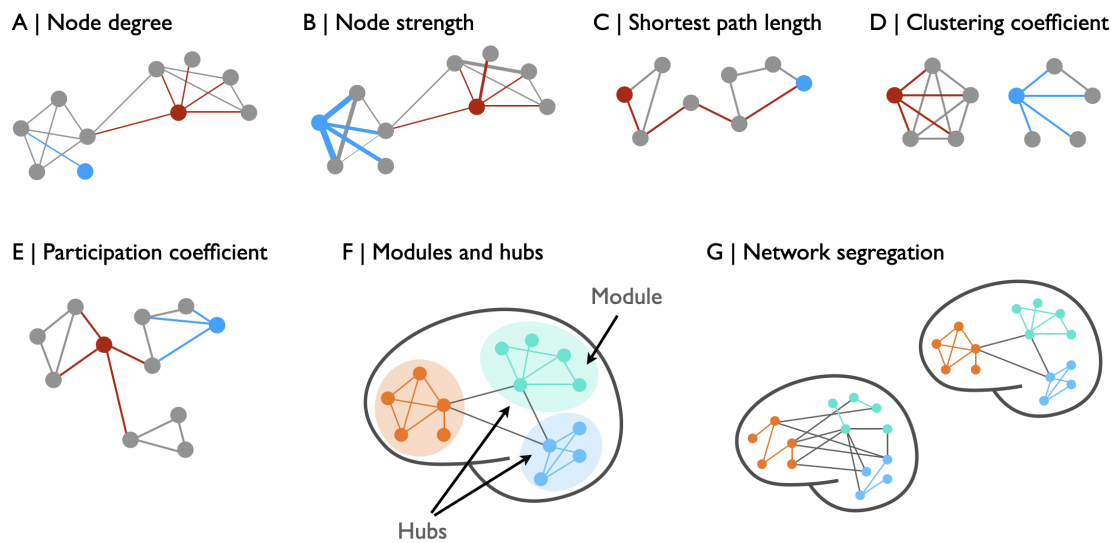


Fig. 1.3 Basic graph metrics: (A) In a binary graph, the node degree indicates the number of edges connecting a given node with all other nodes in the network. The red node has a lower degree than the blue one. (B) In a weighted network, the mean weighted degree is estimated as the average weight over all edges connecting the index node to the rest of the brain. The blue node here may have higher node strength compared to the red node. (C) The shortest path between two nodes is the minimum number of steps, or edges, it takes to connect them. (D) The clustering coefficient is estimated as the number of edges between a node's neighbours divided by the number of edges that could possibly exist between them. The red node's clustering coefficient is high, the blue one's is low. (E) Brain networks are typically modular, meaning that subsets of regions, comprising each of several modules, are more densely interconnected with each other than with nodes that are affiliated to different modules. So-called hubs are nodes with high degree that often mediate information between modules. (F) The participation coefficient is measured as the ratio between a node's intra-modular degree (edges connecting to other nodes in the same module) and its inter-modular degree (edges connecting to other nodes in other modules). (G) Brain networks tend to segregate by strengthening within-module connections and forming a smaller number of long-distance connections between mediating hubs that integrate information between the modules.

1.2 Brain development throughout the lifespan

Throughout the course of life, from conception to old age, the human brain undergoes extraordinary changes in structure (Mills et al., 2014; Sowell et al., 2003; Váša et al., 2018; Whitaker et al., 2016b) and function (Stevens, 2016; Váša et al., 2020). During the prenatal period, the brain initially undergoes a phase of neurogenesis, which is largely completed by 20 weeks post-conception, at which time axons start growing and synapses are formed. Indeed, magnetic resonance imaging of prematurely born infants, born after 24 weeks post-

conception, has demonstrated increases in grey and white matter volume in mid to late fetal periods (Bethlehem et al., 2022). At birth, the brain has reached around 30% of its total grey matter volume (Bethlehem et al., 2022; Gilmore et al., 2012). Recent work on the largest existing MRI dataset ($N \sim 120,000$ brain scans) has confirmed that trajectories of grey and white matter development in the cortex and subcortex can be mapped over the lifespan (Bethlehem et al., 2022). From mid gestation onwards, cortical GM volume increases rapidly, peaking in childhood at 5.9 years of age, then declining over the rest of the lifespan; white matter volume (WM) volume also rapidly increases until early adulthood, at 28.7 years old (yo), before declining gradually throughout adult life, with subsequently accelerated decline in old age; and subcortical grey matter volume follows an intermediate growth trajectory, peaking in adolescence at 14.4 years (Bethlehem et al., 2022). These normative trajectories of cortical development suggest an early post-natal period of differentiation between grey and white matter, which sees a switch from grey matter volume to white matter volume being the proportionally dominant tissue type in the brain after around 3 years. These and other MRI phenotypes of developmental changes in brain macro-structure are thought to represent underlying microscopic neurodevelopmental processes, e.g., synaptic proliferation and axonal myelination, that continue throughout adolescence and into early adult life (Bethlehem et al., 2022; Miller et al., 2012; Petanjek et al., 2011). It is worth noting that all these results were based on univariate models of structural development and no network estimates have been investigated in a comparable sample.

To date, there is less certainty about lifespan changes in fMRI. A widely reported finding is increasing within-network FC until early adulthood, and decreases thereafter (Betzel et al., 2014; Váša et al., 2020). However, no single study has mapped functional connectivity changes over the course of the lifespan in sufficiently large samples (Betzel et al., 2014; Fjell et al., 2017; Ma et al., 2021; Wang et al., 2012) to provide a level of certainty anywhere near that reached using univariate models of structural brain development as described above (Bethlehem et al., 2022).

1.3 Adolescent brain development

Understanding structural (Raznahan et al., 2011; Sowell et al., 2004; Váša et al., 2018; Whitaker et al., 2016a) and functional (Kundu et al., 2018; Váša et al., 2020) development of brain networks during adolescence has been of particular interest to the neuroscientific community. This is because adolescence is well-known to be a time of fundamental changes in cognition and behaviour, and it is also a time of increasing incidence of a variety of

psychiatric illnesses (Costello et al., 2003), including in particular mood disorders. The pathophysiology of these disorders is increasingly understood in connection with atypical maturational changes that occur in the adolescent brain (Paus et al., 2008). Thus, understanding normative adolescent brain development is expected to further our understanding of atypical developmental trajectories on the pathway to mental health disorders, including depression, in young people.

1.3.1 Structural brain development

A large body of work on structural brain development during childhood and adolescence has focused on estimating maturational trajectories of individual (global or regional) morphometric features, e.g., prototypically, cortical thickness. A prominent pattern that has emerged from this work is that from the age of about 3 years, grey matter volume in the brain steadily decreases (Bethlehem et al., 2022). Adolescent structural brain development is shaped by a pattern of continued cortical grey matter volume decreases, largely driven by cortical thinning, with relatively smaller decreases in surface area (Tamnes et al., 2017; Whitaker et al., 2016b), while white matter volume and intra-cortical myelination both show continued increase, albeit at a slower rate than during the first decade (Mills et al., 2016). Further, it has been suggested that there is a difference in timing between subcortical and association cortical adolescent maturation (Mills et al., 2014), with subcortical areas maturing first, followed by later prefrontal maturation.

Studies of structural brain *network* development during this period have so far largely focused on structural covariance networks and DWI-derived connectomes. Cross-species work has highlighted that structural network hubs are established early in life, i.e., studies in *C. elegans* showed that hub neurons are born early in development (Towlson et al., 2013). Work on human subjects demonstrated that the integrative function of hubs as connectors between modules is only fully established during adolescence (Oldham and Fornito, 2018). Further, the above described process of cortical thinning and increasing myelination has been shown to be topologically focused on association cortical hubs in adolescence, consolidating topologically central components of the adult brain network that are less myelinated at the beginning of adolescence (14 yo) and then see faster rates of myelination and cortical shrinkage over the course of adolescence (Whitaker et al., 2016b). Association cortical areas have been shown to support higher cognitive functions and play a topologically important role in the network, such that these findings have been hypothesized to represent an adolescent re-organization of the structural connectome relevant both to normal cognitive and behavioral changes (Whitaker et al., 2016b). Further research has highlighted a process of consolidating

anatomical connectivity between frontal cortex and the rest of the connectome (Váša et al., 2018) during adolescence, possibly representative of an increasing relevance of prefrontal cortex and its central role in cognitive control functions that emerge during adolescence. In summary, these findings suggest that well-known processes of cortical thinning and myelination support the reorganization of structural brain networks during adolescence, in particular shaping the topological importance of association cortical and prefrontal areas, to support adult behavior and cognition

1.3.2 Functional brain development

Two findings in particular have been widely reported by initial studies of developmental changes in functional connectivity during adolescence: (i) an increase in strength of long-range connections; and (ii) an decrease in the strength of short-range connections, hypothesized to represent a shift from localized to distributed networks during adolescence (Dosenbach et al., 2010; Fair et al., 2007). Since most long-range axonal projections start or finish in association cortical areas, the later emergence of long-range functional connections has previously been associated with the idea that primary sensory and motor areas mature during childhood, while association areas undergo changes during late adolescence (Mills et al., 2014; Váša et al., 2020; Whitaker et al., 2016a). Recent work, however, has reported that a large number of developmental results may have been confounded by within-scanner head motion (Power et al., 2012; Satterthwaite et al., 2013). It has been found that head motion both inflates age effects in general, as well as having a heterogeneous effect on distance-dependent fMRI connectivity, such that head motion has a greater effect on long-distance, compared to short-distance connections (Power et al., 2012; Satterthwaite et al., 2013). This may be due to regionally specific effects of motion that inflate the BOLD signal in one region, and decrease it in distant regions on the same axis, leading to anti-correlations between distant regions and increased correlations between locally adjacent regions. These findings are highly relevant for developmental studies since younger subjects tend to move more. Consequently, the effect of head motion in younger subjects may decrease the strength of long distance connectivity in younger subjects leading to a relatively higher long distance connectivity in older subjects who move less (Power et al., 2012; Satterthwaite et al., 2013) putting into question the distance-dependent changes in functional connectivity reported in early developmental studies. This idea is supported by a more recent study that found no distance-dependent effects of age on functional connectivity when applying advanced motion-correction methods (Marek et al., 2015).

Several other aspects of functional connectivity development beyond the controversial question of distance-dependent functional connectivity development have been investigated. It has been suggested that cross-network integration increases with age (Marek et al., 2015). Further, hub regions have been reported to refine their connectivity during adolescence, in particular frontal hubs appear to increase their connectivity with the subcortex early during adolescence, followed by strengthening of connectivity between cerebellar hubs and the cortex (Hwang et al., 2013). Given the above-mentioned finding of timing-differences in subcortical compared to prefrontal structural brain maturation, a last point of focus has been functional connectivity development between subcortical and cortical regions during adolescence (Van Duijvenvoorde et al., 2019; Váša et al., 2020). It has been suggested that subcortico-cortical connectivity develops more heterogeneously during adolescence than cortico-cortical connectivity (Váša et al., 2020). Subcortical programmes of selectively strengthening some connections and weakening others may be representative of a functional reorganization of subcortico-cortical systems, in particular involving reward-related circuits (Van Duijvenvoorde et al., 2019; Váša et al., 2020).

1.4 Sex differences in brain development

Microscopic sex differences, both in terms of gonadal sex steroids, as well as sex chromosomes, are known to shape physiological differences between males and females and have been linked to sexual differentiation of the animal brain (McCarthy et al., 2012), suggesting the existence of similar effects in humans (Raznahan and Disteche, 2021).

Experimental manipulation of gonadal hormones in animal models has been shown to directly affect brain structure and function (Corre et al., 2016). In humans, more indirect methods of linking gonadal hormones to sexual differences in brain structure and function have been employed: by studying subjects displaying longitudinal variation in hormonal levels, either long-term variation, due to developmental phases like adolescence or menopause (Mosconi et al., 2021), or short-term variation, due to the menstrual cycle (Pritschet et al., 2020), or natural variation in testosterone levels over the course of the day (Grotzinger et al., 2022); or by comparing healthy controls to cases of endocrine disorders affecting sex hormone production (Tauber and Hoybye, 2021); or by studying variation due to gender-affirming hormone treatment (Kranz et al., 2020). These studies have demonstrated that sex hormones do indeed affect brain structure and function, both in the short term, i.e. functional brain networks reorganize during the menstrual cycle (Pritschet

et al., 2020), as well as long-term, i.e. menopause appears to effect both grey and white matter volumes (Mosconi et al., 2021).

In the late 1950s, sex chromosomes were first shown to affect sex differences in mammalian brain organization (Phoenix et al., 1959b). Since then, a growing body of literature has suggested that sex chromosomes affect brain organization and may also contribute to phenotypic diversity of the human brain (Arnold, 2012; Raznahan and Disteché, 2021). There are a number of reasons why sex chromosomes are likely to contribute to sex differences in the brain. First, sex chromosomes play a special role in the rapid fixation of mutations and evolution of genes, due to the fact that the X and Y chromosomes are haploid in males. In males recessive mutations on one sex chromosome cannot be masked by the dominant allele from the other chromosome copy. Thus, the recessive allele will be expressed and, when advantageous, it has a higher chance of being passed on to offspring (**Fig. 1.4A**). This process may have contributed to the importance of sex chromosomes for traits advantageous to males, for example, as evidenced by an accumulation of genes relevant for male fertility on both the X and Y-chromosomes. Second, in females, one of the X chromosomes is randomly inactivated, balancing out the fact that males only have one X chromosome. However, about 15% of genes escape X chromosome inactivation (**Fig. 1.4B**). These genes are thus upregulated in females compared to males and may provide a likely source of sexually differentiated phenotypic expression (Disteché, 2016; Oliva et al., 2020). Third, not only is the X chromosome enriched for genes expressed in the brain, X chromosome genes are also heterogeneously expressed across the brain, thus suggesting effects on anatomically patterned and functionally specialised brain systems (**Fig. 1.4C**). And finally, in both sexes, X chromosome expression is upregulated, to ensure that its expression is relatively balanced compared to autosomal gene expression (**Fig. 1.4D**), a process that happens prior to X-inactivation and thereby leads to higher expression of X-linked genes versus autosomal genes in females compared to males cells during embryonic development (DeCasien et al., 2022).

Together, these microscopic sex differences in gonadal hormones and sex chromosomes suggest possible mechanisms for sex differences on the macroscopic level in the form of sexually differentiated brain anatomy and function as measured using MRI.

1.4.1 Sex differences in structural MRI

A range of previous work has investigated sex differences in brain phenotypes, largely focusing on structural MRI and task-activated MRI. The most obvious sex difference observed is that, on average, male brains tend to be larger than female brains, a differences which

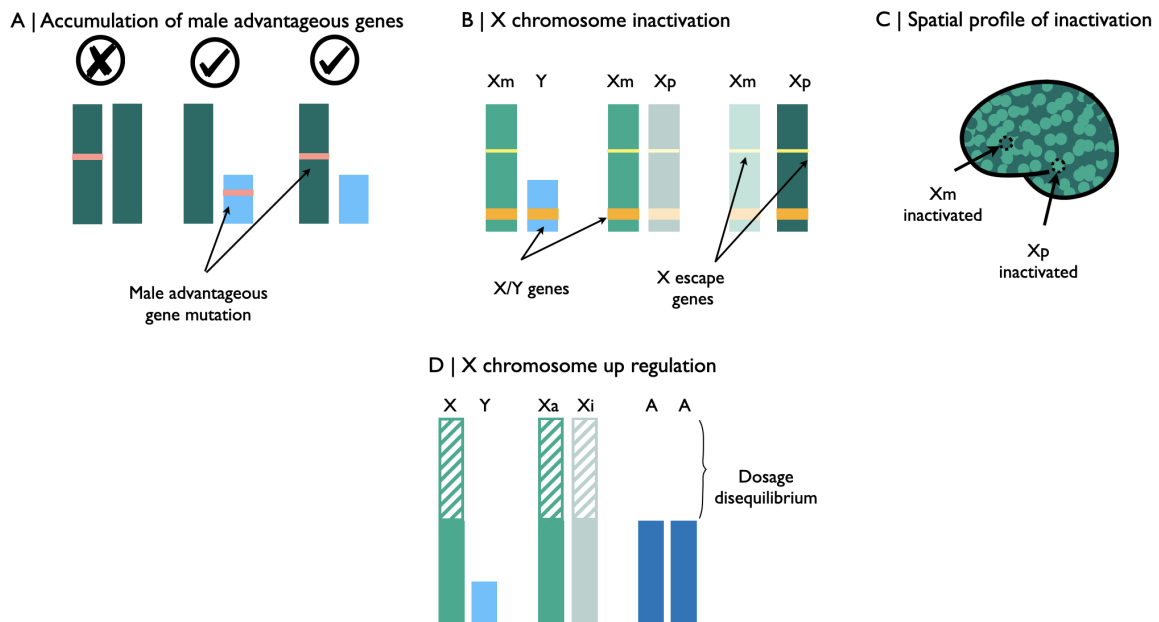


Fig. 1.4 **Microscopic sex differences:** (A) Sex chromosomes are diploid in females and haploid in males. Recessive mutations in females can be masked by dominant alleles on the second copy of the X chromosome. In males, however, such masking cannot occur due to the chromosomes being haploid. When traits are male advantageous, they are more likely to be passed on to offspring, thus leading to an accumulation of male-advantageous genes on sex chromosomes. (B) In females, one X chromosome is randomly inactivated, however, a number of genes escape this inactivation. (C) The inactivation being random leads to a spatially diverse pattern of cells in which the maternal or paternal X chromosome is deactivated. (D) In both males and females, X chromosomes are upregulated such as to avoid a dosage equilibrium between sex chromosomes and autosomes.

is likely due at least partially to a difference in body size (Ruigrok et al., 2014). This sex difference in brain size has been shown to be present at birth, with male brains estimated to be approximately 8% larger than females (Gilmore et al., 2007; Knickmeyer et al., 2017), and persistent throughout life.

Recent work has demonstrated effects of brain size on regional grey matter volume (Eikenes et al., 2022; Warling et al., 2021), white matter tracts (Reardon et al., 2018; Sanchis-Segura et al., 2020), and brain-behavior relationships (Dhamala et al., 2022). The effect sizes of regional sex differences across different structural imaging phenotypes are attenuated when correcting for total brain volume. There has been a long-standing interest in whether there are sex differences in regional brain anatomy above and beyond sex differences in total brain size. A number of MRI studies have reported sex differences in grey matter volume in multiple regions, with effect sizes ranging from small to medium (Liu et al., 2020). Conversely,

a meta-synthesis (i.e. a meta-analysis of meta-analyses) of a large number of studies has reported a lack of coherence in prior findings, and suggested sex differences in grey matter volume may after all be very small (Eliot et al., 2021). This idea stands in contrast to results from recent large-scale studies that find consistent sex differences in grey matter volume across most brain regions (Lotze et al., 2019; Williams et al., 2021). It has since been suggested that a number of factors, including inconsistent approaches to correcting for brain size, and variable sample sizes, may have contributed to the (perceived) lack of consistency in studies of sex differences in grey matter volume (DeCasien et al., 2022), particularly since meta-analyses do not correct for methodological discrepancies between studies. Thus while studies of sex differences in grey matter volume need to be evaluated carefully with respect to sample size and brain size correction methods (Sanchis-Segura et al., 2020), large-scale neuroimaging studies appear to converge on a consistent picture of small to medium-sized sex differences in volume across most brain regions (DeCasien et al., 2022; Williams et al., 2021). However, it is worth noting that within-sex variability in imaging phenotypes is large and also scales with head size (Eliot et al., 2021), and sex differences are statistical differences in the mean of two overlapping distributions.

1.4.2 Sex differences in rsfMRI

In the past, research on sex differences in fMRI have largely focused on task-activated fMRI, often investigating the “brain basis” for assumed sex differences in behavior and cognition. Many such studies have suffered from small sizes and meta analyses have found little overlap between findings (Eliot et al., 2021). It is not yet clear how resting state functional connectivity differs between males and females, either during adolescence or adulthood. One widely reported sex difference is increased functional connectivity of the default mode network (DMN) in females (Allen et al., 2011; Biswal et al., 2010; Bluhm et al., 2008; Filippi et al., 2013; Tomasi and Volkow, 2012). Female-increased connectivity has also been reported in subcortical nuclei and limbic areas (cingulate gyrus, amygdala, hippocampus) (Scheinost et al., 2015); whereas male-increased connectivity has been reported for sensorimotor areas (Biswal et al., 2010; Filippi et al., 2013; Scheinost et al., 2015). However, these effects are not consistently found across studies (Allen et al., 2011; Tomasi and Volkow, 2012; Weissman-Fogel et al., 2010). Importantly, most research on sex differences has focused on pre-selected regions, often including the amygdala (Alarcón et al., 2015; Kilpatrick et al., 2006), with few studies having investigated sex differences comprehensively over all brain regions (Biswal et al., 2010; Casanova et al., 2012; Filippi et al., 2013; Zhang et al., 2016, 2018). While these regionally focused approaches increase

statistical power, they fail to map global patterns. Finally, at least one study failed to observe any sex effects at all (Weissman-Fogel et al., 2010).

It is important to note that almost all studies mentioned here were cross-sectional studies, using either age-balanced, usually adult, samples of males and females, or covering a very limited age range. Most prior rsfMRI studies of brain development have focused on estimating "average" effects of age across both sexes, e.g., by including sex as a covariate in the statistical model for estimation of developmental parameters. Few studies have reported age-by-sex interactions or the conditioning of developmental parameters by sex (Scheinost et al., 2015; Zhang et al., 2018). The lack of longitudinal data may have contributed to the fact that few studies found convincing effects of age-by-sex interaction on functional connectivity. Some interaction effects have been reported in several networks, including the default mode network, the fronto-parietal, visual and auditory networks (Scheinost et al., 2015; Zhang et al., 2016); but often these findings did not survive correction for multiple comparisons. While cross sectional studies can make claims about male-female group differences, no within-subject age-related changes in functional connectivity can be inferred. Thus cross-sectional studies do not allow to determine whether observed differences in functional connectivity are a result of sex, (atypical) maturational trajectories, or a combination of both (Mills et al., 2014). Therefore modelling subject-specific trajectories over time is crucial for our understanding of how sex might intersect with brain development.

Taken together, the current heterogeneity of results concerning the spatial locations and sign of sex differences in brain structure and function suggests a need for further investigation, in particular using large, longitudinal samples, with appropriate correction for motion-related artifacts.

1.5 Vulnerabilities during development

Topological analysis of MRI-derived brain networks has furthered our understanding of structural and functional brain development in health. Additionally, contrasting normative results with patient data from multiple neuropsychiatric disorders has provided insight into atypical deviations of network organization associated with disease. It has been found that even very basic graph theoretical measures, such as degree, can highlight case-control differences in network structure (Morgan et al., 2019; Váša et al., 2018). Contrasting brain networks between healthy controls and cases of neuropsychiatric disorders has also demonstrated how central several topological features are for the healthy functioning of the brain. For example, it has been found that many disorders appear to disrupt the modular

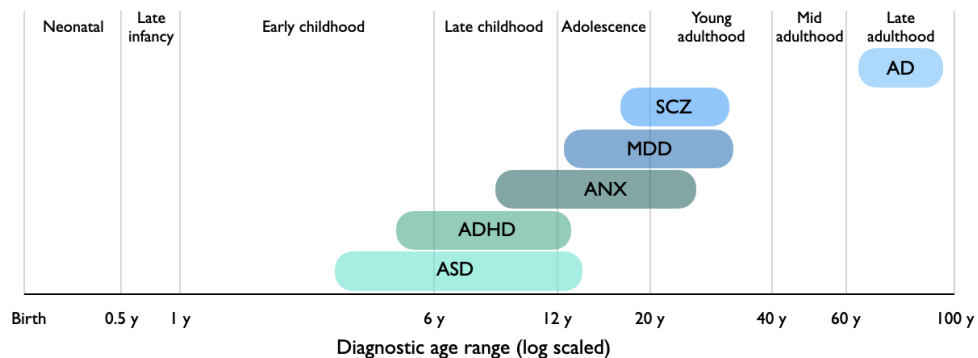
community structure of brain networks, leading to more segregated organization of the connectome (Crossley et al., 2014).

It is notable, that many developmental disorders, e.g., autism spectrum disorder (ASD), are first diagnosed during early to late childhood, whereas psychiatric disorders, in particular mood disorders, e.g., major depressive disorder (MDD) or anxiety disorders, are typically incident during adolescence (**Fig. 1.5A**; (Kessler et al., 2005; Paus et al., 2008)). Both these periods are well-known for being neurodevelopmental phases of major reconfiguration or rewiring of brain networks (Morgan et al., 2018). In line with this coincident timing, it can be argued that atypical trajectories of developmental rewiring may lead to vulnerabilities to disease, i.e. “moving parts get broken” (Paus et al., 2008). For example, it has been suggested that in patients with schizophrenia an “exaggeration of typical adolescent changes” may have occurred (Keshavan et al., 1994).

As mentioned above, many disorders display sex differences in their prevalence or clinical expression profile, including ASD, which is four times as likely to be diagnosed in males than in females, and MDD, which is twice as likely to be diagnosed in females (**Fig. 1.5B**). It is worth acknowledging that socio-cultural as well as structural factors may contribute to this sex difference in diagnosis (Sharma et al., 2021). There is undeniably a gendered influence on health, diagnostic criteria may be sex-biased, and cultural expectations may contribute to a discrepancy in seeking medical help (Phillips, 2005). For example, males often exhibit lower help-seeking behavior, potentially contributing to the sex difference in incidence rates for mood disorders (Galdas et al., 2005). On the other hand, current diagnostic criteria for ASD may lead to under-diagnoses in females, who exhibit more camouflaging behavior (Fusar-Poli et al., 2022), i.e. they show a greater tendency to mask disease-associated behavior either by avoiding some types of behaviors, or conversely by explicitly performing behavior considered to be more neurotypical. However, the concentrated emergence of multiple neuropsychiatric disorders during neurodevelopmentally active periods of the lifespan suggests that sex differences in brain development contribute at least in part to the pathogenesis of these conditions. This is underlined by gene expression studies, i.e. research on postmortem brain tissue suggests that gene expression in ASD is correlated with normative sex differences in gene expression (Kissel and Werling, 2022).

Neuropsychiatric disorders may be associated with alterations in both the timing and/or the shape of developmental trajectories (Di Martino et al., 2014a). For example, attention deficit hyperactivity disorder (ADHD) has been associated with delayed brain maturation, whereas ASD has been associated with an early acceleration of brain development (Shaw et al., 2010). However, to date, neuroimaging studies of atypical brain development have

A | Age of diagnosis



B | Sex difference in prevalence



Fig. 1.5 **Diagnosis of neuropsychiatric disorders:** (A) Many neuropsychiatric disorder show a sex difference in prevalence. (B) Age at first diagnosis of psychiatric disorders according to the literature (Solmi et al., 2022).

largely been cross-sectional. While this allows for estimating case-control group differences, usually corrected for age, it also leads to several fundamental shortcomings (Di Martino et al., 2014a). First, the lack of availability of longitudinal patient data contributes to a lack of understanding of atypical developmental trajectories. Second, when only a single time point is available for an individual, it is impossible to know anything about the shape of this individual's developmental trajectory. **Fig. 1.6** illustrates this issue: while a single timepoint for each subject can reveal their deviation from the norm, it is unclear which trajectory of development they are on. Only a second measure could bring clarity. While the increasing number of longitudinal neuroimaging studies focusing on normative brain development is encouraging, future studies should also attempt to collect longitudinal patient data to allow for mapping atypical trajectories.

A key factor motivating research into brain network changes in disease is that it is likely that symptoms of neuropsychiatric disorder appear after the onset of atypical development, raising the hope that, with advances in normative modelling, neuroimaging may be used to track changes in brain development before symptom onset thus expediting diagnosis or creating opportunities for prevention. It should be pointed out that currently the limited regional availability (i.e. MRI scanners being concentrated in better hospitals, cities, and high-income countries) and the high cost of neuroimaging limit its usefulness in harder-to-

reach populations. A recent development, however, provides hope for the future: portable, low-cost MRI scanners may facilitate reaching more remote populations in the future (Cho, 2023).

One in five adolescents have a mental illness that will persist into adulthood (Kessler et al., 2005), and depression, schizophrenia and addiction are among the top ten leading causes of medical disability worldwide, with no evidence of global reduction in disease burden (Collaborators et al., 2022). Research into the neurodevelopmental basis of neuropsychiatric disorder should thus be of the utmost importance.

A | Cross-sectional vs longitudinal measure

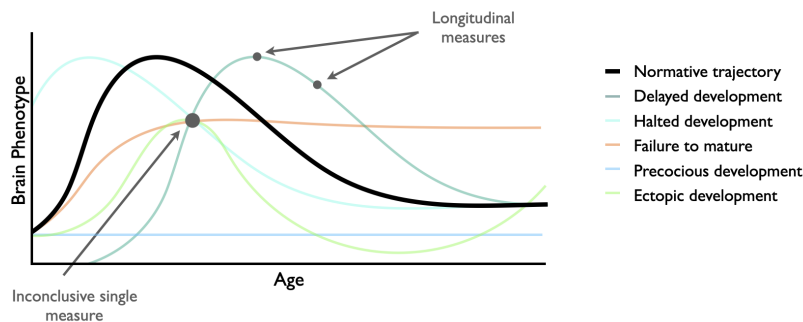


Fig. 1.6 **The value of longitudinal data:** Atypical development can alter both the timing of development (delayed or precocious development) or alter its shape (failure to mature, halted development, ectopic development). A single (cross-sectional) measure for each individual cannot determine the shape of the individual's atypical trajectory.

1.6 Thesis structure

Overall, the findings described above demonstrate that the human brain undergoes various phases of active development during the lifespan. While brain network development is fundamental to the emergence of new cognitive and social capacities, periods of rewiring also expose individuals to an increased risk of neuropsychiatric disorders, highlighting the relevance of understanding normative brain development. Further, many neuropsychiatric disorders are known to display sex differences both in prevalence and clinical presentation, which may be linked to sex differences in brain structure and function. However, while we know that there are sex difference in brain physiology on the microscopic level (Arnold, 2012; Raznahan and Disteche, 2021), less is known about sex differences in macroscopic brain development.

This thesis maps normative functional and structural brain development in adolescence and later life using magnetic resonance imaging. **Chapters 2-3** and **Chapters 5** estimate adolescent changes in functional and structural brain network development in an accelerated longitudinal cohort of healthy adolescents aged 14-25 years (N=298), each scanned between one and three times, with a total of 520 scans. **Chapter 2** asks the question: “*Does adolescent functional brain development differ between males and females?*”. **Chapter 3** builds on the fMRI-derived map of sex differences in adolescent brain development from the previous chapter to ask: “*Are sex differences in adolescent functional connectivity maturation related to major depression?*”. **Chapter 5** moves from functional to structural data, asking: “*Are there adolescent changes in morphometric similarity networks?*”.

Finally, in an effort to move from group level to subject-specific analyses, and acknowledging that brain development is not restricted to adolescence but is a continuous process throughout life, **Chapter 6** aggregates 90,000 scans from 41 prior studies ranging from mid gestation to old age. This allows me to address the question: “*How do subcortical regions develop over the course of the lifespan in health, and how do individuals deviate from these normative trajectories in association with disease?*”.

Finally, **Chapter 7** summarizes the experimental results on adolescent and lifespan development of functional and structural brain networks, and subcortical grey matter volume. It identifies convergent themes and aligns them with the existing scientific literature on brain development, sexual differentiation and risk of psychiatric disorders.

Chapter 2

Sex differences in adolescent development of functional connectivity

2.1 Introduction

As outlined in **Chapter 1**, adolescence is a period of large-scale functional reorganization of the brain (Marek et al., 2015; Sowell et al., 2004; Váša et al., 2020) that coincides with changes in cognition and behaviour. Adolescence is also a period of increased risk to psychiatric disorders many of which show sex differences in prevalence and expression profile (Kessler et al., 2005), raising as the question whether there may be underlying sex differences in brain development. Sex differences on the microscopic scale, in the form of gonadal hormones and sex chromosomes, are known to impact macroscopic measures of brain structure and function (Arnold, 2012; Raznahan and Disteche, 2021). However, to date, little is known about whether, and how, adolescent changes in functional connectivity may differ between males and females. Here, we start from the position that there may indeed be sex differences in adolescent processes of brain maturation.

Recent advances in developmental neuroimaging have produced a number of longitudinal datasets covering the period from late childhood to early adulthood (Kiddle et al., 2017; Satterthwaite et al., 2016), allowing the field estimate age-related changes longitudinally, rather than cross-sectionally. Further, with the newly-gained awareness that head motion differentially affects long-distance connections, previously reported findings suggesting distance-dependent changes in functional connectivity during adolescence were put into question. Thus recent work has endeavored to shed further light on adolescent functional con-

nectivity development, using rigorous motion-controlling strategies and explicitly modelling longitudinal changes during this period.

One such study estimated adolescent changes in regional functional connectivity weighted degree, i.e. the average connectivity across all of a nodes edges to the rest of the brain (Váša et al., 2020). They estimated the baseline connectivity at the beginning of adolescence, and the rate of change in connectivity over the course of adolescence (Váša et al., 2020) for each node (**Fig. 2.1A**) and found that regional functional connectivity weighted degree, was particularly strong in primary motor and sensory cortical areas at the beginning of adolescence, and cortico-cortical connectivity generally increased over the course of adolescence. However, subcortico-cortical connectivity had a varied anatomical distribution, with particularly strong functional connectivity increases between subcortical regions and association cortical areas, and some decreases in connectivity between a number of subcortical regions and primary motor and sensory cortical areas. These findings highlight a special role of subcortico-cortical connectivity changes during adolescence.

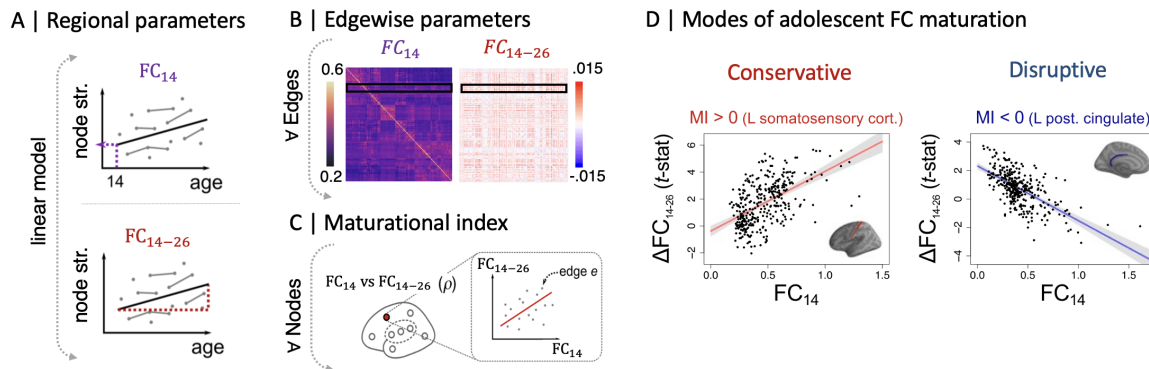


Fig. 2.1 Two modes of adolescent FC development: From a linear model of age effects on FC, two parameters of adolescent development are extracted. (A) First, regionally, the weighted degree of FC of cortical regions and subcortical nuclei is estimated at baseline (14 years), FC_{14} , and the rate of change in connectivity over the course of adolescence, FC_{14-26} . (B) The same parameters can be estimated for each edge. (C) The maturational index is estimated as the correlation between edgewise baseline FC_{14} and the rate of change FC_{14-26} . (D) Visualization of two exemplary regions, displaying (*left*) conservative development ($MI > 0$), where edges that are strong at baseline, become stronger over the course of adolescence, and (*right*) disruptive development ($MI < 0$), where edges that are strong at baseline decrease in strength over the course of adolescence, and edges that are weak increase. Adapted from Váša et al. (2020) under a **CC BY 4.0** licence.

Moving from regional weighted degree to edge-wise connectivity (**Fig. 2.1B**), the authors further developed a new network metric describing edge-wise adolescent functional connectivity maturation. This metric suggested that adolescent development of functional

connectivity can be described as occurring in two modes: a *conservative* mode of consolidating previous phases of development, and a *disruptive* mode of establishing functional connectivity in brain systems that were not previously strongly connected. These developmental modes are measured and differentiated using the maturational index (MI), which describes a system level change in a node's connectivity to the rest of the brain, reflecting maturational changes across all of a node's edges (Váša et al., 2020). Briefly, MI describes how each of a node's connections change during adolescence. It does so by examining the relationship between edgewise functional connectivity strength at the beginning of adolescence, e.g., 14 years old, denoted *baseline connectivity* or FC_{14} ; and the rate of change in functional connectivity over the course of adolescence, e.g., 14-26 years old, denoted *rate of change* or FC_{14-26} (**Fig. 2.1B**). More specifically, MI is estimated for each node by correlating the baseline connectivity and rate of change for all edges connecting the index node to all other nodes in the network (**Fig. 2.1C**). MI defines two distinct modes of adolescent development of brain functional connectivity (**Fig. 2.1D**): (i) conservative development, indicated by a positive MI, which is the result of a node's strong (high FC) edges increasing in functional connectivity over the course of adolescence, and its weak edges decreasing in strength; and (ii) disruptive development, indicated by a negative MI, is the result of a nodes' weak edges gaining strength and its strong edges weakening, leading to a shuffling of a node's ranked edges. Thus, MI describes a "system level" change in a node's wiring, reflecting maturational changes across all of a node's edges (**Fig. 2.2**).

Previous work demonstrated that conservative development was characteristic of primary sensory and motor cortical areas, whereas disruptive development was mainly located in association cortical and subcortical regions. Disruptive development has been suggested to represent metabolically costly remodeling of cortical and subcortical systems to facilitate emergence of adult cognitive and social behaviors (Váša et al., 2020).

Here, using fMRI data from a previously published (Váša et al., 2020) accelerated longitudinal study (N=298; age range 14-26 years; 51% female; **Table 2.1**), stratified by age and balanced for sex per age stratum (Kiddle et al., 2017), we estimated the effects of sex on three parameters of adolescent development of resting-state functional connectivity: (i) baseline connectivity at age 14, FC_{14} ; (ii) the adolescent rate of change, FC_{14-26} , estimated at nodal and edge-wise levels of analysis; and (iii) the maturational index for each node, MI, which is the signed correlation coefficient between FC_{14} and FC_{14-26} across all edges connecting a given node to the rest of the network. We hypothesized that (i) there may be sex differences in parameters of adolescent brain development; and (ii) that these sex differences may be co-located with expression of a weighted function of the whole genome enriched for X chromosome and (iii) developmentally relevant genes.

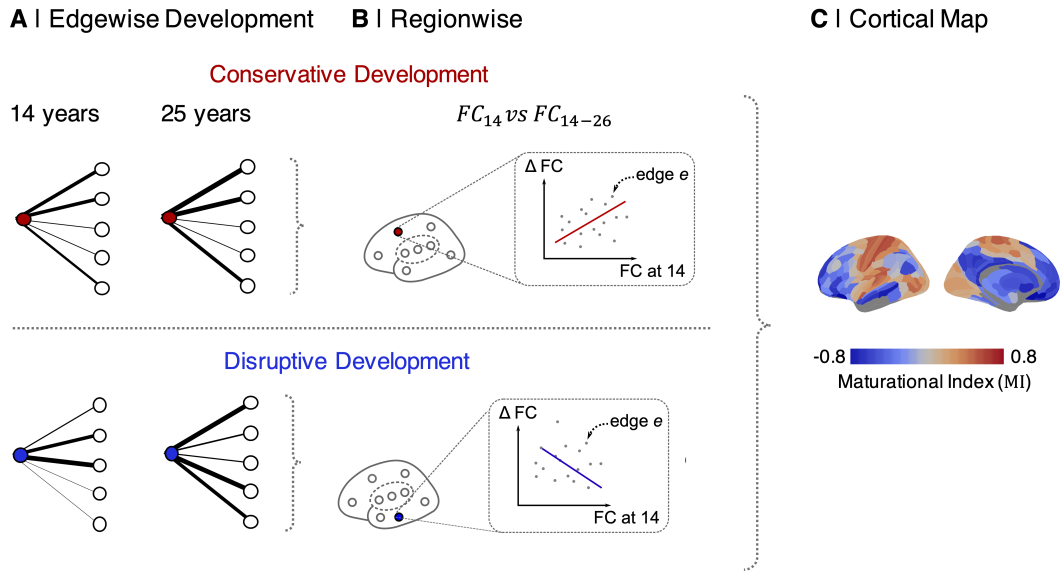


Fig. 2.2 Modes of adolescent development: In conservative development, a node's strong edges get stronger between 14 and 26 years (A; top). Thus, the MI, estimated by Spearman's correlation between baseline connectivity at age 14 (FC_{14}) and adolescent rate of change of connectivity (FC_{14-26}), is positive (B, top). Conversely, in disruptive development, a node's weak edges get stronger over the course of adolescence, while its strong edges weaken (A, bottom). Thus the MI, estimated by the correlation between FC_{14} and FC_{14-26} , is negative. (C) Cortical surface map of MI estimated at each regional node in the brain.

We found that there was a sex-related difference in adolescent brain network development: females had significantly more disruptive development of functional connectivity in a default mode cortical, limbic and subcortical network. Further, we found that this developmentally divergent brain system was co-located with expression of a weighted function of the whole genome enriched for X chromosome genes, and genes expressed during various phases of brain development.

2.2 Methods

2.2.1 Sample

Data Collection

The data analysed in this chapter were collected as part of the Neuroscience in Psychiatry Network (NSPN) consortium, a collaboration between the University of Cambridge and

University College London, with the aim of measuring cognitive and brain developmental changes during adolescence in a healthy adolescent cohort representatively sampled from the population of Greater London and Cambridgeshire (Kiddle et al., 2017). The analyzable sample consisted of 2,402 participants, aged 14 to 26 years, that completed repeated self-assessments of mental health status, with a subset also completing repeated functional and structural magnetic resonance imaging assessments, as detailed below. Participants were recruited in five agebins (14-15 years, 16-17 years, 18-19 years, 20-21 years, older than 22 years), with equal numbers of males and females in each agebin.

All participants aged 16 and older provided informed written consent for each aspect of the study, and parental consent was obtained for those aged 14–15 years. The study was ethically approved by the National Research Ethics Service and was conducted in accordance with NHS research governance standards.

MRI sample

A sub-sample of 306 adolescents drawn from the NSPN cohort consented to complete functional and structural MRI assessments. The age and sex stratification from the larger cohort was maintained, such that each of the five agebins included about 30 males and females. The exclusion criteria for this sample included: a current or past history of neurological disorder or learning disability, and current treatment for psychiatric disorder or drug or alcohol dependence. Each participant in the scanning sample was invited to provide magnetic resonance imaging (MRI) data on at least two occasions: at baseline and at follow-up 12-18 months later, with 29 participants additionally invited to attend follow-up scanning six months after baseline. The fMRI scan was the first in a series of scans collected in each scanning session which also included structural MRI using the multi-parametric mapping (MPM) sequence (Weiskopf et al., 2013), and diffusion weighted imaging. Here, we present results using the functional magnetic resonance imaging (fMRI) scans, whereas **Chapter 5** will focus on complementary analysis of the structural MRI data. A total of 556 resting state functional magnetic resonance imaging (rsfMRI) scans were available for analysis after completion of quality control procedures.

MRI data acquisition

Functional MRI data were acquired at three scanning centres (Wolfson Brain Imaging Centre, University of Cambridge; University College London; and King's College London), on three identical 3T Siemens MRI scanners (Magnetom TIM Trio, VB17 software version)

Sex	# Scans	# Scanned			At Baseline				# Subj./Agebin				
		1	2	3	μ Age	σ Age	μ FD	σ FD	1	2	3	4	5
female	259	54	86	11	19.8	2.9	0.11	0.05	34	39	24	32	22
male	261	41	98	8	19.2	3.8	0.13	0.05	32	33	24	35	23

Table 2.1 Sample of healthy adolescent participants with fMRI data from the NSPN cohort: The final sample after QC included data from $N = 298$ healthy young people who participated in an accelerated longitudinal fMRI study. The recruitment was balanced for sex in each of five age-defined strata. Subjects were scanned between 1 and 3 times with scans taking place at baseline, 6 and/or 18 months later. The number of subjects who were scanned 1, 2 or 3 times respectively is listed under *# Scans*. Framewise displacement (FD), a measure of head movement in mm, was significantly greater in males compared to females on average over all ages, and in the youngest two age strata specifically ($P < 0.05$, *uncorrected*).

with standard 32-channel radio frequency (RF) receive head coils and RF body coils for transmission, using a multi-echo echo-planar imaging (EPI) sequence (Barth et al., 1999) with the following scanning parameters: repetition time (TR), 2.42s; GRAPPA with acceleration factor 2; flip angle, 90° ; matrix size, $64 \times 64 \times 34$; field of view (FOV), 240×240 mm; in-plane resolution, 3.75×3.75 mm; slice thickness, 3.75 mm with 10% gap, with sequential slice acquisition of 34 oblique slices; bandwidth, 2368 Hz per voxel; echo time (TE), 13, 30.55 and 48.1 ms; and total scan time, 11 minutes.

MRI data pre-processing

The data employed here were originally pre-processed in (Váša et al., 2020). We used Freesurfer v5.3.0 to process individual structural scans with a pipeline comprising skull-stripping, segmentation of cortical grey and white matter, and reconstruction of the cortical surface and grey-white matter boundary (Fischl et al., 1999). Subsequently, all scans were visually inspected and manually edited by members of the Neuroscience in Psychiatry Network (NSPN) Consortium. The reconstruction algorithm was re-run after this manual quality control step. Up to 10 iterations of edits were performed (Váša et al., 2018; Whitaker et al., 2016a). For scans to pass final quality control, a complete cortical reconstruction was required.

Analysis of Functional NeuroImages (AFNI) (Cox, 1996b) was used for basic pre-processing of functional MRI scans. All volumes acquired during steady-state equilibration (15 s) were discarded. Motion correction parameters and parameters for anatomical-

functional coregistration were calculated from the images acquired with TE = 30.55 ms. The first volume after equilibration was used as the base EPI image. Matrices for de-obliquing and six-parameter rigid body motion correction were computed. Then, 12-parameter affine anatomical-functional coregistration was computed using the LPC cost functional (Saad et al., 2009), with the EPI base image as the LPC weight mask. Matrices for de-obliquing, motion correction, and anatomical-functional coregistration were combined into a single alignment matrix using the concatenation approach from the AFNI tool *align_epi_anat.py*. The images for each TE were then slice-time corrected and spatially aligned through application of the alignment matrix. Coregistration of structural and functional scans was visually assessed.

The functional MRI data were preprocessed using multi echo independent component analysis (ME-ICA) (Kundu et al., 2012a, 2013a) which identifies and removes sources of variance in the times series that do not scale linearly with TE and are therefore not representative of blood-oxygen-level-dependent (BOLD) contrast. The retained independent components, representing BOLD contrast, were optimally recomposed to generate a broadband denoised fMRI time series at each voxel. Regional time series were averaged over all voxels within each parcel and bandpass filtered by the discrete wavelet transform, corresponding to a frequency range of 0.025-0.111 Hz (Bullmore et al., 2004).

An overall estimate of head motion by each participant, mean FD, was calculated from the six motion parameter time series (three rotation and three translation parameters) estimated during scan re-alignment. More specifically, framewise displacement was calculated as:

$$FD_t = \sum_d |d_{t-1} * d_t| + 50 * \frac{\pi}{180} * \sum_d |r_{t-1} * r_t| \quad (2.1)$$

Scans were parcellated into 360 bilateral cortical regions using the Human Connectome Project (HCP; Glasser et al. (2016a)) template and 16 bilateral sub-cortical regions (amygdala, caudate, diencephalon, hippocampus, nucleus accumbens, pallidum, putamen, and thalamus) were defined by Freesurfer's *aseg* parcellation (Filipek et al., 1994). The Human Connectome Project (HCP) template was chosen for a number of reasons: it is a high-resolution atlas, allowing for suitable regional precision. Further, it was constructed using multi-modal imaging data allowing for robustness of the suggested regional boundaries. Lastly, the HCP parcellation atlas has enjoyed great popularity in the neuroimaging community, allowing for easy comparisons between results from a large number of studies. After within-subject pre-processing and quality control, we retained regional time series for 330 cortical and 16 subcortical nodes. 30 cortical regions were excluded due to low regional mean signal ($Z < -1.96$); see **Fig. 2.3** for a map of retained regions. Individual functional connectivity

2.2.2 Residual motion correction

We found that males tended to display more head movement, particularly in younger age strata (**Fig. 2.4**). This effect did not survive correction for multiple comparisons ($P_{FDR} > 0.05$).

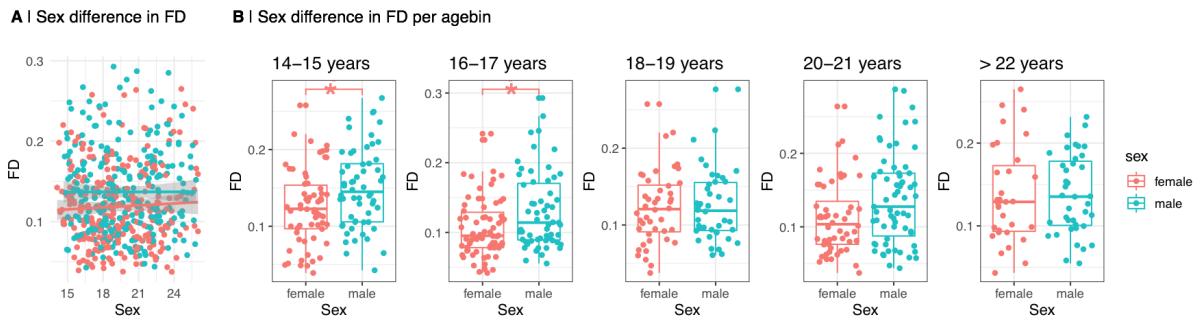


Fig. 2.4 Sex differences in framewise displacement: (A) Across all age strata, males showed higher framewise displacement (FD) than females ($P_{Sex} < 0.05, t(296) = 3.25$). (B) Males showed especially increased FD in the first two age strata ($P_{Sex} < 0.05$), however these differences did not survive correction for multiple comparisons.

Despite the motion correction procedures implemented in the fMRI pre-processing pipeline, there were residual effects of motion on functional connectivity in quality-controlled data. Specifically, we found: (i) that there was a weak relationship between the correlation of FC and head motion (across participants) and the Euclidean distance spanned by edges, i.e., head motion and functional connectivity were more strongly coupled for shorter distance connections; and (ii) that the average edge-wise correlation between FC and motion was non-zero (as evidenced by a non-zero (y-axis) intercept of the fitted linear regression model; **Fig. 2.5A**). In order to remove these residual effects of motion on functional connectivity, we regressed each pairwise correlation or edge on the time-averaged head motion of each participant (mean FD). The residuals of this regression were the estimates of functional connectivity used for further analysis. After this correction, the average head motion, quantified as mean FD, did not change with age ($P_{age} = 0.2, t(220) = 125$) in the full sample (**Fig. 2.5B**). By construction, there was no longer an effect of distance on the correlation between FC and motion, and the average edge-wise correlation between FC and motion was zero (**Fig. 2.5A**). This pre-processed, quality controlled and motion-corrected dataset is identical to the one previous used in Váša et al. (2020) and we will henceforth refer to it as the “analyzable sample” throughout this chapter.

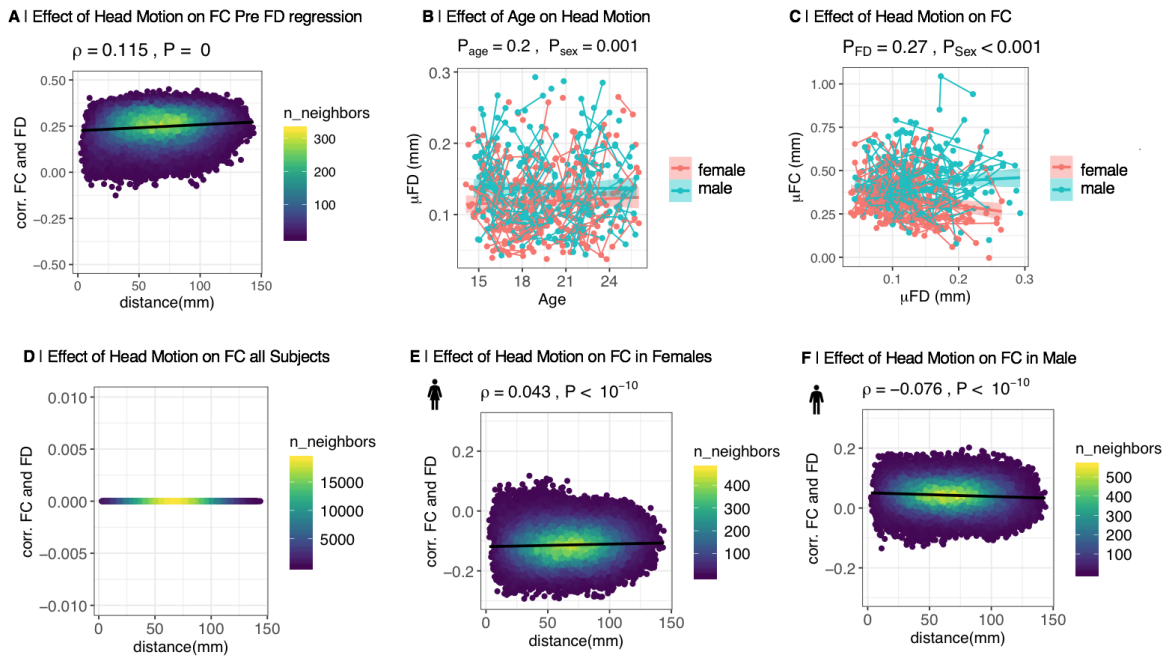


Fig. 2.5 Effect of head motion (FD) on functional connectivity (FC): (A) After ME-ICA pre-processing, there was a weak relationship between the correlation of FC and head motion (across participants) and the Euclidean distance spanned by edges. Further, the average edge-wise correlation between FC and motion was non-zero. (B) To remove the dependence of FC on motion in this sample, mean FD was regressed on each edge; the residuals constituted participant-specific, FD-corrected FC, with intercepts retained to maintain the relative importance of edges across the group as well as the interpretability of FC values. Thus, in the motion-corrected sample, average head motion, quantified as mean framewise displacement (FD), did not change with age ($P_{age} = 0.2, t(220) = 125$). However, there was a weak, but significant effect of sex on FD ($\beta_{sex} = 0.02, P_{sex} < 0.01, t(296) = 3.3$). (C) The effect of head motion (across participants) on global FC was not significant ($P_{FD} = 0.27$). (D) By construction, there was no effect of distance on the correlation between head motion and motion-corrected FC, and the average edge-wise correlation between FC and motion was non-zero (as evidenced by a non-zero (y-axis) intercept of the fitted linear regression model). (E) However, since motion correction was performed across all subjects, we still observed weak, but significant effects of distance on the correlation of FC and FD for females ($\rho = 0.04, P < 0.001$) (F) and males ($\rho = -0.08, P < 0.001$) (G) when the two sexes were analysed separately.

2.2.3 Sex stratified analysis of developmental parameters

Previous work on this dataset did not find evidence for non-linear trajectories of development of functional connectivity between the majority of all possible pairs of regional nodes (Váša et al., 2020). Therefore we used a linear function to model the fixed effect of age on

regional and edge-wise metrics of cortico-cortico, subcortico-cortical and cortico-subcortical functional connectivity, also including the fixed effect of site and a subject-specific intercept as a random effect, in linear mixed effects models fit separately for males and females. For each region i we calculated the mean weighted degree as per **Equation 1.2**.

Briefly, we estimated nodal and edge-wise baseline connectivity (FC_{14}) as the predicted FC at age 14, and the adolescent rate of change (FC_{14-26}) as a linear function of age in the model. We calculated MI for each node as Spearman's correlation of edge-wise FC_{14} and FC_{14-26} (**Fig. 2.2**).

Specifically, we used a sex-stratified approach to analyse developmental parameters over the course of adolescence. This means that we estimated the developmental parameters, FC_{14} and FC_{14-26} , separately for each sex, as detailed below.

First, we estimated FC_{14} and FC_{14-26} locally, i.e. for each node. We used linear mixed effects models to estimate the linear effect of age on functional connectivity. These models included age as the main fixed effect of interest and scanner site as a fixed effect covariate, as well as a subject-specific intercept as a random effect, as follows:

$$FC_{node} \sim 1 + \beta_{age} * age + \beta_{site} * site + \gamma_{subject} * (1|subject) + \varepsilon \quad (2.2)$$

where FC refers to the functional connectivity at nodal level, β refers to coefficients for the fixed effects, $\gamma_{subject}$ refers to the coefficients for random effects, and ε represents the residual error.

We then derived baseline connectivity at age 14, FC_{14} , from **Equation 2.2** as:

$$FC_{14} = 1 + \beta_{age} * 14 + \beta_{site_2} * (1/3) + \beta_{site_3} * (1/3) \quad (2.3)$$

Whereas the adolescent rate of change was simply estimated the β coefficient of age from **Equation 2.2** as:

$$FC_{14-26} = \beta_{age} \quad (2.4)$$

Finally, nodal between-sex differences in FC_{14} and FC_{14-26} were estimated by subtracting each male-specific parameter from the corresponding female-specific parameter:

$$\Delta FC_{14} = FC_{14_{female}} - FC_{14_{male}} \quad (2.5)$$

$$\Delta FC_{14-26} = FC_{14-26_{female}} - FC_{14-26_{male}} \quad (2.6)$$

We then estimated the same measures at the level of individual edges. Thus, for each sex, we predicted functional connectivity using linear mixed effects models as above:

$$FC_{edge} \sim 1 + \beta_{age} * age + \beta_{site} * site + \gamma_{subject} * (1|subject) + \varepsilon, \quad (2.7)$$

where FC_{edge} refers to the functional connectivity at edge level, β refers to coefficients for the fixed effects, $\gamma_{subject}$ refers to the coefficients for random effects, and ε represents the residual error.

We then estimated baseline connectivity at age 14, FC_{14} , from **Equation 2.7** as:

$$FC_{14} = 1 + \beta_{age} * 14 + \beta_{site_2} * (1/3) + \beta_{site_3} * (1/3). \quad (2.8)$$

Whereas the adolescent rate of change was simply estimated by the β coefficient of age from **Equation 2.7** as:

$$FC_{14-26} = \beta_{age}. \quad (2.9)$$

We then combined the sex specific estimates of these two developmental parameters to estimate a sex-specific estimate of MI. Thus in each sex we evaluated at each node the linear relationship (using Spearman's ρ) between the ranked edge-wise parameters FC_{14} and FC_{14-26} for each sex, e.g.:

$$MI_{node} = \frac{cov(FC_{14}, FC_{14-26})}{\sigma_{FC_{14}} \sigma_{FC_{14-26}}} \quad (2.10)$$

where $\sigma_{FC_{14}}$ and $\sigma_{FC_{14-26}}$ are the standard deviations of the ranked variables.

Finally, we estimated the between-sex difference in maturational index by subtracting the male-specific MI from the corresponding female-specific MI:

$$\Delta MI = MI_{female} - MI_{male} \quad (2.11)$$

We parametrically tested for the significance of the sex difference in all developmental parameters using a Z-test (Paternoster et al., 1998). In short, the Z-statistic was estimated as the difference in developmental parameters divided by the standard error of the difference in the parameters. More specifically, the Z-score for sex difference in maturational index (ΔMI) was estimated by:

$$z = \frac{MI_{female} - MI_{male}}{SE_{MI_{female} - MI_{male}}} = \frac{MI_{female} - MI_{male}}{\sqrt{SE_{female}^2 - SE_{male}^2}} \quad (2.12)$$

where MI_{female} and MI_{male} are the maturational indices for each sex, and SE_{female} and SE_{male} are the standard errors of MI for each sex.

For FC_{14} and FC_{14-26} , the standard error of the sex difference in parameters was defined differently. For example, the Z-score for the sex difference in FC_{14} (ΔFC_{14}) was estimated by:

$$z = \frac{FC_{14_{female}} - FC_{14_{male}}}{SE_{FC_{14_{female}} - FC_{14_{male}}}} = \frac{FC_{14_{female}} - FC_{14_{male}}}{\sqrt{\left(\frac{SE_{female}}{N_{female}} - \frac{SE_{male}}{N_{male}}\right)^2}} \quad (2.13)$$

where $FC_{14_{female}}$ and $FC_{14_{male}}$ are the baseline connectivity at age 14 for females and males, respectively; SE_{female} and SE_{male} are the standard errors of FC_{14} for each sex; and N_{female} and N_{male} are the numbers of females and males. The same estimator of Z scores (**Equation 2.13**) was also specified for analysis of between-sex differences in FC_{14-26} . The difference between estimators (**Equations 2.12** and **2.13**) of the sex differences in these developmental parameters results from the fact that the standard error of MI is the standard error of the correlation between FC_{14} and FC_{14-26} , whereas the standard errors of FC_{14} and FC_{14-26} are the standard errors of the regression coefficients which include the number of observations in the denominators. Thus, the Z-score for sex difference in three developmental fMRI parameters was estimated at each of 346 cortical and subcortical regions. We tested for statistical significance using P -values from the standard normal distribution controlled for multiple comparisons by the false discovery rate (FDR). For each whole brain map, comprising 346 regional P -values, we used $FDR = 5\%$ as the threshold for significant sex difference in developmental fMRI parameters.

Our principal reason for choosing a sex-stratified approach was that it allowed the variance of the random effects estimated in **Equation 2.7**, $\text{Var}(\gamma_{subject})$, to differ between sexes. As shown in **Fig. 2.6**, the distributions of random effects were indeed not identical in males and females – males were more variable. Higher variance of random effects was negatively correlated with lower residual variance (denoted ϵ in **Equation 2.7**) in both sexes; but the strength of correlation was greater in females than males, as shown in **Fig 2.6B**. Thus, although the between-sex difference in random effects variance was not statistically significant by a permutation test (**Fig 2.6C**) there was a degree of difference which would influence the residual variance and therefore the significance of the standardised

developmental parameters. It is for this reason that we principally used the sex-stratified approach to linear mixed effects modeling of these longitudinal data. Above, we outlined how we modelled adolescent parameters of functional connectivity development in our principal, sex stratified approach. In the next section, we will introduce the alternative approach, modelling age-by-sex interaction effects. While this work focuses on the former approach, we will show in the results section, that the latter produces highly similar result.

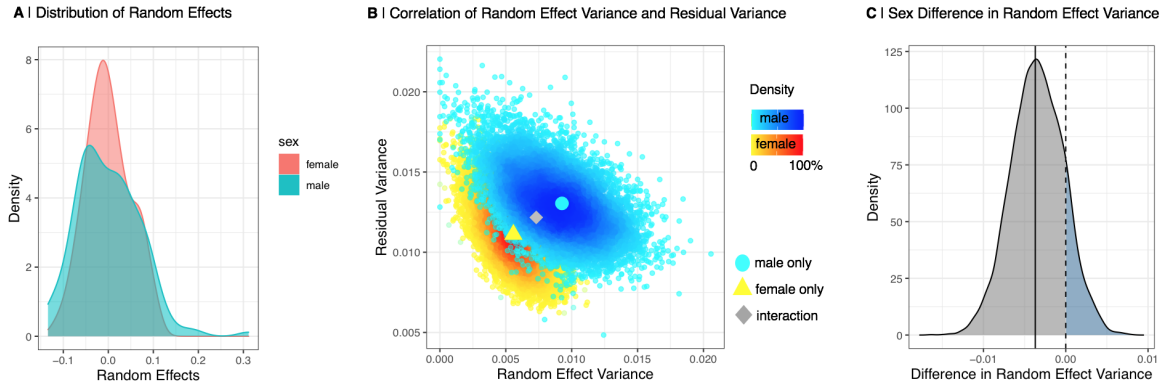


Fig. 2.6 Random effect variance: We estimated the random effects of individual participants on global functional connectivity in a sex stratified approach. We used bootstrapping to resampling participants with replacement 10,000 times within each age stratum, thus sampling the distributions of random effects variance and residual variance. (A) Distribution of random effects estimated in a sex stratified approach. (B) Correlation of random effect variance and residual variance for males and females. The true male and female variance, as well as the random effect variance of an interaction model are marked. This plot shows a clear separation of male and female random effect variance. (C) Using a permutation procedure, we found that there was no statistically significant (at $P < 0.05$) difference in random effect variance between males and females ($P = 0.14$).

2.2.4 Age \times sex interaction model

To demonstrate robustness of our results to an alternative modeling strategy, we also analysed all the data (male and female combined) using a linear mixed effects model to estimate the main effects of age and sex, and the age-by-sex interaction effect, on FC at each edge:

$$FC_{edge} \sim 1 + \beta_{age} * age + \beta_{sex} * sex + \beta_{age*sex} * age * sex + \beta_{site} * site + \gamma_{subject} * (1|subject) + \epsilon \quad (2.14)$$

where FC refers to the functional connectivity at edge level, β refers to coefficients for the fixed effects, γ refers to coefficients for random effects and ε represents the residual error.

On this basis, we can then estimate FC_{14} for males and females as follows:

$$FC_{14_{female}} = \beta_{age} * 14 + \beta_{sex} * 0 + \beta_{age*sex} * 0 * 14 + \beta_{site_2} * (1/3) + \beta_{site_3} * (1/3) \quad (2.15)$$

$$FC_{14_{male}} = \beta_{age} * 14 + \beta_{sex} * 1 + \beta_{age*sex} * 1 * 14 + \beta_{site_2} * (1/3) + \beta_{site_3} * (1/3) \quad (2.16)$$

And likewise we can estimate FC_{14-26} for males and females:

$$FC_{14-26_{female}} = \beta_{age} + \beta_{age*sex} * 0 \quad (2.17)$$

$$FC_{14-26_{male}} = \beta_{age} + \beta_{age*sex} * 1 \quad (2.18)$$

Finally these sex-specific estimates of FC_{14} and FC_{14-26} can be combined to estimate sex-specific estimates of MI and the between-sex difference in MI, ΔMI , as:

$$\Delta MI = MI_{female} - MI_{male} \quad (2.19)$$

As in our principal analysis, we tested the significance of the sex difference in MI by a parametric approach, comparing the slopes of the regression of FC_{14} and FC_{14-26} Paternoster et al. (1998).

2.2.5 Spatial auto-correlation (spin-tests)

In this work, we are interested in identifying the correspondences between the topographies of different brain maps, i.e., the extent of their spatial correlation or co-location. It has been found that standard statistical methods fail to account for the spatial smoothness of brain maps (Alexander-Bloch et al., 2013; Markello and Misic, 2021; Váša et al., 2018). More specifically, brain maps are spatially autocorrelated datasets, such that neighboring

data points on a map cannot be considered as statistically independent and thus violate the assumptions of many statistical frameworks (Markello and Misic, 2021).

To control for the spatial auto-correlation between neighboring brain regions, each analysis of the spatial co-location of two brain maps is reported with both the parametric P -value corresponding to the Pearson correlation (r), as well as a P -value derived from the more conservative spin-test permutation test (Alexander-Bloch et al., 2013; Váša et al., 2018) which conserves the spatial auto-correlation of both maps and is denoted P_{spin} . In brief, P_{spin} -values for the spatial correlation between two maps were estimated by comparing the magnitude of the empirical correlation between the two maps to a null distribution of correlations based on a set of 10,000 random spatial rotations or spins of the observed maps that preserved their internal, spatially autocorrelated structure.

Alexander-Bloch et al. (2013) first suggested a vertex-wise approach to correct for spatial auto-correlation. Our results are estimated at regional level, thus we corrected all tests for spatial co-locations between two autocorrelated cortical maps using a regional adaptation of the spherical permutation test implemented and published by Váša et al. (2018): https://github.com/frantisekvasa/rotate_parcellation. Since the publication by Váša et al. (2018), the effect of regional centroid definition on spatial permutation procedures has been further researched (Markello and Misic, 2021). It has been suggested that the previously used method of estimating the regional centroid by averaging across all vertex coordinates leads to the centroids lying under the surface of the cortical mesh (Markello and Misic, 2021). We therefore defined the centroids by computing the geodesic distance between all vertices in each region and assigning the vertex with the smallest average geodesic distance to all other vertices as the centroid of each region (Markello and Misic, 2021).

More specifically, this implementation of the spatial permutation test generated random permutation matrices by (i) generating three $\{3 \times 3\}$ matrices with coefficients following independent standard normal distributions, (ii) applying a QR decomposition, and (iii) retaining the orthogonal matrices Q which have uniformly distributed parameters. Subsequently the regions of the randomly rotated brain map are matched to the coordinates of the regions in the observed map using Euclidean distance. Starting at the rotated region with the highest average Euclidean distance to all unrotated regions, the algorithm proceeds in descending order to match each rotated region to the unrotated centroid it is closest to.

Spin permutations were applied to both maps, before comparing each permuted map to the observed version of the other map, and then calculating the average P_{spin} -value (Váša et al., 2018).

2.2.6 Sensitivity analyses

Sensitivity of results to alternative motion-correction strategies

In the original sample, we corrected for motion across all subjects by regressing FD at each edge. While this removed the effect of motion on FC across subjects, we still observed a weak, but significant effect of sex on FD ($\beta_{sex} = 0.02, P_{sex} < 0.01, t(296) = 3.3$; **Fig. 2.5C**). We therefore opted to construct three replication samples to test the sensitivity of our results to the specific motion-correction procedures outlined above. (1) *A sample where FD was regressed by sex*: We constructed a sample where FD was regressed on FC at each edge, as in the main sample, but separately by sex. Thus by construction, for each sex separately, there was no longer an effect of distance on the correlation between FC and motion (**Fig. 2.7B**), and the average edge-wise correlation between FC and motion was zero (**Fig. 2.7D,E**). (2) *Motion-matched sample*: We constructed a motion-matched subsample of the NSPN dataset by removing participants with particularly high and low FD values from each agebin in the original sample, until no significant difference in head motion was observed between males and females, while the age and sex stratification of the original sample was maintained. If a participant was included in the sample, all of their follow-up scans were also included. The final sample consisted of 314 subjects (156 females), 124 of which were scanned once, 89 twice and 4 three times (**Table 2.2**). (3) *global signal regression (GSR) regression sample*: We re-processed all data using an alternative pipeline for motion correction. The first pre-processing steps were the same as in the original sample. After ME-ICA pre-processing, however, we performed GSR. The global signal was estimated as the average time series of all cortical voxels. We regressed this time series from each region. From here, we proceeded with wavelet filtering using brainwaver v. 1.6 and all following steps as in the original pre-processing pipeline.

Sex	# Scans	# Scanned			At Baseline			
		1	2	3	μ Age	σ Age	μ FD	σ FD
female	156	67	43	1	18.9	3.0	0.12	0.02
male	158	57	46	3	18.9	2.8	0.12	0.03

Table 2.2 **NSPN fMRI motion-matched sample overview**: We identified a subset of participants such that there was no significant sex difference in framewise displacement (FD) ($P > 0.05$). We resampled subjects within age strata and kept all scans from each single participant together, such that the original structure of the dataset was preserved.

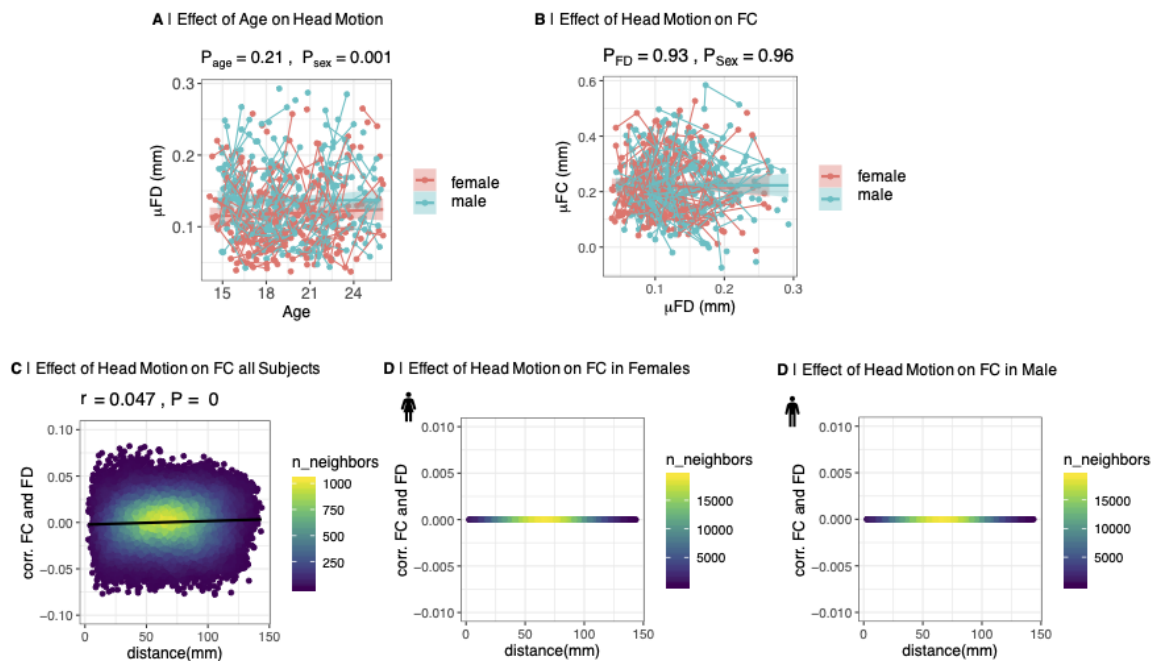


Fig. 2.7 Effect of head motion (FD) on functional connectivity (FC) in the FD regression by sex sample : To remove the sex difference in the dependence of FC on motion, mean FD was regressed from each edge for males and females separately; the residuals constitute participant-specific FD-corrected FC, with intercepts retained to maintain the relative importance of edges across the group as well as the interpretability of FC values. (A) Following this correction, subjects' average head motion, quantified as mean frame-wise displacement (FD), did not change with age ($P_{age} = 0.21, t(220) = 1.25$). However, there was a weak, but significant effect of sex on FD ($P_{sex} < 0.01, t(296) = 3.266$). (B) Mean participant motion was not related to mean FC across participants ($P_{FD} = 0.93, t(221) = 0.09$) and there is no effect of sex on the relationship ($P_{Sex} = 0.93, t(296) = -0.05$). (C) The correlation between FC at each edge and participant motion shows a weak but significant relationship with the Euclidean distance spanned by edges ($r = 0.05, P < 0.001$). The average edge-wise correlation between FC and motion is very close to zero (intercept = -0.002). By definition, the correlation between FC and motion almost completely vanished at the level of individual edges for males and females separately (D) and (E).

Sensitivity of results to intra-cranial volume (ICV)

On average, men tend to have larger ICV than females, hypothetically due to sex differences in body size (Ruigrok et al., 2014). Previous work has demonstrated effects of intracranial volume on grey matter (Eikenes et al., 2022) and white matter volume (Sanchis-Segura et al., 2020), and brain-behavior relationships (Dhamala et al., 2022), which may mediate some of the previously reported sex differences on these measures. Little is known about the effect of

ICV on functional connectivity, so to test for the sensitivity of our results to ICV, we ran an additional sensitivity analysis in which we controlled for ICV.

Specifically, to estimate the effects of total ICV on our main results, we included ICV in both the analysis of global functional connectivity, as well as in the calculation of maturational index. To estimate the effect of ICV on global functional connectivity, we added ICV to our model as a covariate:

$$FC_{global} \sim 1 + age * \beta_{age} + sex * \beta_{sex} + site * \beta_{site} + ICV * \beta_{ICV} + \gamma_{subject} * (1|subject) + \varepsilon \quad (2.20)$$

where FC_{global} refers to the global functional connectivity, β refers to coefficients for the fixed effects, $\gamma_{subject}$ refers to the coefficients for random effects, and ε represents the residual error.

Likewise, we also included ICV in our analysis of edge-wise functional connectivity.

$$FC_{edge} \sim 1 + age * \beta_{age} + site * \beta_{site} + ICV * \beta_{ICV} + \gamma_{subject} * (1|subject) + \varepsilon \quad (2.21)$$

We predicted the mean ICV at age 14 from the model:

$$ICV_{sex} \sim 1 + age * \beta_{age} + site * \beta_{site} + \gamma_{subject} * (1|subject) + \varepsilon \quad (2.22)$$

as:

$$\mu_{ICV_{14sex}} = 1 + 14 * \beta_{age} + 1/3 * \beta_{site_1} + 1/3 * \beta_{site_2} \quad (2.23)$$

We then included the effect of ICV in the calculation of baseline connectivity (FC_{14}) by adding β_{ICV} (from **Equation 2.21**) multiplied by the mean ICV at age 14 for males and females, respectively ($\mu_{ICV_{14sex}}$ from **Equation 2.23**), as an extra term in the regression model used to estimate FC_{14} . Thus for each edge, we estimated baseline connectivity at age 14 as:

$$FC_{14} = 1 + 14 * \beta_{age} + 1/3 * \beta_{site_2} + 1/3 * \beta_{site_3} + \mu_{ICV_{14}} * \beta_{ICV} + \gamma_{subject} * (1|subject) + \varepsilon \quad (2.24)$$

As before, the rate of change is calculated as:

$$FC_{14-26} = \beta_{age}, \quad (2.25)$$

and the MI is the coefficient of the linear relationship between the ICV-corrected FC_{14} and ICV-corrected FC_{14-26} .

Sensitivity of results to global FC

We noted that there was a sex difference in global functional connectivity (FC_{global}) between males and females in our sample (details are described in the results section; **Fig. 2.9A**). In this work, we are interested in analysing sex differences in adolescent edgewise re-organization of functional connectivity. To ensure our results were not confounded by the observed sex difference in FC_{global} , we ran a sensitivity analysis, correcting for the effects of FC_{global} .

Specifically, to estimate the effects of FC_{global} , on our main results, we included FC_{global} in the calculation of maturational index. First, we included FC_{global} in our analysis of edge-wise functional connectivity.

$$FC_{edge} \sim 1 + age * \beta_{age} + site * \beta_{site} + FC_{global} * \beta_{FC_{global}} + \gamma_{subject} * (1|subject) + \epsilon \quad (2.26)$$

We predicted the mean FC_{global} at age 14 from the model:

$$FC_{global_{sex}} \sim 1 + age * \beta_{age} + site * \beta_{site} + \gamma_{subject} * (1|subject) + \epsilon \quad (2.27)$$

as:

$$\mu_{FC_{global_{14_{sex}}}} = 1 + 14 * \beta_{age} + 1/3 * \beta_{site_1} + 1/3 * \beta_{site_2} \quad (2.28)$$

We then included the effect of FC_{global} in the calculation of baseline connectivity (FC_{14}) by adding $\beta_{FC_{global}}$ (from **Equation 2.26**) multiplied by the mean FC_{global} at age 14 for males and females, respectively ($\mu_{FC_{global_{14_{sex}}}}$ from **Equation 2.28**), as an extra term in the regression model used to estimate FC_{14} . Thus for each edge, we estimated baseline connectivity at age 14 as:

$$FC_{14} = 1 + 14 * \beta_{age} + 1/3 * \beta_{site_2} + 1/3 * \beta_{site_3} + \mu_{FC_{global}_{14}} * \beta_{FC_{global}} + \gamma_{subject} * (1|subject) + \epsilon \quad (2.29)$$

As before, the rate of change is calculated as:

$$FC_{14-26} = \beta_{age}, \quad (2.30)$$

and the MI is the coefficient of the linear relationship between the FC_{global} -corrected FC_{14} and FC_{global} -corrected FC_{14-26} .

2.2.7 Gene enrichment analyses

Partial least squares regression

Partial least squares regression (PLS) has been used as a powerful tool to describe the relationship between two sets of variables (represented as two matrices) which uses latent variables to model the covariance them (Abdi, 2003). Its ability to handle situations with a large number of potentially multicollinear predictors has made it useful for analysis of neuroimaging data (Morgan et al., 2019; Vértes et al., 2016; Whitaker et al., 2016a). Briefly, PLS finds mutually orthogonal components that are ranked in order of their importance in explaining the covariance between the dependent and independent variables, so that the first PLS component, denoted first partial least squares regression component (PLS1), defines the weighted functions of both dependent and independent variables with maximal covariance (**Fig. 2.8**). Here, we used PLS to define the weighted gene expression pattern that was most strongly correlated with the anatomical pattern of sex differences in adolescent functional connectivity maturation, ΔMI . Thus we related the 180-length vector of bilaterally averaged sex differences in adolescent FC development, ΔMI , to the 180 by 15,746 matrix of post mortem brain regional gene expression data provided by the Allen Human Brain Atlas (AHBA) from 6 adult brains (5 males) (Arnatkeviciute et al., 2019; Hawrylycz et al., 2015). We analysed whether the first PLS component explained more variance than expected by chance by randomly permuting the rows of the gene expression matrix and comparing the variance explained by PLS regression of ΔMI on the observed transcriptional data with the distribution of variance in ΔMI explained by 1000 random permutations of the brain gene expression matrix. Additionally, we used spherical permutation testing to assess the significance of the PLS analysis. In this case the null distribution was generated by

permuting the order of regions in the dependent variable (Y) according to a spherical rotation of regions the regions, as described in **Section 2.2.5**. For PLS1, which accounted for the greatest proportion of covariance, we estimated the variability of each transcript's weighting coefficient by bootstrap resampling (10,000 times) of the brain regional transcription matrix. The effect size and statistical significance of individual transcript weights on PLS1 were defined by Z -scores (observed weights divided by their bootstrapped standard errors).

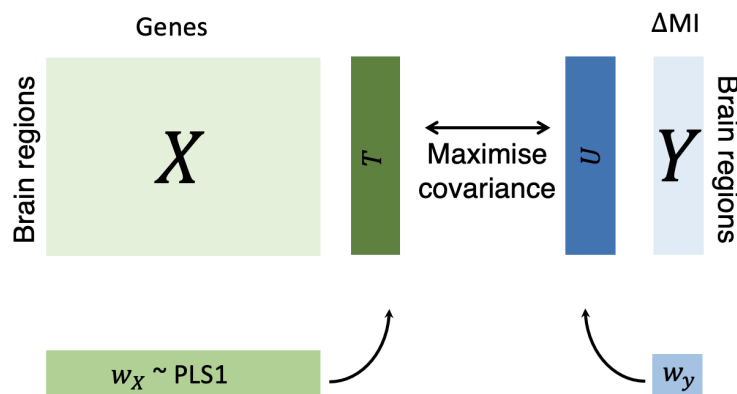


Fig. 2.8 Simplified model of partial least squares analysis: Here, we use PLS to find the weighted pattern of gene expression weights that is maximally co-located with the map of sex differences in adolescent functional connectivity development. We designate the $\{180 \times 15,746\}$ matrix of post mortem gene expression data in 180 brain regions provided by the Allen Human Brain Atlas from 6 adult brains (5 males) (Arnatkeviciute et al., 2019; Hawrylycz et al., 2015) the dependent variable, X ; and the $\{180 \times 1\}$ vector of sex differences in maturational index, ΔMI , the response variable, Y . PLS maximises the covariance between the projections into latent space of X and Y , termed U and T respectively. The PLS components, or weights, w_x , describe the projection of X onto T , i.e. $X = Tw_x + E$, where E is an error term. Since T is estimated by maximizing the covariance with U , w_x defines the weighted functions of both dependent and independent variables with maximal covariance.

Median rank-based gene enrichment

We used a median rank-based approach to assess the enrichment of the PLS1-weighted gene list for previously curated lists of genes with specialised functional roles or associations with psychiatric disorder (Seidlitz et al., 2020). This allowed us to assess whether functionally or pathophysiologically relevant genes were non-randomly represented among the most strongly weighted PLS1 genes that have brain expression anatomically co-located with the spatial pattern of sex differences in maturational index. To do this, each gene on the prior gene list of interest was ranked in terms of its Z -score weighting on PLS1 and the observed median

rank was estimated; then an equivalent number of genes, were randomly selected and their median rank on the PLS1 component was estimated.

Gene length can introduce bias in microarray data analysis. Longer genes produce more RNA molecules, thus they tend to generate stronger signals on the microarray compared to shorter genes, even if their actual expression levels are the same (Oshlack and Wakefield, 2009). This bias can impact data analysis and lead to incorrect conclusions. While routine expression-data quality control aims to adjust for this bias, here we opted to match the randomly selected genes for gene length to control for any residual effects of gene length.

More specifically, in order to ensure that no residual effects of gene length could confound the results of the gene enrichment analysis, we matched the genes in the empirical list with a set of genes in the list of AHBA genes which were similar in length based on the Mahalanobis distance of their gene length to all other genes. We then proceeded to resample from that length-matched subset of AHBA genes to find a set of genes matched for gene length with the empirical gene lists ($P < 0.05$).

This second step of randomly selecting and ranking genes was repeated 10,000 times to sample the permutation distribution of median rank. Finally, the null hypothesis that the observed median rank (for the gene list of interest) was not significantly different from the median rank of a random list of genes (matched for gene length and number of genes) was tested by comparing the observed median rank to the centiles of the permutation distribution. For example, for a two-tailed test of significant enrichment with $P < 0.05$, if the observed median rank was lower than the 2.5th percentile of the permutation distribution, then the gene list of interest was significantly enriched among the most negatively weighted PLS1 genes; whereas if the observed median rank was greater than the 97.5th percentile of the permutation distribution then the gene list of interest was significantly enriched among the most positively weighted PLS1 genes.

Developmental enrichment

We used the Cell Specific Expression Analysis tool (CSEA; <http://genetics.wustl.edu/jdlab/csea-tool-2/>) to test for enrichment of genes co-located with the map of sex differences in functional connectivity development, ΔMI , for developmentally relevant genes across the cortex and subcortical structures (Dougherty et al., 2010; Xu et al., 2014). The CSEA tool uses human data from BrainSpan, an atlas of the developing human brain (Miller et al., 2014), with postmortem human brain specimens collected across 13 developmental stages (4 weeks post conception to 60 years of age) in 8-16 brain structures. We uploaded a ranked list of genes

with significantly negative or positive PLS1 weights ($P_{FDR} < 0.05$) to the CSEA tool under the category *SEA across brain regions and development*.

2.3 Results

2.3.1 Sex differences in parameters of adolescent development of global mean degree

We modeled age and sex effects on global functional connectivity of each participant, estimated as the mean weighted degree over all nodes in the connectome, using linear mixed effects models (LMEs). Global mean degree increased with age ($t(219)=2.3$, $P<0.05$) and males had higher global mean weighted degree than females ($t(296)=5.5$, $P<0.0001$; **Fig. 2.9A**).

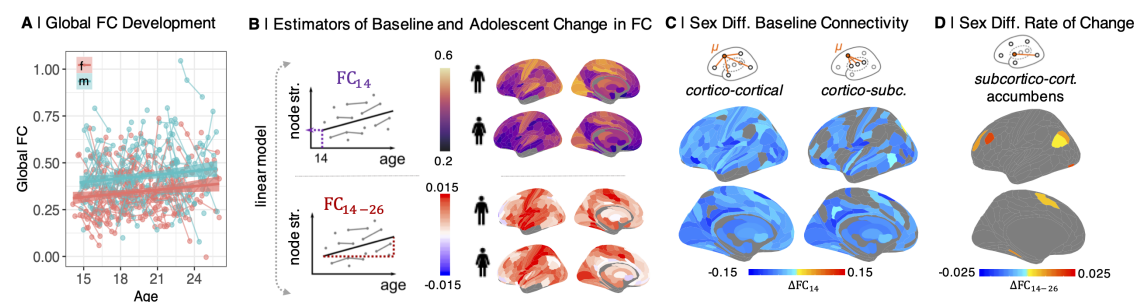


Fig. 2.9 Sex differences in functional connectivity at age 14 (FC_{14}) and adolescent rate of change of connectivity (FC_{14-26}) per year: (A) Global FC strength increased with age ($t(219) = 2.3, P < 0.05$) and was higher in males ($t(296) = 5.5, P < 0.0001$). (B) To estimate two parameters of development at each regional node, we fit a linear model to the relationship between age and weighted degree (nodal strength of connectivity to the rest of the network) for males and females separately. The two model parameters are the intercept, or “baseline” connectivity at age 14 (FC_{14}), and the linear rate of change in connectivity during adolescence (FC_{14-26}). (C) We found 321/330 regions had significantly increased cortico-cortical connectivity, and 230/330 regions had increased cortico-subcortical connectivity, in males compared to females at baseline ($P_{FDR} < 0.05$). (D) FC_{14-26} was only significantly different between sexes (decreased in females) in 27/330 subcortico-cortical connections of the nucleus accumbens.

Regional functional connectivity was estimated between and within cortical and subcortical subsets of nodes by averaging the relevant parts of the connectivity matrix. To model

development of functional connectivity during adolescence, we focused on three parameters: regional baseline connectivity at age 14, FC_{14} (**Fig. 2.10**); regional linear change in connectivity between 14-26 years, FC_{14-26} (**Fig. 2.11**); and the signed Spearman's correlation of these two parameters (**Fig. 2.12A**), or maturational index ($-1 < MI < +1$) (**Fig. 2.12B**; Váša et al. (2020)). Previous work on this sample has reported developmental change (on average over both sexes) in terms of these parameters estimated at each regional node of a whole brain fMRI network (Váša et al., 2020). Here we estimated each of these parameters for males and females separately, and the between-sex difference for each parameter, e.g., $\Delta MI = MI_{female} - MI_{male}$. We tested the significance of the between-sex difference of each regional parameter using parametric tests.

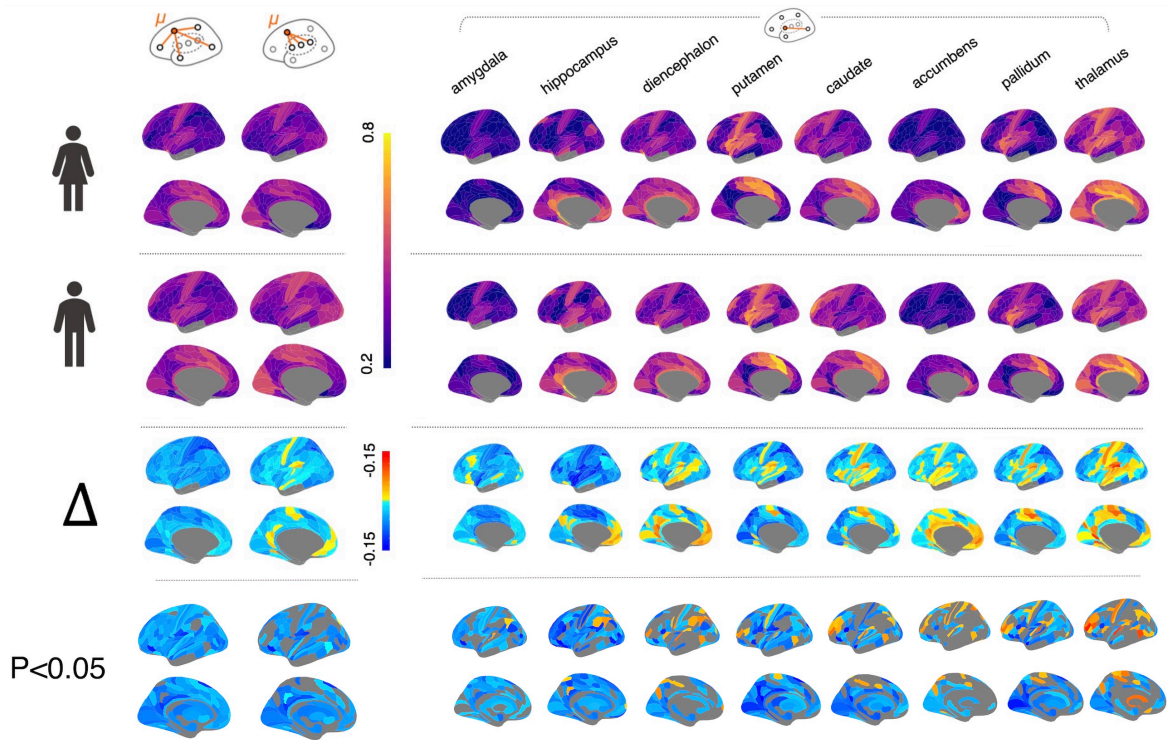


Fig. 2.10 All baseline connectivity FC_{14} plots: Separate linear mixed effects models were fitted for both sexes to model regional functional connectivity development as predicted by age and site for cortico-cortical, cortico-subcortical and subcortico-cortical connections. Baseline connectivity, FC_{14} , was separately estimated using these models for females (*top row*) and males (*second row*) and a difference map was constructed (*third row*). Lastly, this map of sex differences in FC_{14} was thresholded for significance after correction for multiple comparisons at $P_{FDR} < 0.05$ (*last row*).

The pattern of *adolescent rate of change in connectivity* was strongly positive in sensorimotor cortex, and less positive or slightly negative in association cortical and limbic areas,

for both sexes (**Fig. 2.11**). There were no significant sex differences, i.e., $\Delta FC_{14-26} = 0$, for cortico-cortical or cortico-subcortical connectivity; but a subset of 27 subcortico-cortical connections, involving the nucleus accumbens, had significantly more negative rates of change in females compared to males ($P_{FDR} > 0.05$; **Fig. 2.11**).

Qualitatively, *baseline connectivity at age 14* was greater in primary sensorimotor cortex than in association cortex for both sexes (**Fig. 2.10**). As predicted by the sex difference in global functional connectivity at all ages (**Fig. 2.10A**), males had significantly stronger baseline connectivity than females at 14 years, i.e., $\Delta FC_{14} = FC_{14,female} - FC_{14,male} > 0$, in cortico-cortical and cortico-subcortical connections (**Fig. 2.10**).

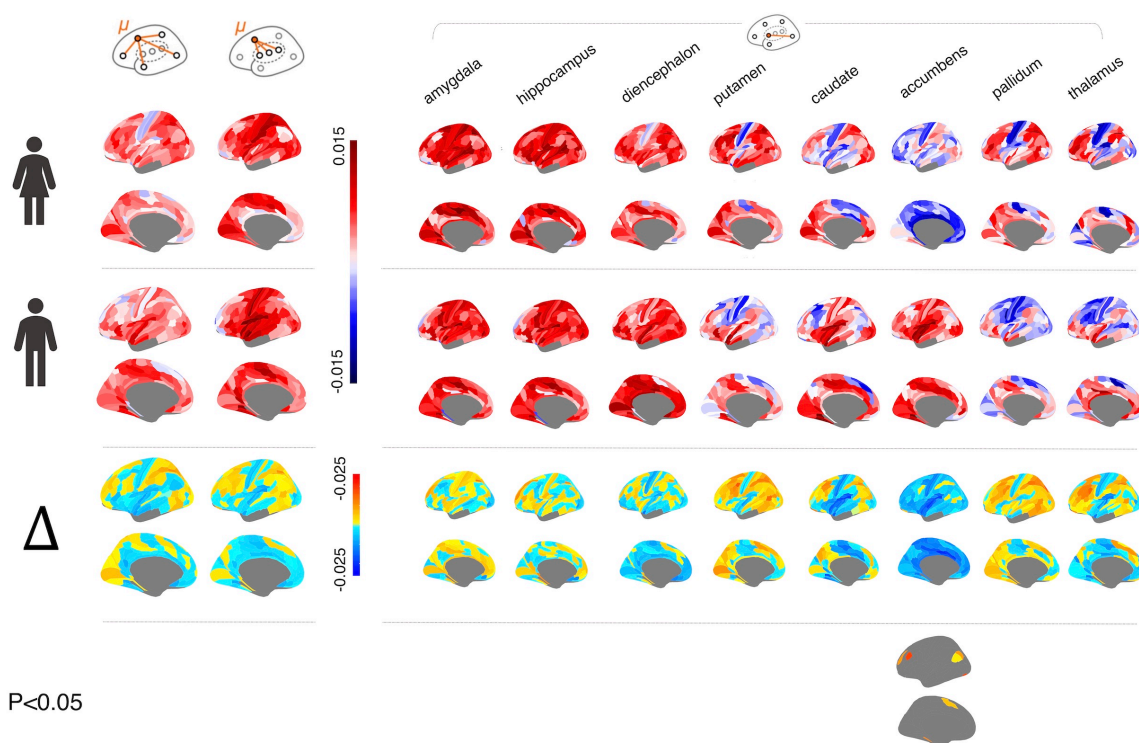


Fig. 2.11 Significance of sex difference in adolescent rate of change FC_{14-26} : The adolescent rate of change, FC_{14-26} , was estimated for females (*top row*) and males (*second row*) separately, and a difference map was constructed (*third row*). This map of sex differences in FC_{14-26} was thresholded for significance after correction for multiple comparisons at $P_{FDR} < 0.05$ (*last row*). ΔFC_{14-26} was significantly non-zero, indicating a difference between males and females, in a subset of 27 subcortico-cortical connections involving the nucleus accumbens

2.3.2 Sex differences in maturational index

Maturational index was positive in sensorimotor cortices, and negative in association cortex and subcortical areas, in both sexes separately (**Fig. 2.12**), as previously reported for both sexes on average (Váša et al., 2020).

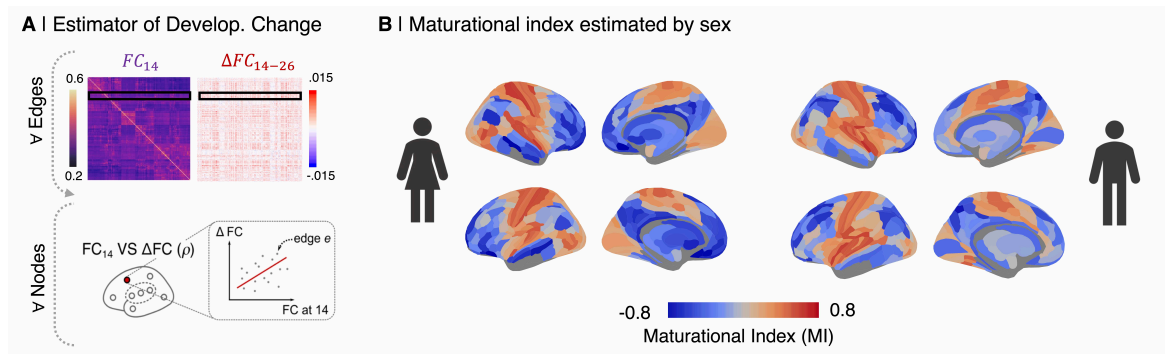


Fig. 2.12 Sex-specific maturational index: (A) maturational index (MI) was estimated as the correlation between edgewise baseline connectivity at age 14 (FC_{14}), and the linear rate of change in connectivity per year (FC_{14-26}), at each regional node. (B) Maturational index for males and females separately, all sides of the brain displayed.

As described above, the sign of MI relates to two modes of maturational development: “disruptive”, i.e. $MI < 0$, and “conservative”, i.e. $MI > 0$. Disruptive development means that edges that are strong at baseline become weaker over the course of adolescence (“strong getting weaker”) and those edges that are weak at baseline become stronger (“weak getting stronger”). Conservative development, in contrast, means that edges that are strong at baseline gain strength over the course of adolescence (“strong getting stronger”) (**Fig. 2.2**), and edges that are weak at baseline become weaker (“weak getting weaker”). We quantified which of these trends was predominant in either developmental mode respectively, by estimating the ratio of edges with positive FC_{14-26} to negative FC_{14-26} (**Fig. 2.13A**). If a region has disruptive development ($MI < 0$), and the ratio of its edges with negative versus positive values of FC_{14-26} is greater than 0.5, we defined the mode of maturational development of that region to be predominantly weak getting stronger; if the same ratio was less than 0.5 we defined it as predominantly strong getting weaker. Conversely, if a region has conservative development ($MI > 0$), and the ratio of its edges with negative versus positive values of FC_{14-26} is greater than 0.5, we mode of maturational development of that region to be predominantly strong getting stronger; and if the same ratio was less than 0.5 we defined it as predominantly weak strong weaker. We find that in both males and females respectively, more than 75% of regions with disruptive development ($MI < 0$) are classified as “weak

getting stronger” (**Fig. 2.13B**), while all conservative regions ($MI > 0$) in both sexes were classified as “strong getting stronger” (**Fig. 2.13C**).

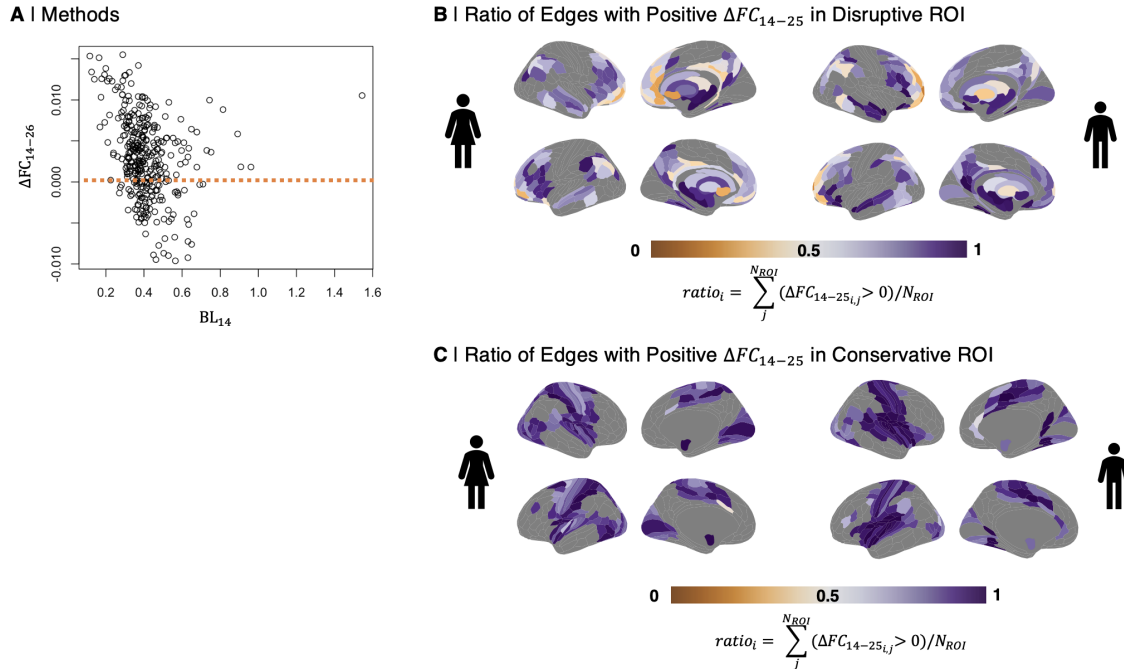


Fig. 2.13 Trends in disruptive and conservative development of connectivity: (A) We estimated trends for regions of disruptive and conservative change in each sex by calculating for each node i the proportion of edges with a positive rate of change connected to it. We then thresholded this ratio map for disruptive and conservative nodes in each sex. (B) In disruptive regions, if this $ratio_i > 0.5$, a region is predominantly strong getting weaker, if $ratio_i < 0.5$, it is predominantly weak getting stronger. We found that disruptive regions were predominantly characterized by weak getting stronger changes (78.5% of regions in females and 81.3% in males). (C) In conservative regions, if this $ratio_i > 0.5$, a region was designated as strong getting stronger, if $ratio_i < 0.5$, it was classified as weak getting weaker. We found that all conservatively maturing regions in both sexes were strong getting stronger.

There were many areas of significant sex difference in MI ($P_{FDR} < 0.05$; **Fig. 2.14D**). Females had more negative MI than males in 107 regions (**Fig. 2.14A,C**; for a full list see **Supplementary Table A.3**). In 84 of these regions, exemplified by the right putamen (**Fig. 2.14B**), there was more disruptive development in females, i.e., weak connections at 14 years became stronger during adolescence, or strong connections became weaker, in females compared to males. In 23 regions, exemplified by right visual area V6 (**Fig. 2.14C**), there was less conservative development in females, i.e., strong connections at 14 years became stronger during adolescence in males compared to females. Thus the brain system defined by regions with a negative ΔMI was predominantly characterized by a weak-getting-stronger

profile of developmental change in functional connectivity that was greater in females than males.

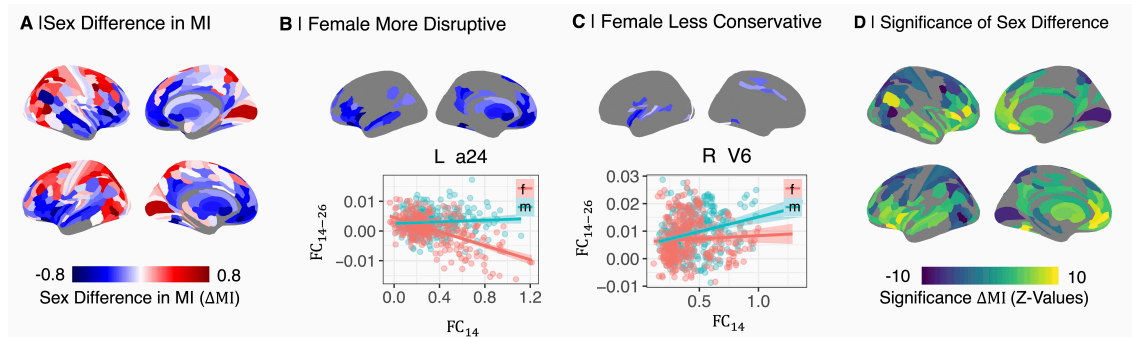


Fig. 2.14 Significance of sex difference in MI: (A) The sex difference in MI was estimated by $\Delta MI = MI_{female} - MI_{male}$. ΔMI was negative in the ventral and medial prefrontal gyrus, ventrolateral prefrontal cortex, anterior and posterior cingulate gyrus, medial temporal gyrus, and subcortical nuclei, indicating sex differences in adolescent development of connectivity of these regions. More specifically, negative ΔMI defined a set of brain regions where adolescent development was either more disruptive (weak connections at 14 years became stronger during adolescence, or strong connections became weaker) or less conservative (strong connections at 14 years became stronger or weak connections became weaker) in females compared to males. (B) Map of brain regions where development was more disruptive in females. As exemplified by data from the right putamen, functional connections of disruptively developing nodes that were strong at 14 years (high FC_{14} , x-axis) became weaker over the period 14-26 years ($FC_{14-26} < 0$, y-axis), and edges that were weakly connected at 14 years became stronger over the course of adolescence, especially in females. (C) Map of brain regions where development was less conservative in females. As exemplified by right visual area V6, connections that were strong at baseline become stronger over the period 14-26 years, especially in males. Due to limited space only these two regions were chosen as examples of the trends described. (C) ΔMI was significant in 230/346 regional nodes ($P_{FDR} = 0.05$). ΔMI thresholded by significance ($P(\Delta MI = 0) < 0.05$).

To further decode the anatomical and functional profile of the observed sex differences in adolescent functional connectivity maturation, the unthresholded map of ΔMI was co-registered with a prior map of cortical cytoarchitectonic classes (**Fig. 2.15A**) and a prior map of resting state networks (Yeo et al., 2011) from an independent component analysis of adult fMRI data (**Fig. 2.15B**). Regions of negative ΔMI were concentrated in secondary sensory, limbic, and insular classes of cortex, and in subcortical structures, defined anatomically (**Fig. 2.15A**); and in default mode, limbic, ventral attentional and subcortical systems defined functionally (**Fig. 2.15B**).

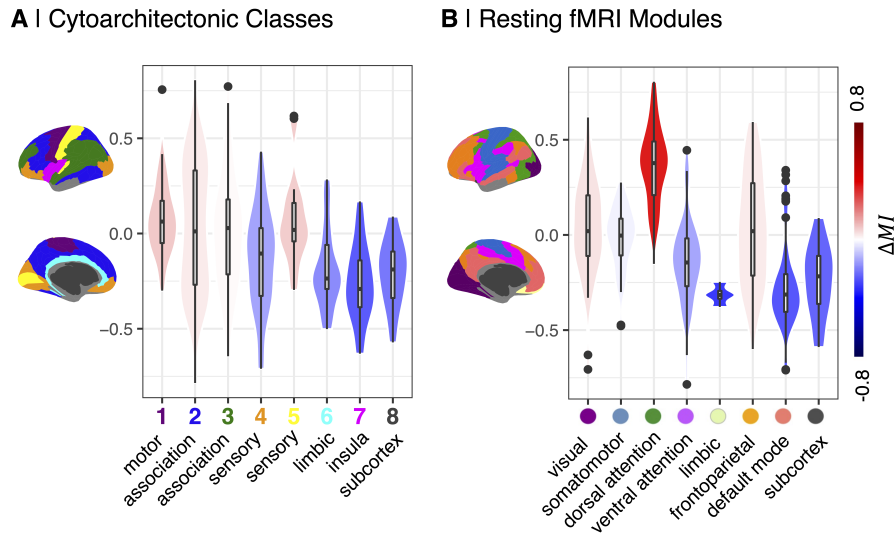


Fig. 2.15 **Cell type and task fMRI enrichment:** (A) ΔMI was most negative in cytoarchitectonically defined secondary sensory, limbic, and insula cortex, and subcortical structures (B) as well as functionally defined (fMRI) default mode network (DMN), ventral attention network, and limbic systems, and subcortical structures. (C) Wordcloud of Neurosynth meta-analytical cognitive terms scaled according to their strength of association with the disruptively developing brain regions (cortical map of $\Delta MI < 0$).

2.3.3 X-chromosome and developmental gene enrichment

To investigate the relationships between gene expression profiles and sexually divergent adolescent brain development, we used partial least squares regression (PLS) regression to find the weighted gene expression pattern that was most closely co-located with the ΔMI map. Whole-genome transcripts were estimated for the average of each of 180 bilaterally homologous cortical regions using adult postmortem data ($N = 6$) provided by the Allen Human Brain Atlas (Arnatkeviciute et al., 2019; Hawrylycz et al., 2015).

The first PLS component (PLS1; **Fig. 2.16A**) explained 34.6% of the variance in ΔMI , significantly more than expected by chance ($P_{perm} < 0.05, P_{spin} < 0.05$). The PLS1 gene expression weights were positively correlated with ΔMI (**Fig. 2.16B**). This means that negatively weighted genes, at the bottom of the ranked PLS1 list, were overexpressed in regions with negative ΔMI , or more disruptive maturational change in females. Conversely, positively weighted genes, at the top of the ranked PLS1 list, were underexpressed in regions with negative ΔMI (**Fig. 2.16B**).

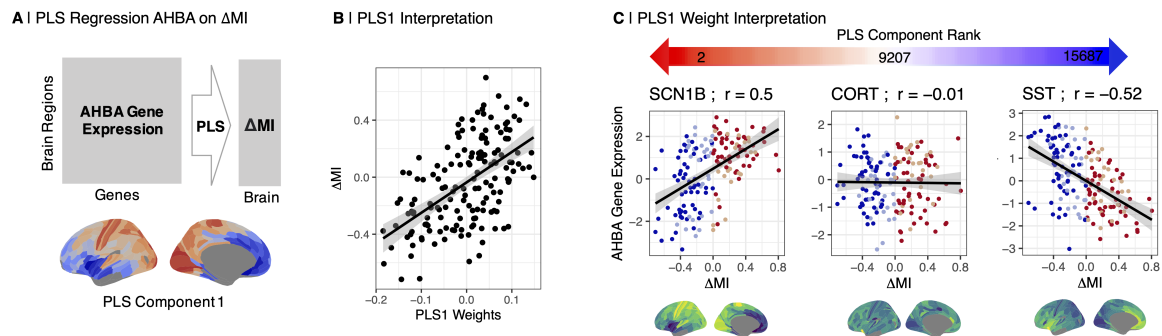


Fig. 2.16 Relationships between gene expression profiles and sexually divergent adolescent brain development: (A) We used PLS regression to map gene expression data (Hawrylycz et al., 2015; Kaczurkin et al., 2019) onto ΔMI . (B) PLS1 was positively correlated with ΔMI ; thus, low PLS1 scores were co-located with low ΔMI or predominantly female more disruptive regions. (C) Relationship of ΔMI to expression of exemplary genes: sodium voltage-gated channel beta subunit 1 (*SCN1B*), a positively weighted gene near the top of the ranked PLS1 weights list; cortistatin (*CORT*), a near-zero weighted gene in the middle of the list; and somatostatin (*SST*), a negatively weighted gene near the bottom. Negatively weighted genes were more strongly expressed in regions of negative ΔMI , that is, predominantly female ΔMI male disruptive regions, whereas positively weighted genes were more strongly expressed in regions with female > male conservative development indicated by positive ΔMI .

We hypothesised that gene expression patterns related to sex differences in adolescent brain development might be enriched for X chromosomal genes. This hypothesis was based on the following considerations. Firstly, genes on the X chromosome are enriched for sex-differential gene expression in multiple tissues, including the prenatal (Lake et al., 2018) and postnatal brain (Polioudakis et al., 2019). Second, the X chromosome is diploid in females (XX) and haploid in males (XY) and while X chromosome inactivation silences transcription of one of the two X chromosomes in females, incomplete inactivation has been shown to affect at least 23% of X-chromosomal genes, which results in sex biases in gene expression and is likely to introduce phenotypic diversity (Oliva et al., 2020). To test this hypothesis, we assessed chromosomal enrichment of the genes weighted on PLS1. We found that the most negatively weighted genes, which were highly expressed in brain regions that demonstrated more disruptive development in females, i.e., regions with negative ΔMI or more negative MI in females, were most strongly enriched for X chromosome genes compared to all other chromosomes ($P_{perm} < 0.001$; **Fig. 2.17**).

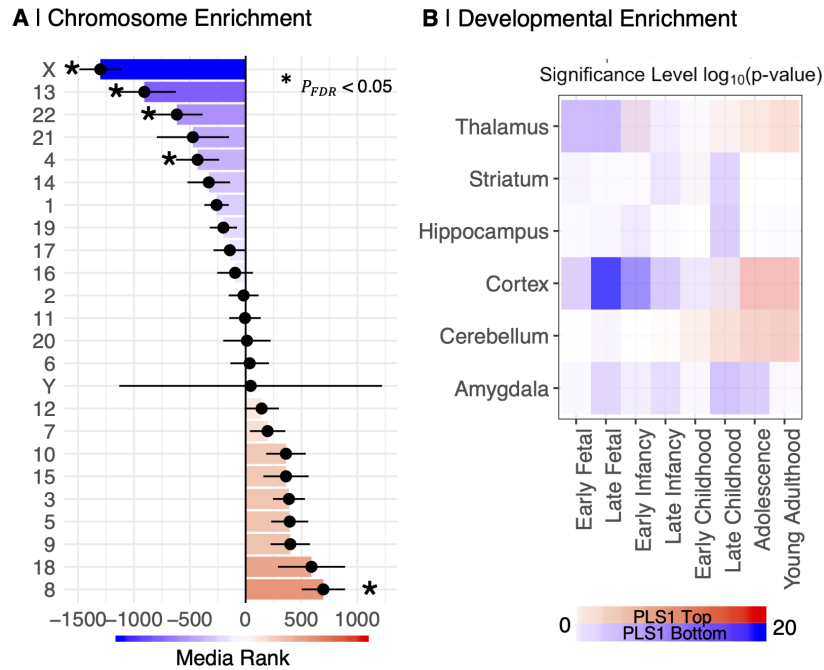


Fig. 2.17 Enrichment for X-chromosome and developmental genes: (A) Enrichment analysis for chromosomal genes. Plot of the median rank of genes from each chromosome on PLS1, with standard deviations. (B) Enrichment analysis for neurodevelopmental genes. Negatively weighted genes (blue) were enriched for genes typically expressed in cortex during late fetal and early post-natal development and for genes expressed in the amygdala, hippocampus and striatum during late childhood and adolescence. Positively weighted genes (red) were enriched for genes typically expressed in cortex and cerebellum during adolescence and early adult life.

2.3.4 Non-linear effects of age

It is conceivable that there could be non-linear effects of age on functional connectivity. However, previous work on the same data set Váša et al. (2020) investigated potential non-linear effects of age and found no substantial evidence for non-linearity in these data. Specifically, Váša et al. (2020) fitted smoothing splines (generalized additive mixed models) to edge-wise trajectories of functional connectivity development, using the “gam” function in R, with the effect of age modelled as the weighted sum of 10 cubic b-splines with knots placed at quantiles of the data and smoothing optimized using restricted maximum likelihood (Reiss et al., 2014). This modeling strategy is adaptive to the non-linearity of age effects, such that non-linear trajectories will be best fitted by spline functions with degrees of freedom (DF) greater than 2, whereas linear trajectories will be best fitted by spline functions with 2

DF, analogous to the intercept and gradient parameters of a simple linear model. Váša et al. (2020) found that approximately 70% of all edges had linear trajectories that were best fit by spline functions with 2 DF (**Fig. 2.18**; Váša et al. (2020)). Moreover, there was no evidence from this analysis that the minority of edges with non-linear trajectories were concentrated on anatomically specific brain regions or systems. For these reasons, we adopted a linear function for age-related effects on functional connectivity in our modeling of these data (**Equation 2.7**). However, to mitigate any residual concerns that non-linearity of age-related changes in functional connectivity might confound sex differences in MI, we examined the relationship between ΔMI and the nodal mean DF for spline functions of age. As shown in **Figure 2.18** there was no significant correlation ($r = 0.006, P = 0.9$). This indicates that there is no evidence for a relationship between non-linear trajectories of functional connectivity development and sex differences in maturational index.

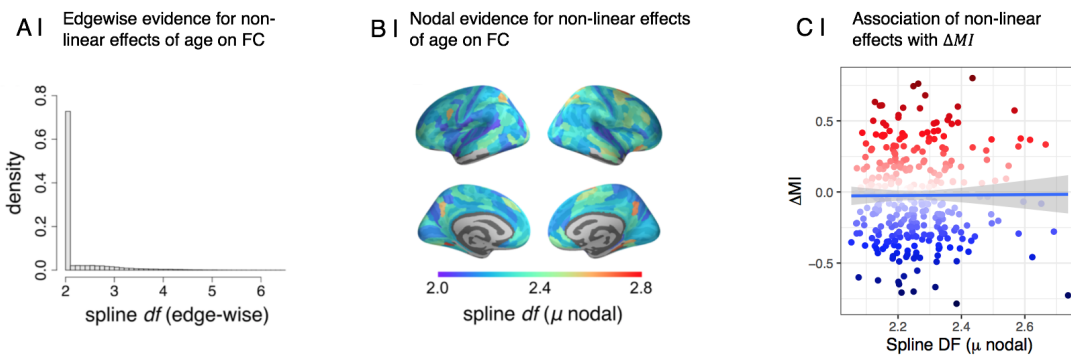


Fig. 2.18 Non-linear effects of age on FC: In previous work on this sample, Váša et al. (2020) fitted locally adaptive mixed effect smoothing splines to edgewise trajectories of functional connectivity development to inspect potential non-linear effects of age on FC. In these models, non-linear trajectories will be best fitted by spline functions with DF greater than 2, whereas linear trajectories will be best fitted by spline functions with 2 DF, analogous to the intercept and gradient parameters of a simple linear model. (A) Distribution of effective DF of smoothing splines across edges: 71.7% trajectories had $DF < 2.1$, suggesting that most trajectories are linear. (B) Cortical distribution of average nodal DF (averaged across all of a node's edges). (C) Lastly, we correlated the cortical map of sex differences in maturational index, ΔMI , with the cortical map of average nodal DF. We show that there is no association between evidence for non-linearities in functional connectivity development with age, as indicated by an effective $DF > 2$ ($r = 0.006, p = 0.9$). Panels A and B are reproduced, with permission, from the Supplementary Information for Váša et al. (2020).

2.3.5 Sensitivity to alternative modelling strategies

We found that the correlation between our principal sex—stratified results and the results of this alternative analysis, based on a fixed term for the sex-by-age interaction were nearly identical, with parameters estimated by sex-stratified and sex-by-age interaction models demonstrating a high degree of correlation, ($r > 0.9$; **Fig. 2.19**). Thus we conclude that our principal results from sex-stratified modelling are robust to an alternative modelling strategy that explicitly includes a fixed term for sex-by-age interaction. However, we continue to prefer the sex-stratified approach because of its greater adaptivity to the evident between-sex differences in random effects variance (**Fig 2.6**).

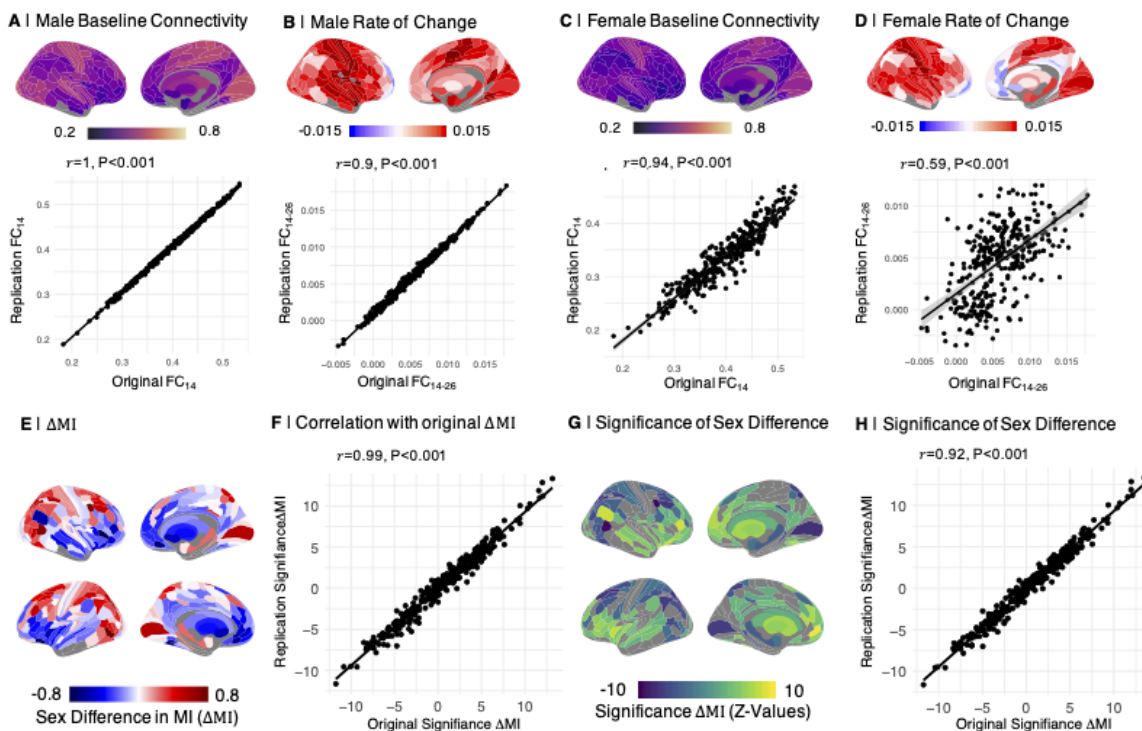


Fig. 2.19 Age \times sex interaction model: We modelled functional connectivity maturational in a joint model for males and females and included an interaction term for the interaction of age and sex. (A)-(D) From this model, we derived updated FC_{14} and FC_{14-26} for males and females. We found that those updated measures are highly correlated with our original measures from the sex stratified approach. (E)-(H) We further found that the sex difference in maturational index (MI), as well as the map of the effect size of this sex difference (Z-values), are highly correlated with our main analysis.

2.3.6 Sensitivity to alternative motion-correction strategies

To assess the robustness of key results to the two-step process for head motion correction, we conducted three sensitivity analyses: (i) sex-specific motion correction - FC matrices were regressed on FD separately for males and females; (ii) GSR correction - the fMRI time series at each node were regressed on the global fMRI signal per participant; and (iii) motion-matched sub-sample analysis - we used a subset of data (N=314), comprising equal numbers of males and females, for which there was no statistical difference in FD. We aimed to replicate our key findings of sexually divergent adolescent development of functional connectivity between DMN, limbic and subcortical regions, as well as an enrichment for X-chromosome genes.

We compared the results from these sensitivity analyses quantitatively to the corresponding results at all stages of the principal analysis. There was a significant correlation between the developmental fMRI metrics (FC_{14} , FC_{14-26} , and MI) estimated by each of these sensitivity analyses, and the same parameters estimated by our principal analysis. Further, we found that the map of sexually divergent adolescent development of functional connectivity of our principal analysis was highly correlated with all replication analysis maps (mean correlation Pearson's $r = 0.8$ between principal and sensitivity analyses of ΔMI).

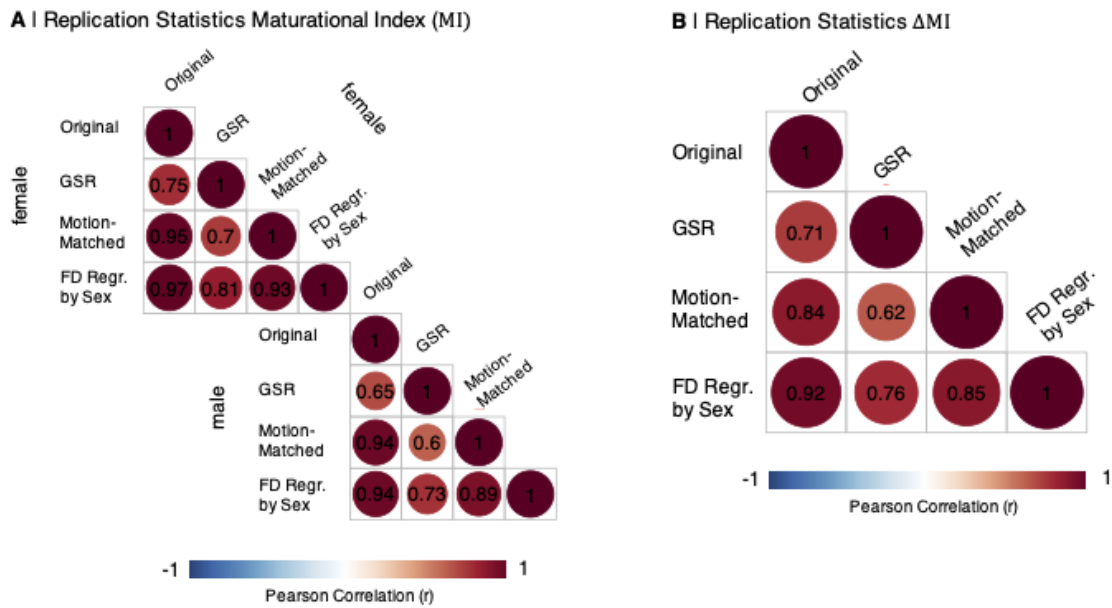


Fig. 2.20 Sensitivity of key findings to motion: Correlation of maps estimated using the principal dataset and analysis pipeline and the three sensitivity analyses designed to test the robustness of these principal results to different strategies for motion correction. (A) Correlation of individual male and female maturational index (MI) maps. (B) Correlation of sex difference in maturational index (ΔMI) maps across all regions calculated from principal and sensitivity analyses.

More specifically, the male and female FC_{14} were highly correlated with the parameters estimated in the original sample, in (i) the sample where FD was regressed by sex ($r_{male} = 0.94, P_{male} < 0.001; r_{female} = 0.95, P_{female} < 0.001$; **Fig. 2.21A, first column**); (ii) in the motion-matched sub-sample ($r_{male} = 0.89, P_{male} < 0.001; r_{female} = 0.98, P_{female} < 0.001$; **Fig. 2.21A, second column**); and moderately correlated with (iii) the same parameters derived in the GSR corrected sample ($r_{male} = 0.45, P_{male} < 0.001; r_{female} = 0.48, P_{female} < 0.001$; **Fig. 2.21A, third column**). Next, the male and female FC_{14-26} were highly correlated with the parameters estimated in the original sample, in (i) the sample where FD was regressed by sex ($r_{male} = 0.99, P_{male} < 0.001; r_{female} = 0.98, P_{female} < 0.001$; **Fig. 2.21B, first column**); (ii) in the motion-matched sub-sample ($r_{male} = 0.94, P_{male} < 0.001; r_{female} = 0.92, P_{female} < 0.001$; **Fig. 2.21B, second column**); and moderately correlated with (iii) the same parameters derived in the GSR corrected sample ($r_{male} = 0.23, P_{male} < 0.001; r_{female} = 0.52, P_{female} < 0.001$; **Fig. 2.21B, third column**).

Further, the original sex difference in maturational index, ΔMI , was highly correlated with the same parameters estimated in (i) the sample where FD was regressed by sex ($r = 0.92, P < 0.001$; **Fig. 2.21C, first column**); (ii) in the motion-matched sub-sample

($r = 0.8, P < 0.001$; **Fig. 2.21C**, *second column*); and moderately correlated with (iii) the same parameters derived in the GSR corrected sample ($r = 0.72, P < 0.001$; **Fig. 2.21C**, *third column*).

With respect to the gene enrichment results observed in our main analysis, we found that in the sensitivity analyses X-chromosome genes ranked towards the bottom of PLS1; however, this enrichment was not always significant at $P < 0.05$ (**Fig. 2.21E**). Specifically, in the GSR-pre-processed data, we found that enrichment for X-chromosome genes was the second-strongest, compared to all other chromosomes. We did observe a negative median rank, thus the effect observed in this sensitivity analysis was in the same direction as in the principal analysis, however the enrichment was not statistically significant.

2.3.7 Sensitivity of results to ICV and global FC

Given the male > female sex difference in intra-cranial volume (Mills et al., 2016; Sanchis-Segura et al., 2020), and the observed sex difference in global functional connectivity reported above, we ran two further sensitivity analyses: (i) intra-cranial volume (ICV) correction - we regressed global and edge-wise fMRI metrics on ICV estimated from structural MRI data on the same sample, and (ii) global functional connectivity correction - we regressed edge-wise fMRI metrics on global FC on the same sample.

We found that our key results replicate well in the sensitivity analysis including ICV (**Fig. 2.21**, *fourth column*). Specifically, original and ICV-corrected baseline connectivity were moderately correlated ($r_{female} = 0.89, P_{female} < 0.001; r_{male} = 0.98, P_{female} < 0.001$), whereas the adolescent rate of change was highly correlated ($r_{female} = 0.94, P_{female} < 0.001; r_{male} = 0.92, P_{female} < 0.001$). The ICV-corrected sex difference in maturational index (ΔMI) is qualitatively and quantitatively similar to the original result from our main analysis ($r = 0.98, P < 0.01$). We further ran the gene enrichment analysis in the replication sample. The original and replication PLS1 components are significantly correlated ($r = 0.92, P < 0.001$). Negatively weighted genes were more strongly expressed in regions of negative ΔMI , that is predominantly female > male disruptive regions; whereas positively weighted genes were more strongly expressed in regions with female > male conservative development indicated by positive ΔMI . We showed that we can replicate the gene enrichment for X-Chromosome genes.

We also found that our key results replicate well in the sensitivity analysis including global functional connectivity (**Fig. 2.21**, *fifth column*). Specifically, original and global-FC-corrected baseline connectivity are highly correlated ($r_{female} = 0.89, P_{female} < 0.001; r_{male} =$

0.98, $P_{male} < 0.0011$), and so is the adolescent rate of change ($r_{female} = 0.94, P_{female} < 0.001; r_{male} = 0.92, P_{male} < 0.001$). The global-FC-corrected controlled sex difference in maturational index (ΔMI) is qualitatively and quantitatively similar to the original result from our main analysis ($r = 0.99, P < 0.01$). Further, we confirmed that we can replicate the gene enrichment for genes on the X-Chromosome.

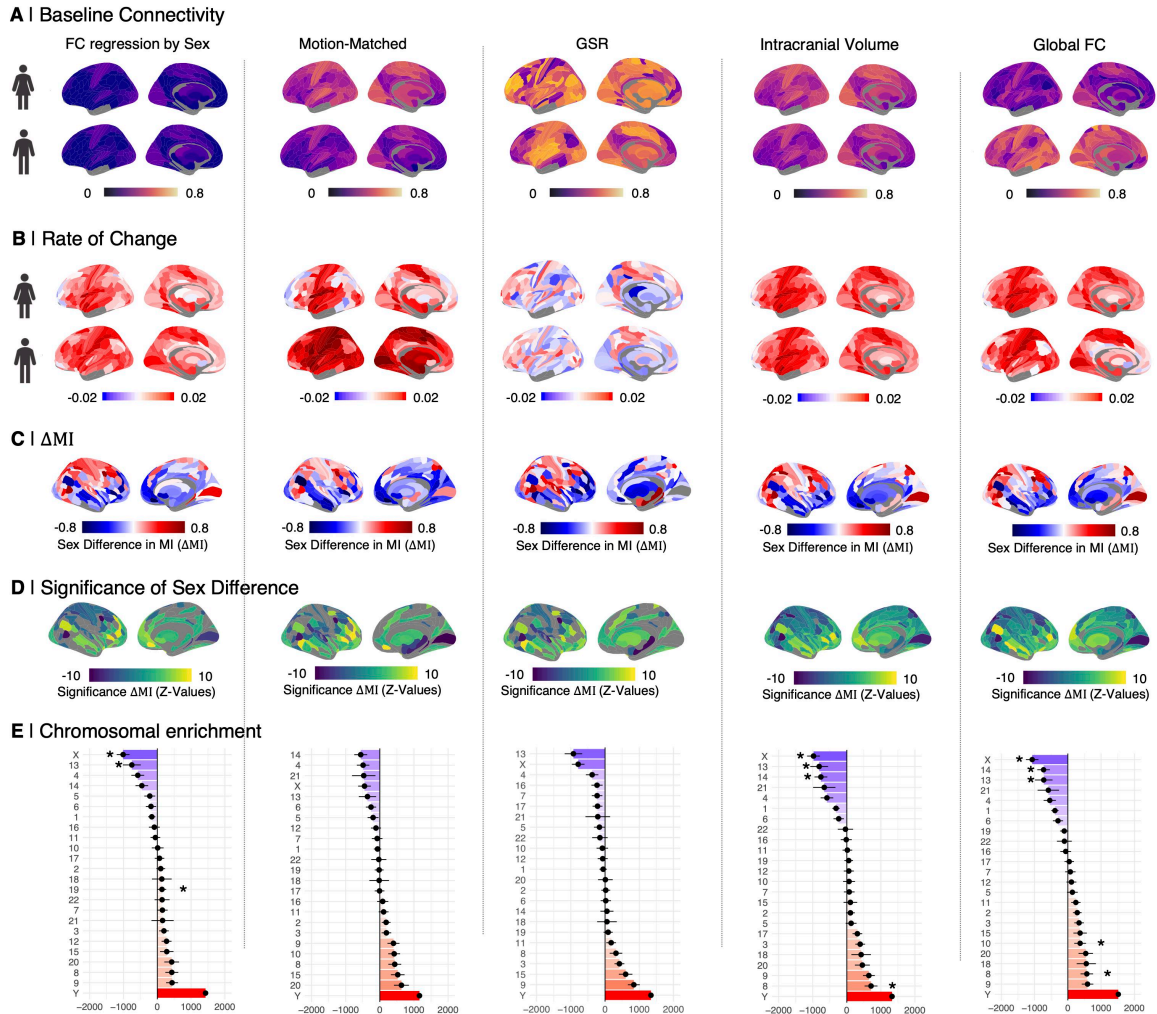


Fig. 2.21 Sensitivity of key results to alternative modeling strategies: We conducted five sensitivity analyses to test the robustness of our results alternative modeling strategies and alternative pre-processing strategies. We found that in all cases, (A) the baseline connectivity (FC_{14}); (B) the adolescent rate of change (FC_{14-26}); (C) the sex difference in maturational index (ΔMI); and (D) the effect size of the sex difference in MI, derived in the replication samples, were significantly correlated with the original parameters at $P < 0.05$.

2.4 Discussion

This study was motivated by the hypothesis that there are sex-divergent differences in brain functional network development of healthy adolescents.

In this accelerated longitudinal fMRI study of healthy young people, we first identified human brain systems that demonstrated a significantly different pattern of adolescent development in females compared to males. We found sex differences in several aspects of functional connectivity (FC): females had lower global mean FC across all ages, and reduced nodal strength of connectivity in most regional nodes at 14 years, FC_{14} . However, there were more anatomically specific sex differences in two developmentally sensitive parameters: the rate of change in FC during adolescence, FC_{14-26} , was significantly reduced in females for connections between one subcortical nucleus (nucleus accumbens) and 27 cortical structures; and the maturational index (MI), a coefficient of the linear relationship between edgewise FC_{14} and FC_{14-26} at each node, was significantly more negative in females for 107 cortical areas concentrated in the DMN, ventral attentional and limbic networks, as well as subcortical nuclei.

The maturational index can be used to define two modes of adolescent brain functional network development (Váša et al., 2020). A conservative node is defined by a positive MI – indicating that it is highly connected or “hub-like” at baseline (14 years) and becomes even more strongly connected over the course of adolescence (14-26 years). Theoretically, conservative nodes could also be weakly connected at baseline and become even more weakly connected during adolescence; however, empirically, we found that this was not the case. A disruptive node is defined by a negative MI – indicating either that it is weakly connected at age 14 but becomes more strongly connected or hub-like during adolescence; or that is a strongly connected node at 14 years but becomes more weakly connected or less hub-like during adolescence. The disruptive developmental profile of weak-getting-stronger during adolescence hypothetically represents a “re-wiring” of the functional connectome, which could be relevant to the acquisition of social, cognitive, and other skills during adolescence (Váša et al., 2020). Similar selective strengthening of connections has also been observed at the cellular level in the developing *C. elegans* connectome (Witvliet et al., 2021). It has also been argued that brain networks that are most developmentally active during adolescence are most likely to contribute to the coincidentally increased risk of mental health symptoms, i.e., “moving parts get broken” (Paus et al., 2008). For these reasons, our analysis focused particularly on sexual differences in weak-getting-stronger disruption in cortico-subcortical networks.

The first explanation we considered for this sex difference in developmental fMRI parameters was that it was attributable to sex differences in potentially confounding variables, including head motion during scanning. Head movement is known to be a potentially problematic confound in developmental fMRI (Power et al., 2012; Satterthwaite et al., 2013, 2012) and males, especially younger males, had more head movement than females in this sample as is consistent with previous studies (Satterthwaite et al., 2013). We initially addressed this issue by a two-stage pre-processing pipeline which statistically corrected each participant's functional connectome for between-subject differences in head motion, indexed by FD. These pre-processed data passed standard quality control criteria for movement-related effects on functional connectivity. Additionally, we conducted three sensitivity analyses of head movement - repeating the entire analysis for a sample where FD was regressed for male and female data separately, for a "motion-matched" subset of the data in which there was no significant sex difference in FD, and for all data after global signal regression (Schölvinck et al., 2010). In parallel, we conducted two additional sensitivity analyses to assess whether the male>female differences in ICV, or global FC, might have confounded our principal results. In all five sensitivity analyses, our key results were qualitatively and quantitatively conserved, e.g., ΔMI maps estimated by the principal analysis were strongly correlated (mean $r \sim 0.8$) with corresponding maps estimated by each sensitivity analysis. We therefore consider that sex differences in head movement, ICV and global FC can be discounted as sufficient explanations for sex differences in these parameters of brain network development.

An alternative explanation is that sex differences in FC_{14-26} and MI reflect divergent development of specific cortico-subcortical circuits. In particular, females have a significantly more disruptive pattern of adolescent development, indexed by negative ΔMI , because functional connections that were weak at 14 years became stronger, and connections that were strong became weaker, over the course of adolescence. This sex difference in terms of functional connectivity could be related to sex differences in an underlying process of reconfiguration or remodelling of cortico-subcortical connectivity at a synaptic or neuronal scale. To assess the plausibility of this biological interpretation, we used pre-existing data on human brain gene expression, and the dimension-reducing multivariate method of PLS, to identify the set of genes that were most over- or under-expressed in brain regions corresponding to the divergent system defined by developmental fMRI. Enrichment analysis demonstrated that the genes that were most strongly expressed in brain regions with more disruptive (or less conservative) development in females included significantly more X chromosome genes than expected by chance. The same set of genes was also significantly enriched for genes that are known *a priori* to be expressed in cortical areas during early

(perinatal) development and in subcortical structures, such as amygdala, during adolescent development.

Sexual differentiation of the brain has been proposed to occur in two stages: an initial “organizational” stage before and immediately after birth, and a later “activational” stage during adolescence (Phoenix et al., 1959a). It has long been argued that these events are driven by gonadal hormones. However, more recent work suggests a complex interplay of sex chromosomes and their downstream products leading to sexual differentiation of brain cells (Arnold et al., 2004; Carruth et al., 2002; McCarthy and Arnold, 2011). The results of our enrichment analysis, indicating co-location of the sexually divergent fMRI-derived map with brain regions enriched for expression of X chromosomal and neurodevelopmental genes, are compatible with interpretation of adolescent change in fMRI connectivity as a marker of an underlying program of transcriptional changes in genes previously linked to post-natal sexual differentiation at a neuronal level.

It is a strength of the study that our analysis of sexually divergent brain network development is based on a large, accelerated longitudinal fMRI dataset with approximately equal numbers of males and females in each stratum of the adolescent age range. However, previous work has found substantial overlap in male and female distributions of multiple brain measures (Cahill, 2006; Kaczkurkin et al., 2019), and the metrics analysed here (FC_{14} , FC_{14-26} and ΔMI) are group-level parameters. Thus all reported sex differences are reflective of a group mean difference, estimated from functional connectivity distributions that substantially overlap between the sexes. On this basis, we are not arguing that female and male brains are distinctly dimorphic (Eliot et al., 2021).

It is also worth acknowledging that males and females are often exposed to fundamentally different environmental conditions spanning almost all domains of life (Shankar Mishra and Joe, 2021), including professional work environments (Quinn and Smith, 2018), medical treatment (Phillips, 2005) and education (United Nations Educational and *UNESCO*, 2022). Many of these differences in environmental conditions start at birth and as such likely have effects throughout the lifespan. It is conceivable that these widespread sex differences across disciplines of life shape brain organization at the group level. In humans, however, it is fundamentally difficult to systematically study these different environmental responses to being perceived as male or female, due to our at best limited ability to manipulate environmental factors in an experimentally controlled way.

Limitations of the study include our reliance on gene expression maps from post-mortem examination of six adult, mostly male, brains. Previous work has suggested that gene expression is sexually differentiated (Dewing et al., 2003), and varies throughout the lifespan (Li

et al., 2018b). In particular, there is evidence for pronounced changes in gene expression during adolescence (Snoek et al., 2014). Biological validation of this divergent fMRI system would be more directly informed by human brain maps of whole genome transcription that are (i) sex-specific and (ii) are derived from adolescent donor brains; but to the best of our knowledge such data are not currently available. It will also be important in the future to test the hypothesis that an anatomically homologous cortico-subcortical system has divergent adolescent development in animal models that allow more precise but invasive analysis of the cellular and molecular substrates of fMRI phenotypes than is possible in humans.

We conclude that there are sex differences in normative adolescent development of a cortico-subcortical brain functional networks, with females showing more disruptive functional connectivity development in the default mode network, limbic cortex, and subcortical nuclei.

Chapter 3

Anatomical, psychological and genetic characteristics of sex-differences in adolescent development of functional connectivity that are relevant to depression

3.1 Introduction

Multiple psychiatric disorders are known to display sex differences both in their prevalence and clinical expression profile. Further, psychiatric disorders are increasingly understood in the context of atypical developmental changes, which may be the reason that phases of neurodevelopmental change coincide in timing with periods of increased risk for psychiatric disorders (Paus et al., 2008). Major depressive disorder (MDD) is a mood disorder, which occurs more frequently in women than men (Faravelli et al., 2013). One explanation for this sex difference in the risk for mood disorders is that it may be related to underlying sex differences in brain development (Paus et al., 2008).

3.1.1 Adolescent depression

Before puberty, the prevalence of depressive symptoms is generally low. However, advancing pubertal stages carry a substantially higher risk of depressive symptoms for girls as opposed

to boys (Patton et al., 2008). Small sex differences have been reported to start occurring from the age of 11, and by the age of 15 females are about twice as likely to be depressed as boys (Cyranowski et al., 2000; Faravelli et al., 2013; Hankin et al., 1998).

Magnetic resonance imaging (MRI) has emerged as a powerful tool to investigate alterations in brain function in patients with MDD. Possibly the most widely reported finding is increased functional connectivity (FC) in the default mode network (DMN) (Greicius et al., 2007; Korgaonkar et al., 2020; Yang et al., 2021), which has been suggested to relate to rumination and self-referential processing (Broyd et al., 2009). Other areas found to be included in depression include cognitive control networks and limbic regions (Mulders et al., 2015).

Most studies have focused on adult depression and it remains uncertain whether adolescent depressive patients show the same changes. Adolescent depression has been associated with areas that mediate emotion processing. One of the most replicated findings is altered connectivity in the anterior cingulate (ACC) (Connolly et al., 2013; Cullen et al., 2009), which has also been found to play a role in adult depression (Davey et al., 2012; Drevets et al., 1997). Further, reduced connectivity between amygdala and the dorsolateral prefrontal cortex (DLPFC) as well as ventromedial prefrontal cortex (VMPFC) has been reported in case-control studies of adolescent depression (Connolly et al., 2017). Considering that the DLPFC is a key region in the volitional regulation of emotions (Phillips et al., 2008), and the VMPFC has been implicated in affect processing and regulation (Mitchell, 2011), these findings suggest that adolescent depression is driven by dysfunction in volitional and automatic regulation of emotion.

Despite the well known sex difference in prevalence of depression, few studies have investigated sex differences in structural (Carlson et al., 2015; Kong et al., 2010) or functional (Talishinsky et al., 2022) MRI in patients with depression. Yao et al. (2014) found sex differences in the amplitude of low frequency fluctuations (ALF) in frontoparietal and attention networks, but not in limbic regions. Further, Talishinsky et al. (2022) studied sex differences in functional connectivity between the DMN and the rest of the brain and found hyperconnectivity within the default mode network, as reported by multiple prior studies, was largely driven by males, not females. Further, the authors reported that regional differences in the expression of depression-related genes modulated the neuroanatomical distribution of connectivity effects in men and women with depression (Talishinsky et al., 2022).

3.1.2 Summary and hypotheses

Taken together, these findings suggest that the occurrence of mood disorders differs by age and sex, with a higher risk for females to develop mood disorders overall, and generally an increasing occurrence of depressive symptoms with age during puberty. When investigating adolescent brain maturation in relation to mood disorders it is therefore of crucial importance to understand the sex differences in healthy development.

In **Chapter 2** we noted that little was known about sex difference in normative development of functional connectivity. We hypothesized that there may indeed be sex differences in adolescent functional connectivity development. Using data from an accelerated longitudinal study of adolescents, ages 14 to 25 years, stratified by age and balanced for sex per age stratum (Kiddle et al., 2017), we estimated the effects of sex on three parameters of adolescent development of resting state FC: (i) baseline connectivity at age 14, FC_{14} , i.e. the predicted functional connectivity at age 14; (ii) the adolescent rate of change in connectivity, FC_{14-26} , estimated as the regression of a linear function of age on functional connectivity at nodal and edgewise levels of analysis; and (iii) the maturational index (MI) for each node, which is the signed correlation coefficient between FC_{14} and FC_{14-26} over all edges connecting a given node to the rest of the network (Dorfschmidt et al., 2022; Váša et al., 2020).

In this chapter, we started from the position that the sexually divergent risk trajectory for depression, with higher depressive symptom scores for adolescent females than males (Cyranski et al., 2000; Faravelli et al., 2013), could be the psychological or clinical representation of underlying sex differences in adolescent brain network development (Allen et al., 2011; Biswal et al., 2010; Zhang et al., 2016). To investigate this overarching hypothesis experimentally, we made use of the unthresholded map of sex differences in healthy adolescent brain development identified in the previous chapter (see **Fig. 2.14**) and tested the anatomical co-location of sexually divergent functional magnetic resonance imaging (fMRI) systems with prior maps of task-related brain activation, human brain gene expression, and depression-related abnormalities of functional dysconnectivity.

We found that this developmentally divergent brain system was co-located with loci of brain activation by reward-related tasks; with an anatomical map of depression-related differences in functional connectivity from an independent case-control fMRI study of MDD (Kitzbichler et al., 2020); and with expression of a weighted function of the whole genome enriched for genes identified by genome-wide association studies (GWAS) of MDD.

3.2 Methods

3.2.1 Adolescent functional connectivity sex difference

We derived a map of sex differences in functional connectivity development during adolescence using data from an accelerated longitudinal study ($N = 298$; age range 14 to 26 years; 51% female; **Table 2.1**). Methods are described in detail in **Chapter 2**. Briefly, in a sex-stratified approach, we estimated the linear effect of age on edgewise functional connectivity using linear mixed effects models with a fixed effect of age, sex, and imaging site, as well as a random effect of subject. From this model, we derived the baseline connectivity at age 14, FC_{14} and the adolescent rate of change, FC_{14-26} . From these parameters, we estimated the maturational index (MI), at each node, as the signed Spearman correlation coefficient between FC_{14} and FC_{14-26} of all edges that connect the node with the rest of the brain. We then estimated the sex difference in MI, ΔMI , by subtracting the male from the female MI, and tested the significance of this sex difference using parametric testing (Z -scores).

3.2.2 Psychological co-location with depression

First, we assessed the psychological relevance of sex differences in adolescent functional connectivity development by estimating the co-location of the brain system defined by sex differences in MI with prior data on the coordinates of task-related fMRI activation. Specifically, we performed automated meta-analytic referencing of the unthresholded map of ΔMI using the NeuroSynth database Yarkoni et al. (2011). First, we generated a volumetric version of the sex difference map by assigning the ΔMI value of each region to its respective parcel in the volumetric nifti file of the parcellation. Next, we uploaded this map to the database. The Neurosynth decoder registered our map with its set of cognitive terms and their coordinates in standard space generated through automatic parsing of the literature as follows:

1. The decoder extracts activation coordinates from published manuscripts.
2. The full text of each manuscript is parsed and the article is tagged with the set of terms that are mentioned frequently.
3. The database of activation coordinates of all studies parsed is divided into two sets for each term: articles that do contain the term and articles that do not.

4. A meta-analysis compares the coordinates reported for studies with and without the term of interest, resulting in statistical inference maps (Z and P – value maps), as well as posterior probability maps, which indicate the likelihood of a given term being mentioned in an article if activation is observed at a particular coordinate.

Using the generated maps of task activation, the neurosynth decoder returned a ranked list of cognitive terms with their correlation values describing the strength of association to our map of sex differences in MI . The correlation values generated indicate whether a given term was positively or negatively associated with our map, i.e. a positive correlation between a Neurosynth term and our map indicates that this term is more often mentioned in studies that show activation in regions where we observe a positive ΔMI . Conversely, a negative correlation value indicates that a given term is more frequently mentioned in studies that see activation in regions where we observe a negative ΔMI . It is worth mentioning that this automated process of generating meta-analytical maps is not perfect, i.e. each individual coordinate extraction may not be faultless, however, the number of articles parsed results in highly accurate meta-analytical maps.

3.2.3 Anatomical co-location with depression

Major depression sample

To assess the anatomical co-location of the sexually divergent system derived in **Chapter 2** with network dysconnectivity patterns in major depressive disorder (MDD), we included an independent dataset from the Biomarkers in Depression study (BioDep) study (Aruldass et al., 2021; Kitzbichler et al., 2020), which is a case-control study of adult subjects, aged 25-50 years, with and without a diagnosis of MDD. More specifically, data was collected from a total of 129 subjects: 46 healthy controls, and 83 MDD cases. Subjects were assessed for depressed using a structured clinical interview for DSM-V (SCID) (First, 2014), as defined by the Diagnostic and Statistical Manual of Mental Disorders fifth edition (DSM-5) (American Psychiatric Association et al., 2013), and all depressed cases had a global score greater than 13 on the Hamilton Rating Scale for Depression (HAM-D). This study was originally designed to assess inflammation in depression, using C-reactive protein (CRP) as a peripheral marker of inflammation to stratify the cases. Thus the MDD group contained cases with low CRP < 3 mg/L (N=53), and MDD cases with high CRP > 3 mg/L (N=34). Inflammation-linked depression only affects a sub-group of MDD cases and is thought to manifest differently in brain structural and functional alterations (Aruldass et al., 2021; Kitzbichler et al., 2020). In

this work, we focused on the low CRP cases only, excluding the high CRP cases, to avoid any confounding effects of inflammation-linked depression on our results. Consequently it is worth noting that our results may not generalize to subjects with inflammation-linked depression. The final sample after quality control (see below) contained 46 healthy controls and 50 MDD cases (**Tab. 3.1**).

MRI processing of the MDD sample

A multi-echo echo-planar imaging (EPI) sequence (Poser et al., 2006) was used to collect fMRI data under resting state conditions with the following parameters: repetition time (TR) = 2.57 s; echo time (TE) ($TE_{1,2,3}$) = 15, 34 and 54 ms; acquisition time = 10 mins 42.5 s = 250 time points in each fMRI time series. Multi-echo EPI data were collected as 32 slices at -30 degrees to the AC-PC line, field of view: 240 mm, matrix size: 64 ×64, voxel resolution: 3.75 ×3.75 ×4 mm.

The first 6 volumes were discarded to ensure scanner equilibrium and the remaining data were pre-processed using multi echo independent component analysis (ME-ICA) (Kundu et al., 2012a, 2013a) to identify sources of variance in the fMRI time series that scaled linearly with TE and could be confidently regarded as representing blood-oxygen-level-dependent (BOLD) signal. Other non-BOLD sources of variance, such as head movement, that do not scale with TE, were identified by ME-ICA and discarded. The retained independent components, representing BOLD contrast, were optimally recomposed to generate a broadband denoised fMRI time series at each voxel. This was bandpass filtered, using the Maximal Overlap Discrete Wavelet Transform using Daubechies' orthonormal compactly supported wavelets, resulting in a BOLD signal oscillating in the frequency range 0.02-0.1 Hz (wavelet scales 2 and 3) (Patel et al., 2014).

Geometric re-alignment was used to estimate 6 motion parameters for each participant (3 translation and 3 rotation parameters) which were used to calculate an overall estimate of motion - framewise displacement (FD), defined as the Euclidean norm of motion and rotation derivatives in mm: $FD^2 = |\vec{\Delta x}|^2 + |\vec{\Delta \theta}|^2$. For each participant, mean FD was calculated by averaging the FD time series. A total of 3 scans were excluded due to high in-scanner motion $\langle FD \rangle_{RMS} > 0.3$ mm or $\max(FD) > 1.3$ mm and one subject was dropped due to excessively high mean correlation > 0.7 .

Each pre-processed fMRI image was regionally parcellated into the set of 360 cortical regions defined by the Human Connectome Project (HCP) template (Glasser et al., 2016b) and 8 bilateral subcortical regions provided by freesurfer and the regional mean fMRI time

series were estimated for each cortical and sub-cortical region using the non-zero mean variant of the Analysis of Functional NeuroImages (AFNI) *3dROIstats* command (Cox, 1996a). Thus we estimated a 376×244 regional time series matrix for each participant.

The functional connectivity between each regional pair of fMRI time series was estimated by Pearson's correlation coefficient r for each possible pair of regions, resulting in a 376×376 symmetric association or functional connectivity matrix. The row (or column) means of this matrix comprise the vector of regional or nodal weighted degree as defined in **Equation 1.2**.

Group	Sex <i>female</i>	μ Age	σ Age	μ FD	σ FD	Centre		
						Cambridge	Kings	Oxford
Control	27	35.5	7.5	0.08	0.05	36	6	4
MDD	29	36.8	7.1	0.01	0.05	37	8	5

Table 3.1 **MDD case-control sample characteristics:** A total of $N=96$ subjects, comprising 50 MDD cases and 46 healthy controls, balanced for group mean age and sex were scanned at three MRI imaging centres.

Major depression case-control map

We constructed an MDD case-control difference map by estimating the effect (t -value) of group (case vs. control) differences on regional FC strength or weighted degree, controlling for age, sex and imaging site by the following linear model:

$$FC_i \sim 1 + \beta_{group} * group + \beta_{age} * age + \beta_{sex} * sex + \beta_{site} * site + \varepsilon \quad (3.1)$$

where FC_i refers to the weighted degree of the i th node, β refers to coefficients for the fixed effects, and ε represents the residual error. The case-control map was derived as the t -value of the group effect in **Equation 3.1** and tested for statistical significance using the false discovery rate to correct for multiple comparisons across regions ($P < 0.05$, FDR-corrected).

3.2.4 Gene enrichment analysis

To assess whether the map of sex differences in adolescent functional connectivity development was enriched for depression-related genes, we estimated the cortical map of weighted

gene expression that was most strongly co-located with the neuroimaging phenotype represented by the map of sex differences in adolescent brain maturation (ΔMI) and tested the enrichment of this weighted gene list for cell-type specific genes, as well as genes previously associated with MDD by a genome wide association study (GWAS). The gene-enrichment analysis methods were described in depth in **Chapter 2**. Briefly, we used data from the Allen Human Brain Atlas (AHBA) which includes post mortem transcriptomic gene expression data collected from 6 donor brains (5 males). Using partial least squares regression (PLS) regression, we found the weighted gene expression pattern that was most strongly correlated with the cortical map of ΔMI . The first partial least squares regression component (PLS1), explained significantly more variance than expected by chance. Using a median rank-based approach, we assessed whether a given reference gene list, e.g., from MDD GWAS, was non-randomly represented among the most strongly weighted PLS1 genes.

Prenatal cell type enrichment

We tested PLS1 for prenatal cell type-specific enrichment using single-cell transcriptomic gene expression data from mid gestation (gestation week 17 to 18; (Polioudakis et al., 2019)). These data included 16 unique clusters: endothelial cells (End), excitatory deep layer 1 (ExDp1), excitatory deep layer 2 (ExDp2), maturing excitatory (ExM), newborn excitatory neurons (ExN), intermediate progenitor cells (IP), microglia (Mic), oligodendrocyte precursor cells (OPC), outer radial glia (oRG), pericytes (Per), cycling progenitor G2/M phase (PgG2M), cycling progenitor S phase (PgS), and ventricular radial glia (vRG). Using these gene lists allowed us to estimate the early developmental relevance of the gene expression profile associated with the sexually divergent system of functional connectivity development.

Adult cell type enrichment

We also tested PLS1 for postnatal cell type specific enrichment using gene expression data on 33 distinct adult brain cell types (Lake et al., 2018), including excitatory neurons (Ex) and inhibitory neurons (In), cerebellar granule cells (Gran), and purkinje cells (Purk), as well as non-neuronal cells, including endothelial cells (End), smooth muscle cells or pericytes (Per), astrocytes (Ast), oligodendrocytes (Oli), oligodendrocyte precursor cells (OPC), and microglia (Mic). We excluded cell types expressed in the cerebellum only, since the cerebellum was not included in our fMRI analyses.

MDD risk gene enrichment

Finally, we tested whether PLS1 was enriched for genes associated with increased risk for MDD (Li et al., 2018a). For this analysis, risk genes for MDD were defined by a prior study, in which single nucleotide polymorphisms (SNIPs) significantly associated with MDD in one of the largest available genome wide association study (GWAS) (Edwards et al., 2013; Sey et al., 2020; Wray et al., 2018) were mapped to functionally relevant genes using epigenetic (Hi-C) data to guide the interpretation of GWAS-significant SNIPs in non-coding loci (Li et al., 2018a). We chose this particular gene list, in preference to other GWAS study results, because over 80% of risk variants identified by GWAS are found in the non-coding genome, which makes the interpretation of underlying genetic mechanisms challenging without the additional information provided by Hi-C data analysis. The genome's three dimensional structure allows for distal enhancers to be brought into contact with sequentially distant promoters, which allows non-coding SNIPs to regulate distal genes via long-range regulatory interactions. Hi-C data analysis is informed by the 3D structure of the genome and is therefore able to link variants in non-coding regions to the protein-coding genes they regulate, even if regulatory and coding sequences are separated by long linear distances on the genome.

3.2.5 Diagnostic specificity

To assess the diagnostic specificity of the co-location of the map of sex differences in adolescent functional connectivity maturation with major depression, we also included a further independent case-control dataset, the COBRE study (Çetin et al., 2014), which includes fMRI data from adult cases of schizophrenia and healthy controls.

Schizophrenia sample overview

The Center for Biomedical Research Excellence (COBRE) (Çetin et al., 2014) study is an open schizophrenia case-control fMRI study of adults, aged 18 to 65 years, in which individuals are identified as either healthy controls or cases of schizophrenia, bipolar or schizoaffective disorder, diagnosed using the structured clinical interview for DSM-V (SCID). Exclusion criteria included confirmed or suspected pregnancy, any history of neurological disorders, or a history of mental disabilities. We downloaded the data from the SchizConnect database (<http://schizconnect.org>), where it had been obtained using the Collaborative Infor-

matics and Neuroimaging Suite Data Exchange tool (COINS; <http://coins.mrn.org/dx>). We excluded 6 cases with a diagnosis of bipolar disorder.

MRI preprocessing

These data were originally pre-processed for a prior study (Morgan et al., 2021). Single echo fMRI was collected using an echo-planar imaging sequence with the following parameters: 150 volumes; acquisition time = 5 minutes; 32 slices; TE = 29 ms; TR = 2000 ms; voxel size = $3 \times 3 \times 4$ mm³. A prior pipeline (Patel et al., 2014) was used to pre-process the fMRI data. This pipeline included: slice acquisition correction, rigid-body head motion correction, co-registration to the T1-weighted image, a standard space transform to the MNI152 template in Talairach space, spatial smoothing, and intensity normalization. We excluded 19 subjects due to excess motion using previously defined criteria. We bandpass filtered the timeseries using wavelet scale 2 (Patel et al., 2014), corresponding to the frequency ranges 0.0625–0.125 Hz.

Each pre-processed fMRI image was regionally parcellated into 360 bilateral cortical regions using the HCP (Glasser et al., 2016b) template and 16 bilateral sub-cortical regions (amygdala, caudate, diencephalon, hippocampus, nucleus accumbens, pallidum, putamen, and thalamus) defined by Freesurfer’s “aseg” parcellation template (Filipek et al., 1994; Fischl et al., 2002). Nine regions were excluded due to signal dropout in one or more subjects (missing data or low regional mean signal of $Z < -1.96$), leaving 367 regions.

The functional connectivity between each regional pair of Z -scored fMRI time series was estimated by Pearson’s correlation coefficient r for each possible pair of regions, resulting in a $\{ 367 \times 367 \}$ symmetric association or functional connectivity matrix. The functional connectivity r values were subsequently transformed to Z -scores by Fisher’s transformation (Fisher, 1915). The mean across rows (or columns) of this motion-corrected, Z -transformed connectivity matrix yields the vector of regional or nodal weighted degrees (Fornito et al., 2016). Thus, for each region i we calculated the mean weighted degree k as per **Equation 1.2**.

Schizophrenia case-control map

After pre-processing and quality control, the analysable fMRI sample included 148 subjects, 81 healthy controls and 67 cases (58 with a diagnosis of schizophrenia and 9 with a diagnosis of schizoaffective disorder).

We constructed a case-control difference map by estimating the effect (t -value) of group (case vs. control) on region-wise functional connectivity strength (or weighted degree), controlling for sex, age and mean framewise displacement (FD), as in **Equation 3.1**. This schizophrenia case-control dysconnectivity map was finally tested for significant co-location with the ΔMI map using the spin test procedure to control for spatial auto-correlation in calculation of the P -value.

3.2.6 Robustness of results to alternative pre-processing strategies

Since previous research has demonstrated the sensitivity of fMRI studies to motion, in particular in younger samples, we repeated our main analyses in three replication samples that used different pre-processing strategies. Details of the constitution of these samples have been outlined in **Chapter 2**. Briefly, we constructed (i) a sample where FD was regressed for male and female data separately, (ii) a “motion-matched” sub-sample of the data in which there was no significant sex difference in FD, and (iii) a sample after global signal regression (Schölvinck et al., 2010). Further, given the well-established sex difference in total intracranial volume and the observed sex difference in global functional connectivity reported in **Chapter 2**, we also repeated our analyses correcting for total intracranial volume and global functional connectivity.

3.3 Results

3.3.1 Anatomical and psychological co-location with depression

Having derived a map of sex differences in adolescent functional connectivity maturation, termed ΔMI , in **Chapter 2**, we first assessed the psychological co-location of this sexually divergent system with depression. Sex differences indexed by negative ΔMI were located primarily in the default mode network, limbic cortical and subcortical regions, which showed more disruptive development in females. This means that in females these regions showed a greater tendency to change the rank ordering of their connections to other regions of the brain network, such that connections that were weak at baseline became stronger over the course of adolescence, and connections that were strong at baseline became weaker.

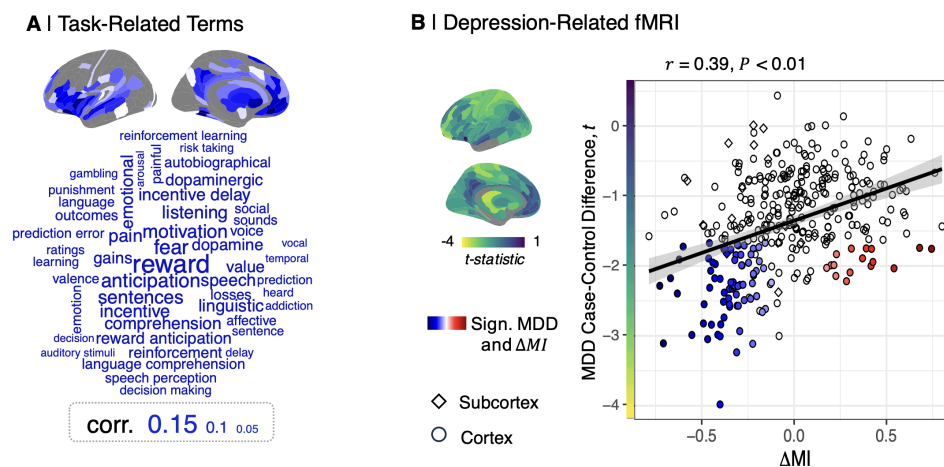


Fig. 3.1 Anatomical and psychological co-location with depression: (A) Wordcloud of Neurosynth meta-analytical cognitive terms scaled according to their strength of association with the disruptively developing brain regions (cortical map of $\Delta MI < 0$). (B) Scatterplot of MDD case-control t -statistics (y -axis) versus ΔMI (x -axis). Each point represents one of 346 cortical or subcortical regions; regional nodes that show a significant MDD case-control difference, $t \neq 0$, and a significant sex difference in MI, $t \neq 0$, are highlighted. The fitted line and 95% confidence interval indicate the positive correlation ($r = 0.4, P < 0.001$) between the spatial maps of MDD case-control differences, t , and ΔMI , shown alongside the y and x axes, respectively. Regions with sexually divergent disruptive development in adolescence (negative ΔMI) had reduced degree of connectivity (negative t) in adult MDD cases.

To investigate the psychological relevance of this sexually divergent development of functional connectivity in cortico-subcortical circuits, comprising the unthresholded set of regions with negative ΔMI , we conducted an automated meta-analytic referencing analysis using the Neurosynth database of task-related fMRI activation coordinates (Yarkoni et al., 2011). This analysis indicated that regions with more disruptive (or less conservative) development in females were typically activated by tasks related to reward processing, emotion, motivation, incentive delay, and dopamine (**Fig. 3.1A**).

In contrast, when registering the map of positive ΔMI regions to the Neurosynth database, we find that these regions were more typically activated by tasks related to primary sensory regions, i.e. visual and spatial perception, movements and attention (**Fig. 3.2**).

A | Neurosynth Terms



Fig. 3.2 **Neurosynth analysis of positive ΔMI regions:** (A) Wordcloud of Neurosynth meta-analytical cognitive terms scaled according to their strength of association with the cortical map of $\Delta MI > 0$.

To assess the anatomical correspondence between the sexually divergent disruptive brain system, and mood disorder-related changes in fMRI connectivity, we used resting state fMRI data from a prior case-control study of adult MDD cases (N=50) and healthy controls (N=46) to derive a map of case-control differences in functional connectivity in major depression. We correlated the parcellated, unthresholded map of MDD case-control differences in weighted degree (comprising 346 regional t statistics) with the map of sex differences in MI, ΔMI . We found that the two maps were significantly co-located ($P = 0.4$, $P < 0.001$, $P_{spin} < 0.001$; **Fig. 3.1B**). Thus, brain regions with sexually divergent development in adolescence (negative ΔMI) had reduced degree of functional connectivity in MDD cases compared to controls. Considering the focus on subcortical structures later in this thesis, we note that while there are widespread sex differences in MI in subcortical regions, as well as apparent MDD-associated decreases in functional connectivity in the same regions, the latter are not always statistically significant (**Fig. 3.1B**).

3.3.2 Celltype-specific and MDD risk gene enrichment

We explored developmental aspects of the sexually divergent system by testing for enrichment by genes specific to pre-natal and post-natal cell types (Lake et al., 2018; Polioudakis et al., 2019). We found that genes which were over-expressed in disruptively developing brain regions were enriched for prenatal cell types (Polioudakis et al., 2019), including

oligodendroglial precursor cells (OPC), microglia, astrocyte progenitor radial cells, inhibitory and excitatory cortical neurons (**Fig. 3.3A**), as well as for multiple adult glial and neuronal cell classes (**Fig. 3.3B**).

Extending the enrichment analysis to consider depression-related genes, we found that the list of genes strongly co-expressed with sexually divergent disruptive brain systems was significantly enriched for risk genes for MDD from an epigenetically-informed, large prior GWAS study (Li et al., 2018a). Over 80% of risk variants identified by genome wide association studies (GWAS) are found in the non-coding genome, which makes the interpretation of underlying biological mechanisms challenging. Non-coding single nucleotide polymorphisms (SNPs) can regulate distal genes via long-range regulatory interactions, since the 3D structure of the genome allows for distal enhancers to be brought into contact with promoters far downstream. Therefore, we used a gene list which mapped SNIP hits from one of the largest available MDD GWAS studies (Wray et al., 2018) to functionally relevant genes using epigenetic (Hi-C) data, to guide the interpretation of hits in non-coding loci (Edwards et al., 2013; Sey et al., 2020). Our enrichment results showed that the MDD risk genes were negatively weighted and ranked towards the bottom of the PLS1 list, indicating that they were more highly expressed in brain regions with disruptive development, indexed by negative ΔMI (**Fig. 3.3C**). In other words, regions in which females tended to show more disruptive adolescent FC development during healthy adolescence appear to show greater expression of genes associated with risk to MDD.

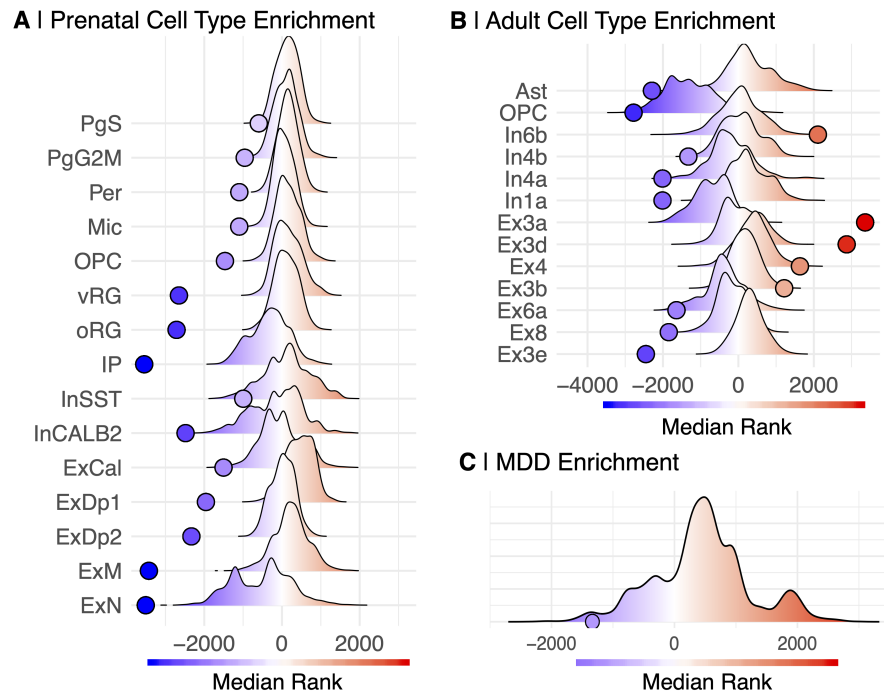


Fig. 3.3 Sexually divergent, disruptive brain systems are co-located with brain tissue transcripts enriched for cell type-specific and MDD risk-related genes: (A) Enrichment analysis for prenatal cell type-specific genes. Negatively weighted genes (blue) were significantly enriched for genes expressed by prenatal radial glia (vRG, oRG), microglia (Mic), oligodendrocyte precursor cells (OPC), and excitatory neurons. (B) Enrichment analysis for adult cell type-specific genes. Negatively weighted genes were significantly enriched for genes expressed by adult astrocytes, OPC, and excitatory neurons. (C) Enrichment analysis for MDD risk-related genes. Negatively weighted genes were significantly enriched for genes associated with major depressive disorder by an independent genome wide association study (Li et al., 2018a)

Anecdotally contextualizing the genes that were found to be significantly over-expressed in regions displaying more disruptive development in females, we noticed that this list included two (*somatostatin (SST)* and *neuropeptide Y (NPY)*) out of three genes previously reported (Anderson et al., 2020) as specifically expressed by adult neuronal and glial cells and linked to neuroimaging phenotypes of depression. This illustrates a partial convergence of significant results for *SST* and *NPY* between a prior study (Anderson et al., 2020) and the current study (**Fig. 3.4**). Specifically, regions with more disruptive development in females ($\Delta MI < 0$; dark blue points) have increased expression of *SST* ($Z_{FDR} = -10.05$) and *NPY* ($Z_{FDR} = -4.63$), compared to regions with more conservative development in females ($\Delta MI > 0$; dark red points). Whereas expression of *cortistatin (CORT)* is not correlated with regional variation in ΔMI ($Z_{FDR} = -0.25$; **Fig. 3.4**). This finding is largely anecdotal, but

does spark interest due to the role of inter-neurons in coordinating information flow across, and their relation to depression as evidenced using in-vivo MRI, GWAS and ex vivo cortical gene dysregulation (Anderson et al., 2020).

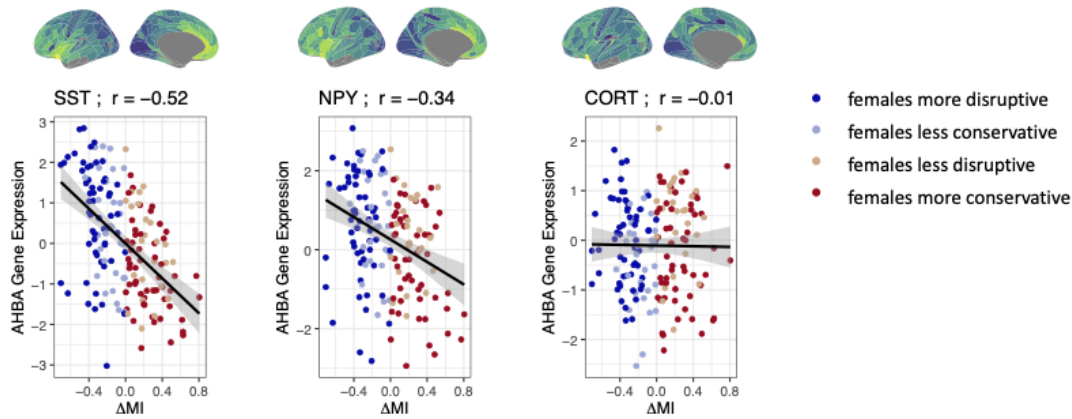


Fig. 3.4 Illustrative correlations between ΔMI and three genes (*SST*, *NPY* and *CORT*): *SST*, *NPY* and *CORT* are three genes that were previously highlighted by an independent study of gene expression and MRI phenotypes of MDD (Anderson et al., 2020). We noted that two of these genes (*SST* and *NPY*) were also included in the list of genes with significantly non-zero weights on PLS1 ($|Z| > 2.58$). The Z-scored PLS1 weights for each gene were as follows: *SST* ($Z_{FDR} = -10.05$), *NPY* ($Z_{FDR} = -4.63$), and *CORT* ($Z_{FDR} = -0.25$). These three scatterplots show expression of each gene at each region of the Allen Human Brain Atlas (AHBA; y-axis) versus ΔMI of each region (x-axis) with each region colour-coded according to its sexually divergent developmental profile. The small brain maps above each scatterplot represent the anatomical expression of each gene in the AHBA dataset.

3.3.3 Diagnostic specificity

To assess the specificity of the relationships between sexually divergent brain development (indexed by the ΔMI map) and (i) MDD case-control differences in functional connectivity and (ii) brain expression profiles of MDD risk genes, we repeated our key analyses of anatomical co-location with a case-control map, and a genetic enrichment for disorder risk-related genes using comparable independent data on schizophrenia. First, we tested the co-location of the ΔMI map with a map of functional connectivity differences in schizophrenia cases compared to healthy controls, reported in a prior case-control resting state functional magnetic resonance imaging (rsfMRI) study (Morgan et al., 2021; Çetin et al., 2014) (**Fig. 3.5A**). We found that schizophrenia case-control differences in weighted degree were not significantly co-located with the unthresholded map of ΔMI ($r = 0.05$, $P = 0.35$, $P_{spin} = 0.47$; **Fig. 3.5B**). Second, we tested the list of genes transcriptionally co-located with ΔMI for

enrichment by schizophrenia-related risk genes. We used the largest currently available GWAS study of schizophrenia, which identified 270 schizophrenia-associated SNIPs and mapped these SNIPs to genes using epigenetic information (Trubetskoy et al., 2022). We found that genes transcriptionally co-located with ΔMI were not significantly enriched for genes associated with schizophrenia ($P = 0.25$; **Fig. 3.5C**).

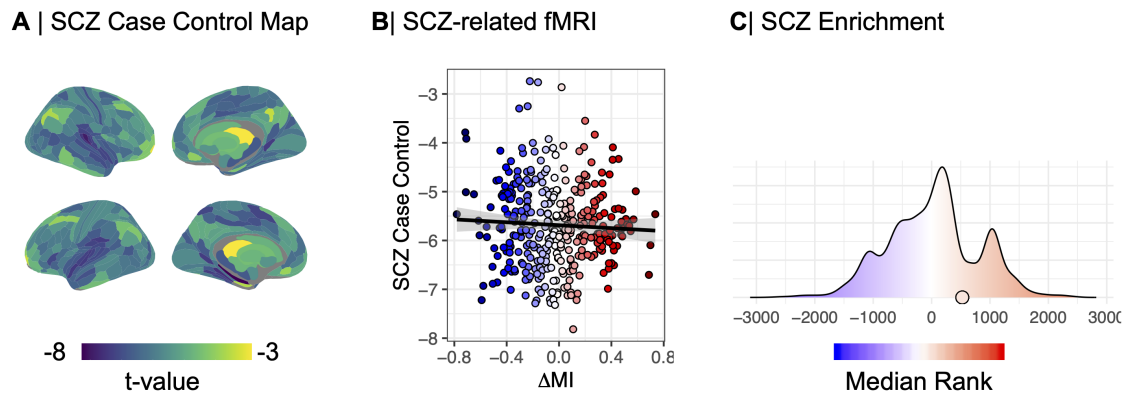


Fig. 3.5 Diagnostic specificity: We tested the diagnostic specificity of the relationship between sexually divergent brain functional development and major depression by repeating the key analyses using comparable data from independent studies of schizophrenia. (A) We constructed a map of case-control differences in functional connectivity, using rsfMRI data from healthy controls ($N=81$) and schizophrenia cases ($N=67$) from a prior study (Çetin et al., 2014). We estimated the case-control effect on regional functional connectivity strength using linear mixed effects models, with a random effect for subject ID and fixed effects of group, age, sex, and mean framewise displacement. The t -statistics for case-control difference in regional weighted degree are mapped on the cortical surface; $t < 0$ indicates areas of reduced degree in schizophrenia. (B) Scatterplot of schizophrenia case-control t -statistics (y-axis) versus ΔMI (x-axis). Each point represents one of 346 cortical or subcortical regions. There was no significant correlation ($r = 0.05$, $P = 0.35$, $P_{spin} = 0.47$) between the spatial map of schizophrenia case-control differences in weighted degree, t , and the spatial map of ΔMI . (C) Analysis for enrichment of 130 schizophrenia-related genes in the list of genes transcriptionally co-located with the ΔMI map and strongly weighted on the first PLS component (PLS1). The density plot shows the distribution of the median rank of 183 genes randomly sampled under the null hypothesis and the observed median rank of the 183 genes significantly associated with schizophrenia (Trubetskoy et al., 2022) is indicated by an open circle on the x-axis. There was no evidence that genes transcriptionally co-located with ΔMI were significantly enriched for these schizophrenia-related genes.

3.3.4 Robustness of results to alternative processing strategies

To assess the sensitivity of our main results, i.e. the anatomical co-location with an MDD case-control map and a gene enrichment for MDD risk genes, we conducted five sensitivity analyses: (i) using a sample where FD was regressed by sex; (ii) using a sample that was pre-processed by a pipeline including global signal regression (GSR) regression; (iii) using a sample where a motion-matched subset of data was chosen, such that there was no significant difference in motion between males and females; and (iv) using an alternative analysis pipeline which included intra-cranial volume (ICV) as a covariate in the statistical models to control for potentially confounding effects of head size; and similarly (v) using an alternative analysis pipeline which included global functional connectivity as a covariate.

We found that all the main findings replicated well across the different sensitivity analyses. First, we found that across all sensitivity analyses there was a significant correlation of ΔMI with the MDD case-control map (FD regression by sex sample: $r = 0.39, P < 0.0001, P_{spin} < 0.001$; GSR sample: $r = 0.12, P < 0.05, P_{spin} = 0.06$; motion-matched sample: $r = 0.5, P < 0.0001, P_{spin} < 0.001$; ICV-corrected processing: $r = 0.41, P < 0.0001, P_{spin} < 0.001$; global FC-corrected processing: $r = 0.41, P < 0.0001, P_{spin} < 0.001$; **Fig. 3.6A-D, top row**). Notably, the spatial correlation between the two maps using GSR-processed data for estimation of ΔMI was small but significant at $P < 0.05$, with a spin-test P -value of 0.06 (**Fig. 3.6B, top row**). Second, we found that the sexually divergent system derived from each of the sensitivity analyses was significantly enriched for MDD risk genes (**Fig. 3.6, middle row**). Third, the cell-specific enrichment was largely conserved across all sensitivity analyses, with PLS1 consistently enriched for excitatory neurons (**Fig. 3.6, third, fourth row**).

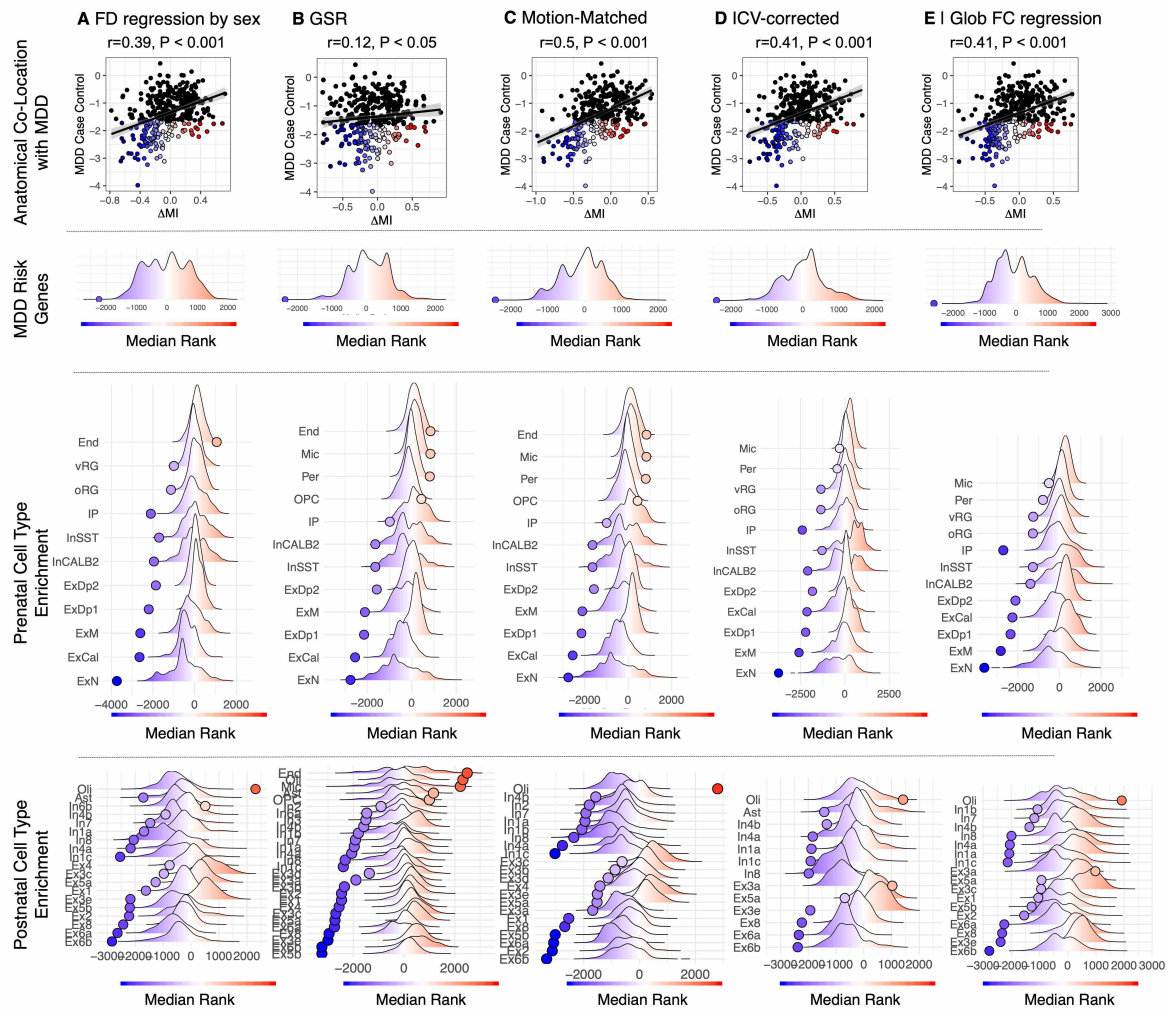


Fig. 3.6 **Robustness of MDD co-location results to alternative processing strategies:** We evaluated the robustness of our key findings to alternative processing strategies. *Top row:* Each point represents one of 346 cortical or subcortical regions. Regions that show a significant MDD case-control difference, $t \neq 0$, and a significant sex difference in ΔMI , $t \neq 0$, are highlighted. *Second row:* MDD risk gene enrichment. *Third row:* Prenatal cell type enrichment. *Fourth row:* Postnatal cell type enrichment.

3.4 Discussion

We assessed the psychological, anatomical and genomic relevance to depression of a sexually divergent profile of adolescent brain network development. Anatomically, the DMN and subcortical structures that had more disruptive development in females (e.g., the ventral medial prefrontal cortex, medial temporal gyrus, anterior and posterior cingulate cortex)

have previously been implicated as substrates of depressive disorder (Connolly et al., 2013; Cullen et al., 2009). This anatomical convergence was quantified by the significant spatial correlation between the whole brain map of sex differences in MI and an independent map of MDD case-control differences in nodal degree of functional connectivity. Cortical and subcortical areas with reduced degree of connectivity or “hubness” in MDD cases had more disruptive development in adolescent females.

Genomically, the list of genes transcriptionally co-located with this divergently developing network was enriched for risk genes from a prior genome-wide association study of MDD. In the context of gene enrichment results for genes on the X chromosome in **Chapter 2**, it is also notable that major depressive disorder has been previously associated with up-regulation of X-linked escapee genes and genes that control X-inactivation (Ji et al., 2015). Psychologically, by meta-analysis of a large prior database of task-related fMRI studies, we found that brain regions comprising the sexually divergent system were psychologically specialised for reward- and emotion-related processes that are fundamental to core depressive symptoms, e.g., anhedonia.

Collectively, these results do not prove there is a causal relationship between sexually divergent brain development and risk of depression. However, they demonstrate that there is indeed a sexually divergent process of adolescent development of a cortico-subcortical system that is anatomically, genomically and psychologically relevant to depression. These insights motivate and focus future studies purposively designed to test the hypothesis that sexual divergence of adolescent brain development causes contemporaneous or subsequent sex differences in the risk for mood disorders. While the Neuroscience in Psychiatry Network (NSPN) cohort used in this study included a cohort of exceptionally healthy adolescents, it is conceivable that large enough longitudinal studies may include subjects that change diagnostic labels over the course of the study, allowing for the direct assessment of sex differences in relationship to the onset of psychiatric disorders.

It is increasingly recognised that clinical phenotypes, as well as genetic and environmental risk factors, may be shared in common between depression and other mental health disorders arising in adolescence (Elliott et al., 2018; Gandal et al., 2018). In particular, abnormalities in fMRI connectivity have been reported as trans-diagnostic phenotypes, characteristic of multiple, diagnostically distinct disorders (Elliott et al., 2018); and risk genes associated with individual mental health and neurodevelopmental disorders have been found to overlap across disorders, implying that some genes confer trans-diagnostic risk for multiple neuropsychiatric disorders (Gandal et al., 2018). In this context, it is reasonable to ask if the significant associations we have demonstrated between ΔMI and both fMRI and genetic data on MDD

are specific to depression, or if they are representative of a trans-diagnostic association between ΔMI and functional dysconnectivity and/or risk genes for mental health disorders more generally. As a first step in addressing this question, we tested for spatial co-location of the ΔMI map and a map of functional dysconnectivity derived from a prior case-control fMRI study of schizophrenia. We found no significant association, indicating that the abnormalities of functional connectivity associated with adult schizophrenia do not coincide anatomically with the cortico-subcortical network that demonstrated sex differences in adolescent development. In a second step, we tested for enrichment by schizophrenia-associated genes of the list of genes that were identified by PLS analysis as transcriptionally co-located with the ΔMI map. We found no evidence for significant enrichment of this gene list by risk genes for schizophrenia. In summary, these two specificity analyses indicated that the brain systems demonstrating sexually divergent development in adolescence were not anatomically or genetically linked to schizophrenia, suggesting that this normative neurodevelopmental process may be specifically relevant to depression. However, we note that we have only tested for a relationship between ΔMI and two mental health disorders (MDD and schizophrenia). It will be important in future to explore this relationship across a wider range of disorders to characterise its diagnostic specificity more comprehensively and conclusively. It is conceivable that sex differences in development of this system could be relevant to sex differences in risk for other mental health disorders.

3.4.1 Limitations

Social and environmental factors are relevant modulators of psychiatric disorders (Crossley et al., 2019) and have not been assessed in this study. These factors can be (i) neurodevelopmentally relevant, i.e. childhood socioeconomic status influences the pace of brain development (Tooley et al., 2021) and (ii) can help explain sex and gender differences in mental health outcomes, i.e. previous studies have demonstrated a relationship between social inequality and gender disparities in mental health (Yu, 2018). This naturally leads to the question of how sexually divergent functional network development might be modulated by socio-economic deprivation, or other environmental risk factors for mental health disorder. Lastly, this dataset did not include information on pubertal timing, which we consider may affect subject-specific development of adolescent brain maturation, i.e. prior work has found that pubertal stage is better predictor of mood disorder prevalence than chronological age (Paus et al., 2008). We suggest that deeper understanding of such potential interactions between biological programmes of sexually divergent brain development on one hand, and gendered or generic social stressors in childhood and adolescence on the other hand, over the

course of an individual's pubertal development, will be an important strategic goal for the future of mental health science.

In summary, we found that normative sexual divergence in adolescent development of a cortico-subcortical brain functional network that is psychologically, anatomically and genetically relevant to depression.

Chapter 4

A review of cortical similarity and connectivity networks

4.1 From histological stains to whole-brain connectomics

A longstanding interest in brain structure led to the development of *histological stains* (e.g. the Golgi stain, Nissl stain) in the late 19th and early 20th centuries. These advances first allowed researchers to visualize (i) the cellular composition of cortical layers, i.e. the size, shape and arrangement of the neuronal cell bodies in the cortex, which developed into the field of cytoarchitectonics, as well as (ii) the myelin composition of cortical layers, which developed into the field of myeloarchitectonics (Kaes, 1907; Vogt, 1910). These early studies provided a valuable window into the histological complexity of individual brain regions. However, it was only with the invention of *tract tracing* methods in the mid-20th century that researchers were able to map axonal pathways between individual brain regions, providing early insights into the organization of large-scale brain networks and moving from studying regional characteristics to inter-regional connectivity. To date, tract tracing is seen as the “gold standard” for measuring axonal pathways between brain regions, but the invasive nature of the method limits it to use in animals only. The invention of magnetic resonance imaging (MRI) enabled measurement of brain anatomy *in vivo* in humans, and univariate methods were first developed (Bethlehem et al., 2022; Sowell et al., 2003) to analyze structural features at each of multiple discrete locations in the brain. However, the brain has been shown to be organised as a complex network, thus a univariate focus on regionally localised structural features misses the opportunity to observe the coordinated brain architecture that gives rise to cognition and behavior (Bullmore and Sporns, 2009). In recognising the need to estimate

the anatomical connectivity between brain regions, several methods have been developed to represent the human brain as a network.

4.2 Approaches to structural brain network construction

4.2.1 Diffusion weighted imaging

From the mid-1990s onwards, computational tractography methods using diffusion tensor imaging (DTI) data have been employed to reconstruct or “dissect” white matter fiber tracts between pre-defined grey matter regions. DTI contrasts are generated by measuring the diffusion of water molecules and inferring the direction of axonal tracts from the direction of maximal diffusion, i.e., water is expected to diffuse more rapidly in parallel to the orientation of axonal tracts than perpendicular to them. This method first provided researchers with the ability to map axonal connectivity between brain regions in humans *in vivo*. DTI has been particularly useful in measuring axonal tracts between regions of interest when the number of regions are limited and within a short geodesic or Euclidean distance from one another; but the limitations of the method were encountered when the field moved from region-of-interest analyses to whole-brain connectomics. Concerns were raised that whole-brain connectivity networks generated from DTI suffered from a systematic under-representation of long-distance connections (Dauguet et al., 2007; Donahue et al., 2016), likely due to greater difficulties in accurately measuring intersecting, branching or touching white matter paths over the course of longer distances, since DTI lacks the ability to definitively determine which fiber tract the measured signal originates from. Additionally, DTI networks include a large number of false-positive connections (Maier-Hein et al., 2017; Thomas et al., 2014). Lastly, due to long acquisition times of DTI data, head movement has been shown to significantly affect the derived networks (Walker et al., 2012), a finding that is particularly relevant in the context of developmental studies, knowing that younger participants tend to move more in the scanner than older ones.

4.2.2 Inter-subject structural covariation

In searching for an alternative to DTI tractography, between-subject *similarity* has been proposed as a proxy measure of axonal connectivity between spatially distant brain regions. It was noted that brain structure varies between individuals in a spatially organized pattern, i.e., it has been noted that inter-individual differences in a regional imaging phenotype often

co-vary with inter-individual differences in the structure of other spatially distant regions. Based on this observation, structural covariance networks (SCNs), have been proposed as a means to estimate anatomical connectivity in terms of inter-individual variation between spatially distant regions, also known as structural covariation (Alexander-Bloch et al., 2013). Structural covariation networks are constructed by correlating a single regional morphometric feature, e.g., cortical thickness or volume, across multiple subjects, resulting in a group-level network, where each edge describes the inter-regional correlation of a single macro-structural (or micro-structural) MRI phenotype across subjects (**Fig. 4.1D,F**). However, these networks also suffer from a number of limitations: group level networks lack the ability to map developmental changes in network configuration (even though sliding-window approaches have been suggested as a mitigating measure (Váša et al., 2018)); they only make use of a single morphometric feature at a time, thus failing to leverage the growing capacity of multi-modal MRI to measure multiple different structural MRI phenotypes near-simultaneously in the same scanning sequence or session (Lerch et al., 2017); and, perhaps most importantly, the biological and mechanistic interpretation of these networks is debatable.

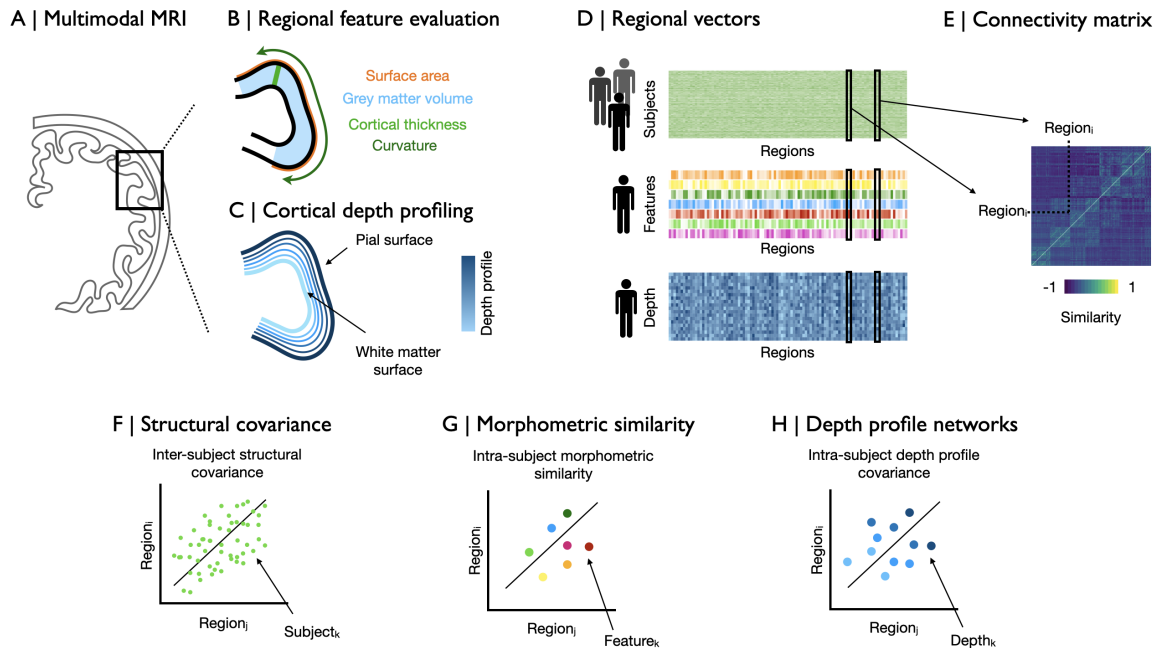


Fig. 4.1 Cortical similarity and connectivity network estimation: (A) Structural brain networks can be derived from multi-modal magnetic resonance imaging (MRI) data. These images are parcellated into pre-defined brain regions. (B) Regional features, like CT, GM, and SA can be estimated at each region. (C) Additionally, depth-dependent profiling can be used to construct multiple cortical surfaces between the white matter surface and the pial surface, at each of which an MRI phenotype can be measured. (D) Similarity-based structural connectivity networks can subsequently be estimated from regional feature vectors, to estimate either (*top*) (i) between-subject covariation, based on a single structural feature estimated across subjects at each region, resulting in a single group-level $\{Regions \times Subjects\}$ unimodal MRI data matrix; or (ii) between-regional similarity using (*middle*) multiple features estimated at each region for each individual subject, resulting in a subject-specific $\{Regions \times Features\}$ multi-modal MRI data matrix; or (*bottom*) a single feature estimated at multiple cortical depths for each subject, resulting in a subject-specific $\{Regions \times Depth\}$ depth-dependent unimodal MRI data matrix. (E) Structural MRI association matrices are generally estimated as the pairwise correlation between all possible combinations of regional feature vectors. Specifically, (F) structural covariance networks (SCNs) are estimated as the inter-subject structural covariance (or in practice often correlation) between the regional values of a single feature estimated for each subject, resulting in a single group-level structural covariance network; (G) morphometric similarity networks (MSNs) are estimated on the single subject level, as the pairwise correlations between regional feature vectors comprising multiple features estimated at each region, resulting in a subject-specific morphometric similarity network; and (H) microstructure profile covariance networks (MPCs) are estimated at the single-subject level as the pairwise correlation between regional feature vectors comprising a single feature estimated at multiple cortical depths, resulting in a subject specific microstructure profile covariance network (MPC) matrix.

4.2.3 Intra-subject structural similarity

It has long been understood that variations in cytoarchitectonic differentiation follow a non-random and graded spatial pattern in both humans and other species (Barbas and Hilgetag, 2023; von Economo and Koskinas, 1925). More specifically, cortical tissue is non-uniformly differentiated, with the granular cortex exhibiting a clearly eulaminal (6-layer) structure and high neuronal density; conversely, the agranular cortex largely lacks clearly identifiable layers, and has a low neuronal density. Between these two extremes, the dysgranular cortex displays an intermediate profile of less clearly distinguishable layers and moderate neuronal density. Recent work in primates has further demonstrated that similarity in laminar structure and cellular composition, rather than other measures like distance or cortical thickness, is decisive in determining the strength of axonal connections between brain regions (**Fig. 4.2**; (Hilgetag et al., 2016a)). The strongest connections are formed between regions with highly similar (i) lamination and/or (ii) myelination of cortical tissue, whereas the weakest connections are between highly dissimilar regions (Hilgetag et al., 2016a). For example, Beul et al. (2017) stereologically quantified the neuron density, a well-established proxy measure of cytoarchitectonic differentiation (Dombrowski et al., 2001), in the macaque cortex and estimated the similarity in neuron density between all pairs of cortical regions. They find that the projection density, measured using systematic anatomical tract tracing, between to regions was higher for regions with highly similar neuron density architecture (**Fig. 4.2**). One mechanistic explanation for these findings is that regions with similar laminar organization are likely involved in similar functions, since their structure is capable of processing similar types of information, and are thus are more likely to be connected.

A | Cytoarchitectonic similarity vs tract tracing

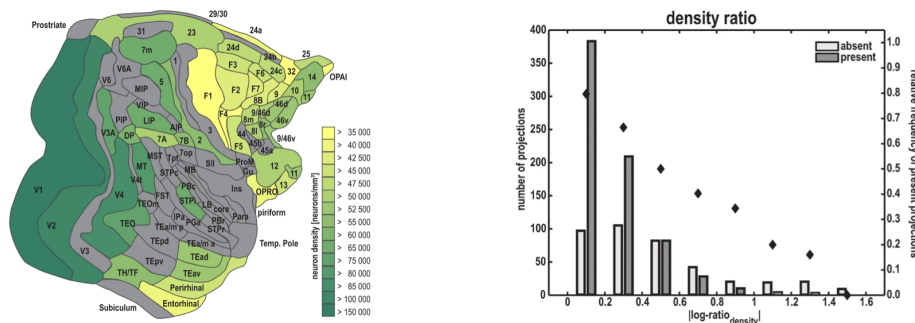


Fig. 4.2 **Cytoarchitectonic similarity predicts projection density:** (*left*) Neuron densities, a measure of cytoarchitectonic differentiation, in the macaque cortex. Gray areas mean no density data is available. (*right*) Comparison of neuron density similarity and projection frequency. The number of projections is plotted against the ratio of neuron density ($|\log - ratio_{density}| = \ln(density_{source-region} / density_{target-region})$), i.e. the log-ratio of neuron density values for each pair of connected areas, between two distant regions. Adapted from Beul et al. (2017) under a **CC BY 4.0** licence.

High-resolution MRI has emerged as a powerful tool for approximating laminar organization in human brain in vivo (Trampel et al., 2019), (i) through the increasing availability of multi-modal imaging sequences capturing a variety of anatomical properties hypothetically related to cytoarchitecture at each brain region (**Fig. 4.1B**), and (ii) due to the ability to measure individual MRI imaging features at multiple cortical depths, gaining insight into changes in microstructure across multiple cortical depths at each region (**Fig. 4.1C**) (Paquola and Hong, 2022; Paquola et al., 2019). The latter approach has so far largely been employed using magnetization transfer (MT) contrasts as an estimate of intra-cortical myelination (**Fig. 4.3**), but can be extended to a number of volumetrically estimated MRI measures including T1 images (Ferguson et al., 2018), as well as fractional anisotropy (FA), mean diffusivity (MD), neurite orientation dispersion and density imaging (NODDI).

Building on the idea that axo-synaptic connectivity is stronger between brain regions with similar cytoarchitecture and laminar organization (Goulas et al., 2016, 2017), two approaches to estimate similarity-based structural brain connectivity using MRI have been suggested: (i) *Microstructure profile covariance networks (MPCs)* are constructed, for each subject, by estimating for each possible pairwise combination of regions, the correlation (or covariance) between the cortical depth profiles of an MRI metric measured separately for each region (**Fig. 4.1C,D,H**; (Paquola and Hong, 2022)); (ii) *Morphometric similarity networks (MSNs)* are constructed, for each subject, by estimating the correlation between each possible regional pair of standardized MRI feature vectors (**Fig. 4.1B,D,G**; (Seidlitz et al., 2018)).

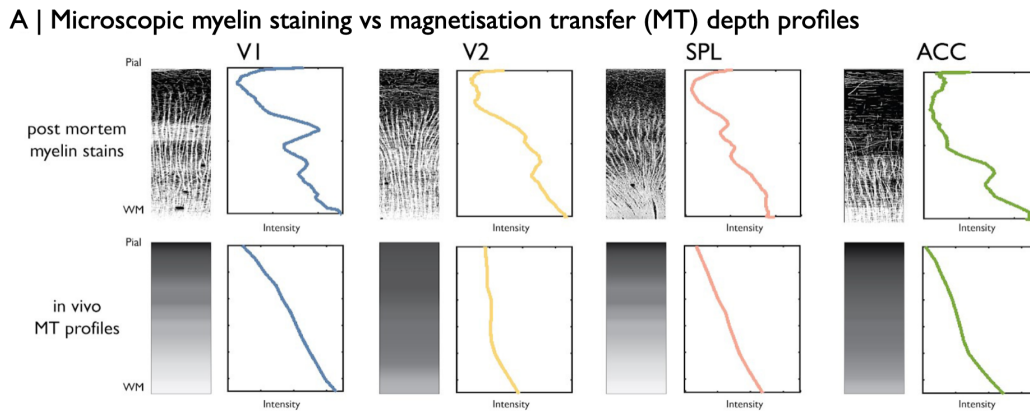


Fig. 4.3 Cortical depth profiles for MT: Gradients in magnetization transfer (MT) measured at multiple cortical depths can approximate microscopic myelin-staining. (A) Exemplary microscopic myelin-stained sections of the primary (V1) and secondary (V2) visual cortex, the superior parietal lobule (SPL) and the anterior cingulate cortex (ACC) (Vogt, 1910) with the inverted image showing myelin in lighter tones; and the corresponding in vivo MT profiles from the same regions averaged over $N=300$ subjects from the HPC cohort. Adapted from Paquola et al. (2019) under a **CC BY 4.0** licence.

In summary, the validity of MRI inter-regional similarity as a measure of anatomical connectivity rests on two assumptions: Firstly, that similarity at cellular scale leads to axonal connectivity, and secondly, that similarity of their MRI feature vectors is a meaningful reflection of the similarity of two cortical areas at a cellular scale. In relation to the second assumption, micro-structural MRI markers of tissue composition, e.g., myelination, neurite density, are expected to be informative elements of the MRI feature vectors used to estimate similarity.

Below, we review relevant literature to understand the impact MSNs have had in recent years (**Table 4.10**).

4.3 Mapping to cytoarchitectonics and tractography

MSNs are thought to link macro-scale MRI phenotypes with their neurobiological substrates. They have been shown to improve our ability to represent cortical cytoarchitectonic classes (von Economo and Koskinas, 1925) and brain organizational principles (Seidlitz et al., 2018). However, MRI is an indirect or proxy measure of structural connectivity; thus any networks derived from MRI metrics must be evaluated for their ability to accurately approximate the “gold standard” of (anterograde) tract-tracing methods in animal models,

which map monosynaptic connectivity, from cells of origin, through axonal projections, to synaptic terminals. Indeed, cross-species work has demonstrated that MSNs are able to approximate axonal connectivity measured by tract-tracing (Seidlitz et al., 2018). While this mapping is not perfect, and it is only possible to estimate the correspondence in animal models, it appears safe to assume that reasonable levels of correspondence can also be reached in humans. This anatomical validation of MSNs suggests that these similarity-based networks are able to further our understanding of structural brain connectivity and connectomes in health and disease.

4.4 Predicting cognitive and behavioral outcomes

A fundamental objective of structural brain network analysis is to help us better understand how brain anatomy gives rise to cognition and behavior. As such, it is noteworthy that MSNs have been shown to be associated with intelligence quotient (IQ) in two independent samples thus demonstrating their relevance to fundamental cognitive abilities (Seidlitz et al., 2018; Wu et al., 2022). Increased modular differentiation in MSNs between cortex and subcortex has also been linked to better scores on multiple cognitive questionnaires in a pediatric sample (Wu et al., 2022). This finding is of particular relevance in the developmental context, suggesting a developmental differentiation of segregated cytoarchitectonic areas. Further, it goes in line with prior literature on pediatric and adolescent development of DTI networks that also display a process of modular segregation (Baum et al., 2017).

4.5 Bridging from micro to macro scales

Brain networks are organized on multiple spatial scales from the micro-scale of gene expression measured using transcriptomics in post mortem brains (Kaczurkin et al., 2019) to the macro-scale of MRI-defined grey matter brain regions. In order to further our understanding of the brain as a complex system influenced by genetics, gene expression, cell types, and spatial constraints, bridging scales of analysis is of fundamental importance. MSNs have been proven to be a promising avenue for linking cortical transcriptomic data from the Allen Human Brain Atlas averaged across six donor brains (Hawrylycz et al., 2015) with single-subject structural MRI-derived networks. These advances have demonstrated two key properties of MSNs: First, changes in morphometric similarity as a result of chromosomal copy number variation (CNV) disorders have been shown to closely relate to spatial expression patterning

of genes from the affected chromosomes (Seidlitz et al., 2018), suggesting that MSNs are able to map changes in brain anatomy due to genetic changes. Second, MSNs have been used widely to map phenotypic associations with risk genes for multiple psychiatric (Morgan et al., 2019; Xue et al., 2023; Zong et al., 2023), and neurodegenerative disorders (Zhang et al., 2021a). These findings promise to support our understanding of gene-brain-structure relationships in health and disease.

4.6 Identifying neuroanatomical differences in health and disease

A key motivation for mapping structural brain networks is the identification of deviations in brain anatomy due to disorders. Morphometric similarity networks have been used to identify such differences for a wide variety of neuropsychiatric disorders (Lei et al., 2022; Li et al., 2022, 2018b; Morgan et al., 2019; Xue et al., 2023; Zhang et al., 2021a; Zong et al., 2023). For example, patients with psychosis across three independent datasets have been shown to have globally decreased morphometric similarity, and a regionally specific profile of decreases in MSNs nodal strength in the hubs of the “normative” MSN connectome, located in frontal and temporal cortical areas, as well as increased regional strength of the non-hubs of the normative connectome, in parietal cortex (Morgan et al., 2019). Epilepsy has been associated with decreased regional morphometric similarity in primary motor, prefrontal and temporal regions and increased nodal strength of inter-regional similarity, i.e. weighted degree, in occipital, insular and posterior cingulate cortices (Li et al., 2022). It has been argued that neuropsychiatric disorders often affect the most highly connected nodes of the network, i.e. the hubs. Case-control studies of differences in morphometric similarity in Alzheimer’s disease have provided further evidence to support this theory (Li et al., 2018b), integrating recent work on MSNs into a long-standing history of research on disease. Notably, MSNs have also been used to distinguish different groups of healthy subjects. It has long been reported that skill acquisition can lead to changes in brain structure and function (Maguire et al., 2006). RaviPrakash et al. (2021) estimated individual differences in morphometric similarity in healthy controls with different skill sets, namely chess players, suggesting that skill acquisition, or some pre-determined aptitude to learn skills, may directly shape morphometric similarity. However, these analyses were conducted in a small sample (N=40) and future work should provide further evidence for these findings.

4.7 Clinical applications

Much neuroscientific research is conducted with the ultimate intention of advancing our understanding of diseases, such that findings will translate into clinical practice. While morphometric similarity networks were designed with the goal of exploiting multi-modal magnetic resonance imaging data which is increasingly acquired in research settings, it has been noted that the core structure of these networks is stable across various combinations of imaging phenotypes, including when features are derived only from commonly clinically acquired T1-weighted images (King and Wood, 2020; Li et al., 2017). Indeed, several of the case-control differences reported above were measured in MSNs derived exclusively from features measured in T1-weighted images. (Li et al., 2018b; Morgan et al., 2019).

Further work has explored the use of MSNs in clinical practice by estimating structural brain network changes in response to anti-psychotic treatment (Zong et al., 2023). This work found an association between whole-brain MSN architecture and treatment response, potentially related to MSN's ability to capture multi-dimensional brain organization architectures related to cognitive function changes (Zong et al., 2023). It appears the reported changes in morphometric similarity in response to treatment may be in the opposite direction of case-control differences from a prior study (Morgan et al., 2019). However, prior work on univariate models of cortical thickness have suggested a similar trend of apparent intensification of cortical thickness differences despite an improvement of symptoms after treatment (Voineskos et al., 2020). Further work is needed to relate morphometric similarity changes in response to treatment with prior case-control studies.

It is worth noting that a large number of studies using morphometric similarity networks are currently adopting relatively coarse-grained parcellations, e.g., the Desikan-Killiany anatomical atlas (DK) which includes 34 bilateral cortical regions (**Table 4.10**). While a low number of regions will increase the statistical power to detect case-control differences at a nodal level by limiting the number of statistical tests that need to be corrected for multiple comparisons in the context of whole-brain analyses, they do not provide neuroanatomical specificity on par with more fine-grained parcellations now available such as the Human Connectome Project (HCP) parcellation (Glasser et al., 2016b).

4.8 Leveraging multimodal imaging

The theoretical basis of MSNs rest in the idea that brain regions that are cytoarchitecturally more similar to one another are more likely to be connected. This raises the question of how

cytoarchitecture can best be represented using MRI. No consensus has been reached on which combination of MRI features best approximate underlying anatomical connectivity. While many microstructural MRI measures, in particular when measured at different cortical depths, have been shown to approximate cytoarchitectonic organization well (Paquola et al., 2019), the link with macrostructural MRI measures relate is less intuitive. Recent work in animal models has suggested that cortical thickness is not a good predictor of cytoarchitectonic similarity (Hilgetag et al., 2016b). However, cortical thickness measurements using MRI are based on computationally finding the boundary between the cortical sheet grey matter sheet and the underlying white matter, a measurement that can be confounded by greater intra-cortical myelination in deeper cortical layers, leading to a systematic under-estimation of cortical thickness in such regions. Thus while cortical thickness measures in MRI differs from histological studies, this confound may actually provide relevant information on cytoarchitecture. More work is needed to address the question of how individual MRI features relate to cytoarchitect similarity.

A key motivation in developing morphometric similarity networks was the exploitation of multi-modal imaging data, yet many studies have so far only used T1-image derived features. One explanation for this may be that T1 imaging data are more readily available. Indeed a number of studies used legacy datasets to study morphometric similarity networks (Zong et al., 2023). Both the age of these datasets and the fact they were not specifically acquired to derive multi-modal structural networks may have contributed to the small feature vectors used. Conversely, it can be seen as a strength that MSNs provide the ability to derive single-subject networks from T1 data only, since, as several studies reviewed here have demonstrated (Fenchel et al., 2020; Galdi et al., 2018; He et al., 2020; King and Wood, 2020; Vuksanović, 2022; Wu et al., 2022; Zhang et al., 2021a; Zhukovsky et al., 2022), this opens up the possibility to use any of the large number of openly available neuroimaging datasets that routinely include T1 images, but not necessarily other imaging modalities.

However, it is key to note that inter-regional correlations estimated on the basis of short feature vectors comprising five features derived from T1 data only, inevitably have larger errors than correlations estimated on the basis of longer feature vectors comprising 10 or more features derived from T1 in addition to other modalities of MRI data (Seidlitz et al., 2018). Thus, while T1-only MSNs are pragmatically convenient, they are less robust statistically and may be less sensitive to detect individual differences between subjects due to the relatively high error in estimation of each MSN.

On a related note, exploiting multi-modal data also allows expansion of the anatomical range of MSNs from focusing only on cortico-cortical structural connectivity to also

include subcortical connections. Specifically, the output from common T1-image processing pipelines, e.g., *FreeSurfer*, typically includes a number of regional cortical features, but often only grey matter volume is measured for subcortical structures. Recent work has demonstrated the value of examining subcortical structural connections by deriving a developmental signature of decreasing morphometric similarity, or hypothetically increasing cytoarchitectonic segregation, between cortex and subcortex during childhood (Wu et al., 2022). Future studies should further explore subcortico-cortical morphometric similarity, for example integrating FA and MD measured subcortically.

4.9 Tracking developmental changes in brain anatomy

A core focus of neuroscientific research is understanding brain development over the lifespan. Studying network changes in development can inform our understanding of neuropsychiatric disorders by highlighting key maturational processes which may be vulnerable to atypical development (Paus et al., 2008). Previous work on structural brain network development, in particular in youth, has been limited by the difficulty of obtaining high quality diffusion weighted imaging (DWI) connectomes, and the fact that SCNs are only estimated at the group level. While discrete group comparisons (Khundrakpam et al., 2013) and sliding-window approaches (Váša et al., 2018) have been employed to approximate developmental network changes using SCNs, no continuous process of development can be modeled. A key advantage for using single-subject MSNs is the ability to model continuous trajectories of brain network development, but to date, this potential advantage of MSNs has not been exploited widely. Out of the 25 studies reviewed here, 17 were conducted on adult subjects without a developmental perspective (**Table 4.10**). However, the limited number of developmental studies already in the literature does support the idea that MSNs could be used to map maturational network changes. For example, Fenchel et al. (2020) reported detectable network modules in MSNs derived from infant MRI data. These modules were comparable to known adult network modules and within-module morphometric similarity was shown to increase with age, suggesting that infancy is a period of consolidating intra-modular connectivity (Fenchel et al., 2020). Further, using a sample of infants aged 38 to 45 weeks post menstrual age (PMA), showed that morphometric similarity networks were predictive of chronological brain age in the perinatal period Galdi et al. (2018). Together, these findings suggest that MSNs are indeed able to model developmental changes in network structure.

4.10 Future directions

To date, the potential of morphometric similarity networks to study developmental changes in brain structure have not been entirely fulfilled.

A number of studies reported here had small sample sizes, speculatively at least partially due to the fact that morphometric similarity approaches allow for construction of structural brain networks from older, smaller sample size legacy datasets. Recent work has suggested that sample sizes of around 20,000 are required to establish brain-behavior relationships (Marek et al., 2022). This finding suggests that a number of brain-behavioral relationships evaluated using MSNs may have been under-powered. While comparatively simpler case-control difference studies may be better-powered, larger sample sizes, with at least two longitudinal measurements of each subject, will still be needed to improve our ability to detect small-scale developmental changes in brain network structure.

A key limitation of structural brain network construction using morphometric similarity networks is that they collapse the diverse information included in vertex-level data on each metric into a single number, e.g., cortical thickness, for each regional node. Previous work has explored single-subject structural similarity matrices estimated at the vertex-level, but to date vertex-level similarity was usually estimated from a single morphometric feature only (Homan et al., 2019; Kong et al., 2015; Leming et al., 2021). There is a notable exception to this trend: Sebenius et al. (2022) proposed a method to estimate morphometric similarity that makes use of the rich, multidimensional vertex-level data derived from multiple MRI phenotypes by estimating the divergence between between the multivariate distributions of their structural features.

Future research should also focus on making use of the increasing number of features that can be derived from multi-modal imaging data. Further, the value of integrating features measured at multiple depths, i.e. in line with MPCs, could be considered. So far, cortical depth profiles have largely been measured in MT (Paquola and Hong, 2022; Paquola et al., 2019) and T1-weighted images (Eickhoff et al., 2005), but theoretically they could be derived in multiple other modalities, opening up opportunities to further characterize the multi-layer structure of the cortex using MRI.

A key motivation in generating similarity-based structural brain networks is to study connectivity between brain regions. To date, work on MSNs has largely focused on analyses of node degree, i.e., the sum over a node's edge-wise similarities with all the other nodes in the network. Relatively little attention has been paid to the rich information available in the edge-wise connections themselves.

One challenge in the future will be to link the detailed knowledge derived from monosynaptic connectivity studies in animals with structural connectivity models from in vivo MRI. One avenue for further research may be the acquisition of datasets that combine multimodal MRI with tract-tracing data, and possibly also transcriptomics, or histology to create an in-depth view into brain structure in animals.

Paper	Age	Dx	Features	T1	N	Atlas
Galdi et al. (2020)	Infancy	Ctrl	GM, T1/T2, NODDI, DKI	No	105	Makrop.
Galdi et al. (2018)	Infancy	Ctrl	GM, T1/T2, FA, MD, AD, RD, ICFV, VISO, ODI	No	95	Makrop.
Fenchel et al. (2020)	Infancy	Ctrl	CT, MC, MI, SA, FA, MD, NDI, ODI	No	241	In-house
Wang et al. (2022)	Childhood	Ctrl	CT, SA, MC, GC, FI, CI, GM	Yes	130	DK
Wu et al. (2022)	Childhood	Ctrl	CT, CA, SD, CV, T1w intensity, T2w intensity, +12	No	8,908	DK
Lei et al. (2022)	Childhood	BP	GM, SA, CT, MC, IC, FA, MD	No	102	HCP
Morgan et al. (2019)	Adulthood	SCZ	GM, SA, CT, IC, MC, FA, MD	No	412	308
Yang et al. (2021)	Adulthood	Ctrl	GM, SA, CT, CI, MC	Yes	119	Gradient
King and Wood (2020)	Adulthood	Ctrl	T1 derived only	Yes	1,113	DK
Wei et al. (2021)	Adulthood	IG	CT, SA, IC, MC, CI, FI, GM, GA, MD, RD, AD,	No	101	308
Xue et al. (2023)	Adulthood	MDD	GM, CT, SA, CI, IC, MC,	Yes	142	DK
Martins et al. (2022)	Adulthood	Pain	GM, CT, SA, IC, CI, MC	Yes	158	DK
Zong et al. (2023)	Adulthood	SCZ	CT, GM, SA, IC, MC, FI, CI, FA, MD	No	80	DK
Zhukovsky et al. (2022)	Adulthood	SUD	GM, SA, CT, MC, IC, CI, MC, FI	Yes	331	
Li et al. (2021)	Adulthood	MDD	FA, MD, GM, SA, CT, IC, MC	No	473	308
Li et al. (2022)	Adulthood	Epilep.	GM, CT, SA, MC, IC, CI, FI	Yes	251	308
RaviPrakash et al. (2021)	Adulthood	Ctrl	GM, SA, CT, CI, FI	Yes	47	Yeo-17
Tian et al. (2021)	Adulthood	Ctrl	GM, CT, SA, MC, CI, IC, FI	Yes	216	DK
He et al. (2020)	Adulthood	Ctrl	Nvertex, SA, GM, CT, sdCT, MC, IC, CI, FI,	Yes	361	DK
Tian et al. (2020)	Adulthood	CT	GM, CT, SA, MC, CI, IC, FI	Yes	216	DK
Li et al. (2017)	Adulthood	Ctrl	GM, CT, SA, MC, CI, IC, FI	Yes	55	DK
Zhang et al. (2021a)	Old Age	AD	All? GM, Curvature, FA, MD	No	212	308
Li et al. (2018b)	Old Age	AD	CT, GM, SA, MC, FI	Yes	40	DK
Vuksanović (2022)	Lifespan	Ctrl	T1 derived only	Yes	198	DK
Seidlitz et al. (2020)	Lifespan	CNV	CT, SA, GM, MC, IC	Yes	462	308

Table 4.1 Previously published studies using morphometric similarity networks. The studies were identified by a *pubmed* search in January 2022 using the search terms *morphometric similarity network* or *MSN*.

Chapter 5

Adolescent morphometric similarity development

5.1 Introduction

5.1.1 Adolescent brain development

Chapter 2 and **Chapter 3** have illustrated that the human brain undergoes extensive functional reorganization during adolescence. Functional reorganization is thought to be based, at least partially, on changes in brain structure during the same period (Gu et al., 2021). Previous work on adolescent structural brain development has established two major processes that dominate this period: (i) after peaking in early childhood, cortical grey matter volume decreases during adolescence through synaptic pruning; while (ii) protracted myelination of the cortex sees peak white matter volumes reached in early adulthood (Bethlehem et al., 2022). These neurodevelopmental programs are thought to be fundamental to the emergence of adult cognitive functions and social behaviours (Mills et al., 2016; Sowell et al., 2004; Váša et al., 2018), but to date, they have largely been studied in isolation using univariate models (Mills et al., 2016; Whitaker et al., 2016b). This chapter will focus on adolescent changes in structural magnetic resonance imaging (MRI) markers of brain network development during adolescence and will test the hypothesis that these changes are linked to functional connectivity.

5.1.2 Structural network studies of adolescent development using MRI

Magnetic resonance imaging can be used to map developmental changes in brain structure at various anatomical scales. The adolescent changes in brain structure outlined above likely represent a process of network reorganization. However, research on adolescent structural brain development so far has largely focused on univariate phenotypes (Mills et al., 2014; Whitaker et al., 2016a), and research into network changes has often been limited by the lack of access to good quality individual connectomes measured longitudinally. Previous work has largely focused on structural covariance networks, which are estimated at the group level, or connectomes generated from diffusion weighted imaging (DWI) data. However, the biological interpretation of structural covariance networks, that are based on the between-subject covariance in a single phenotype, is difficult, and in addition to the limited availability of good-quality longitudinal DWI connectomes in young subjects, DWI-based networks generally also suffer from underestimation of long-range connections, e.g., between bilaterally symmetric cortical areas (refer to **Chapter 4** for details).

Building on the idea that cytoarchitectonically similar regions are more likely to be axonally connected, morphometric similarity networks (MSNs) quantify the similarity between distant cortical areas in terms of multiple MRI parameters measured at each area, thus constructing whole-brain anatomical networks for individual subjects. MSN can be build from any combination of structural MRI metrics, including (i) macro-structural metrics, like cortical thickness (CT), grey matter volume (GM) and surface area (SA), which aggregate data from multiple voxels representing an anatomical region to estimate its geometric properties on centimetre scale; and (ii) micro-structural metrics, like magnetization transfer (MT), which are representative of some aspect of brain tissue composition on millimetre scale, e.g., MT is a proxy for cortical myelination. MSN-construction and validation is described in-depth in **Chapter 4** but, briefly, MSNs have been shown to correlate with the “gold standard” of anatomical connectivity, white-matter tract tracing data, in the macaque monkey, thus validating the status of morphometric similarity as a proxy for axonal connectivity; they have been used to predict individual differences in intelligence quotient (IQ) (Seidlitz et al., 2018) and case-control differences in schizophrenia (Morgan et al., 2019), demonstrating their ability to map to relevant cognitive and psychiatric outcomes; and they have been linked to genetic variation in studies of sex chromosome aneuploidies and other neurodevelopmental disorders (Seidlitz et al., 2020). However, to date, little is known about how MSNs change over the course of normal development. Here, we will leverage MSN’s ability to incorporate multi-modal imaging data, including features previously found to represent relevant pro-

cesses of adolescent structural maturation like CT and MT, to explore changes in adolescent structural brain networks longitudinally.

5.1.3 Functional and metabolic correlates of structural network development

Structure is thought to underlie the functional realization of spontaneous activity across the cortex. While the mapping between the two is imperfect - at best, structural connectivity is thought to explain 50% of the variance in functional connectivity (Suárez et al., 2020) - at least some of the known adolescent changes in functional connectivity (Marek et al., 2015; Váša et al., 2020) may be driven by structural changes. Adolescence is a time of increasing social and cognitive individualization, which is likely underpinned by development of increasing functional flexibility during this time (Baum et al., 2017, 2020). One may expect that such changes in functional organization could result from changes in how underlying structure supports coordinated fluctuations in neural activity underlying cognition (Baum et al., 2017). Prior work has suggested that tightly coupled structural and functional connectivity, often reported in highly myelinated sensory-motor regions, may represent strong structural constraints on function, where activity is directly supported by local white matter pathways, potentially reflecting highly conserved programming that ensures the early development of specialized sensory hierarchies (Buckner and Krienen, 2013). Conversely, it has been suggested that less tightly coupled structural and functional connectivity may support functional flexibility and dynamic recruitment during diverse task demands (Baum et al., 2020). Indeed, Baum et al. (2020) found that longitudinal changes in structure-function coupling were associated with longitudinal changes in the diversity of inter-regional functional connectivity.

To date there is no consensus on how best to estimate the coupling between structural and functional connectivity, and various methods have been used to define both structural and functional networks (Baum et al., 2020; Liu et al., 2022; Zamani Esfahlani et al., 2022), which may contribute to the lack of consistency in the overall pattern of previously reported results. Notably, structure has so far been defined from DWI networks (Baum et al., 2020) or downstream graph theoretical properties of such networks (Zamani Esfahlani et al., 2022). It is conceivable that new insights can be gained into how structure constrains function by employing different structural network modeling approaches, including more directly modelling relevant maturational processes of increasing myelination paired with cortical thinning as is possible using MSNs.

5.1.4 Summary and Hypotheses

Here, we analysed 469 structural MRI and 448 functional MRI scans in an accelerated longitudinal design, with one to three scans per participant. First, we estimated age related changes in six macro- and micro-structural MRI metrics individually. Then, we estimated the morphometric similarity between 358 cortical areas on a feature vector comprising those six structural metrics. For each scan, this resulted in a morphometric similarity network, with edge weights and nodal weighted degrees, for modeling of anatomical connectome development and for comparison with functional MRI connectivity. We hypothesized that (i) MRI macrostructural features would decrease over the course of adolescence, while MRI microstructural measures of myelination would increase, respectively reflecting known processes of synaptic pruning and increases in myelination; (ii) we could map these diverging processes to a profile of changes in morphometric similarity over the course of adolescence; and (iii) that this structural re-wiring would be linked to changes in structure-function coupling over the course of adolescence.

5.2 Methods

5.2.1 Sample

The work in this chapter makes use of the same dataset presented in **Chapters 2-3**, which was collected as part of the Neuroscience in Psychiatry Network (NSPN), a joint initiative by the University of Cambridge and University College London, with the aim of using an accelerated longitudinal design to measure developmental brain changes in a sample drawn from the population of Greater London and Cambridgeshire that was broadly representative of the populations of England and Wales. A total of 306 adolescents were invited to undergo functional and structural neuroimaging assessments. The exclusion criteria for this subsample included a current or past history of neurological disorders, current treatment for psychiatric disorder or drug or alcohol dependence, as well as learning disabilities. Each participant was invited to provide data on at least two occasions; at baseline and at a one year follow-up assessment, with a subset of the sample invited to come in six months after baseline for an additional scan. The cohort was scanned a total of 556 times. The study was ethically approved by the National Research Ethics Service and conducted in accordance with U.K. National Health Service research governance standards. While the previous chapter focused

on the functional MRI data acquired for each participant, here we will focus on the structural MRI data.

5.2.2 Structural MRI acquisition and pre-processing

The anatomical MRI data were acquired using a multi-parametric mapping (MPM) sequence (Weiskopf et al., 2013) at three sites, on three identical 3T Siemens MRI scanners (Magnetom TIM Trio, VB17 software version) with a standard 32-channel radio-frequency (RF) receive head coil and RF body coil for transmission. The diffusion weighted data were collected during the same session. A single-shot echo planar imaging sequence (63 gradient directions with b -value = 1000 mm^2/s^2 and 5 unweighted B_0 images) was used to acquire a high-angular resolution diffusion-weighted image (HARDI) with the following scanning parameters: slice number = 70 consecutive; slice thickness = 2 mm; field of view = 192×192 mm; echo time (TE) = 90 ms; repetition time (TR) = 8700 ms; voxel size = 2.0 mm isotropic.

We pre-processed the anatomical data using the `recon-all` command in Freesurfer v5.3.0 (Fischl, 2012). In short, the pipeline included the following steps: non-uniformity correction, projection to Talairach space, intensity normalisation, skull stripping, automatic tissue and subcortical segmentation, and construction of smooth representations of the gray/white interface and the pial surface. Subsequently, the DWI volumes were aligned to the T1 image for each subject.

We parcellated the anatomical and DWI scans into 360 bilateral parcels, using the Human Connectome Project (HCP) parcellation atlas (Glasser et al., 2016b).

5.2.3 Functional magnetic resonance imaging (fMRI) acquisition and pre-processing

The functional MRI data were acquired using a multi-echo (ME) echo-planar imaging sequence with the following scanning parameters: TR = 2.42 s; GRAPPA with acceleration factor = 2; flip angle = 90° ; matrix size = $64 \times 64 \times 34$; field of view = 240 mm by 240 mm; in-plane resolution = 3.75 mm by 3.75 mm; slice thickness = 3.75 mm with 10% gap, with sequential acquisition of 34 oblique slices; bandwidth = 2368 Hz/pixel; and echo times (TE) = 13, 30.55, and 48.1 ms.

The full pre-processing pipeline has been described in depth in 2. Briefly, this included: multi-echo independent component analysis (ME-ICA) to remove non-BOLD

components (Kundu et al., 2012b, 2013b); CSF-regression using Analysis of Functional NeuroImages software (AFNI; (Cox, 1996b)); parcellation into 360 bilateral cortical regions using the HCP template (Glasser et al., 2016b); band-pass filtering (frequency range 0.025 to 0.111 Hz); removal of 30 dropout regions, defined by a low Z score of mean signal intensity in at least one participant ($Z < -1.96$); functional connectivity estimation using Pearson's correlation between all possible combinations of regional timeseries; and Fisher's $r - Z$ transformation. Finally, to remove any residual effects of head motion on functional connectivity, we regressed each pairwise correlation between regions on the time-averaged head motion of each participant (mean framewise displacement (FD)). We retained the residuals of this regression, i.e., motion-corrected Z scores, as the estimates of functional connectivity (FC) for this analysis.

5.2.4 Morphometric feature estimation and quality control

We used FreeSurfer's standard morphometric features: cortical thickness (CT), grey matter volume (GM), surface area (SA), intrinsic curvature (IC), mean curvature (MC), intrinsic curvature (IC), and folding index (FI). Previous work on this sample had indicated that MT adolescent changes with age were most pronounced at 70% cortical depth from the pial surface (Whitaker et al., 2016b); thus regional MT values were estimated at that depth. Lastly, regional volumes for fractional anisotropy (FA) and mean diffusivity (MD) were derived from the DWI scans.

In order to identify potential outliers, first we standardized each (global) morphometric feature using the non-parametric metric median absolute deviation (MAD). We normalized each features across nodes within each scan, i.e.:

$$MAD_{f,s} = \frac{X_{f,s} - \text{median}(X_{f,s})}{k * \text{median}(|X_{f,s} - \text{median}(X_{f,s})|)} \quad (5.1)$$

where $X_{f,s}$ is the vector of regional feature values for a single feature f across regions for a single scan s , and $k \approx 1.4826$ is a constant, which ensures that for large N the median absolute deviation is approximately equal to the standard deviation. Thus $MAD_{f,s}$ is a vector of standardized feature values for a single feature f across regions for a single scan s .

We excluded 11 subjects due to outliers, with $MAD \geq 5$ set as the threshold based on visual interpretation of the distributions of data, in at least one global morphometric measure (Fig. 5.1).



Fig. 5.1 **Global morphometric outliers:** We estimated MAD scores across subjects for each of 10 morphometric features: CT, GM, SA, FA, MT, MD, CI, FI, IC, and MC. We defined outliers as subjects with $MAD \geq 5$ in at least one morphometric feature. Here, global (raw) feature values, colored by their respective MAD scores, are shown to highlight which datapoints were removed.

We then estimated MAD locally, as in **Equation 5.1**, for each morphometric feature across subjects. First, we excluded regions with signal dropout, defined as $MAD = 0$, which led to the exclusion of two regions (L_H , R_H ; see **Supplementary table A.2** for a list of full regions names), such that the total number of regions analysed henceforth was 358. Next, within each subject, we excluded all regions with $MAD \geq 5$ (**Fig. 5.2**). At this step of the quality control pipeline, we found that the curvature features, MC, IC, CI, and FI, demonstrated much larger numbers of outliers across all regions. We thus chose to exclude them from further analyses and proceeded with the six previously mentioned micro- and macro-structural MRI features only (CT, GM, SA, MT, FA, MD).

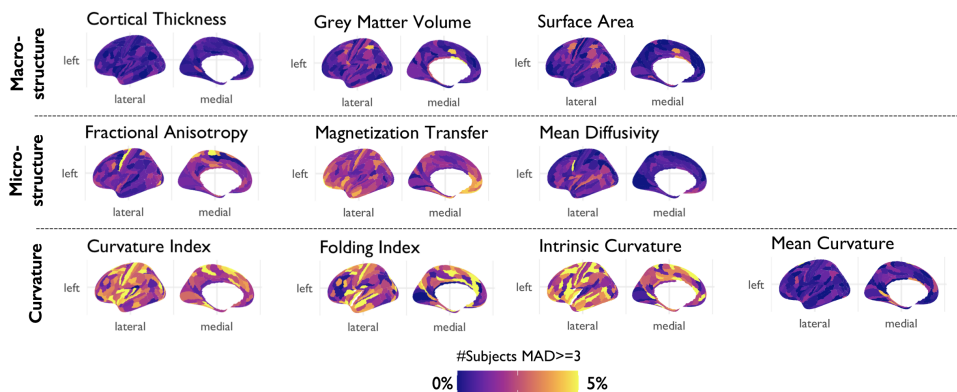


Fig. 5.2 **Local morphometric outliers:** We estimated the local MAD score for each subject at each region within each morphometric feature. Here, we show the percentage of subjects with $MAD \geq 3$ in each region.

5.2.5 Modeling of developmental change in morphometric features

We estimated linear age-related changes or development in six morphometric features at global scale, i.e., on average for each feature over all regions, and locally, for each feature at each region, using linear mixed effects models, with a fixed effect of age, sex and site, and a random effect for the repeated measures on each participant, as follows:

$$F_i \sim 1 + \beta_{age} * age + \beta_{sex} * sex + \beta_{site} * site + \gamma_{subject} * (1|subject) + \epsilon \quad (5.2)$$

where F_i refers to the morphometric feature at region i , β refers to the coefficients for the fixed effects, $\gamma_{subject}$ refers to the coefficients for the random effect, and ϵ represents the residual error.

5.2.6 Adolescent changes in morphometric similarity

We derived subject-specific structural connectomes using morphometric similarity networks. To this end, we standardized each morphometric feature within each subject using MAD. We then estimated morphometric similarity networks for each subject by calculating the Pearson correlation between their standardized feature vectors for each possible pair of regions. This resulted in a 358×358 symmetric matrix, indicative of morphometric similarity between cortical regions.

A | Adolescent longitudinal MSN development

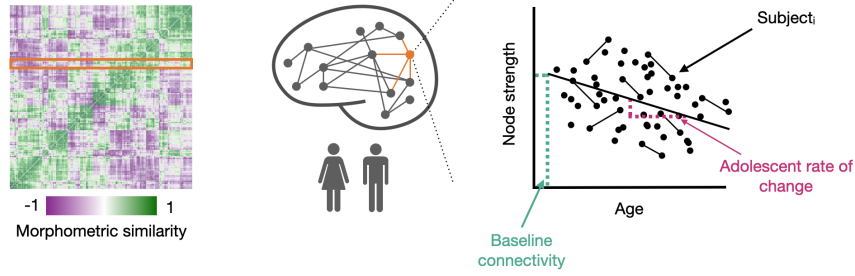


Fig. 5.3 Estimation of age effects on morphometric similarity: First, for each subject, we estimated weighted degree as the mean over all of a node's edges. Then, we estimated the linear effect of age on weighted degree using linear mixed effect models with a fixed effect of age, sex and site, and a random effect of subject. From this model, we estimated two parameters: the baseline connectivity at age 14, as the predicted nodal degree at age 14; and the adolescent rate of change, as the slope of the regression line fitted to the effect of age on nodal degree.

We first estimated regional morphometric similarity, or weighted degree as the mean across a region's edges (**Equation 1.2**). Then we estimated the linear effect of age on MSN weighted degree, using linear mixed effects models (**Fig. 5.3A**) with a fixed effect of age, sex, and site and random effect of subject, as follows:

$$s_i \sim 1 + \beta_{age} * age + \beta_{sex} * sex + \beta_{site} * site + \gamma_{subject} * (1|subject) + \epsilon \quad (5.3)$$

where s_i refers to the morphometric similarity strength, or weighted degree, of regional node i , β refers to coefficients for the fixed effects, $\gamma_{subject}$ refers to the coefficients for random effects, and ϵ represents the residual error.

From this model, we estimated the adolescent rate of change in morphometric similarity, or the age effect on weighted degree at each node of MSN, as the β -coefficient of age.

In order to decode the regional changes in morphometric similarity by cell type, we averaged weighted degree over all regions within each cytoarchitectonic class of cortical areas defined *a priori* by a reference brain atlas (Whitaker et al., 2016b).

We then estimated the correlation between age-related changes (t -values) in individual morphometric features, estimated by **Equation 5.3**, and age-related changes (t -values) in morphometric similarity, estimated by **Equation 5.3**. Each analysis of spatial co-location or correlation between two cortical maps was reported with both the parametric P -value corresponding to the Pearson correlation (r), as well as a P -value derived from the more

conservative "spin-test" permutation. Spin tests based on spatial permutation have been introduced in detail in **Chapter 2**. Briefly, spatial autocorrelation of statistical brain maps can cause inflated estimates of the probability of spatial co-location or correlation between two maps (Alexander-Bloch et al., 2013; Váša et al., 2018). The spin test procedure addresses this issue by conserving the spatial autocorrelation of the maps by randomly “spinning” or spherically rotating each map over the surface of the brain and calculating the spatial co-location statistic after each spin permutation.

We estimated the anatomical co-location of the map of age-related changes in morphometric similarity with various gradients of cortical organization, including metabolic rates, blood volume, and functional hierarchy (Sydnor et al., 2021). To do this, we correlated the ranked map of age-related changes in morphometric similarity with each prior map, and then estimated the significance of the correlation while controlling for spatial auto-correlation using a spin-test (Váša et al., 2018).

We further assessed the psychological relevance of the map of age-related changes in morphometric similarity using Neurosynth, an automated meta-analytical tool (Yarkoni et al., 2011). Details of this analysis have been described in **Chapter 3**. Briefly, we generated a volumetric version of the regional map of adolescent changes in morphometric similarity (code available at https://github.com/LenaDorfschmidt/neurosynth_analysis) and uploaded it for automated comparison to the Neurosynth database (<https://neurosynth.org>) of task-related fMRI activation coordinates, which returned the correlation values of the map with a wide set of terms related to fMRI task activation experiments.

5.2.7 Co-location with adolescent changes in functional diversity

We were interested in assessing whether changes in morphometric similarity during adolescence were associated with changes in functional diversity, which might represent adolescent changes in cognition and behavior. To this end, we used subjects’ functional connectivity matrices to estimate the regional participation coefficient, a measure of inter-modular connectivity mediated by each node, such that nodes with high participation coefficient have been designated “connector hubs” because of their important role in communication between functionally specialised modules (**Chapter 1, Fig. 1.3**). We then used linear mixed effects models to estimate the linear effect of age on the participation coefficient in each region i as follows:

$$PC_i \sim 1 + \beta_{age} * age + \beta_{sex} * sex + \beta_{site} * site + \gamma_{subject} * (1|subject) + \varepsilon \quad (5.4)$$

where PC_i refers to the participation coefficient at region i , β refers to the coefficients for the fixed effects, $\gamma_{subject}$ refers to the coefficients for random effects, and ε represents the residual error.

5.2.8 Adolescent changes in structure-function coupling

We estimated global structure-function coupling as the Spearman correlation between the upper triangle of each subject's structural (MSN) and functional (FC) networks at each timepoint (Fig. 5.4A,B). We opted to use Spearman's rank correlation due to its robustness to possible outliers. Local structure-function coupling was estimated at each node as the Spearman correlation between the node's edges in the structural and functional networks (Fig. 5.4A,C).

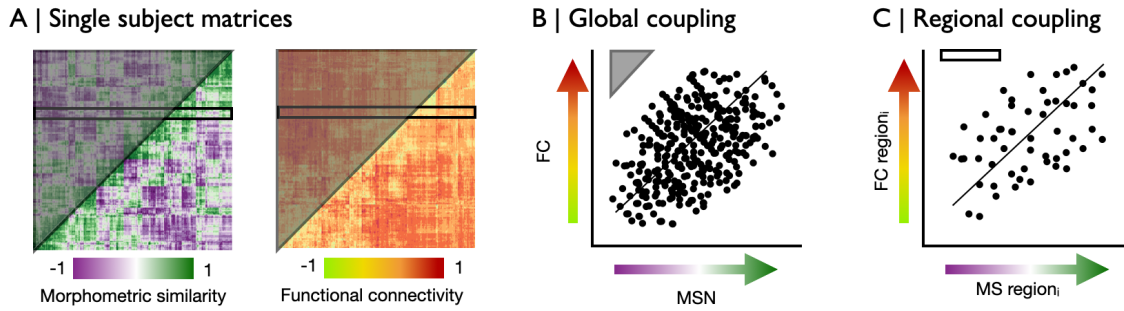


Fig. 5.4 **Structure-function coupling estimation:** (A) For each subject, we estimated the coupling between their structural (MSN) and functional (FC) connectomes. (B) Global coupling was estimated as the Spearman correlation between the upper triangle of both matrices. (C) Regional coupling was estimated as the Spearman correlation between all edges of each region.

Then, we estimated parameters of adolescent change in structure-function coupling. Specifically, we estimated the linear effect of age on regional structure-function coupling strength using linear mixed effects models, with a fixed effect of age, sex and site, and a random effect of subject, as follows:

$$CS_i \sim 1 + \beta_{age} * age + \beta_{sex} * sex + \beta_{site} * site + \gamma_{subject} * (1|subject) + \varepsilon \quad (5.5)$$

where CS_i refers to the strength of structure-function coupling at region i , β refers to the coefficients for the fixed effects, $\gamma_{subject}$ refers to the coefficients for random effects, and ε represents the residual error.

We proceeded to derive the local structure-function coupling at baseline (age 14) as the predicted coupling value from **Equation 5.5**, i.e.,

$$CS_{14_i} = 1 + 14 * \beta_{age} + 0.5 * \beta_{sex} + 1/3 * \beta_{site}; \quad (5.6)$$

and the rate of change in coupling over the course of adolescence, as the t – values of the effect of age, β_{age} , estimated by **Equation 5.5**.

Finally, we estimated intra-individual changes between baseline and follow-up assessments in participation coefficient, ΔPC : :

$$\Delta PC = PC_{follow-up} - PC_{baseline}; \quad (5.7)$$

and comparable changes in structure-function coupling, $\Delta Coupling$:

$$\Delta Coupling = Coupling_{follow-up} - Coupling_{baseline}; \quad (5.8)$$

and then estimated the correlation between ΔPC and $\Delta Coupling$ for each regional node.

5.3 Results

5.3.1 Analyzable sample

The final sample of morphometric feature data after quality control consisted of 469 scans from 291 subjects in 358 regions. The fMRI sample included 448 scans from 283 subjects at 330 regions (**Table 5.1**). We conducted each analysis on the largest possible dataset, thus analyses of brain structure were conducted on 291 subjects across 358 regions, whereas analyses of structure-function relationships were conducted on an extensively overlapping sample of 283 subjects across 330 regions.

agebin	Baseline		6 Months		Follow Up	
	female	male	female	male	female	male
1	29	28	3	2	19	25
2	34	28	2	2	24	22
3	23	24	3	2	14	13
4	30	32	5	5	15	21
5	20	18	1	2	8	15

Table 5.1 NSPN structural MRI data sample overview: The NSPN sample was a sex-balanced, age-stratified longitudinal cohort, with subjects recruited in five age bins: 14-15 years, 16-17 years, 18-19 years, 20-21 years and older than 22 years at baseline. Approximately 30 subjects per sex were recruited in each age bin. Subjects were invited for scanning at a baseline and follow-up visit approximately one year later, with a small subset of subjects also invited for an intermediate scan about six months after baseline. Here, we list the number of structural scans available in the final sample (after quality control) per age-bin, for each of the visits, stratified by sex.

5.3.2 Adolescent changes in global and regional MRI metrics

We first estimated adolescent changes at global and regional scales for six morphometric features: (i) three macro-structural MRI metrics, cortical thickness (CT), grey matter volume (GM), and surface area (SA); (ii) and three micro-structural metrics, magnetization transfer (MT), magnetization transfer (MT) and mean diffusivity (MD).

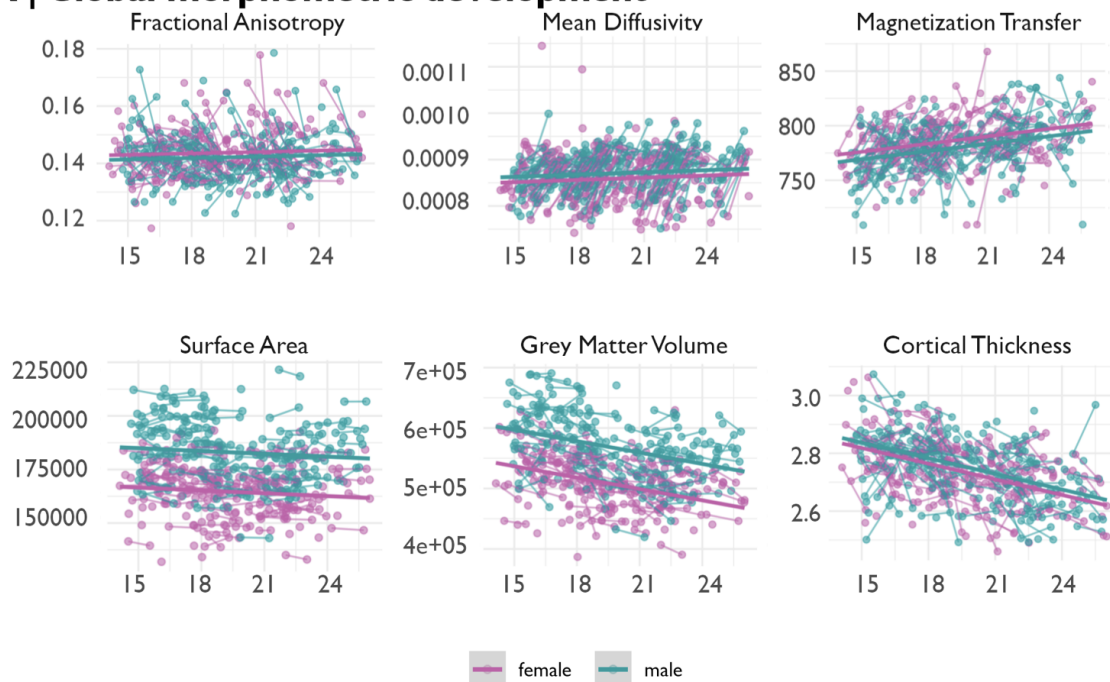
A | Global morphometric development

Fig. 5.5 Adolescent changes in global macro-structural and micro-structural MRI metrics: (A) We modeled the linear effect of age on six morphometric features: 3 macro-structural MRI metrics (GM, CT, SA) all decreased over the course of adolescence ($P_{FDR} < 0.05$ for each), while 1 of the 3 micro-structural MRI metrics was significantly increased during adolescence (MT, $P_{FDR} < 0.05$) but not MD or FA.

Globally, we found that all macro-structural metrics significantly decreased during adolescence: SA, $t_{age} = -2.33, P_{FDR} < 0.05$; GM, $t_{age} = -5.23, P_{FDR} < 0.01$; and CT, $t_{age} = -7.29, P_{FDR} < 0.01$. Of the micro-structural metrics, MT significantly increased ($t_{age} = 3.19; P_{FDR} < 0.01$) while FA ($t_{age} = 1.78$) and MD ($t_{age} = -0.42$) showed no significant changes after correction for multiple comparisons (**Fig. 5.5A, Table 5.2**). We also found that there were significant sex differences in one feature, GM, $t_{sex} = 2.85, P_{FDR} < 0.05$.

	t_{age}	P_{age}	t_{sex}	P_{sex}	P_{ageFDR}	P_{sexFDR}
Fractional Anisotropy	1.78	0.08	1.13	0.26	0.09	0.31
Mean Diffusivity	-0.42	0.67	-2.01	0.05	0.67	0.07
Magnetization Transfer	3.19	0.00	-2.10	0.04	0.00	0.07
Surface Area	-2.33	0.02	2.20	0.03	0.03	0.07
Grey Matter Volume	-5.23	0.00	2.85	0.00	0.00	0.03
Cortical Thickness	-7.29	0.00	-0.11	0.91	0.00	0.91

Table 5.2 **Age and sex effects on individual morphometric features:** We estimated the linear effect of age on individual morphometric features (FA, MD, MT, SA, GM, CT) using linear mixed effects models with a fixed effect of age, sex and site, and a random effect of subject. Above, we list the t and P -values from this model.

Regionally, we found that macro-structural MRI metrics tended to decrease, in particular in association and motor cortical areas, and micro-structural metrics tended to increase, in particular in association and sensory cortical areas (**Fig. 5.6A,B**); We found that this effect was strongest for MT, where 289 regions significantly ($P_{FDR} < 0.05$) increased in weighted degree over the course of adolescence, and in CT and GM, where 336 and 296 regions, respectively, significantly decreased (for full results see **Appendix Table A.4**).

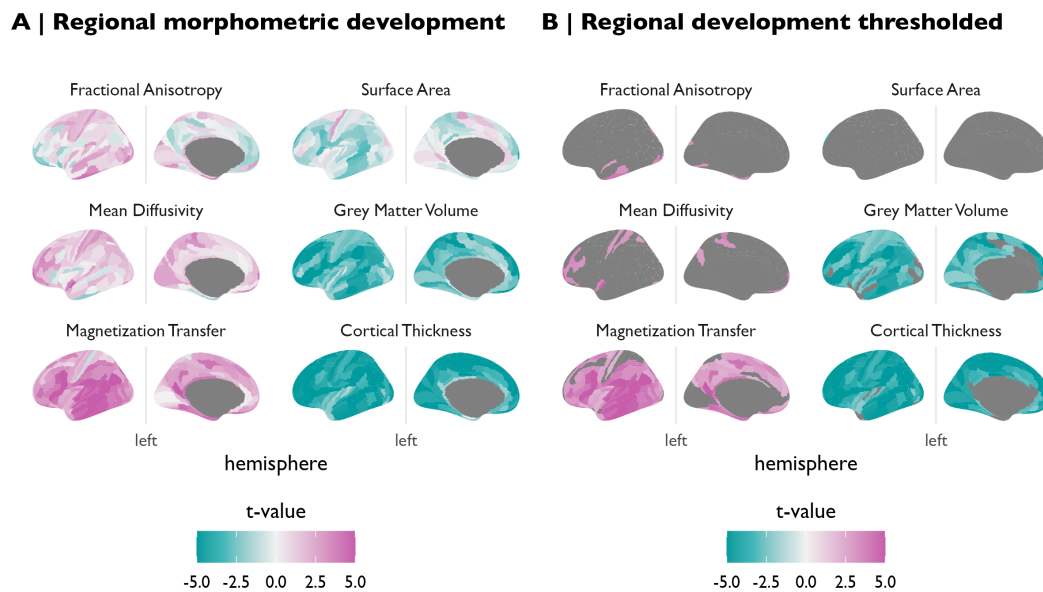


Fig. 5.6 Adolescent changes in regional macro-structural and micro-structural MRI metrics: (A) We modeled the linear effect of age on six morphometric features at each of 179 bilateral cortical areas to resolve the anatomical patterning of decreased macro- and increased micro-structural metrics during adolescence. We largely observed increases ($t > 0$) in micro-structural features, and decreases ($t < 0$) in macro-structural features. (B) We thresholded the results from panel (A) for significance after correction for multiple comparisons, $P_{FDR} < 0.05$. The results were highly symmetric across hemispheres, so here only the left hemisphere is shown.

We were interested in the extent to which the age related changes in regional morphometric features followed the respective global trends. To this end, we estimated the rates of change in each morphometric feature regionally while correcting for its global values. We thus derived a map of change relative to a feature's global development, where negative values indicated that the region increased in strength less than the respective global phenotype, and a positive value indicated that the region increased in strength more than the respective global phenotype. We found that the rate of change after global effect correction was regionally varied (**Fig. 5.7A**). Overall, the micro-structural features tended to increase more strongly in temporal regions, whereas they increased less strongly in medial frontal regions.

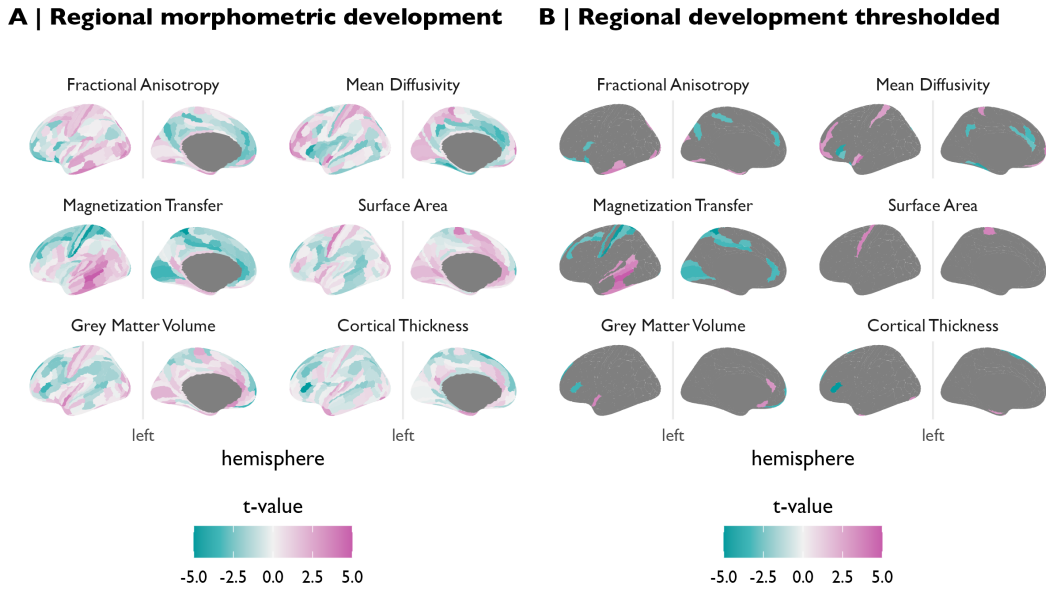


Fig. 5.7 Adolescent changes in macro-structural and micro-structural MRI metrics corrected for global effects of age: We estimated age-related changes in regional features correcting for their respective global values, i.e., regional rates of change relative to each feature’s global rate of change. (A) We modeled the linear effect of age on 6 micro-structural and macro-structural MRI features in each of 180 bilateral cortical areas to resolve the anatomical patterning of decreased macro- and increased micro-structural metrics during adolescence. (B) We thresholded the results from panel (A) for significance after correction for multiple comparisons $P_{FDR} < 0.05$. The results were highly symmetric across hemispheres, so here only the left hemisphere is shown.

5.3.3 Adolescent change in morphometric similarity

We constructed MSNs for each participant’s set of T1 and DWI MRI scans, at each time-point, by estimating the Pearson correlation between all pairwise regional feature vectors comprising the six MRI metrics, resulting in a $\{358 \times 358\}$ symmetric morphometric similarity matrix or weighted, undirected morphometric similarity network (MSN) (for details, see **Chapter 4.1**). The weighted degree of each regional node in each MSN is a measure of its morphometric similarity with all other regions, and high degree nodes or hubs are morphometrically similar to many other nodes in the brain.

Because we constructed a MSN model of the connectome for each scanning session completed by each participant, we could estimate developmental changes in MSN parameters using the same linear mixed effects model (LME) model as previously used for analysis

of age-related change in global and regional MRI metrics. We found that weighted degree decreased with age in frontal and occipital cortical nodes, meaning that these areas became more morphometrically dissimilar from the rest of the brain, and increased with age in temporal and limbic cortical nodes, meaning they became more morphometrically similar to the rest of the brain (**Fig. 5.8A**). 33 regional MSN nodes, primarily located in association (N=13), limbic (N=6) and insular (N=8) cortical regions, had significant changes in weighted degree after correction for multiple comparisons ($P_{FDR} < 0.05$; see **SI Table A.4**).

To assess potential cytoarchitectonic drivers of the observed adolescent change in morphometric similarity, we estimated the mean effect of age on weighted degree of all regions in each of seven cytoarchitectonic classes of cortex (**Fig. 5.8B**). Limbic and insular cytoarchitectonic classes of cortex had increased MSN degree during adolescence, whereas motor, association and sensory cytoarchitectonic classes had decreased MSN degree. Next, we averaged the morphometric similarity over all edges within and between each cytoarchitectonic class to estimate the age effect on the within- and between-class morphometric similarity strength.

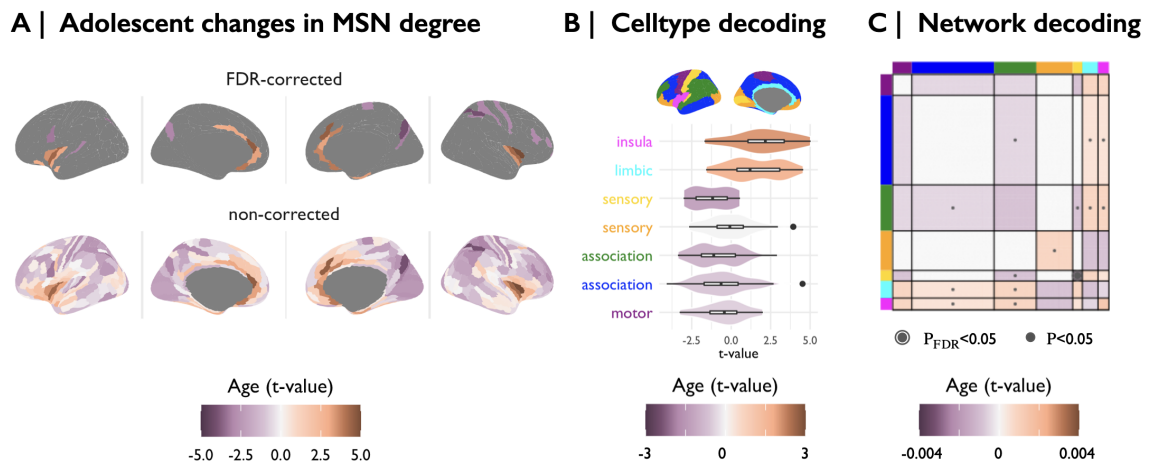


Fig. 5.8 Adolescent changes in morphometric similarity: We estimated morphometric similarity networks for each subject by correlating their standardized morphometric feature vectors for each possible combination of regions. (A) We estimated linear changes in morphometric similarity with age at each region. We found that that morphometric similarity decreased in frontal and occipital cortical regions, and decreased in medial and temporal cortical regions. These changes were significant after correction for multiple comparisons in 33 regions. (B) We estimated the mean effect of age on all regions within each of the von Economo cytoarchitectonic classes and found that morphometric similarity increased in insular and limbic cytoarchitectonic classes and decreased in all other classes. (C) We estimated the effects of age on the average similarity across edges within and between each of the von Economo classes. We found that adolescent change in morphometric similarity was more pronounced between than within cytoarchitectonic classes, however these changes were only nominally significant $P < 0.05$ and did not survive correction for multiple comparisons.

In order to further dissect adolescent morphometric similarity changes between cytoarchitectonic classes, we estimated the age-related change in connectivity of all nodes in each cytoarchitectonic class to the rest of the brain (**Fig. 5.9A**). Qualitatively, we found that each cytoarchitectonic class changed its connectivity to the rest of the brain in a distinctive way, e.g. secondary association cortical areas decreased in strength, or became more dissimilar to the rest of the network, whereas connections between limbic areas and the rest of the brain tended to increase in strength, becoming more similar to the rest of the brain over the course of adolescence (**Fig. 5.9B**).

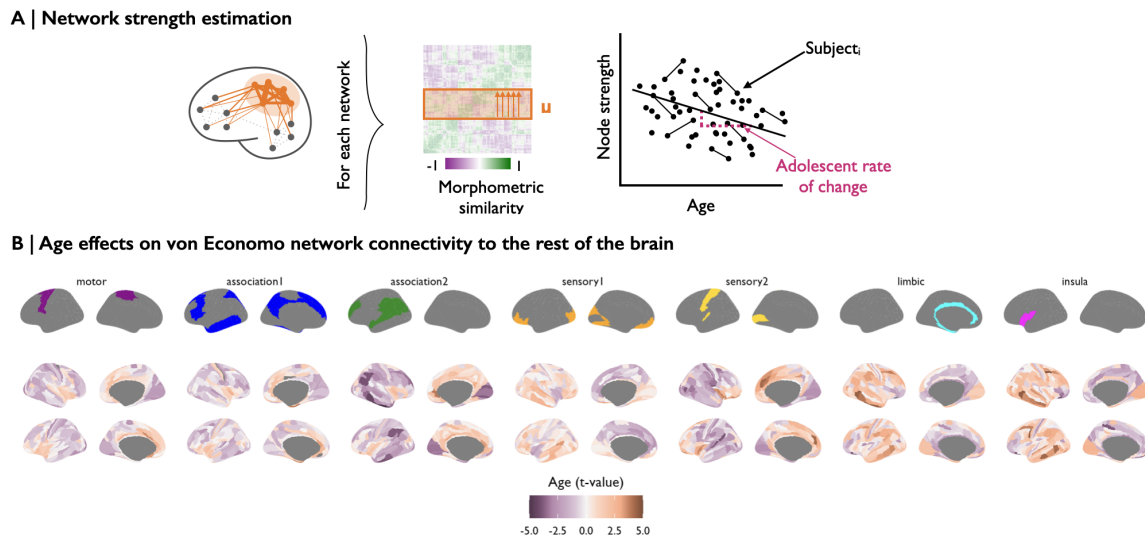


Fig. 5.9 Cytoarchitectonic class-specific changes in morphometric similarity: (A) For each cytoarchitectonic class, we estimated the strength of similarity of all other cortical regions to the nodes in the class by summing the relevant sections of the connectivity matrix, and then estimated age-related change of each class-specific measure of similarity. (B) We found that the patterns of adolescent rate of change in morphometric similarity differed qualitatively between cytoarchitectonic classes. For example, secondary association cortical areas (green) became more dissimilar to the rest of the network, whereas limbic areas became more similar to the rest of the brain over the course of adolescence.

In the context of **Chapter 2** and **Chapter 3** it is relevant to emphasize that we did not find evidence for widespread sex differences in morphometric similarity during adolescence (**Fig. 5.10**). After correction for multiple comparisons, we found only seven regions (*L_5mv*, *L_OP4*, *L_PFop*, *L_VMV3*, *R_RI*, *R_PHT*, *R_PPF*; see **Supplementary table A.2** for a list of full regions names) with significant sex differences in morphometric similarity ($P_{FDR} < 0.05$). Overall, the pattern of observed (non-significant) sex effects included increased morphometric similarity in females in limbic and default mode network regions, and increased morphometric similarity in males elsewhere in the cortex.

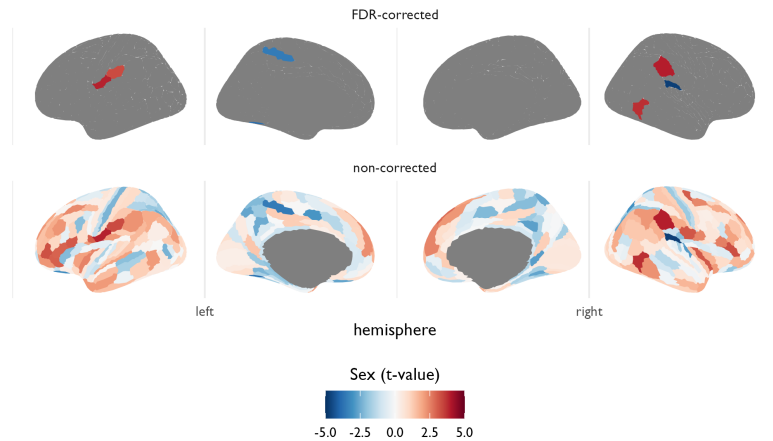


Fig. 5.10 Sex effects on adolescent changes in morphometric similarity: We estimated sex effects on adolescent changes in morphometric similarity at each region (*bottom*). Positive t -values indicate that morphometric similarity increased with age more strongly in males compared to females. After correction for multiple comparisons, we found that seven regions (L_5mv , L_OP4 , L_IP0 , L_VMV1 , R_52 , R_TF , R_IP0 ; ; see **Supplementary table A.2** for a list of full regions names) displayed significant sex differences in age-related changes in morphometric similarity ($P_{FDR} < 0.05$).

In an effort to understand the contribution of each of the six individual morphometric features to the adolescent change in morphometric similarity, we correlated the age effect on the individual features (**Fig. 5.6B**) with the age effect on regional weighted degree (**Fig. 5.8A**). We observed a divergent pattern (**Fig. 5.11A**), whereby the age effect on micro-structural features was negatively correlated with adolescent changes in MSN nodal strength or weighted degree (MD: $r = -0.4$, $P_{spin} < 0.05$; MT: $r = -0.15$, $P_{FDR} < 0.05$; FA: $r = -0.1$), whereas macro-structural feature changes were positively correlated with adolescent changes in MSN nodal degree (GM: $r = 0.32$, $P_{spin} < 0.05$; CT: $r = 0.31$, $P_{spin} < 0.05$; SA: $r = 0.26$, $P_{spin} < 0.05$). This result indicates that regions which showed strongest increases in myelination, as measured by MD, MT, and FA, became cytoarchitecturally less similar, or more differentiated, compared to the rest of the brain over the course of adolescence (**Fig. 5.11B**). Furthermore, these same regions were associated with the strongest age-related decreases in cortical thickness, grey matter volume and (to a lesser extent) surface area. In summary, the well-known adolescent processes of cortical thinning and increased myelination appeared to drive increasing morphometric dissimilarity or differentiation of the corresponding nodes in the morphometric similarity network. Conversely, regions that increased in morphometric similarity over the course of adolescence were associated with comparatively smaller adolescent changes over all MRI features as indicated by t -values closer to zero (**Fig. 5.11B**).

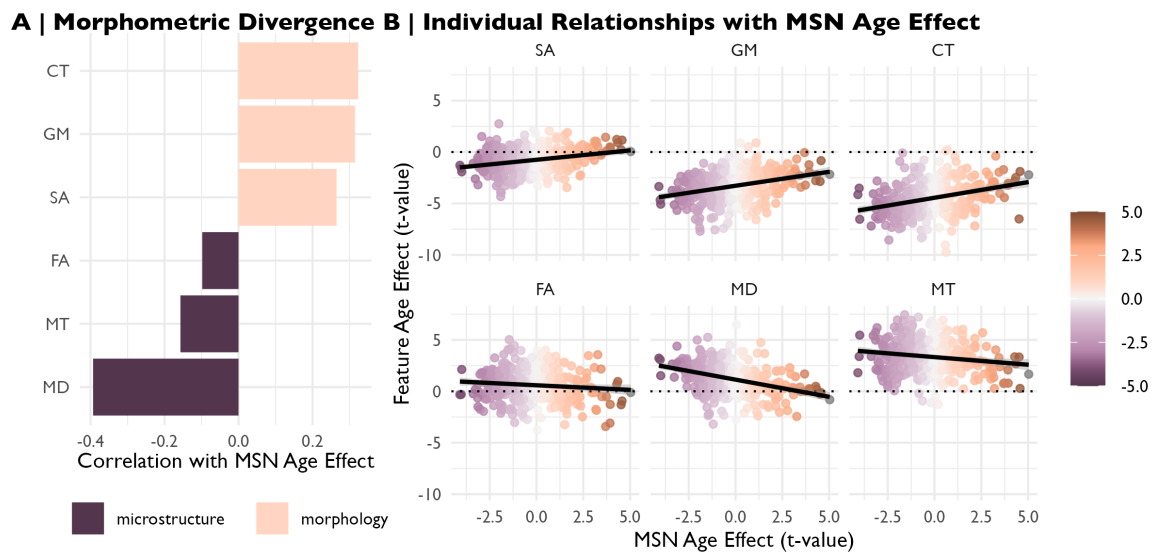


Fig. 5.11 Divergent profile of morphometric similarity: (A) We estimated the correlation between the age effects on individual morphometric features at each region (cf. **Fig. 5.6B**) and the age effect on morphometric similarity of each node in the network. (B) We found that micro-structural MRI features were negatively correlated with adolescent change in morphometric similarity, i.e., they increased with age in regions that become more morphometrically dissimilar during adolescence. Conversely, macro-structural MRI features were positively correlated with adolescent change in morphometric similarity, thus they tended to decrease in regions that decreased in morphometric similarity during adolescence.

5.3.4 Neurobiological and psychological context of adolescent changes in anatomical connectomes

We were interested in contextualizing age-related changes in MSNs in relation to prior maps of transcriptional and functional gradients, evolutionary change, and metabolic requirements (Sydnor et al., 2021). We found that the whole brain map of adolescent change in weighted degree of each regional node MSN node was significantly negatively correlated with commensurate maps of aerobic glycolysis ($r = -0.32; P_{spin} < 0.05$) and the rates of oxygen ($r = -0.44; P_{spin} < 0.001$) and glucose metabolism ($r = -0.48; P_{spin} < 0.001$). Thus association and other cortical nodes that had decreased MSN degree during adolescence tended to have increased metabolic demands in adulthood (**Fig. 5.12A**). Conversely, we found a positive correlation with a map of cerebral blood volume ($r = 0.19; P_{spin} < 0.05$), meaning that regions that saw decreases in morphometric similarity tended to have decreased cerebral blood volume (**Fig. 5.12B**).

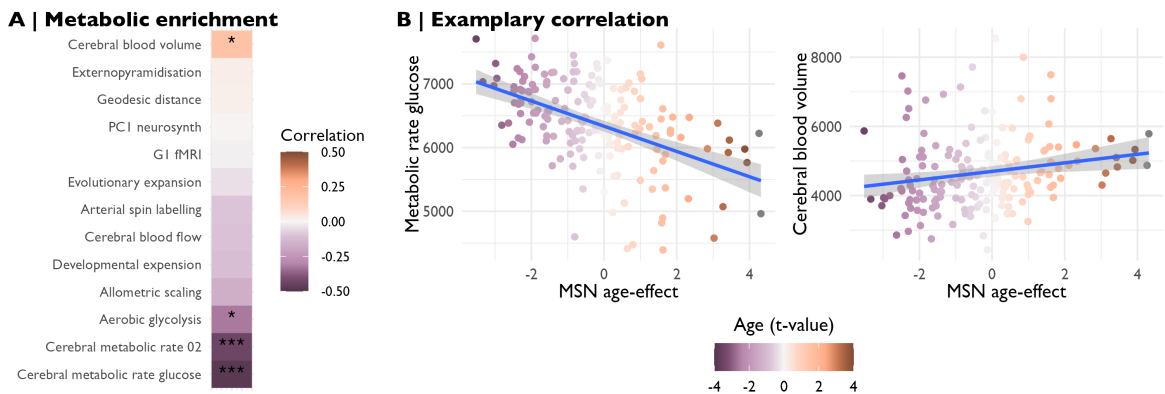


Fig. 5.12 Neurobiological relevance of adolescent changes in MSN: (A) We estimated the correlation between the age effect on morphometric similarity and several prior maps of brain organization. (B) We found a negative correlation between the effects of age on MSN nodal degree and several brain maps of metabolic rates, meaning that regions that showed decreases in degree of morphometric similarity tended to have increased metabolic rates. Conversely, the positive correlation between the age effect on MSN nodal degree and a map of cerebral blood volume means that regions that had decreased morphometric similarity over the course of adolescence had lower cerebral blood volume.

Next, we explored the psychological relevance of the map of age-related changes in morphometric similarity. We conducted automated meta-analytic referencing using the NeuroSynth database of task-related fMRI activation coordinates. This analysis revealed that regions that showed decreases in morphometric similarity ($t \leq 0$) were typically activated by tasks related to visual processing and imagery, motor control, and working memory. Conversely, regions that showed increases ($t \geq 0$) in similarity were associated with self-evaluation of emotional content, nociception, and pain (**Fig. 5.13A**).

or structural differentiation from the rest of the brain, were associated with increasing diversity of functional connectivity, measured as a relative strengthening of inter-modular connectivity, potentially representing an increased ability to integrate information across multiple, structurally differentiated and functionally specialised modules.

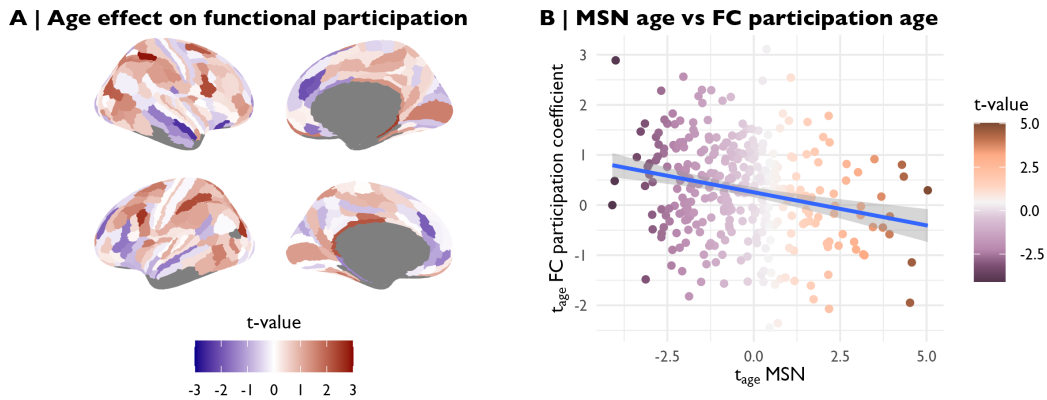


Fig. 5.14 Morphometric dissimilarity was associated with functional participation: (A) We estimated age-related changes in the participation coefficient of regional nodes in fMRI connectomes over the course of adolescence. Functional participation increased in association cortical regions and decreased in primary motor and sensory regions, as well as medial prefrontal regions. (B) We estimated Spearman's correlation between age-related changes in morphometric similarity and age-related changes in functional participation coefficient. We found that regions that became more morphometrically dissimilar over the course of adolescence tended to increase in their functional participation.

Next, we hypothesized that these increases in functional participation coefficient, supported by increased morphometric dissimilarity, may be driven by changes in structure-function coupling. To test this hypothesis, we first estimated global structure-function coupling as the correlation between the ranked elements of the functional connectivity matrix and the morphometric similarity matrix for each subject, at each time-point. We modeled the linear effect of age on structure-function coupling using the same linear mixed effects model as previously used for global, local and MSN metrics. We found that global structure-function coupling decreased over the course of adolescence ($t = -5.04, P < 0.001$; **Fig. 5.15A**), indicating a decoupling of functional connectivity from morphometric similarity.

Then, we tested the same hypothesis regionally. We thus estimated the linear effect of age on structure-function using a linear mixed effects model, with a fixed effect of age, sex and site, and a random effect of subject. From this model of age-related change in regional structure-functional coupling, we derived a map of baseline coupling, or the predicted coupling at age 14 years (**Fig. 5.15B**), as well as a map of adolescent changes in regional

coupling (**Fig. 5.15C**). Baseline coupling was high in secondary sensory and association cortical areas, and to a lesser degree in motor cortex (**Fig. 5.15**). Coupling decreased most strongly in sensorimotor and association cortical regions, and increased in limbic and insular cortical regions (**Fig. 5.15C**). It is notable that the majority of regions decreased in coupling over the course of adolescence (blue in **Fig. 5.15C**).

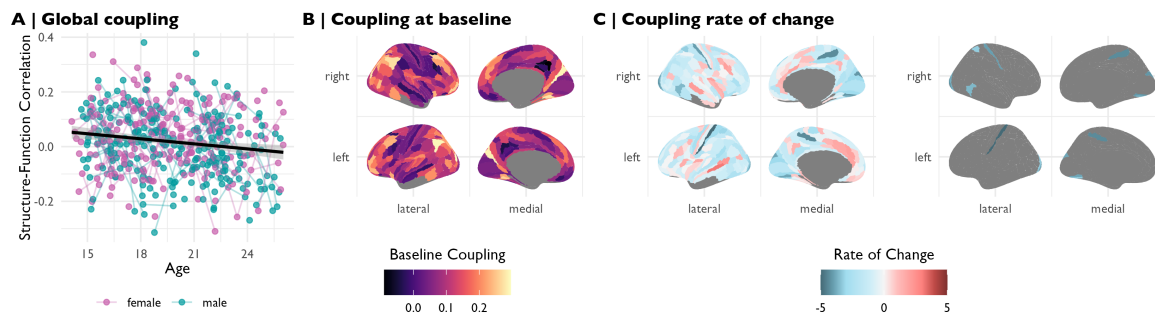


Fig. 5.15 Adolescent development of structure-function coupling: (A) We modeled the linear effect of age on global structure-function coupling by correlating the ranked edgewise connectivity vectors derived from a subject's FC matrix and MSN, respectively. We found that there was a significant decline in global structure-function coupling over the course of adolescence. (B-C) We estimated regional structure-function coupling as the correlation between the ranked vector of a region's edges derived from the FC matrix and the MSN, respectively. We estimated the linear effect of age on regional structure-function coupling using linear mixed effects models. From this model, we derived a map of baseline structure-function coupling as the predicted coupling at age 14, and a map of the rate of change in coupling, or the t -value of the effect of age. We found that 10 regions showed significant changes in structure-function coupling after correction for multiple comparisons ($P_{FDR} < 0.05$).

We further investigated how adolescent changes in morphometric similarity were related to this signature of adolescent structure-function decoupling. We found that baseline morphometric similarity, i.e., weighted nodal degree at age 14 years, and baseline structure-function coupling were weakly correlated ($r = 0.15, P_{spin} < 0.05$), such that regions that had high MSN degree also had strong structure-function coupling at baseline. We also found that structure-function coupling at baseline and the rate of change in coupling were negatively correlated ($r = -0.35; P_{spin} < .001$), thus regions that were more strongly coupled at baseline tended to have greater decreases in coupling over the course of adolescence (**Fig. 5.16B**). Lastly, regions that most strongly de-coupled also tended to show the strongest decreases in weighted degree of MSN regional nodes during the same developmental period ($r = 0.36, P_{spin} < 0.01$; **Fig. 5.16C**).

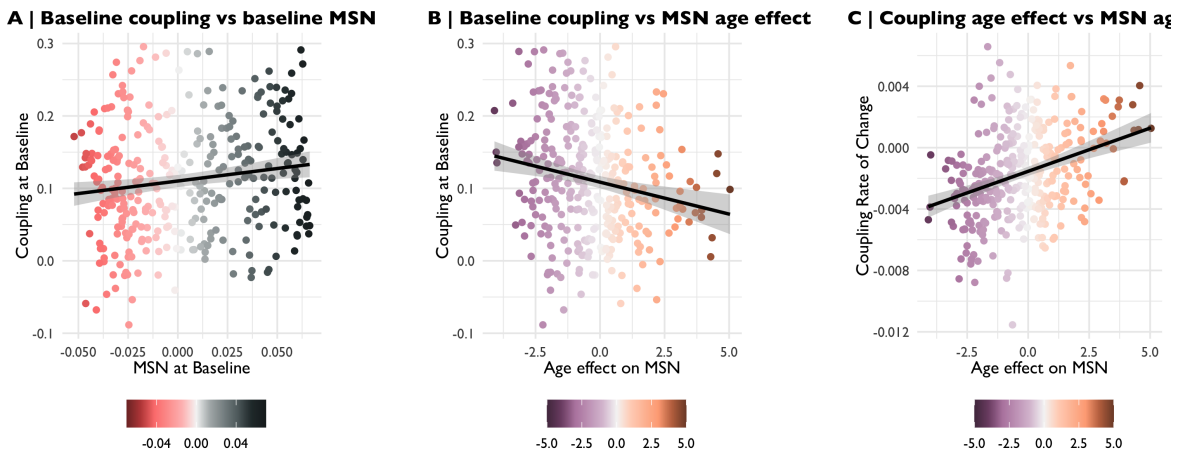


Fig. 5.16 Structure-function coupling in relation to adolescent changes in MSN: (A) We found that weighted degree of MSN regional nodes at 14 years was significantly correlated with baseline structure-function coupling, thus regions with high degree had stronger structure-function coupling at baseline. (B) There was a significant negative correlation between the age effect on MSN weighted degree and structure-function coupling at 14 years, meaning that regions that decreased in MSN degree during adolescence had increased structure-function coupling at baseline. (C) The age effect on MSN weighted degree was significantly positively correlated with the rate of change in structure-function coupling. Thus, regions that became more morphometrically dissimilar tended to have decreased coupling, or become more functionally independent, over the course of adolescence.

Thus having established that: (i) decreases in structure-function coupling during adolescence were associated with increases in morphometric dissimilarity (**Fig. 5.16C**); and (ii) increasing morphometric dissimilarity was associated with increased functional diversity over the course of adolescence (**Fig. 5.14C**), we aimed to assess whether age-related decreases in structure-function coupling during adolescence were also associated with changes in functional participation. We found that the inter-individual rate of change in coupling was not significantly associated with the inter-individual rate of change in participation coefficient ($t = -0.05, P = 0.3$). However, we did observe a significant relationship between the intra-individual development of structure–function coupling ($\Delta Coupl$; **Equation 5.8**) and the intra-individual changes in the participation coefficient (ΔPC ; **Equation 5.7**), estimated on the subset of participants that had both a baseline scan and a follow-up scan. This relationship suggested that intra-individual increases in functional participation coefficient were associated with intra-individual increases in coupling of frontal and temporal regions and decreases of primary sensory regions. Finally, we found that this association between intra-individual changes in structure-function coupling and functional participation ($\Delta Coupl \sim \Delta PC$) was significantly correlated with the age-related changes in weighted degree of MSN nodal degree

($r = -0.16, P_{spin} < 0.05$), such that regions in which increases in functional participation were associated with decreases in structure-function coupling tended to have increased morphometric dissimilarity over the course of adolescence.

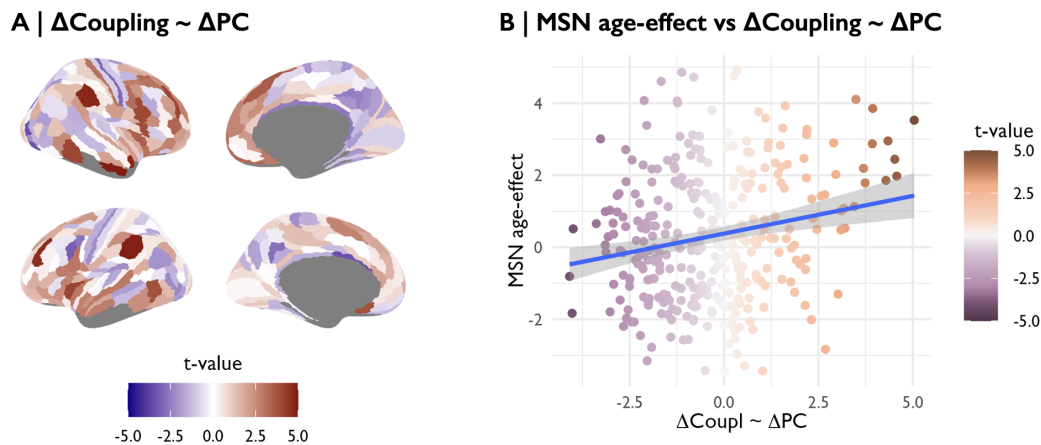


Fig. 5.17 Morphometric dissimilarity partially explains adolescent age-related changes in functional participation: We estimated the effect of the intra-subject difference (between baseline and follow-up scans) in participation coefficient (ΔPC) on the intra-subject difference in structure-function coupling ($\Delta Coupling$). (A) We found that ΔPC was positively associated with $\Delta Coupling$ in prefrontal and medial frontal cortex, as well as temporal cortical regions; but negatively associated with $\Delta Coupling$ in primary sensory cortical regions and medial parietal cortex. (B) The association between intra-individual changes in coupling and participation coefficient ($\Delta Coupling \sim \Delta Coupling$) was positively correlated with adolescent changes in weighted degree of MSN weighted degree ($r = -0.16, P_{spin} < 0.05$), meaning that regions that became morphometrically dissimilar (indexed by age-related decrease in weighted degree) over the course of adolescence tended to show decreases in participation coefficient in fMRI networks that were associated with decreases in structure-function coupling between MSN and fMRI networks.

5.3.6 Exploratory analysis of lifespan changes in morphometric similarity

It is of note that the adolescent changes in morphometric similarity reported in this chapter are less pronounced than the changes in functional connectivity identified in the same sample and reported in previous chapters. Considering the evidence for early development of global or regional measures of grey matter volume (Bethlehem et al., 2022), it is likely that structural brain networks, in absolute terms, change more strongly during the first decade of life compared to adolescence.

To situate adolescent changes in MSN more securely in the context of brain development over the course of the entire life-cycle, we conducted an exploratory analysis to investigate the timing of changes in MSNs. To this end, we combined datasets from all five available HCP Lifespan Projects, each of which includes multimodal MRI data acquired using highly similar scanning protocols, and which collectively cover the lifespan from preterm birth to old age: Developing Human Connectome Project (dHCP; N=1500; 20-44 weeks post-conception; Makropoulos et al. (2018)), Baby Connectome Project (BCP; N=500; 0-5 years; Howell et al. (2019)), Human Connectome Project Development (HCP-D; N=1350; 5-21 years; Somerville et al. (2018b)), Human Connectome Project (HCP; N=1200; 22-35 years; Glasser et al. (2013); Van Essen et al. (2013)), and Human Connectome Project Ageing (HCP-A; N=1200; 36-100 years; Bookheimer et al. (2019)). We adjusted these MRI data for between-site differences using ComBat (Fortin et al., 2018). We then binned the data, into one week age bins for preterm to term birth, into half year age bins before two years of age, and into one year age bins thereafter. Subsequently, we constructed group average MSNs for each age bin and estimated the pairwise correlation between average MSNs for all possible pairs of age bins. This preliminary analysis allowed us to highlight timepoints at which MSN change more rapidly in that the correlation between two adjacent age bins is lower compared to the correlation between age-adjacent MSN during other periods of life. These data confirm the prediction from whole life-cycle modeling of univariate global or regional metrics that MSN changes markedly in the first 5-6 years of development, and then undergo more gradual changes over the course of later life (**Fig. 5.18**). Despite between-study harmonization by ComBat, between-study differences remained visible in this analysis, as indicated by relatively abrupt changes in correlation between adjacent age bins when the MSN had been derived from data acquired in the different component studies. However, the changes in network organization associated with age were generally larger than the differences between MSN derived from different dataset, with largely gradual trends from one age bin to another. Thus this preliminary analysis of MSN development over the course of the entire life-cycle does provide some support for the hypothesis that structural networks are more extensively reconfigured in the first decade compared to the second decade of life.

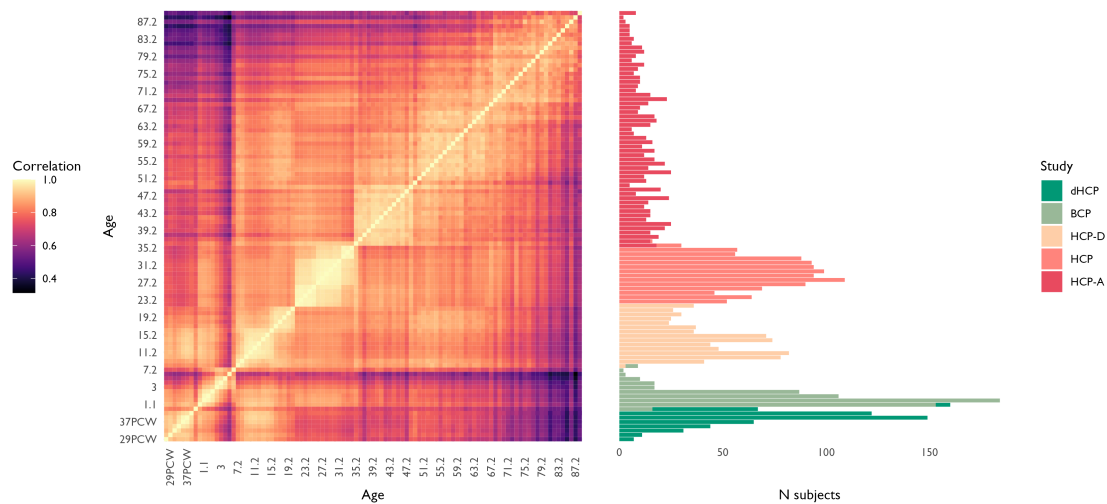


Fig. 5.18 Morphometric similarity network development over the life-cycle: Five HCP datasets were combined to cover the lifespan from preterm birth to old age, and harmonized using ComBat. The data were binned by age and group-level MSNs were estimated for each age bin before estimating the correlation between all pairwise combinations of age-binned MSNs over the course of the lifespan. Darker colours in the plot indicate a lower correlation of MSNs between age-related bins. On the right is shown the number of subjects per age bin, as well as the primary study in which they recruited.

5.4 Discussion

Here, we assessed adolescent changes in micro-structural and macro-structural features using structural MRI data on $N=298$ healthy adolescents, each scanned one to three times within a timespan of approximately one year, in a sex-balanced, age-stratified, accelerated longitudinal design. We found that (i) during adolescence, association and sensory cortical areas became more morphometrically dissimilar to the rest of the brain; (ii) increasing morphometric dissimilarity was a metabolically expensive process associated with increasing micro-structural metrics of myelination and decreasing macro-structural metrics such as cortical thickness and volume; (iii) regions that became more morphometrically dissimilar over the course of adolescence were co-located with regions that had increased diversity of functional connections as measured using the participation coefficient; and (iv) regions that become most morphometrically dissimilar during adolescence also showed the greatest decoupling between structural and functional connectivity over the same period.

Increases in myelination and decreases in cortical thickness are well-established developmental trends over the course of adolescence (Mills et al., 2016; Whitaker et al., 2016b).

Here, we assessed the related adolescent changes in micro-structural and macro-structural MRI features. As expected, we found increases in micro-structural metrics of myelination and decreases in macro-structural features, both globally and locally.

We used morphometric similarity networks to quantify adolescent changes in structural network configuration. This allowed us to quantify the complex interplay between micro- and macro-structural changes, or network reorganization, during adolescence. We found that association cortical regions tended to become more morphometrically dissimilar. We hypothesize that this increasing morphometric dissimilarity is an expression of the increasing cytoarchitectonic or myleoarchitectonic differentiation of these late-maturing cortical areas from the rest of the brain during adolescence. We found that this signature of age-related changes in morphometric similarity was related to a divergent profile of increases in univariate micro-structural metrics and decreases in univariate macro-structural metrics. Prior work using DWI has supported the idea that adolescence is a time of increasing network segregation, a process that sees targeted strengthening of network edges to support the development of executive function (Baum et al., 2017). We argue that the evidence of increasing morphometric dissimilarity shown here represents a similar process of cellular differentiation of association cortex to support emergence of “higher order” cognitive functions during adolescence.

In an exploratory analysis over the whole life-cycle, we contextualised these principal results on adolescent brain network development by demonstrating that age-binned average morphometric similarity networks change more markedly during early childhood, compared to the more incremental age-related changes witnessed thereafter. This finding helps us to explain the relatively less-extensive changes in structural connectivity observed in this chapter, compared to adolescent changes in functional connectivity reported in the same dataset in **Chapters 2-3**. On a related note, while we did observe sex differences in FC in **Chapters 2-3**, structurally, we only found widespread sex differences in GM in this chapter. Speculatively, sex differences in structural features may be less extensive, or, the timing of sexually different development in structure may not fall into adolescence, the period observed in this chapter. Future work is required to fully reconcile the two findings from these chapters.

We found that adolescent changes in MSN weighted degree were co-located with maps of metabolic rates for oxygen and glucose measured in adults. Regions that became more morphometrically dissimilar over the course of adolescence tended to have increased rates of glucose metabolism, aerobic glycolysis and oxidative metabolism. We hypothesize that the

protracted development of these regions throughout adolescence is associated with relatively increased metabolic demands.

We had hypothesized that changes in structural brain network development during adolescence might be associated with increasing diversity of functional connectivity. Indeed we found that adolescent increases in morphometric dissimilarity, hypothetically representing regional differentiation, were associated with increases in the participation coefficient of the same nodes in fMRI networks. We interpret this association to mean that regions that become structurally more differentiated during adolescence also diversify the topological profile of their functional interactions by becoming more connected to other nodes in different modules of the fMRI connectome (Yeo et al., 2015). It is assumed that regions that are morphometrically similar are more likely to be connected by white matter tracts (Seidlitz et al., 2018). On this assumption, increases in morphometric dissimilarity during adolescence would indicate a weakening of direct axonal connectivity between these regions and the rest of the brain, such that functional connectivity of these regions may rely more on polysynaptic (indirect) axonal connections or circuit-level modulation of neuronal activity (Baum et al., 2020).

Pursuing this hypothesis, we assessed whether the association between changes in morphometric similarity and functional participation was related to changes in structure-function coupling. Indeed, we found that during adolescence structural MRI-derived morphometric similarity networks became increasingly decoupled from fMRI derived functional connectivity networks. Locally, we found that regions that showed increased morphometric dissimilarity tended to have decreased structure-function coupling over the course of adolescence. Prior work has found decreases in global structure-function coupling over the course of adult life (Zamani Esfahlani et al., 2022). Our findings indicate that this process of structure-function decoupling may start earlier in life than previously reported and could be linked to local processes of cortical differentiation indexed by morphometric dissimilarity.

While we observed no significant correlation between adolescent changes in functional participation coefficient and changes in structure-function coupling, we did find that intra-individual changes in functional participation coefficient had a regionally varied association with intra-individual changes in coupling. We further observed that the regions in which decreased structure-coupling was associated with increased functional participation also had increased inter-individual age-related changes in morphometric similarity. We thus conclude that there is some evidence that developmental changes in cytoarchitectonic organization of late-maturing cortical areas, operationalized as increased morphometric dissimilarity, may contribute to adolescent changes in diversity of functional connections between different

modules of the functional connectome. However, further work is required to test this novel hypothesis and to assess its importance in explaining the emergence of “higher order”, more individualised cognitive functions during adolescence.

We estimated structure-function coupling between morphometric similarity networks and static resting state functional connectivity networks, because we were interested in how changes in the interplay between brain micro- and macro-structure were related to brain function. This stands in contrast to previous work on structure-function coupling, which has been focused on estimating how white matter architecture develops to support coordinated functional activity. Previous work has largely found strong structure–function coupling in primary sensory cortex and relatively weak structure-function coupling of transmodal or association cortical regions (Baum et al., 2020; Gu et al., 2021; Liu et al., 2022). When focusing on structural networks defined by inter-regional morphometric similarity, rather than white matter tracts, we see only partially overlapping results.

However, it is worth noting that a number of approaches to estimation of structure-function coupling have been suggested (Baum et al., 2020; Liu et al., 2022; Suárez et al., 2020; Zamani Esfahlani et al., 2022). Most published work has used diffusion-weighted MRI data to derive structural networks, either directly using tractography, or through graph theoretical analysis of the resulting connectomes (Baum et al., 2020; Zamani Esfahlani et al., 2022). Functional networks have been defined using resting state fMRI (Gu et al., 2021; Zamani Esfahlani et al., 2022), task-based fMRI (Baum et al., 2020), as well as dynamic fMRI data (Liu et al., 2022). These methodologically different approaches inevitably lead to only partially overlapping results across the literature. This methodological heterogeneity in analysis of structure-function coupling should be surveyed more systematically in further work so that future studies of developmental changes in structure-function coupling can proceed on a more secure methodological basis.

We conclude overall that during adolescence the complex anatomical network of the brain is reorganized in a metabolically expensive process that is consistent with increased cytoarchitectonic or myeloarchitectonic differentiation which is associated with age-related increases in the topological diversity of functional connections to these late-maturing cortical areas, and with increased independence (uncoupling) of functional and structural connectivity. This complex interplay between developmental changes in structural and functional network configuration is presumably relevant to the greater individualisation of higher-order cognitive functions that occurs over the same phase of development, and this important hypothesis emerging from these results will merit further, purposive investigation in future.

Chapter 6

Beyond human adolescence: lifespan trajectories

6.1 Introduction

The previous chapters have highlighted functional (**Chapter 2** and **Chapter 3**) and structural (**Chapter 5**) changes in human brain development during adolescence, demonstrating the extensive functional and structural reconfiguration the brain undergoes during this period of maturational development. However, adolescence is neither the only, nor the most fundamental, brain developmental period. Further, those chapters focused on group effects and no analysis was performed on subject-specific variability in development, largely due to the sample size of the datasets involved. This chapter aims to look beyond adolescence, focusing on normative lifespan structural development of the brain and subject-specific deviations from the norm.

Routine pediatric health assessments involve measuring a child's height and weight to reference them against normative "growth charts", allowing for early detection and intervention in cases of atypical development. Recent work (Bethlehem et al., 2022; Rutherford et al., 2022) has highlighted the potential of normative reference standards to quantify individual differences in neuroimaging metrics over the course of life. This work has produced interactive open resources to benchmark brain morphology derived from any current or future sample of magnetic resonance imaging (MRI) data, e.g., <http://www.brainchart.io/>. However, so far these resources only focus on global brain volumetric phenotypes (total grey matter volume, total white matter volume, total subcortical volume, and ventricular volume), and selected cortical regional phenotypes (grey matter volume, cortical thickness, surface

area) derived from structural magnetic resonance imaging (MRI). In this work, we extended the normative modeling approach to estimate non-linear trajectories of regional subcortical structural development for the first time over the entire life-cycle.

6.1.1 Normative modelling

Normative modelling aims to benchmark an individual against a reference model by charting (per)centiles of variation in the population and estimating an individual's deviation from these norms. Possibly the most well-known applications of normative models are the World Health Organization's (WHO's) growth charts for children's height and weight (Borghetti et al., 2006). There is a general understanding that child growth is a health and nutrition marker, thus estimating a child's individual trajectory of development compared to a population mean is internationally recognized as a highly informative measure of quality of early life.

The WHO's charts are constructed by pooling together data from various datasets. They typically show the development with age of a phenotype (i.e. height, weight, body-mass-index) for males and females separately in terms of (per)centiles, where a centile indicates the value below which a given percentage of observations in the population falls.

A successful normative model needs to overcome a number of challenges, including (i) pooling sufficient amounts of data over a number of primary studies, (ii) ensuring that the sample used is sufficiently diverse to represent the "norm", and (iii) harmonising across measurement instruments and data processing strategies. In the case of the WHO's height measurements, at least the latter issue is likely less of a concern, since height is comparatively simple to measure. In the field of neuroimaging, however, primary studies are conducted on a variety of scanners, and with different imaging protocols, as well as processed using a number of preprocessing tools, introducing significant "study-specific" or "batch effects".

6.1.2 Lifespan development of subcortical regions

Normative models have long attracted interest in the neuroimaging community (Sowell et al., 2003). More recently, the availability of several large-scale neuroimaging cohorts (Garavan et al., 2018; Somerville et al., 2018a; Sudlow et al., 2015; Van Essen et al., 2012), as well as an increasing number of openly shared datasets, has made it possible to aggregate multiple primary studies, thereby extending the age-range and sample size significantly (Bethlehem et al., 2022; Rutherford et al., 2022). However, while some studies have focused on normative subcortical development, "lifespan" models covering the subcortex have so far been limited

in the age range covered (Dima et al., 2022; Pomponio et al., 2020; Romero et al., 2021; Rutherford et al., 2022), likely due to the small number studies covering the prenatal and early infancy age range, and the lack of accessible, automated subcortical parcellation tools for infant brains that are comparable to adult processing pipeline outputs. Prior work has established early cortical development as a critical period (Gilmore et al., 2020) in which “developmental milestones” are reached (Bethlehem et al., 2022), thus emphasising the need for full lifespan models of subcortex.

6.1.3 Subcortical volume differences in atypical development

A key motivator in constructing normative reference models is to further our understanding of individual trajectories in health and disease across the lifespan. Traditionally, neuroimaging work has largely focused on group differences between patients and healthy controls. However, it is becoming increasingly clear that clinical diagnoses do not translate into easily detectable, clear group differences in neuroimaging measures. Rather, there appears to be normative variation in neuroimaging phenotypes that overlaps with disease-related variation. Further, when group mean differences are indeed detected, these may be driven by “extreme” examples in the patient group (Bethlehem et al., 2020).

Several psychiatric disorders have been associated with decreases in subcortical volume. Major depression, for example, has been associated with decreases in volume of the amygdala and hippocampus, compared to non-depressed controls (Stratmann et al., 2014). Similarly, schizophrenia has been associated with reduced grey matter volume in several subcortical regions, including the amygdala, thalamus, putamen and pallidum (Velakoulis et al., 2006). Further, the same regions have been shown to respond to treatment, i.e., there is evidence that treatment with antidepressants can lead to increased volume of the hippocampus and amygdala in depression (Frodl et al., 2008; Zhou et al., 2020), and treatment with antipsychotics has been associated with volume increases in the amygdala in schizophrenia (Ho et al., 2011). Also, there is some evidence that the length and severity of disease effects the magnitude of subcortical volumetric reductions, i.e., in major depressive disorder (MDD) amygdala and hippocampal volume has been shown to be more markedly reduced in patients with recurrent depressive episodes than in first-episode patients (Stratmann et al., 2014). Neurodegenerative diseases like Alzheimer’s disease (AD) have also been associated with decreases in hippocampal volume, with late mild cognitive impairment seen as a prodromal stage of AD, mirroring these results (Whitwell et al., 2007).

Taken together, this evidence for deviations in subcortical volume in disease highlights the potential value of benchmarking individuals against a normative trajectory of subcortical development, maturation and senescence.

6.2 Methods

6.2.1 Aggregated dataset

We aggregated data across 41 primary cross-sectional and longitudinal MRI imaging studies, covering an age range from mid gestation (180 days post conception), to 100 years (**Fig. 6.1**). Details of each individual study are compiled in **Appendix A.5**.

A | Aggregated Dataset

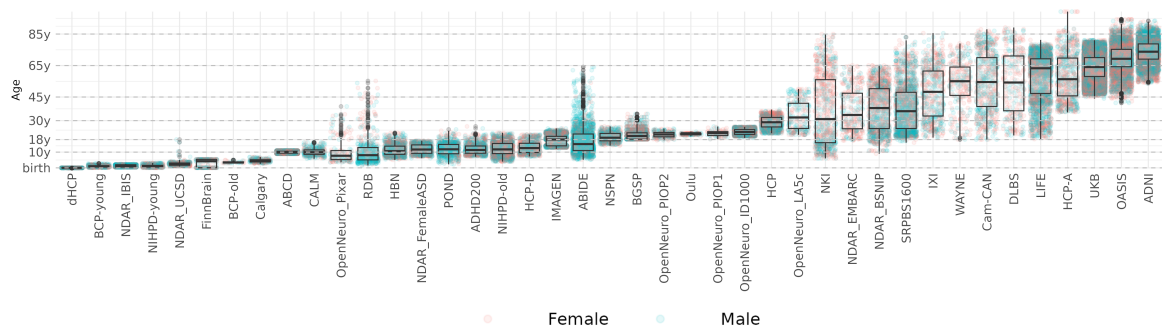
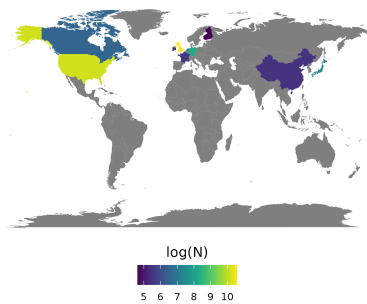


Fig. 6.1 Aggregated lifespan MRI dataset: We collected T1- and T2-weighted MRI data from 41 primary studies to form an aggregated dataset of 90,763 scans from 78,832 subjects that collectively spanned the age range from mid-gestation to 99 postnatal years. The box-plots show the age distribution for each study, with individual points colored by sex.

Previous work has defined major epochs of lifespan brain development, ranging from conception to old age (Kang et al., 2011). No neuroimaging data is available prior to about 16 post conception week (PCW), but our aggregated dataset includes scans from all developmental stages from 24 PCW (**Fig. 6.2B**): it includes 206 scans from the *late fetal* (24-38 PCW) stage, 1124 scans from *early infancy* (0-6 months), 1103 scans from *late infancy* (6 months - 1 year), 2784 scans from *early childhood* (1-6 years), 15073 scans from *mid to late childhood* (6-12 years), 8435 scans from *adolescence* (12-20 years), 10068 scans from *young adulthood* (20-40 years), 16575 scans from *mid adulthood* (40-60 years), and 35394 scans from *late adulthood* (older than 60 years). Notably, the ages <2 years, as well as the mid-life range from 25 to 50 years, spanning two developmental stages, are represented by comparatively few scans.

An ideal sample to estimate generalisable brain “growth charts” should be as representative of the world’s population as possible, and cover the entire lifespan. However, in general, the availability of neuroimaging studies is strongly biased for datasets from Western Europe and North America. This is reflected in our aggregated dataset, too (**Fig. 6.2A**). While we were able to aggregate data from 41 primary studies, these data were largely collected in the aforementioned regions. Only a subset of data were acquired outside these regions, in Japan and China, for example.

A | Country of study



B | Age distribution

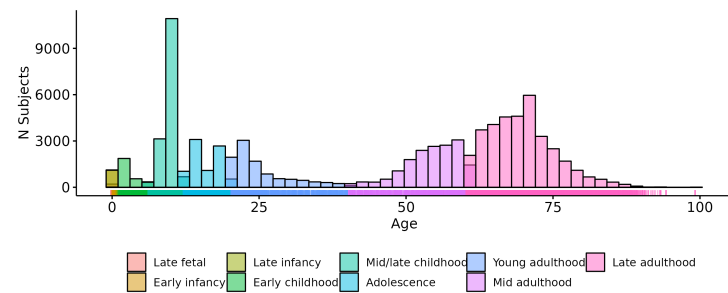


Fig. 6.2 Dataset demographics: (A) World map showing the number of subjects per country included in the aggregated dataset. (B) Histogram and density plot indicating the number of subjects by age. Further, the coloring indicates which developmental stage the subject falls into. Notably, the dataset includes fewer scans early in life, in the prenatal window until early childhood, as well as between 25 and 50 years of age.

6.2.2 MRI pre-processing

The primary studies included in this dataset ranged from openly available data, to data only shareable in derived format, i.e. regional volume values rather than raw imaging files. Whenever possible, the data were processed locally on the same server located at Cambridge, UK, with the most recent FreeSurfer version at the time. For this study, we were able to include a large number of studies originally pre-processed for a previous publication (Bethlehem et al., 2022) using FreeSurfer 6.0.142. However, Bethlehem et al. (2022) only aggregated the phenotypes used in their study, such that here, we went back to the original freesurfer output files where available to extract subcortical data from the *aseg.stats* files. We further added a number of new studies not included in the prior publication. For these newly added data, we used the most recent FreeSurfer version available, version 7.0.1. For Infant FreeSurfer we used version v1108.

Wherever T1- and T2/FLAIR-weighted raw images were available, these data were processed with FreeSurfer’s combined T1-T2 recon-all pipeline. If only raw T1-weighted

data were available, and subjects were aged over 2 years, the data were processed with a FreeSurfer standard recon-all pipeline. Lastly, if subjects were aged 0–2 years, data were processed with Infant FreeSurfer. An overview of FreeSurfer versions used for each dataset (and site) is provided in **Supplementary Table A.5**.

Briefly, the recon-all processing function includes the following steps: non-uniformity correction, projection to Talairach space, intensity normalisation, skull-stripping, automatic tissue and subcortical segmentation, surface interpolation, tessellation and registration.

Regional subcortical volume was estimated for each of 8 bilaterally averaged subcortical regions (thalamus, caudate, putamen, pallidum, hippocampus, amygdala, nucleus accumbens and ventral diencephalon), as well as the main sections of the corpus callosum (anterior, mid anterior, medial, mid posterior, posterior), and the cerebellum grey and white matter volume, defined by the aseg parcellation template following the final stages of the recon-all pipeline and using the “aseg.stats” files generated by FreeSurfer.

6.2.3 Lifespan trajectories

We used generalized additive models for location scale and shape (GAMLSS), a robust and flexible framework for modelling non-linear growth trajectories recommended by the World Health Organization (Borghini et al., 2006; Stasinopoulos and Rigby, 2008), to derive developmental curves from the aggregated life-spanning neuroimaging dataset (**Fig. 6.3**). This modelling strategy allowed us to estimate non-linear age-related trends (in median and variance) stratified by sex over the entire lifespan, and to account for site- or study-specific effects on MRI phenotypes in terms of multiple random effect parameters. To estimate these models, we used the code published by Bethlehem et al. (2022), which is available on github: <https://github.com/brainchart/Lifespan>.

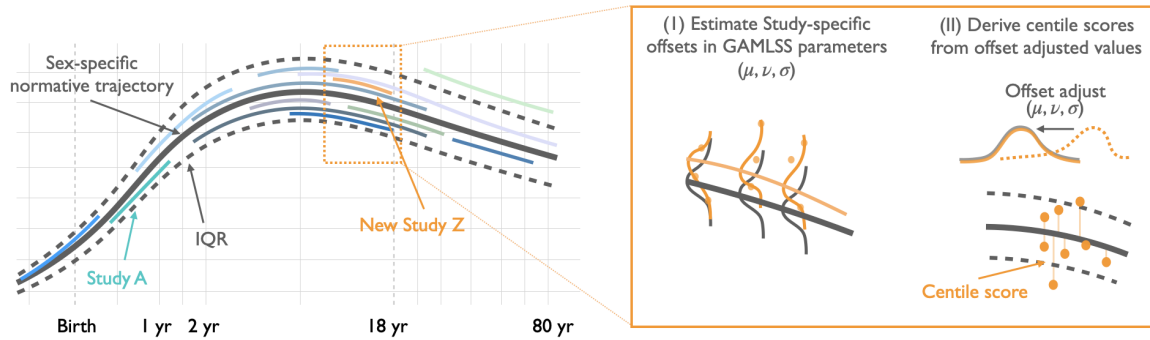


Fig. 6.3 **Normative modelling:** (*left*) We estimated normative trajectories of various imaging phenotypes as a non-linear function of age, stratified by sex, using GAMLSS models on an aggregated dataset of cross-sectional primary studies. This resulted in sex-specific lifespan trajectories of development of the median of each phenotype. (*right*) We controlled for study-specific offsets, or random effects, in the first two parameters of the underlying statistical distributions, μ , σ . After correction for these study-specific offsets, we can derive subject-specific centile scores, which measure an individual's deviation from the benchmark of the normative age- and sex-matched growth chart.

6.2.4 GAMLSS models

GAMLSS is a class of regression models where all the parameters of the outcome distribution can be modelled as additive functions of the explanatory variables. A strong asset of GAMLSS models is that they allow modeling not only of the central tendency of the outcome distribution (Y), but also other parameters of the distribution of Y , as linear, nonlinear, parametric, or additive non-parametric functions of explanatory variables and random effects. Prior evidence suggests that brain phenotypes do not only vary in mean, but also in variance across the lifespan. With GAMLSS we chose a modelling framework that could account for variation with age in the first (mean) and second (variance) moment of the outcome distributions. Further, GAMLSS models allow for the distribution of the response variable to be drawn from a general family of distributions which includes, among others, skewed and kurtotic continuous and discrete distributions.

In the GAMLSS framework, the outcome vector Y , consisting of independent observations $y_1, y_2, y_3, \dots, y_N$, follows the probability distribution F , with:

$$F \sim F(\mu, \sigma, \nu, \tau) \quad (6.1)$$

where F is parameterised by typically up to four distribution parameters (μ, σ, ν, τ). These parameters can correspond to the mean, variance, skewness, and kurtosis of the outcome distribution, i.e. the first four moments. However, for many distributions there is no direct mapping between the parameters and the moments of the distribution.

More specifically, each of these components, k , is defined in terms of a link-function g_k , i.e. a regression on potential covariates. Importantly, the covariates do not have to be the same between the parameters and in fact parameters can reduce to constants, a fact that becomes relevant further below. The link function, g_k , thus includes includes N_k fixed effects, parametrised by their coefficients $\beta_k = (\beta_{k,1}, \beta_{k,2}, \dots, \beta_{k,J_k})$, and their design matrix, X_k ; random effects, γ_k , with design matrix Z_k ; and non-parametric smoothing functions $s_{k,i}$ applied to the i th covariate for each parameter, with $i = 1, 2, \dots, N_k$:

$$g_\mu(\mu) = X_\mu \beta_\mu + Z_\mu \gamma_\mu + \sum_{i=1}^{N_\mu} s_{\mu,i}(x_i) \quad (6.2)$$

$$g_\sigma(\sigma) = X_\sigma \beta_\sigma + Z_\sigma \gamma_\sigma + \sum_{i=1}^{N_\sigma} s_{\sigma,i}(x_i) \quad (6.3)$$

$$g_\nu(\nu) = X_\nu \beta_\nu + Z_\nu \gamma_\nu + \sum_{i=1}^{N_\nu} s_{\nu,i}(x_i) \quad (6.4)$$

$$g_\tau(\tau) = X_\tau \beta_\tau + Z_\tau \gamma_\tau + \sum_{i=1}^{N_\tau} s_{\tau,i}(x_i) \quad (6.5)$$

The outcome distribution determines the appropriate link function and which parameters (i.e. how many) are modelled. Bethlehem et al. (2022) optimised GAMLSS model specification and parameterization to estimate non-linear normative growth trajectories of lifespan brain structural development and determined that the generalized gamma distribution appropriately models their data using a model comparison approach. Here, we use a largely overlapping sample on similar phenotypes, thus we also model a generalized gamma distribution.

We used fractional polynomials to model age-related changes in MRI phenotypes. Using the alternative, non-parametric smoothers (i.e. smoothing splines), would have been more flexible, but also more unstable. Within the GAMLSS framework the appropriate power of the fractional polynomials is chosen in an iterative fitting process across the “standard” set of powers, $p \in \{-2, -1, -0.5, 0, 0.5, 1, 2, 3\}$.

We estimated GAMLSS models to derive trajectories of subcortical volume development. Briefly, in a sex-stratified approach, we estimated lifespan development in the first order (μ) and second order (σ) distributional parameters of brain phenotypes using GAMLSS with fixed effects of age and pre-processing pipeline, and a random effect of study, using fractional polynomials to model non-linear age-related trends.

We modeled the effect of study as a random effect, as opposed to a fixed effect. These random effects are assumed to follow a normal distribution with mean zero and a variance term. We chose to use the simple case of random intercept, i.e. a group-level intercept. The advantage of this procedure is that we can estimate the (random) effect of a new study, i.e., a study that is not included in the original dataset used to fit the normative growth chart, from the random-effect covariance structure.

The third distributional parameter, ν , was only modeled as a constant, since previous work using GAMLSS models to estimate lifespan trajectories (Bethlehem et al., 2022), found that including age, sex and study parameters for this term lead to numerical instability. Since we have no *a priori* reason to assume age-dependent or random effects on skewness in subcortical volume, we chose not to model lifespan changes in this parameter. This means that **Equation 6.4** reduces to:

$$\nu = \alpha_\nu \tag{6.6}$$

All trajectories fitted here are represented in terms of centile scores rather than the outcome measures directly, or Z-scores. The reasoning behind this is that GAMLSS models allow for the outcome distribution to be highly skewed, in which case Z-scoring is invalid. For clarity, it is worth emphasizing that while the GAMLSS parameters can map to the moments of the outcome distribution, this depends on the specific distribution that is used. In the case of the generalized gamma distribution used here, the distributional parameters (μ, σ, ν) do not directly map to the mean, variance and skewness of the distribution. Thus, while as specified in **Equation 6.4** ν does not change with age, the skewness of the outcome distribution can. All trajectories shown are the median (50th percentile) of the distribution of normative trajectories.

6.2.5 Developmental milestones

We defined key developmental milestones by estimating the peaks of the modelled trajectories, as well as the peak rates-of-change for each subcortical structure. The peak grey or

white matter volume was determined as the peak of the median trajectory of each regional subcortical phenotype. The peak rate-of-change, or velocity, was estimated as the peak of the first derivative of each normative median trajectory. We further estimated bootstrap confidence intervals around these measures by estimating the derivatives of the bootstrapped curves, as described below.

6.2.6 Centile score estimation

We obtained the relative distance of each individual's observation from the normative trajectory of each brain phenotype, as the relative distance from the median of the age-normed distributions of the reference model, stratified by sex. This distance is termed "centile" and describes the percentage rank of the individual's brain phenotype measurement benchmarked by the normative distribution of the corresponding phenotype. More specifically, we derived the study-specific centile q_i for an individual's observation, i , as:

$$q_i = F'(y, x | \beta, z) \quad (6.7)$$

where F' is the inverse cumulative density function of (**Equation 6.1**) of a brain phenotype, β are the coefficients of the fixed effects, z is the random effect of study, x are the individual's covariates, and y is the outcome measure, i.e., the brain MRI phenotype.

6.2.7 Case-control differences in centile scores

Using the centile scores derived above, we estimated deviations from normative development in healthy controls (CNs) in multiple psychiatric and developmental disorders.

To this end, the aggregated dataset included a total of 17,406 subjects with diagnoses of mental health or developmental disorders (**Table 6.1**). In order to ensure an increased level of certainty in our results, we chose to only focus on "large" patient groups, which we defined as including 400 or more cases. These were: Alzheimer's disease (AD; 1200 subjects, 49-94 years), attention deficit hyperactivity disorder (ADHD; 879 subjects, 5-57 years), anxiety/phobia (ANX; 1741 subjects, 7-64 years), autism spectrum disorder (ASD; 2376 subjects, 0-79 years), mild cognitive impairment (MCI; 565 subjects, 54-91 years), major depressive disorder (MDD; 4965 subjects, 10-81 years), schizophrenia and other developmental disorders (SCZ; 449 subjects, 9-70 years). A total of 4089 (0-93 years) subjects had been diagnosed with a range of other disorders, none of which included more

than 400 subjects. These diagnoses have been grouped together as “other” and were not included in further analyses.

Diagnosis	Sex	#Subjects	Age_{min}	Age_{max}	μ Age
AD	Female	514	49.27	94.30	74.13
AD	Male	506	55.17	89.59	74.72
ADHD	Female	228	5.06	50.03	12.67
ADHD	Male	651	5.41	57.04	12.10
ANX	Female	1127	7.11	80.05	63.00
ANX	Male	614	6.81	80.05	63.56
ASD	Female	469	0.47	79.05	12.03
ASD	Male	1907	0.47	76.05	14.10
CN	Female	30863	-0.21	99.24	43.07
CN	Male	30554	-0.21	99.24	43.11
MCI	Female	220	54.27	87.69	72.10
MCI	Male	345	53.67	90.69	74.07
MDD	Female	3219	10.37	81.05	59.41
MDD	Male	1746	15.54	81.05	60.24
Other	Female	2202	0.47	92.30	50.47
Other	Male	1887	0.47	93.30	44.73
Other Developmental	Female	434	9.01	10.93	9.95
Other Developmental	Male	888	9.01	10.93	10.01
SCZ	Female	166	10.59	70.05	39.03
SCZ	Male	283	9.43	77.05	34.86

Table 6.1 **Subject numbers for diagnostic groups of cases and controls:** Here, stratified by sex, we list the number of subjects, the group minimum (Age_{min}), maximum (Age_{max}) and mean (μ Age) age in years for each diagnostic group that includes more than 400 cases in the sample. Diagnostic groups including less than 400 subjects were deemed too small for stable centile-score group difference estimations and are summarized as “Other”.

We estimated differences in centile scores between healthy controls and patients using a bootstrapped (500 bootstraps) non-parametric generalization of Welch’s one-way analysis of variance (ANOVA). We then conducted post-hoc comparisons for all case-control combinations using a non-parametric Monte Carlo permutation test with 10,000 permutations. The results were corrected for multiple comparisons using FDR correction. Lastly, we estimated effect sizes of the case-control differences using Cohen’s d .

6.2.8 Quality control

Given the very large number of scans in this aggregated dataset, we did not perform manual quality control of each individual scan. Rather, we estimated the Euler index (EI) for each scan as a measure of image quality. The EI is an automated, quantitative measure of data quality in scans processed by FreeSurfer and as such is only available for FreeSurfer processed data. It measures the number of “surface holes”, or topological defects, in the cortical surface reconstruction, across hemispheres prior to correction. More specifically, surface holes are regions on the surface mesh where there are missing or disconnected vertices, resulting in gaps in the surface for example as a result of image artifacts, or partial volume effects. This work focuses on volumetric measures which are likely less affected by surface holes, however the EI has previously been used as a general measure of raw scan quality, which is how we have used it here. Previous work has provided evidence that there likely is no single EI threshold that is generalizable as a valid criterion of image quality across studies (Rosen et al., 2018).

First, we assessed the potential relationship between age and image quality. Specifically, in a sex-stratified approach, we estimated the linear effect of age on EI using linear mixed effects models with a random effect of study:

$$EI \sim 1 + \beta_{age} * age + \beta_{sex} * sex + \gamma_{study} * (1|study) + \varepsilon \quad (6.8)$$

where EI is the Euler index for a given subject, β refers to the coefficients for the fixed effects, $\gamma_{subject}$ refers to the coefficients for random effects, and ε represents the residual error.

Secondly, we estimated the effects of image quality on model-derived centile scores. In a sex-stratified approach, for each study, we estimated the Spearman correlation between the subject-specific centile scores and the EI.

6.2.9 Leave-one-study-out

Despite the size of the aggregated dataset used in this study - to the best of our knowledge, its size is second only to the dataset used by (Bethlehem et al., 2022) - concerns could be raised about the fact that a large proportion of the data is derived from two cohorts: the UK Biobank (UKB) (Sudlow et al., 2015), and the adolescent brain cognitive development study (ABCD) (Garavan et al., 2018). Thus in an effort to demonstrate the reliability of the derived

normative development curves, i.e. to estimate their dependence on individual datasets, we performed a leave-one-study-out (LOSO) jackknife analysis. Specifically, we re-estimated all trajectories while leaving out each study in turn. A direct comparison of the individual LOSO models to another is impeded by the fact that each of the models, by definition, is derived from different data. Thus model comparison techniques like Bayesian information criterion (BIC) are not of use in this case. Therefore, we estimated the consistency of the model fit across leave-one-out-iterations by estimating the standard deviation across all iterations to derive confidence intervals. From the bootstrap distribution for each parameter, we can derive its confidence interval as the ± 1.96 the standard deviation of the distribution.

6.2.10 Bootstrap analyses

In an effort to evaluate the reliability and stability of the derived lifespan trajectories, we estimated confidence intervals around all parameters by a bootstrap procedure. More specifically, we randomly resampled with replacement 1,000 times and re-estimated the lifespan trajectories for each regional phenotype. Each of these bootstrap iterations was restrained to ensure a random dataset that was comparable to our original dataset in terms of the sex distribution, the age distribution, and the relative size of the original primary studies. Retaining the relative proportions of males and females in the resampled dataset is relevant, since we stratified our original models by sex, i.e. we included sex as a fixed effect. Our original models included a random effect of study. In order to derive bootstrap confidence intervals around this study parameter, we constrained the resampling to retain the original age distribution and study size. Failing to constrain the resampling to consider study size could lead to individual studies being omitted in some iterations, and otherwise skew the bootstrap value, leading to inappropriate comparisons between original and bootstrap values.

6.3 Results

6.3.1 Lifespan development of subcortical structures

First, we used GAMLSS models to estimate lifespan development trajectories of bilateral volume of eight subcortical structures: the thalamus, caudate, putamen, pallidum, hippocampus, amygdala, accumbens and ventral diencephalon. The full models are listed in **Appendix C.2**. We found that, in general, volume of all subcortical structures increases from mid gestation and peaks during adolescence in most regions (**Fig. 6.4B**), with the thalamus peaking at

17.9 years ($CI_{bootstrap}$ 17.4-18.3 years), the caudate at 9 years ($CI_{bootstrap}$ 8.8-9.0 years), the putamen at 12 years ($CI_{bootstrap}$ 11.8-12.1 years), the pallidum at 18.4 years ($CI_{bootstrap}$ 17.9-18.4 years), the hippocampus at 19.2 years ($CI_{bootstrap}$ 19.0-19.4 years), the amygdala at 18.3 years ($CI_{bootstrap}$ 17.7-18.6 years), and the ventral diencephalon at 27.1 years ($CI_{bootstrap}$ 26.9-28.3 years). The nucleus accumbens forms an exception to these trends described above, peaking at 0.1 years ($CI_{bootstrap}$ 0.2-0.3 years). Visual inspection of the models compared to the raw data suggested a poor model fit in the nucleus accumbens and ventral DC below one year of age. We suggest this is due to the fact that these two regions were not included in one of the early-life datasets, leading to great model uncertainty at those ages. However, the trajectories appear to fit well after one year of age, and the age at peak volume for the ventral DC appears unaffected. Thus here, we continue to report on down-stream analyses in these models.

Next, we estimated the peak rate-of-change in volume for those same structures. We found that the developmental rate-of-change tended to peak in early infancy (**Fig. 6.4D**). Specifically, the thalamus peaked at 0.9 years ($CI_{bootstrap}$ -0.2-1.0 years), the caudate peaked at 0.9 years ($CI_{bootstrap}$ 0.9-0.9 years), the putamen at 0.6 years ($CI_{bootstrap}$ 0.6-0.7 years), the pallidum at 1.3 years ($CI_{bootstrap}$ 1.2-1.3 years), the hippocampus at 1.7 years ($CI_{bootstrap}$ 1.6-1.7 years), the amygdala at 1.8 years ($CI_{bootstrap}$ 1.7-1.9 years), and the nucleus accumbens at 0.1 years ($CI_{bootstrap}$ 0.1-14.2 years). Notably, the caudate displayed a second inflection point, with the rate of change increasing in late life (**Fig. 6.4D**).

We explicitly modeled lifespan development of normative variance, or between-subject variability, in subcortical phenotypes using GAMLSS models. In general, the normative variance tended to increase from mid gestation. Notably, in the hippocampus, pallidum, caudate and putamen, the variance increased into late life, with caudate and putamen having a second period of strong increases in variance in late adulthood, after a peak in adolescence. Further, we found that males consistently demonstrated higher variance than females across all subcortical regions.

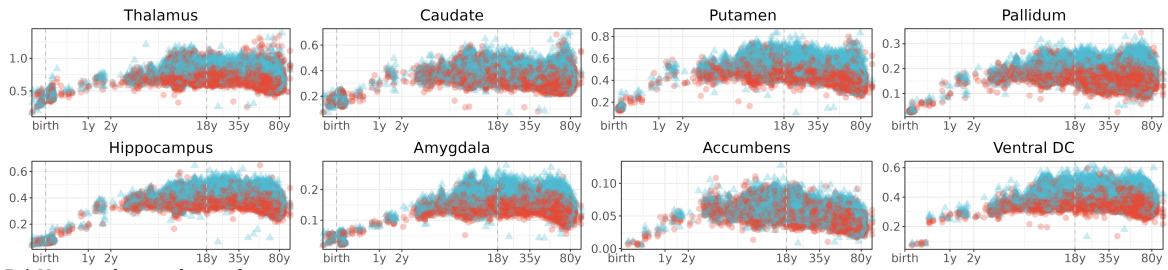
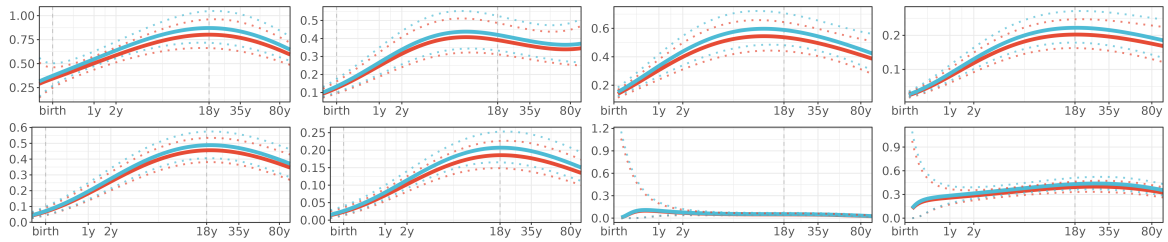
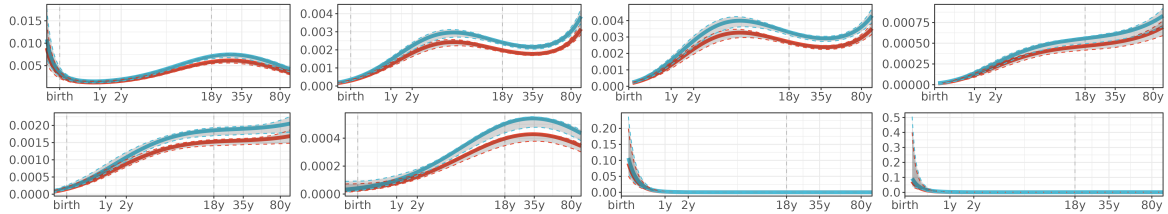
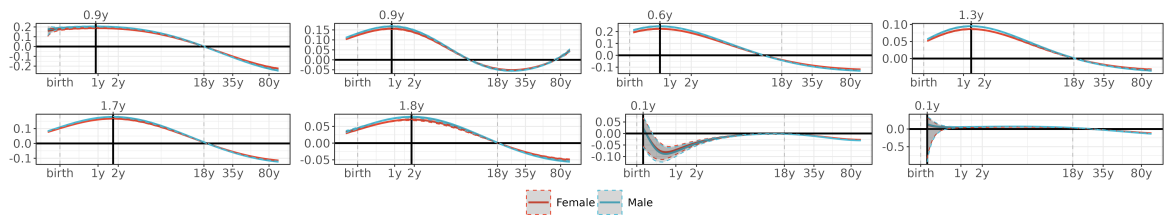
A | Cerebrum tissue volumes**B | Normative trajectories****C | Normative variance****D | Normative rate-of-growth**

Fig. 6.4 Lifespan development of subcortical structures: (A) First, we show the non-centiled, “raw” bilateral subcortical volumes for each structure (thalamus, caudate, putamen, pallidum, hippocampus, amygdala, nucleus accumbens, ventral diencephalon) plotted for each cross-sectional control scan as a function of age (log-scaled). Sex is shown by the colour of the points. (B) We estimated normative trajectories of subcortical volume using GAMLSS, stratified by sex, with site- and study-specific batch effects. Non-linear trajectories of the median volume of all the structures (with 2.5% and 97.5% centiles denoted as dotted lines) are shown as a function of age. (C) We estimated trajectories of median between-subject variability, with the 95% confidence intervals estimated by sex-stratified bootstrapping. (D) We estimated rates of change in subcortical tissue volume across the lifespan, stratified by sex, as the first derivatives of the median volumetric trajectories. The points at which this derivative cross the horizontal line ($y = 0$), indicate the age at which the subcortical structure stops growing and starts shrinking, i.e., its peak volume, whereas the age of maximum growth is indicated as a vertical line ($x = 0$) for each tissue.

6.3.2 Lifespan cerebellar and corpus callosum development

We estimated lifespan trajectories of white matter volume in the sections of the corpus callosum, the grey matter volume in the cerebellar cortex, as well as the volume of the cerebellar white matter (**Fig. 6.5B**).

From these lifespan trajectories, we estimated the peak volume of each structure (**Fig. 6.5C**). We found that the volume of the corpus callosum generally peaked in early to mid adulthood. Specifically, the volume peaked at 42.7 years ($CI_{bootstrap}$ 41.4-43.5 y) in the posterior section, at 31.6 years ($CI_{bootstrap}$ 31.3 - 31.7 y) in the mid posterior section, at 24.1 years ($CI_{bootstrap}$ 24.2-24.6 y) in the central section, at 26.2 years ($CI_{bootstrap}$ 26.1-26.4 y) in the mid anterior section, and at 33.2 years ($CI_{bootstrap}$ 32.4-33.4 y) in the anterior section. The cerebellum cortical volume peaked at 12.9 years ($CI_{bootstrap}$ 12.6-13.5 y), whereas the cerebellum white matter volume peaked at 28.3 years ($CI_{bootstrap}$ 27.4-28.2 y).

We further estimated the peak rate-of-growth in volume for each structure. We found that the rate-of-growth in the posterior corpus callosum peaked at 8.2 years ($CI_{bootstrap}$ 6.8-8.8 y), in the mid posterior corpus callosum it peaked at 12.4 years ($CI_{bootstrap}$ 12.4-12.9 y), at 8.6 years in the central corpus callosum ($CI_{bootstrap}$ 7.3-9.5 y), at 10.3 years in the mid anterior corpus callosum ($CI_{bootstrap}$ 9.1-11.1 y), at 13.5 years in the anterior corpus callosum ($CI_{bootstrap}$ 13.5-13.6 y), at 0.4 years in the cerebellar cortex ($CI_{bootstrap}$ 0.3-0.5 y) and at 8.7 years in the cerebellar white matter ($CI_{bootstrap}$ 7.7-9.8 y).

As was the case in the prior analysis of subcortical grey matter volume, we found that between-subject variance of white matter volumes was higher in males compared to females in most regions.

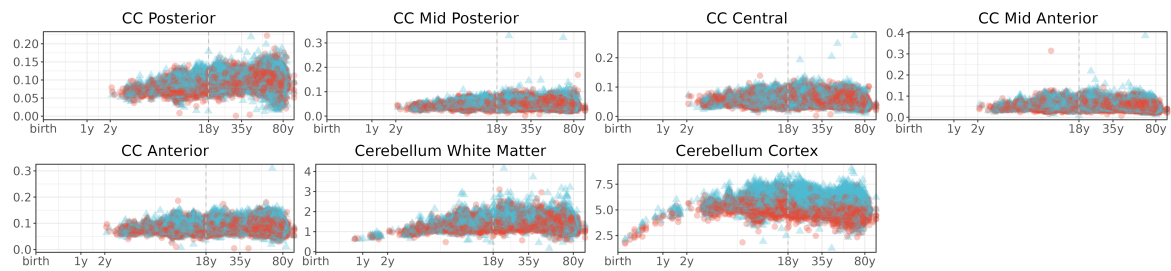
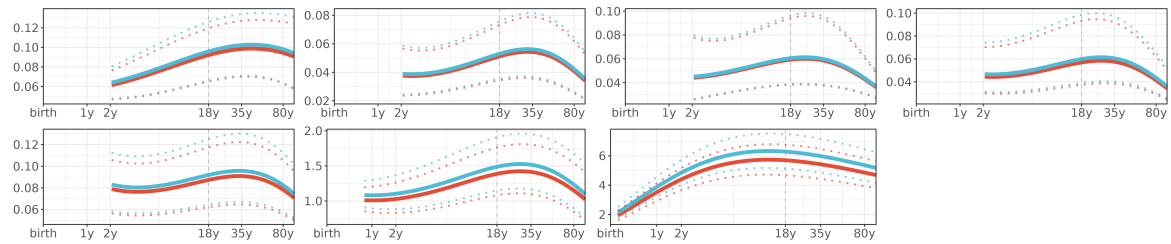
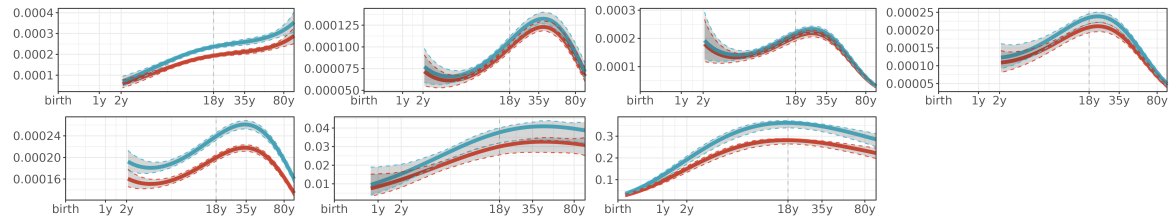
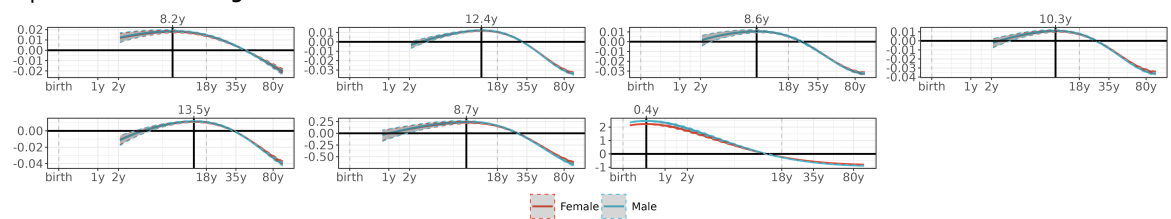
A | Tissue volumes**B | Normative trajectories****C | Normative variance****D | Normative rate-of-growth**

Fig. 6.5 Lifespan development of cerebellum and corpus callosum: (A) First, we show the non-centiled, “raw” grey and white matter volumes of unilateral white matter tracts (corpus callosum) and bilateral (cerebellum) subcortical structures, plotted for each cross-sectional control scan as a function of age (log-scaled). Sex is shown by the colour of the points. (B) We estimated normative trajectories of median GM or WM volume using GAMLSS, stratified by sex, with site- and study-specific batch effects. Non-linear trajectories of the median volume for each structure are shown as a function of age (with 2.5% and 97.5% centiles denoted as dotted lines). (C) We estimated trajectories of median between-subject variability, with the 95% confidence intervals estimated by sex-stratified bootstrapping. (D) We estimated rates of change in subcortical tissue volume across the lifespan, stratified by sex, as the first derivatives of the median volumetric trajectories. The point at which each derivative crosses the horizontal line ($y = 0$), indicates the age at which the corresponding subcortical structure stops growing and starts shrinking, i.e., the age of its peak volume, whereas the age of maximum growth is indicated as a vertical line ($x = 0$) for each subcortical structure.

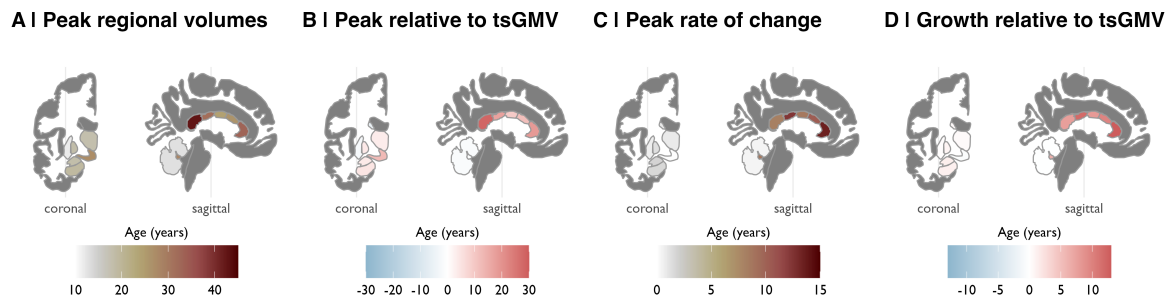


Fig. 6.6 Developmental milestones: Maps of developmental milestones for bilaterally averaged subcortical structures. (A) Map of subcortical regional peak volumes in grey matter and white matter, respectively. Apart from one outlier due to poor model fit (nucleus accumbens), these values ranged from 12 (putamen) to 42 years (cerebellar white matter). (B) Subcortical map of the difference in years between the regional peak volume and the respective peak of the global measure: total subcortical grey matter volume (tsGMV) and total white matter volume (tWMV). This map highlights regions that peak earlier (blue) or later (red) than the respective global volume phenotype. (C) Subcortical map of regional peaks in the rate-of-change in volume, i.e. the inflection points of the first derivative of the normative trajectory in volumetric growth for each region. (D) Difference in years between the peak regional rate-of-change and the respective peak global rate-of-change.

We compared the developmental milestones derived above, i.e., the ages at which the peak volume (**Fig. 6.6A**) and the peak rate-of-change (**Fig. 6.6C**) were reached, to the equivalent milestones derived from the respective global phenotypes: total white matter volume (tWM) for the cerebellar white matter, and total subcortical volume for all others (**Fig. 6.6B,D**; Bethlehem et al. (2022)). We found that there was an inner-outer gradient of age of peak volume in subcortex, whereby the putamen peaks early on, with the pallidum peaking at an intermediate age, and the thalamus peaking last (**Fig. 6.6B**). Further, we observed a near-perfect antero-posterior gradient across the corpus callosum, with the posterior section forming an exception. The peak rate-of-change followed the same antero-posterior trend as the peak age (**Fig. 6.6D**).

6.3.3 Sensitivity of results to image quality

This aggregated dataset included data from across the entire lifespan, it was acquired on a variety of scanners in many locations, and included data from multiple disorders. All of these factors contribute to the image quality varying between subjects. We therefore carefully assessed the effect of image quality, as estimated by the Euler index, on our results.

First, we examined the relationship between age and image quality (**Fig. 6.7**) using linear mixed effects models. We found that, in general, younger cohorts tended to have worse image quality ($P < 0.01; t = 18$; **Fig. 6.7**).

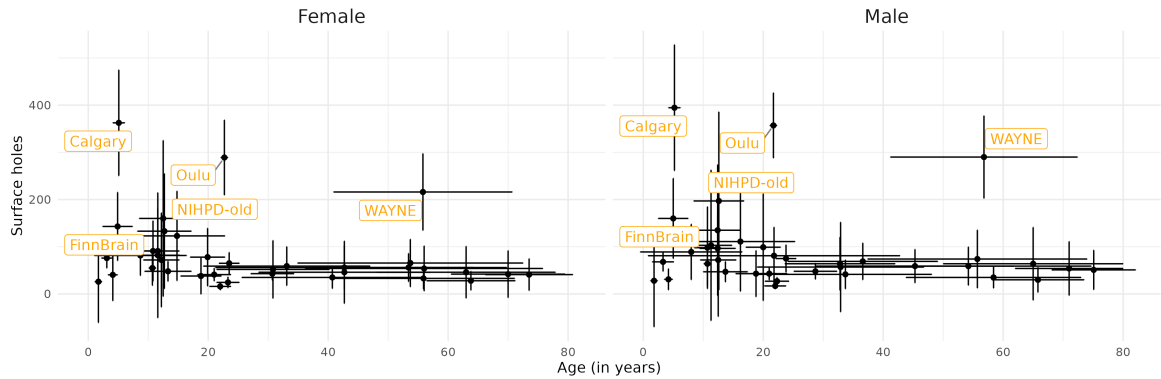


Fig. 6.7 Age-related variation in image quality: We measured image quality as the EI for each scan. Here, we show the relationship between median age and median Euler Index by study. Crosshairs indicate the standard deviations of both measures. We highlight the 10 studies with the highest ranking median Euler Index. We found cohorts with younger median age at scanning tended to have worse image quality ($P < 0.01; t = 18$).

Next, we estimated the effect of data quality on an individual's deviation from the norm, i.e. the relationship between centile scores and EI. Here, we show an illustrative example of the relationship between centile scores and EI in the thalamus (**Fig. 6.8A**). We found that the Spearman correlation between subjects' centile scores (stratified by sex) and their EI scores was statistically significant ($P < 0.05$), but negligible, i.e. for all regions $|\rho| < 0.08$ (**Fig. 6.8B**).

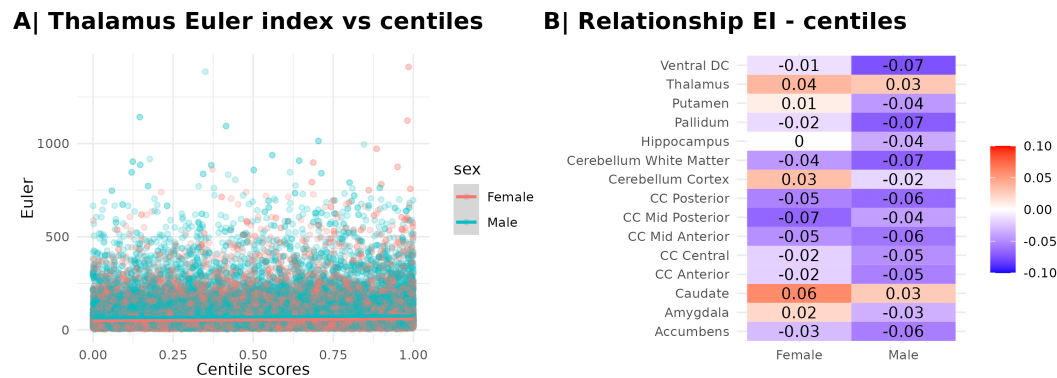


Fig. 6.8 Associations between centile scores and MRI scan quality defined by EI: (A) We estimated the Spearman correlation between centile scores (stratified by sex) and Euler index, illustrated here by the thalamus. (B) These relationships between subcortical centile scores and EI were statistically significant ($P < 0.05$), but materially negligible, i.e., for all regions $|\rho| \leq 0.06$.

6.3.4 Sensitivity of trajectories to specific studies

We tested for the sensitivity of the normative trajectories of subcortical brain development to inclusion/exclusion of specific studies using a permutation approach. We systematically re-estimated the normative developmental curves while leaving one study out. This procedure resulted in the models being estimated from different datasets in each iteration, thus direct quantitative comparison between the models using for example Akaike information criterion (AIC) or BIC is not possible. Instead, we derived confidence intervals around the original model by estimating the standard deviation across leave-one-study-out iterations. We found that these confidence intervals were so small that they were difficult to discern when overlaid on the original model (**Fig. 6.9A**). Magnifying the confidence intervals 50-fold demonstrated that they followed the original model very closely, with a tendency for stronger deviations in early age (**Fig. 6.9B**). In particular, we found the confidence intervals were larger for the age range below 1 postnatal year in the nucleus accumbens and ventral diencephalon. The increased confidence intervals around these two regions are likely related to the issue mentioned above, where one study does not have estimates for these two features, thus when removing further studies, the amount of data in the younger age range may not be enough to reliably estimate models.

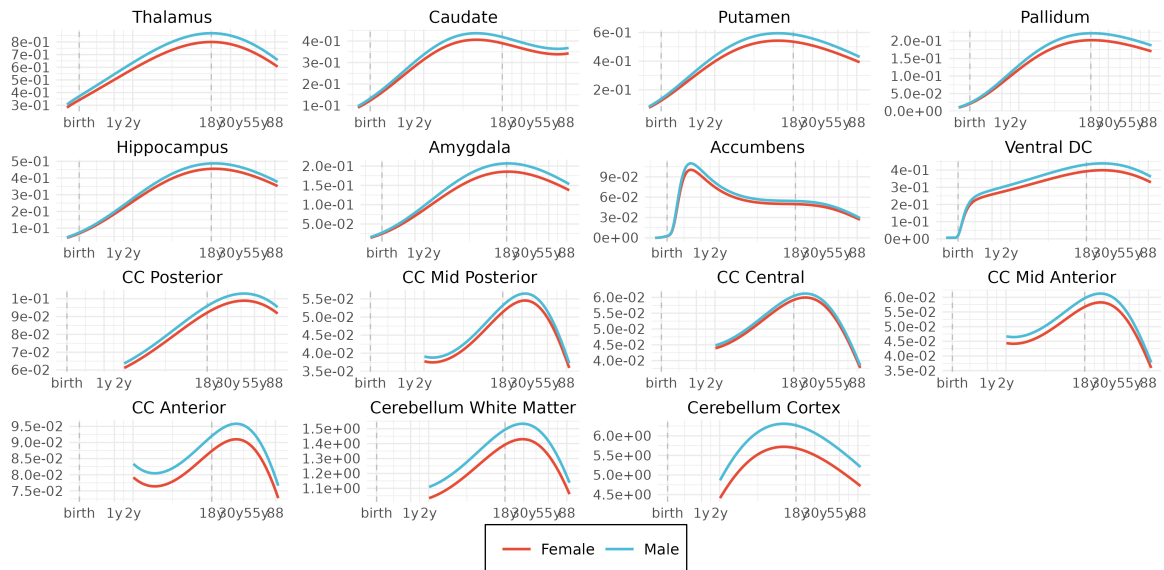
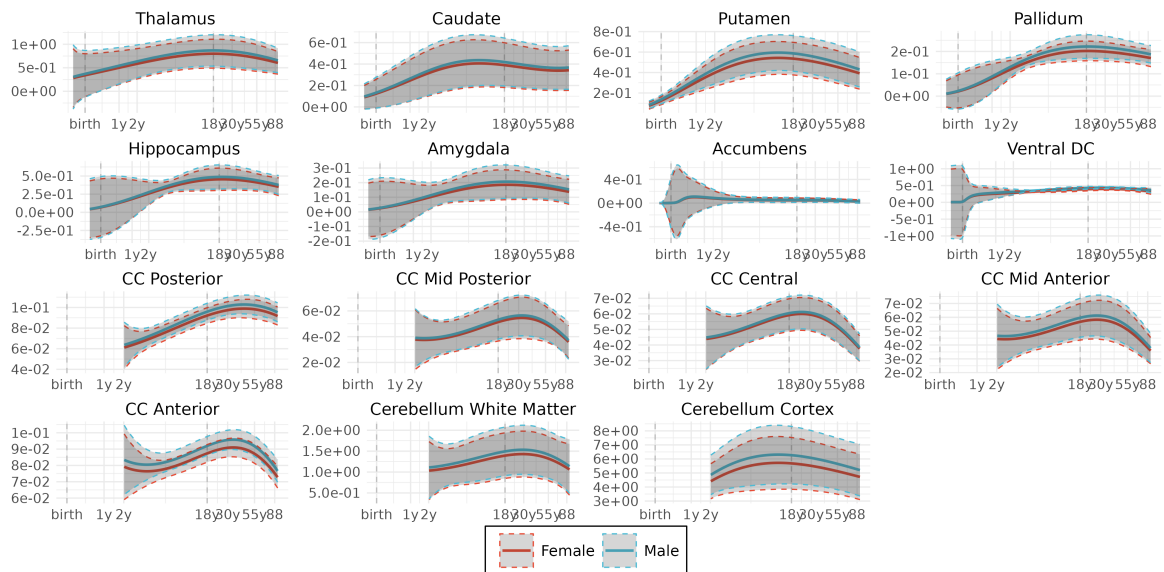
A| Leave-one-study-out with CI**B| Leave-one-study-out with CI x50**

Fig. 6.9 Leave-one-study-out sensitivity analysis: (A) We estimated 95% confidence intervals around the normative trajectories estimated by the original model after leaving out (excluding from analysis) each primary study in turn. Confidence intervals were estimated from the mean and the standard deviation of the resulting distribution of leave-one-out trajectories. (B) Here, we show the same data as above, however we have magnified the confidence intervals 50-fold in order to enhance their visibility.

6.3.5 Bootstrapping studies of reliability and stability

In order to assess the reliability and stability of the fitted normative trajectories, and to obtain confidence intervals on all parameter estimates obtained from the GAMLSS fitting procedure, we ran 1,000 bootstrap iterations, resampling our data with replacement. These bootstrap iterations were stratified by sex and study size, thus retaining approximately the same distribution of study size and age range in each of the bootstrapped resamples as in the original sample from the aggregated dataset.

Further, we derived bootstrap confidence intervals around the study-specific random effects, i.e., the first (μ) and second (σ) parameters of the gamma distribution. This analysis addressed the question of whether empirically derived parameters were more extreme than expected by chance, given the size and sex-balance of each study. Visual inspection of point-range plots of the bootstrapped study-specific random effects on regional subcortical volumes indicated that all study-specific offsets were well within their bootstrapped confidence intervals. In general, the confidence intervals around the σ -parameters were larger than around the μ -parameters **Fig. 6.10**.

6.3.6 Case-control differences in subcortical volumes

We estimated changes in centiled subcortical volume in psychiatric disorders, benchmarked appropriately against normative trends in subcortical volume development. We found that each disorder showed significant case-control differences (Cohen's d , d) in centile scores for at least a few subcortical regions (**Fig. 6.11**). Notably, AD was associated with decreased subcortical volume (blue) across all subcortical structures, with a particularly strong effect in the hippocampus ($d_{female} = -1.2$; $d_{male} = -1.2$) and amygdala ($d_{female} = -1.2$; $d_{male} = -1.1$). We observed a very similar, but less strong, pattern of case-control deficit of centiled subcortical volumes in MCI, and these results were extensively overlapping with the case-control differences identified in SCZ. More specifically, the pattern of schizophrenia case-control differences also saw strong disease-related decreases in subcortical volume in the hippocampus and amygdala, but conversely, saw increases in volume in patients compared to controls in the pallidum and putamen in males, and to a lesser extent also in females (**Fig. 6.11**).

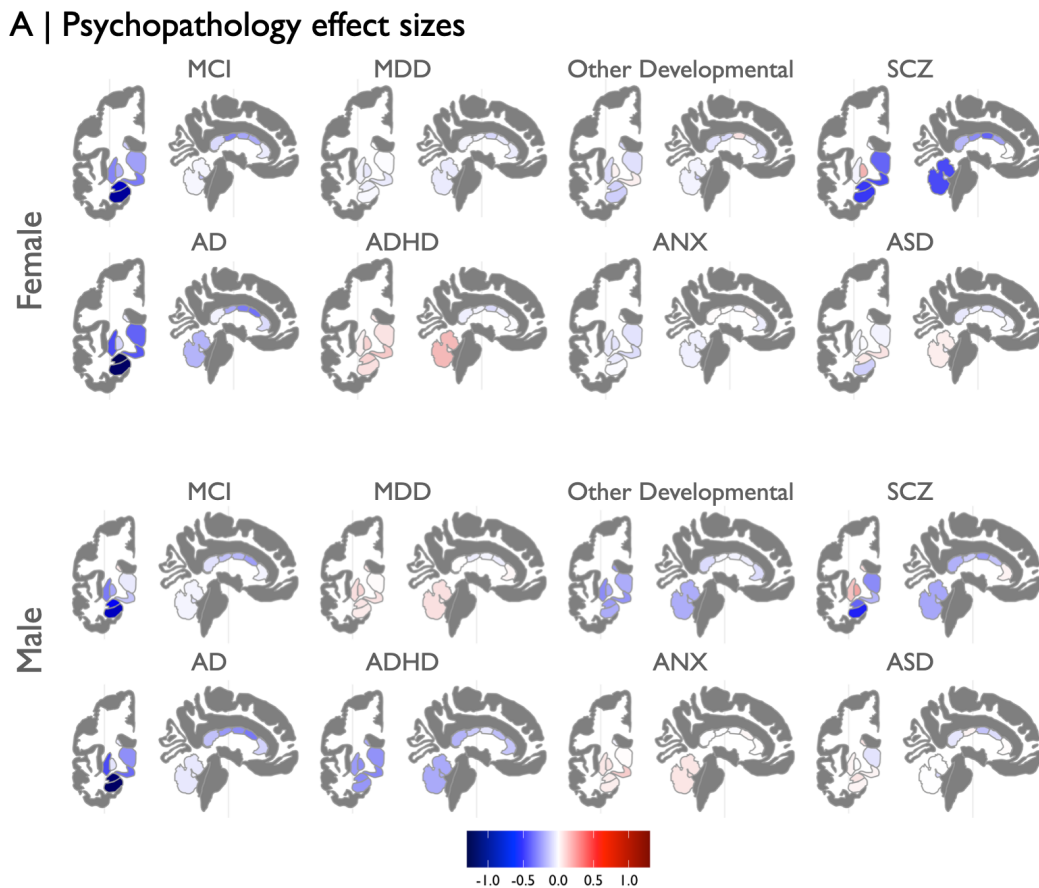


Fig. 6.11 Case-control differences in centile scores of subcortical volumes for multiple neuropsychiatric disorders: Case-control differences between the normative sample (CN) and each diagnostic category of clinical cases, using Cohen's d , for males and females separately, to demonstrate the standardised effect size for case-control differences for each disorder in both (A) subcortical regions, and (B) cerebellum and corpus callosum.

We observed that for several disorders, and in a number of different regions, the sign of the case-control differences in grey or white matter volume differed between the sexes. Most notably, we observed divergent patterns of case-control increases of subcortical volumes in female ADHD cases, compared to case-control volumetric decreases in male ADHD cases, in almost all subcortical regions, with most of these effects being significant (**Fig. 6.12A**).

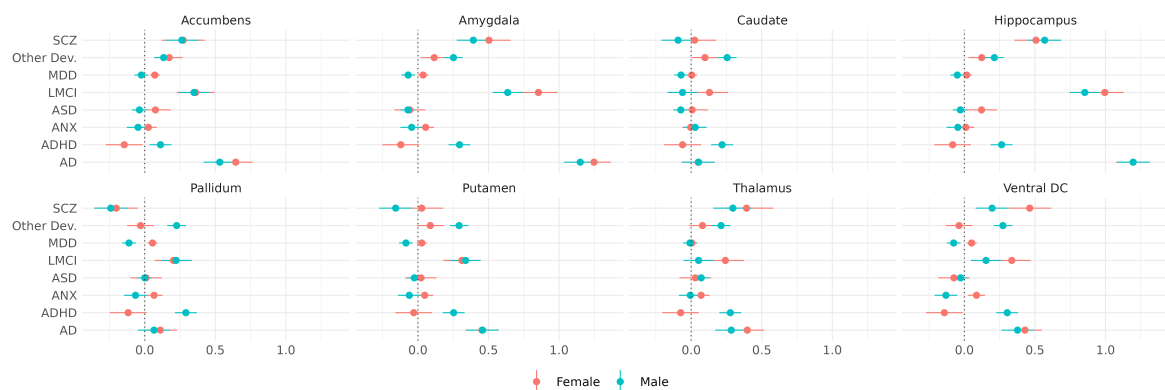
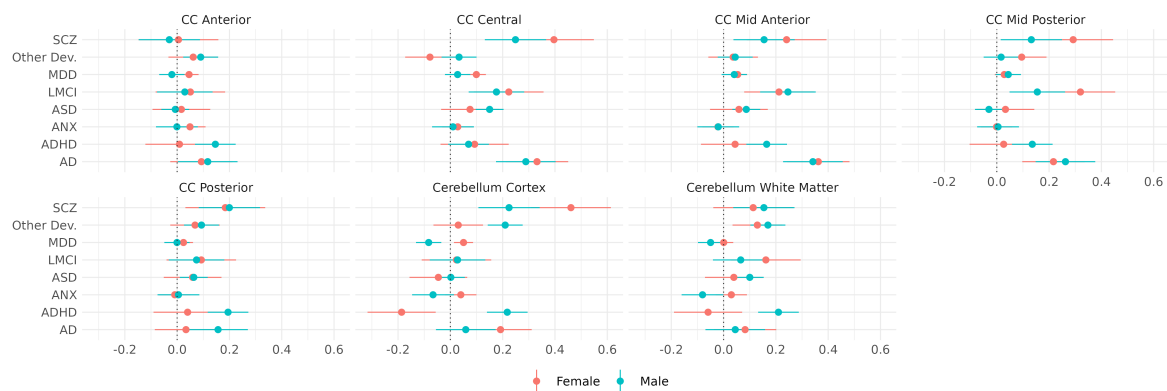
A | Psychopathology effect sizes in subcortex**B | Psychopathology effect sizes in cerebellum and corpus callosum**

Fig. 6.12 Neuropsychiatric case-control differences in subcortical volumetric centile scores by subcortical structure: Case-control differences between the normative sample (CN) and each diagnostic category of clinical cases. We compared each diagnostic group to controls using Cohen's d , both in (A) subcortical regions, and (B) cerebellum and corpus callosum. For each region, we show the magnitude of standardised effect size d , and its confidence interval, for males and females separately.

6.4 Discussion

Using a large aggregated neuroimaging dataset, we derived growth charts of normative subcortical human brain development, estimated developmental milestones in subcortical volume development, and demonstrated that individual centile scores benchmarked against the appropriate norms showed significant differences in most regions tested in multiple neuropsychiatric disorders.

First, we aggregated one of the largest neuroimaging samples to date. We derived normative trajectories of subcortical phenotypes, with the aim of making them available

to the neuroimaging community. Such normative referencing standards are very useful for benchmarking individual brain scans that were not included in the dataset used to model normative brain charts. In this work, we included a random effect of study, which theoretically allows us to estimate centile scores for individual scans from new studies (cf. **Fig. 6.3**). We aim to include the subcortical phenotypes normatively modelled here for the first time into the published “BrainChart” toolbox <https://brainchart.shinyapps.io/brainchart/>.

We found that subcortical structures, including the thalamus, caudate, putamen, pallidum, hippocampus, amygdala, nucleus accumbens and ventral DC, as well as the cerebellar grey matter, peaked during adolescence and early adulthood, and showed their peak rate-of-growth during early infancy. Conversely, the different corpus callosum sections, as well as the cerebellar white matter, peaked later in life, during mid adulthood, and reached their peak rate-of-growth during childhood or early adolescence. The age of peak volume reported here is later than previously suggested for many subcortical regions (Dima et al., 2022). We speculate that this may be due to prior samples using smaller datasets and not fully mapping the entire lifespan, which may have led to boundary-problems in prior models (Rutherford et al., 2022). Lastly, the age-differences at which developmental milestones are reached between different structures may indicate that the subcortex develops in at least two developmental windows: the earlier maturation of grey matter volume is followed by later peaks in white matter tracts.

In line with previous work on variance of subcortical structures, we observed greater between-subject variability in males compared to females in most regions (Wierenga et al., 2022). This finding is of particular relevance, because recent work has suggested a potential link between variance in brain phenotypes and the development of psychiatric disorder (Wierenga et al., 2022). Differences in variance across the sexes highlights the need to consider individual differences within the sexes and how they may underpin the sex-specific vulnerability to disorders (Wierenga et al., 2022).

Individual centile scores benchmarked against these normative trajectories were associated with multiple neuropsychiatric disorders, demonstrating the possible clinical value of charting subcortical brain development. In particular, we find the strongest associations between deviations from normative subcortical development and Alzheimer’s disease, with mild cognitive impairment showing a very similar pattern. With MCI seen as an intermediary state between healthy aging and Alzheimer’s disease the similarity in the pattern of case control differences, but differences in effect size strength provides support for the sensitivity of centile scores to individual disorders. We believe that this work is likely showing the most extensive effects of disorders on subcortical volumes reported to date, largely owing to

the large sample size of the aggregated sample and the power of GAMLSS modeling to fit non-linear trajectories to datasets collected from different scanners.

We would like to point out that the strongest effect sizes were observed for the neurodegenerative Alzheimer's disease, with smaller effect sizes found across most psychiatric disorders. It may not be surprising that using structural MRI effect sizes are particularly strong in neurodegenerative diseases which have well-characterized patterns of atrophy and pathology, such as for example the presence of abnormal protein aggregates. In contrast, to date no clear structural brain biomarkers of psychiatric disorders are known. Further, neurodegenerative diseases are typically more clearly defined, compared greater heterogeneity of symptoms in psychiatric disorders. While these factors combined may lead to greater difficulty in observing case-control differences in normative trajectories of subcortical development, this study has provided reasonable evidence for such differences across multiple psychiatric disorders.

It is worth noting that due to the nature of the aggregated nature of this dataset, each disease group contained subjects from several studies. Inevitably, the criteria for these diagnoses varied by study. Here, we carried forward the diagnostic labels as they were designated by the primary studies. It may be that the variation in diagnostic labels contributes to relatively small effect sizes in some disorders. For example, MDD is the largest patient group in this sample, but case-control effect sizes for this group were generally small. However, 86% MDD cases stem from the UKB sample, such that this analysis may be biased towards the diagnostic criteria used by this one large population study which labeled all subjects with a lifetime history of depression as MDD cases (rather than recruiting specifically for symptomatic MDD patients as would usually be done in a traditional case-control study).

We note that for two subcortical structures, the nucleus accumbens and the ventral diencephalon, the normative trajectories did not appear to fit the underlying raw data well for the period before 1 year of age. We believe that this effect was likely caused by the fact that the youngest dataset available (dHCP) did not include estimates of grey matter volume in the nucleus accumbens and ventral DC. Consequently, this effect will likely be mitigated in the future by adding further datasets providing more complete coverage of the age range below 2 years.

In this work, based on known differences in structural brain development and in line with the WHO growth chart methodology, we stratified by sex. Thus, age-by-sex interaction effects are not specifically modelled; however, this is theoretically possible and while not practically needed for centile score estimation, it may be interesting for scientific purposes. Modelling age-by-sex interactions in the future would be particularly interesting in the

context of psychiatric disorders. Using our sex-stratified centile scores, we found a variation in the direction and effect size of case-control differences in multiple disorders, most notably in ADHD, where prevalence and behavioral symptoms are known to differ between males and females (Arnett et al., 2015; Murray et al., 2019). It has been difficult in the past to study sex differences in disorders like ADHD and ASD which are more commonly diagnosed in males, since datasets often do not include many females. Aggregating data across multiple studies and benchmarking them against a robust normative framework, may thus provide a promising avenue for studying sex differences in these disorders. In the context of our findings in **Chapter 3** it is also worth noting that we do observe different patterns of MDD case-control differences in this study, and it will also be interesting in the future to more directly explore potential sex differences in MDD. Most neuroimaging studies only collect information on sex, not gender. It would be interesting, in the future, to move away from models stratified by a binary sex variable. Indeed prior work has suggested that brain phenotypes are best described as a continuum (Zhang et al., 2021b). Further, there is evidence that androgyny on a brain-gender continuum may be associated with better mental health in line with psychological androgyny (Zhang et al., 2021b), highlighting the relevance of assessing gender compared to biological sex only.

It is worth noting that the sample sizes for the different patient groups varied widely (**Table 6.1**), such that inevitably, the statistical power to detect an effect will have been larger for some patient group, compared to others. For some disorders (i.e. ASD, ADHD) there was a sex imbalance, as is common in studies of these conditions. Since the case-control differences are estimated for each sex separately, statistical power would have been larger one sex compared to the other. Future work should attempt to increase the sample sizes of smaller patient groups.

Multiple regions included in this work are only defined in FreeSurfer output files. However, a number of studies included in this aggregated dataset were processed with other pipelines. In particular subjects aged younger than two years were usually processed with InfantFreeSurfer or custom processing pipelines that did not include all subcortical regions analysed here. Further work is required to increase the number of studies that do include all regions, or to re-preprocess existing datasets with pipelines that include them. Processing scans from subjects aged younger than one year poses difficulties due to pronounced intensity and contrast changes taking place during early postnatal development. However, recent advances on automated segmentation pipelines has seen the development of promising new tools based on deep-learning models that may facilitate this process (Billot et al., 2023a,b; Shang et al., 2022)

It is worth noting that any difficulties with pre-processing pipelines are limited to subjects aged 2 years and younger. These younger subjects do not directly inform the modelling at later ages when all subcortical volumes reported here peak, thus the key results reported here are likely unaffected at large.

Adding additional data covering early-life period may likely address a number of limitations in the findings reported here. First of all, we note that we did observe a significant relationship between age and image quality across studies. Some of those effects may be inevitable. For example, it is widely reported in the functional magnetic resonance imaging (fMRI) literature that younger subjects tend to move more in the scanner, contributing to decreased image quality (Satterthwaite et al., 2013), and work on structural MRI has similar effects on scan quality in those data (Alexander-Bloch et al., 2016). However, increasing the number of studies may help to mitigate concerns about data quality of individual studies. Reassuringly, our results indicated that at large there was no meaningful effect of image quality on individual centile scores, and no individual study appeared disproportionately to bias the estimated normative trajectories.

The landscape of openly available neuroimaging datasets is strongly biased in favour of (mostly affluent) participants from white Western European and North American populations (Kopal et al., 2023). This increasingly well-recognised demographic bias in the field at large was inevitably also reflected in our aggregated dataset. While we were able to gather data from three continents, further work is needed to increase the geographical, and thereby ethnic, diversity of the studies included in this work to enable more population-representative normative trajectories. A further point of concern in relation to diversity of neuroimaging datasets is the effect of socio-economic status (SES) on brain structure. There is a growing body of evidence suggesting that SES significantly impacts brain structure throughout the lifespan (Rakesh and Whittle, 2021). It is notable that recent work has shown that SES may impact brain development as early as in-utero, with low parental SES associated with decreased fetal grey and white matter volume (Lu et al., 2021; Spann et al., 2020). Further, there is ample evidence that SES is associated with worse cognitive outcomes during multiple stages of development (Zhou et al., 2015), and a number of studies have provided evidence that discrepancies in cognitive outcomes as a result of SES may be mediated to by changes in brain structure (Whittle et al., 2017). The relationship between SES and brain morphology is thought to be complex, and proposed contributing factors include SES being associated with increased levels of stress (Hackman et al., 2012), and differences in nutrition, health, cognitive stimulation, and parenting behaviour (Whittle et al., 2017). Taken together, these results highlight a great need for the neuroimaging community to address the lack of diverse datasets (Benkarim et al., 2021; Kopal et al., 2023).

Of further note is that the data used in this study were processed using multiple pre-processing pipelines. It is conceivable that pipelines are differently good at reconstructing the cortical surface, resulting in differing numbers of surface holes. The authors note, however, that there is advantages of including multiple processing pipelines into their models: in order for these models to remain up to date, upgrading to the respectively most recent version appears essential, while re-preprocessing all legacy data is infeasible given the size of the dataset. Future work should address concerns regarding multiple processing pipelines and in particular will have to disentangle potential interaction effects between FreeSurfer version, participant age, year of data acquisition, MRI scanner and surface holes.

The most well-known example of normative reference charts, the World Health Organization's pediatric growth charts (Group and de Onis, 2006; Organization et al., 2006), were primarily estimated from data acquired by a multi-center longitudinal study of children under two years of age, with cross-sectional data included subsequently (Group and de Onis, 2006; Organization et al., 2006). In our work, we aggregated both cross-sectional and longitudinal studies initially. However longitudinal scans comprised only 13% of the total number of scans, thus we decided not to explicitly model longitudinal changes, i.e., by adding a term to the model for subject-specific random effects. Further work is needed to validate these models by estimating whether analysis of multiple repeated measures from a single individual result in similar centile scores to the scores obtained for the same individual when their data are analysed cross-sectionally. Previous work using the same normative modelling framework on cortical data has shown that the GAMLSS modeling framework is capable of generating centile scores that remain within the same centile boundaries across multiple measures (Bethlehem et al., 2022), thus it is reasonable to expect that this should also be the case for subcortical structures. Of particular interest are cases of subjects that changed diagnostic labels between their longitudinal scans. We would expect changes in neurodegenerative and psychiatric diagnoses to be accompanied by longitudinal step-changes in an individual's centile scores for subcortical volume. For example, it would be interesting to include subjects that shift from being considered healthy controls or having MCI to receiving an AD diagnosis. Such changes in diagnosis are results of known neurodegenerative process underlying diagnostic transitions (Risacher et al., 2009), and we would expect to see them reflected in individuals' centile score (Bethlehem et al., 2022). Other examples of diagnostic or treatment transitions with known underlying changes in brain structure that may trigger a "jump" in individuals' centile scores include subjects transitioning from first episode psychosis to chronic schizophrenia, or from untreated first episode psychosis to treated first episode psychosis.

It is worth pointing out that the “growth charts” developed here, although analogous to pediatric growth charts, merely demonstrate the feasibility of deriving lifespan trajectories of subcortical development, and thus are not immediately suitable for clinical use. However, there is reason to believe that centile scores derived from trajectories of structural brain phenotypes may in the future support clinical practice (Bedford et al., 2022). First, there is evidence for neuroanatomical alterations in neurodevelopmental disorders in early development, i.e. it has been shown that increased surface area at 6 months of age can precede a diagnosis of autism in children at 24 months (Hazlett et al., 2017). Given our lack of understanding of underlying biology or causal mechanisms for many neurodevelopmental disorders, it is unlikely that brain growth charts would lead to a diagnosis, but rather they could form part of a broader individual screening and help support early diagnosis. The neurobiology of neurodegenerative diseases like AD, however, are comparatively better understood (Coupé et al., 2019), with deviations in brain anatomy seen up to 10-15 years prior to diagnosis (Coupé et al., 2019), suggesting that longitudinal changes in centile score may be indicative of risk or a prodromal phase for neurodegeneration (Bedford et al., 2022).

In a promising recent development, Schabdach et al. (2023) demonstrated the feasibility of using clinically acquired scans, rather than research data, to derive normative trajectories of brain development. While this first sample is rather small (N=372, 0-22 years), the prospect of being able to use "real-world" clinical data is an exciting development, which may be able to solve a number of concerns addressed above, including availability of scans from younger subjects and population diversity, since tens of thousands of additional scans are routinely acquired in medical settings around the world (Schabdach et al., 2023). Including such data into lifespan models for research would present a major expansion of data availability and diversity.

We conclude that the GAMLSS framework is well-suited for estimating normative lifespan trajectories of subcortical volume. In one of the biggest neuroimaging samples to date, we have mapped for the first time lifespan trajectories of subcortical volume from preterm birth to old age, demonstrated the feasibility of benchmarking individual subjects to normative trajectories, and using centile scores as a standardized measure of atypical brain structure, revealed patterns of neuroanatomical variation across multiple neuropsychiatric disorders.

Chapter 7

Summary and concluding remarks

7.1 Summary of findings

This thesis has examined changes in adolescent functional and structural brain development and their relationships to psychiatric disorders.

In **Chapter 2**, a sexually divergent system of adolescent functional connectivity development, primarily located in the association cortex and subcortex, was identified. In these regions functional connectivity developed more disruptively in women, meaning that females demonstrated a greater tendency for weak functional connections (at age 14 years) to become more strongly connected over the course of adolescence, resulting in greater changes to the rank ordering of each node's edge-wise connections to the rest of the network in females compared to males. We further showed that these sex differences in adolescent brain development were spatially co-located with brain regions that were enriched for expression of genes located on the X-chromosome and developmentally relevant genes. In **Chapter 3** the anatomical, psychological and genetic relevance of this sexually divergent development of functional connectivity to the well-known sex differences in incidence of depressive and other mood disorders during adolescence was investigated. More specifically, the map of sex differences in development of functional connectivity during adolescence was spatially co-located with (i) a map of case-control differences in major depression, such that regions that developed more disruptively in healthy females tended to show stronger decreases in functional connectivity in patients with major depressive disorder compared to healthy controls; (ii) with prior loci of reward-related brain activation; and (iii) an adult brain gene transcriptional profile enriched for major depressive disorder (MDD) risk genes.

Chapter 4 reviewed the literature on similarity-based structural connectivity networks and made suggestions for future work, including studying developmental changes in morphometric similarity networks (MSNs). **Chapter 5** used the same dataset as in **Chapter 2** and **Chapter 3**, to focus on adolescent changes in brain structure. It identified a pattern of increasing morphometric dissimilarity, hypothetically representing increasing cytoarchitectonic differentiation of structural brain networks over the course of adolescence. Increasing morphometric dissimilarity was found to be driven by increases in myelination and decreases in cortical thickness. This process of structural segregation was further co-located with a map of age related changes in functional participation coefficient, suggesting that cytoarchitectonic differentiation during adolescence may allow for more varied functional realizations to meet adult cognitive and social demands.

Finally, in **Chapter 6** sex-specific lifespan trajectories of subcortical development were estimated using a normative modelling approach. This chapter defined milestones of subcortical grey matter volume development, which tended to peak during adolescence and decrease thereafter in putamen, pallidum, hippocampus, amygdala, ventral diencephalon, accumbens, thalamus and caudate, while the corpus callosum and cerebellar white matter volume peaked in early adulthood. Further, this chapter showed that individual centile scores benchmarked against normative trajectories of brain development show significant differences across multiple neuropsychiatric disorders.

7.2 Convergent themes

7.2.1 Brain development during adolescence - and beyond

Prior work on the NSPN sample (Váša et al., 2020), and further analyses in **Chapter 2 - 3**, are consistent with literature indicating wide-spread functional re-organization during adolescence (Dosenbach et al., 2010; Fair et al., 2007; Váša et al., 2020). The adolescent changes in brain structure observed in **Chapter 5** are comparatively less extensive. Research on univariate phenotype development has shown that grey matter volume, both globally and locally, undergoes a rapid period of development from mid-gestation until about six years of age. Although white matter volume also increases rapidly from mid-gestation until early childhood, there is a more gradual and prolonged period of white matter development subsequently, which peaks during early adulthood (Bethlehem et al., 2022). An exploratory analysis in **Chapter 5**, estimating lifespan changes in morphometric similarity networks, provided evidence that the strongest changes in morphometric similarity may indeed be seen

in early life, until the age of six years. However, little is known about lifespan changes in functional network measures, such that no direct comparison of the magnitude of changes in structure and function during different periods of life can be made.

Further, while **Chapter 6** found that many subcortical regions peak in volume during adolescence, subcortex was not considered in **Chapter 5**, since not all morphometric features used for the network construction could be derived for subcortical regions. Future work should address adolescent changes in morphometric similarity between the subcortex and cortex.

7.2.2 Sex differences

Historically, animal studies have focused on studying male animals, based on the assumption that the male can serve as representative of the species (Simon, 2005). Females have been argued to be more variable, due to their menstrual cycle. However, empirical research in mice demonstrates there is no evidence for greater in variability in females in behavioral, morphological, physiological, or molecular traits (Prendergast et al., 2014), or even suggest greater variability in males (Smarr and Kriegsfeld, 2022).

Further, there has been a distinct lack of focus on sex differences in both clinical trials as well as basic science animal studies. This is of particular concern, because (i) there is ample evidence that sex can effect the expression profile of a number of (psychiatric) disorders, which cannot be fully understood without studying sex; (ii) treatment may affect men and women differently. In the United States of America, it was not until 1994 that the U.S. National Institute of Health (NIH) published guidelines to include women in federally funded clinical research (of Health et al., 1994). As an illustrative example, an analysis by the U.S. Food and Drug Administration (FDA) of drugs removed from the market between 1997 and 2000 showed that eight out of 10 of them had greater side effects in women than in men (Carey et al., 2017; Heinrich et al., 2001), further supporting the urgency with which sex differences in treatment response must be investigated in the course of drug development.

Modern science inherits a history of studies dedicated to finding the “neural basis” of sex differences in behavior, which it has been argued have suffered from misogynistic assumptions that women and men were “hard-wired” to be different (Fine, 2005, 2014). The early 2010s saw a rise in criticism of studies using small sample sizes to investigate stereotypically gendered behavior, and the term “neurosexism” was coined (Fine, 2008).

However, this work has also provided evidence for the relevance of considering sex differences in neuroscientific research. **Chapter 2** and **Chapter 3** of this thesis have demon-

strated the anatomical, psychological and genetic relevance of sex differences in adolescent functional brain development to MDD, while **Chapter 6** provided tentative evidence for sex differences in grey matter volume deviations in a number of psychiatric disorders. Taken together, these findings highlight the importance of estimating sex differences during development and in the neuropsychiatric context.

Media attention and popular interpretation of scientific findings can - and should - be of concern to researchers studying sex differences in the brain. However, avoiding reporting sex differences may contribute to gender disparities in health. Thus instead of avoiding the study of sex differences altogether, we should focus instead on responsible communication of research findings.

7.2.3 Cortex vs subcortex

Prior work has highlighted the importance of subcortico-cortical connectivity during development and in neuropsychiatric disorders. Multiple neuropsychiatric disorders have been associated with case-control differences in both structural and functional subcortical phenotypes, i.e. decreased grey matter volume in the hippocampus, amygdala, thalamus, and accumbens has been reported in patients with schizophrenia (Van Erp et al., 2016); MDD has been associated with amygdala hyper-connectivity, hypothetically representing increased emotional evaluation and rumination (MacMaster et al., 2008).

It has been suggested that there may be a “mismatch”, i.e., a difference in developmental timing, between subcortical regions and prefrontal regions (Mills et al., 2014). More specifically, it has been argued that prefrontal regions, which are involved in cognitive control, may undergo a more prolonged development compared to subcortex, which is involved in reward processing, hypothetically leading to increases in risk-taking and sensation-seeking behaviours (Miller et al., 2014).

Early neuroimaging work has reported both increases (Marek et al., 2015; van Duijvenvoorde et al., 2016) and decreases (Supekar et al., 2009) in subcortico-cortical functional connectivity between childhood and adolescence. However, many of these studies were seed-based analyses and did not investigate whole-brain connectivity. Recent work on the NSPN sample has suggested that individual subcortical regions show distinct maturational profiles of functional connectivity (Váša et al., 2020).

Chapter 2 and **Chapter 3** highlighted sex differences in adolescent functional connectivity development. Of the eight bilateral subcortical regions examined, almost all were found to display significant differences between males and females, with females displaying more

disruptive development than males, meaning that in females, there was a greater tendency for change in the rank ordering of functional connections between subcortical regions and the rest of the brain.

Chapter 5 explored adolescent structural brain development from a network perspective. Many of the metrics we used to construct the morphometric similarity networks in this chapter are commonly measured only in cortex, thus no subcortical regions were included in this analysis. Previous studies have demonstrated that subcortico-cortical morphometric similarity is predictive of cognitive outcomes during childhood (Wu et al., 2022). It is conceivable that there may be adolescent changes in subcortico-cortical morphometric similarity not detected in our current work. Future work could thus explore how subcortico-cortical morphometric similarity changes during adolescence. **Chapter 6** provided further evidence that indeed subcortical structures may contribute to structural brain network changes during adolescence. The univariate models of structural brain development used to derive lifespan trajectories of subcortical grey matter volume for multiple regions suggested that many of them peak in volume during adolescence. Further analysis is required to understand how the maturational dynamics of a single phenotype relate to brain network changes during the same period of life and whether the peak in subcortical grey matter volume relates to changes in maturational functional connectivity development.

7.2.4 Vulnerabilities during development

There is an intricate relationship between developmental changes in the brain and vulnerabilities to psychiatric disorders (Paus et al., 2008; Silbereis et al., 2016). **Chapter 3** found that the regions that demonstrate more fundamental re-organization in their connectivity to the rest of the brain are also implicated in MDD in various ways. This finding aligns with the suggestion that “moving things get broken” (Paus et al., 2008), i.e. re-organization of the brain network architecture results in increased vulnerabilities to disorders. **Chapter 3** has highlighted vulnerabilities to one disorder, MDD, during a single period of development, adolescence. However, there is evidence that, despite the fact that many psychiatric disorders are first diagnosed during adolescence, vulnerabilities may be conferred during much earlier development, including prenatally, and may contribute to the later occurrence of disorders (Markham and Koenig, 2011; Selemon and Zecevic, 2015). Thus future work should investigate other developmental periods outside adolescence to further our understanding of vulnerabilities to mental health disorders during development. While further analyses are required to disentangle how centile score differences in disease emerge over the course of the lifespan, the univariate models of structural brain development in **Chapter 6** nevertheless

have laid the groundwork for examining case-control differences in subcortical volume by the innovative approach of normative modeling.

7.3 A note on open science

Openly sharing data is essential to ensure reproducibility and to maximize the impact of public investments in scientific research. Further, despite the long-standing interest of the field in understanding lifespan changes in the brain, to date no single dataset has fully covered the lifespan with a sufficient sample size to estimate lifespan trajectories of subcortical and cortical brain development. A number of factors can contribute to neuroimaging data not being shared publicly (Bethlehem et al., 2022; White et al., 2022), including (i) privacy concerns, often originating from a lack of informed consent for open data sharing being obtained from participants at the time of data collection; (ii) requirements by funding bodies to include senior authors in secondary work on the acquired data; and (iii) national or institutional data protection regulations preventing sharing of raw data.

Only recent increases in publicly available datasets have made it possible to aggregate a sufficient number of studies covering extended periods of the lifespan with sufficient sample size. Such efforts have furthered our understanding of lifespan trajectories of cortical and subcortical brain development (Bethlehem et al., 2022; Rutherford et al., 2022), and **Chapter 6** of this thesis aims to contribute to these advances. In collecting the studies aggregated into a larger dataset in **Chapter 6**, a number of factors crystallised that may hamper progress in future large-scale neuroimaging work.

1. **Data format:** The organization of shared datasets differed vastly between datasets. Recent efforts by the neuroscientific open science community have attempted to standardize magnetic resonance imaging (MRI) data organization in the Brain Imaging Data Format (BIDS) format, and the NIH common data elements (CDE) proposed a standardized framework for data collection, organization, and sharing in biomedical research in general which would, for example, also cover neuroimaging-associated behavioral data (Kuplicki et al., 2021; Kush et al., 2020), but to date these standards are not universally applied. Data-sharing in non-standardized formats makes data aggregation more difficult not least because scripts need to be adapted on a single-case basis, an effort that becomes less manageable with increasing numbers of studies aggregated. There is no doubt that larger sample sizes have improved our ability to estimate brain development in health and disease (Bethlehem et al., 2022; Rutherford

et al., 2022), and indeed specific suggestions have been made for minimal sample sizes needed to investigate brain-behavior relationships (Marek et al., 2022).

2. **Ease of access:** There are large differences in the “openness”, i.e. the accessibility of primary datasets, without further negotiation, to secondary data users. Some neuroimaging studies were shared only via personal communication, some studies were accessible by well-managed but lengthy formal application processes, and some were accessible by a one-click download. Of particular note in the latter category are the OpenNeuro platform (Markiewicz et al., 2021), which facilitates the sharing of neuroscientific data on a single website in the standardized BIDS format; and the SRPBS1600 study (Tanaka et al., 2021b), a single large study available through a one-click download. While the work in **Chapter 6** benefitted immensely from data shared through personal communication, such efforts should not be necessary and indeed may bias data sharing with specific author groups.
3. **Authorship:** Usage requirements differed even between “openly shared” datasets. While it was generally sufficient to cite the datasets used, other data owners requested the inclusion of authors in the author list, sometimes specifying specific positions in the list. This clearly stretches the definition of open science. Further, including authors due to data-sharing for some datasets, but not others that are fully openly shared may disincentivize open data sharing.

On a related note, please refer to **C.3** for data and code availability. All methods and overview figures created for **Chapter 1** have been made available to download and reuse under a **CC BY 4.0** licence at [10.5281/zenodo.7782905](https://doi.org/10.5281/zenodo.7782905).

7.4 Future directions

Beyond the specific suggestions made in each of the previous chapters, two key themes covered in this thesis may provide avenues for future research (i) network approaches to lifespan development, and (ii) brain-gene-interactions (over the course of the lifespan).

Structurally, this thesis started from a network position, examining changes first in functional, then in structural brain networks during adolescence. It then proceeded to expand the scope of analysis to examine lifespan change in univariate structural brain phenotypes. One future direction will be to move from univariate to network models of lifespan development. As a first step, morphometric similarity networks may provide

a suitable avenue for exploring lifespan development of structural brain networks given the ease with which they can be estimated from T1 scans only which have already been aggregated for **Chapter 6**. While it would be difficult to aggregate enough multi-modal datasets to fully leverage the potential of MSNs, it may therefore be worth considering measuring phenotypes at multiple depths, both to increase the number of features, as well as to improve microstructural information.

Lastly, a growing body of work is exploring the interaction between genes and brain structure and function. **Chapter 2-3**, in line with multiple prior studies (Morgan et al., 2019; Whitaker et al., 2016b) have explored transcriptomic data from a high-resolution transcriptomic atlas generated from a set of six post-mortem brains (Arnatkeviciute et al., 2019; Hawrylycz et al., 2015) to better understand patterns of gene expression associated with changes in brain function. While the use of this dataset has furthered our understanding of gene expression patterns associated with (changes in) brain structure and function (Dorfschmidt et al., 2022; Seidlitz et al., 2020; Whitaker et al., 2016b), a number of limitations to this approach have been outlined, including the limited age-range, as well as sex imbalance of this dataset. Alternative datasets which expand the sample size and age range covered do exist, they are so far limited in their spatial resolution (i.e. the number of brain regions sampled) (Miller et al., 2014). Thus, to deepen our understanding of gene-expression linked to neuroimaging phenotypes new methods will be needed to fully leverage the potential of more diverse, but lower-resolution alternatives to the Allen Human Brain Atlas (AHBA).

Additionally, a recent move towards larger samples and thorough phenotyping, including whole genome sequencing for individuals enrolled in neuroimaging studies (Alfaro-Almagro et al., 2018; Casey et al., 2018), has opened up a further avenue for exploring gene-brain-interactions. For example, prior work has examined individual risk of disorders, via the means of polygenic risk scores, and could thereby examine the association between normal variation in polygenic risk score (PRS) and MRI phenotypes of brain morphometry and tissue composition (Stauffer et al., 2021). It has also become increasingly clear that brain structural and functional phenotypes are substantially heritable and influenced by common genetic variation (Warrier et al., 2022). Specifically, genome-wide association studies (GWASs) have been used to identify common genetic variants linked to human cortical development and organisation (Warrier et al., 2022) and to examine shared genetic effects on psychiatric disorders and brain structure (Stauffer et al., 2023). Remarkably, such studies offer the opportunity to explore causal links between brain and cognitive phenotypes (Shen et al., 2020) promising to further our understanding of the emergence of psychiatric disorders. Future work could expand these research directions to examine (changes in) gene-brain-interactions over the course of lifespan for example by examining the relationship between

PRS and centile scores. To this end, the neuroimaging community will have to make efforts to acquire large-scale datasets covering multiple periods of life.

7.5 Conclusion

Collectively, the work in this thesis has highlighted maturational changes in brain structure and function during adolescence, and the lifespan more generally, and strengthened evidence for the intimate relationship between development and vulnerabilities to disorders. In particular, it has highlighted the relevance of considering sex differences when exploring normative development and risk of psychiatric disorders.

References

- Hervé Abdi. Partial least square regression (pls regression). *Encyclopedia for research methods for the social sciences*, 6(4):792–795, 2003.
- Sophie Achard, Raymond Salvador, Brandon Whitcher, John Suckling, and ED Bullmore. A resilient, low-frequency, small-world human brain functional network with highly connected association cortical hubs. *Journal of Neuroscience*, 26(1):63–72, 2006.
- Gabriela Alarcón, Anita Cservenka, Marc D Rudolph, Damien A Fair, and Bonnie J Nagel. Developmental sex differences in resting state functional connectivity of amygdala sub-regions. *NeuroImage*, 115:235–244, 2015. ISSN 1053-8119. doi: 10.1016/J.NEUROIMAGE.2015.04.013.
- Lindsay M Alexander, Jasmine Escalera, Lei Ai, Charissa Andreotti, Karina Febre, Alexander Mangone, Natan Vega-Potler, Nicolas Langer, Alexis Alexander, Meagan Kovacs, et al. An open resource for transdiagnostic research in pediatric mental health and learning disorders. *Scientific data*, 4(1):1–26, 2017.
- Aaron Alexander-Bloch, Armin Raznahan, Ed Bullmore, and Jay Giedd. The convergence of maturational change and structural covariance in human cortical networks. *Journal of Neuroscience*, 33(7):2889–2899, 2013. ISSN 0270-6474. doi: 10.1523/JNEUROSCI.3554-12.2013. URL <https://www.jneurosci.org/content/33/7/2889>.
- Aaron Alexander-Bloch, Liv Clasen, Michael Stockman, Lisa Ronan, Francois Lalonde, Jay Giedd, and Armin Raznahan. Subtle in-scanner motion biases automated measurement of brain anatomy from in vivo mri. *Human brain mapping*, 37(7):2385–2397, 2016.
- Fidel Alfaro-Almagro, Mark Jenkinson, Neal K Bangerter, Jesper LR Andersson, Ludovica Griffanti, Gwenaëlle Douaud, Stamatios N Sotiropoulos, Saad Jbabdi, Moises Hernandez-Fernandez, Emmanuel Vallee, et al. Image processing and quality control for the first 10,000 brain imaging datasets from uk biobank. *Neuroimage*, 166:400–424, 2018.
- Elena A Allen, Erik B Erhardt, Eswar Damaraju, William Gruner, Judith M Segall, Rogers F Silva, Martin Havlicek, Srinivas Rachakonda, Jill Fries, Ravi Kalyanam, Andrew M Michael, Arvind Caprihan, Jessica A Turner, Tom Eichele, Steven Adelsheim, Angela D Bryan, Juan Bustillo, Vincent P Clark, Sarah W Feldstein Ewing, Francesca Filbeyand, Corey C Ford, Kent Hutchison, Rex E Jung, Kent A Kiehl, Piyadasa Kodituwakku, Yuko M Komesu, Andrew R Mayer, Godfrey D Pearlson, John P Phillips, Joseph R Sadek, Michael Stevens, Ursina Teuscher, Robert J Thoma, and Vince D Calhoun. A baseline for the multivariate comparison of resting-state networks. *Frontiers in systems neuroscience*, 5:2, 2011. ISSN 1662-5137. doi: 10.3389/fnsys.2011.00002.

- D American Psychiatric Association, American Psychiatric Association, et al. *Diagnostic and statistical manual of mental disorders: DSM-5*, volume 5. American psychiatric association Washington, DC, 2013.
- Kevin M Anderson, Meghan A Collins, Ru Kong, Kacey Fang, Jingwei Li, Tong He, Adam M Chekroud, Thomas B T Yeo, and Avram J Holmes. Convergent molecular, cellular, and neural signatures of major depressive disorder. *bioRxiv*, 2020. doi: 10.1101/2020.02.10.942227.
- A Arnatkeviciute, B D Fulcher, and A Fornito. A practical guide to linking brain-wide gene expression and neuroimaging data. *NeuroImage*, pages 353–367, 2019. ISSN 189. doi: 10.1016/j.neuroimage.2019.01.011.
- Anne B Arnett, Bruce F Pennington, Erik G Willcutt, John C DeFries, and Richard K Olson. Sex differences in adhd symptom severity. *Journal of Child Psychology and Psychiatry*, 56(6):632–639, 2015.
- Arthur P Arnold. The end of gonad-centric sex determination in mammals. *Trends in genetics*, 28(2):55–61, 2012.
- Arthur P Arnold, Jun Xu, William Grisham, Xuqi Chen, Yong-Hwan Kim, and Yuichiro Itoh. Minireview: Sex Chromosomes and Brain Sexual Differentiation. *Endocrinology*, 145(3):1057–1062, 2004. ISSN 0013-7227. doi: 10.1210/en.2003-1491.
- Athina R Aruldass, Manfred G Kitzbichler, Sarah E Morgan, Sol Lim, Mary-Ellen Lynall, Lorinda Turner, Petra Vertes, Jonathan Cavanagh, Phil Cowen, Carmine M Pariante, et al. Dysconnectivity of a brain functional network was associated with blood inflammatory markers in depression. *Brain, behavior, and immunity*, 98:299–309, 2021.
- Helen Barbas and Claus C Hilgetag. From circuit principles to human psychiatric disorders. *Biological Psychiatry*, 93(5):388–390, 2023.
- Markus Barth, Jürgen R Reichenbach, Ramesh Venkatesan, and Ewald Moser and Mark E Haacke. High-resolution, multiple gradient-echo functional MRI at 1.5 T. *Magnetic Resonance Imaging*, 17(3):321–329, 1999. ISSN 0730-725X. doi: 10.1016/S0730-725X(98)00191-X.
- Graham L Baum, Rastko Ciric, David R Roalf, Richard F Betzel, Tyler M Moore, Russell T Shinohara, Ari E Kahn, Simon N Vandekar, Petra E Rupert, Megan Quarmley, et al. Modular segregation of structural brain networks supports the development of executive function in youth. *Current Biology*, 27(11):1561–1572, 2017.
- Graham L. Baum, Zaixu Cui, David R. Roalf, Rastko Ciric, Richard F. Betzel, Bart Larsen, Matthew Cieslak, Philip A. Cook, Cedric H. Xia, Tyler M. Moore, Kosha Ruparel, Desmond J. Oathes, Aaron F. Alexander-Bloch, Russell T. Shinohara, Armin Raznahan, Raquel E. Gur, Ruben C. Gur, Danielle S. Bassett, and Theodore D. Satterthwaite. Development of structure–function coupling in human brain networks during youth. *PNAS*, 117(1):771–778, 2020. doi: 10.1073/pnas.1912034117. URL <https://www.pnas.org/doi/abs/10.1073/pnas.1912034117>. Publisher: Proceedings of the National Academy of Sciences.

- Saashi A Bedford, Jakob Seidlitz, and Richard AI Bethlehem. Translational potential of human brain charts. *Clinical and Translational Medicine*, 12(7), 2022.
- Oualid Benkarim, Casey Paquola, Bo-yong Park, Valeria Kebets, Seok-Jun Hong, Reinder Vos de Wael, Shaoshi Zhang, BT Thomas Yeo, Michael Eickenberg, Tian Ge, et al. The cost of untracked diversity in brain-imaging prediction. *bioRxiv*, pages 2021–06, 2021.
- Matt A Bernstein, Kevin F King, and Xiaohong Joe Zhou. *Handbook of MRI pulse sequences*. Elsevier, 2004.
- R. a. I. Bethlehem, J. Seidlitz, S. R. White, J. W. Vogel, K. M. Anderson, C. Adamson, S. Adler, G. S. Alexopoulos, E. Anagnostou, A. Areces-Gonzalez, D. E. Astle, B. Auyeung, M. Ayub, J. Bae, G. Ball, S. Baron-Cohen, R. Beare, S. A. Bedford, V. Benegal, F. Beyer, J. Blangero, M. Blesa Cábez, J. P. Boardman, M. Borzage, J. F. Bosch-Bayard, N. Bourke, V. D. Calhoun, M. M. Chakravarty, C. Chen, C. Chertavian, G. Chetelat, Y. S. Chong, J. H. Cole, A. Corvin, M. Costantino, E. Courchesne, F. Crivello, V. L. Croypley, J. Crosbie, N. Crossley, M. Delarue, R. Delorme, S. Desrivieres, G. A. Devenyi, M. A. Di Biase, R. Dolan, K. A. Donald, G. Donohoe, K. Dunlop, A. D. Edwards, J. T. Ellison, C. T. Ellis, J. A. Elman, L. Eyler, D. A. Fair, E. Feczko, P. C. Fletcher, P. Fonagy, C. E. Franz, L. Galan-Garcia, A. Gholipour, J. Giedd, J. H. Gilmore, D. C. Glahn, I. M. Goodyer, P. E. Grant, N. A. Groenewold, F. M. Gunning, R. E. Gur, R. C. Gur, C. F. Hammill, O. Hansson, T. Hedden, A. Heinz, R. N. Henson, K. Heuer, J. Hoare, B. Holla, A. J. Holmes, R. Holt, H. Huang, K. Im, J. Ipser, C. R. Jack, A. P. Jackowski, T. Jia, K. A. Johnson, P. B. Jones, D. T. Jones, R. S. Kahn, H. Karlsson, L. Karlsson, R. Kawashima, E. A. Kelley, S. Kern, K. W. Kim, M. G. Kitzbichler, W. S. Kremen, F. Lalonde, B. Landeau, S. Lee, J. Lerch, J. D. Lewis, J. Li, W. Liao, C. Liston, M. V. Lombardo, J. Lv, C. Lynch, T. T. Mallard, M. Marcelis, R. D. Markello, S. R. Mathias, B. Mazoyer, P. McGuire, M. J. Meaney, A. Mechelli, N. Medic, B. Misic, S. E. Morgan, D. Mothersill, J. Nigg, M. Q. W. Ong, C. Ortinau, R. Ossenkoppele, M. Ouyang, L. Palaniyappan, L. Paly, P. M. Pan, C. Pantelis, M. M. Park, T. Paus, Z. Pausova, D. Paz-Linares, A. Pichet Binette, K. Pierce, X. Qian, J. Qiu, A. Qiu, A. Raznahan, T. Rittman, A. Rodrigue, C. K. Rollins, R. Romero-Garcia, L. Ronan, M. D. Rosenberg, D. H. Rowitch, G. A. Salum, T. D. Satterthwaite, H. L. Schaare, R. J. Schachar, A. P. Schultz, G. Schumann, M. Schöll, D. Sharp, R. T. Shinohara, I. Skoog, C. D. Smyser, R. A. Sperling, D. J. Stein, A. Stolicyn, J. Suckling, G. Sullivan, Y. Taki, B. Thyreau, R. Toro, N. Traut, K. A. Tsvetanov, N. B. Turk-Browne, J. J. Tuulari, C. Tzourio, É Vachon-Presseau, M. J. Valdes-Sosa, P. A. Valdes-Sosa, S. L. Valk, T. van Amelsvoort, S. N. Vandekar, L. Vasung, L. W. Victoria, S. Villeneuve, A. Villringer, P. E. Vértes, K. Wagstyl, Y. S. Wang, S. K. Warfield, V. Warrier, E. Westman, M. L. Westwater, H. C. Whalley, A. V. Witte, N. Yang, B. Yeo, H. Yun, A. Zalesky, H. J. Zar, A. Zettergren, J. H. Zhou, H. Ziauddeen, A. Zugman, X. N. Zuo, E. T. Bullmore, and A. F. Alexander-Bloch. Brain charts for the human lifespan. *Nature*, 604(7906):525–533, 2022. ISSN 1476-4687. doi: 10.1038/s41586-022-04554-y. URL <https://www.nature.com/articles/s41586-022-04554-y>. Number: 7906 Publisher: Nature Publishing Group.
- Richard A. I. Bethlehem, Jakob Seidlitz, Rafael Romero-Garcia, Stavros Trakoshis, Guillaume Dumas, and Michael V. Lombardo. A normative modelling approach reveals age-atypical cortical thickness in a subgroup of males with autism spectrum disorder.

- Communications Biology*, 3(1):1–10, September 2020. ISSN 2399-3642. doi: 10.1038/s42003-020-01212-9. URL <https://www.nature.com/articles/s42003-020-01212-9>. Number: 1 Publisher: Nature Publishing Group.
- Richard F. Betzel and Danielle S. Bassett. Multi-scale brain networks. *NeuroImage*, 160: 73–83, October 2017. ISSN 1053-8119. doi: 10.1016/j.neuroimage.2016.11.006. URL <https://www.sciencedirect.com/science/article/pii/S1053811916306152>.
- Richard F Betzel, Lisa Byrge, Ye He, Joaquín Goñi, Xi-Nian Zuo, and Olaf Sporns. Changes in structural and functional connectivity among resting-state networks across the human lifespan. *Neuroimage*, 102:345–357, 2014.
- Sarah F Beul, Helen Barbas, and Claus C Hilgetag. A predictive structural model of the primate connectome. *Scientific reports*, 7(1):1–12, 2017.
- R Bilder, R Poldrack, T Cannon, E London, N Freimer, E Congdon, K Karlsgodt, and F Sabb. "ucla consortium for neuropsychiatric phenomics la5c study", 2018.
- Benjamin Billot, Douglas N Greve, Oula Puonti, Axel Thielscher, Koen Van Leemput, Bruce Fischl, Adrian V Dalca, Juan Eugenio Iglesias, et al. Synthseg: Segmentation of brain mri scans of any contrast and resolution without retraining. *Medical Image Analysis*, page 102789, 2023a.
- Benjamin Billot, Colin Magdamo, You Cheng, Steven E Arnold, Sudeshna Das, and Juan Eugenio Iglesias. Robust machine learning segmentation for large-scale analysis of heterogeneous clinical brain mri datasets. *Proceedings of the National Academy of Sciences*, 120(9):e2216399120, 2023b.
- Bharat Biswal, FZerrin Yetkin, Victor M. Haughton, and James S Hyde. Functional connectivity in the motor cortex of resting human brain using echo-planar mri. *Magnetic Resonance in Medicine*, 34(4):537–541, 1995. ISSN 07403194. doi: 10.1002/mrm.1910340409.
- Bharat B Biswal, Maarten Mennes, Xi-Nian Zuo, Suril Gohel, Clare Kelly, Steve M Smith, Christian F Beckmann, Jonathan S Adelstein, Randy L Buckner, Stan Colcombe, Anne-Marie Dagonowski, Monique Ernst, Damien Fair, Michelle Hampson, Matthew J Hoptman, James S Hyde, Vesa J Kiviniemi, Rolf Kötter, Shi-Jiang Li, Ching-Po Lin, Mark J Lowe, Clare Mackay, David J Madden, Kristoffer H Madsen, Daniel S Margulies, Helen S Mayberg, Katie McMahon, Christopher S Monk, Stewart H Mostofsky, Bonnie J Nagel, James J Pekar, Scott J Pekar, Steven E Petersen, Valentin Riedl, Serge A R B Rombouts, Bart Rypma, Bradley L Schlaggar, Sein Schmidt, Rachael D Seidler, Greg J Siegle, Christian Sorg, Gao-Jun Teng, Juha Veijola, Arno Villringer, Martin Walter, Lihong Wang, Xu-Chu Weng, Susan Whitfield-Gabrieli, Peter Williamson, Christian Windischberger, Yu-Feng Zang, Hong-Ying Zhang, F Xavier Castellanos, and Michael P Milham. Toward discovery science of human brain function. *Proceedings of the National Academy of Sciences of the United States of America*, 107(10):4734–9, 2010. ISSN 1091-6490. doi: 10.1073/pnas.0911855107.
- Robyn L Bluhm, Elizabeth A Osuch, Ruth A Lanius, Kristine Boksman, Richard W J Neufeld, Jean Théberge, and Peter Williamson. Default mode network connectivity: effects of age, sex, and analytic approach. *NeuroReport*, 19(8):887–891, 2008. ISSN 0959-4965. doi: 10.1097/WNR.0b013e328300ebbf.

- Susan Y Bookheimer, David H Salat, Melissa Terpstra, Beau M Ances, Deanna M Barch, Randy L Buckner, Gregory C Burgess, Sandra W Curtiss, Mirella Diaz-Santos, Jennifer Stine Elam, et al. The lifespan human connectome project in aging: an overview. *Neuroimage*, 185:335–348, 2019.
- E. Borghi, M. de Onis, C. Garza, J. Van den Broeck, E. A. Frongillo, L. Grummer-Strawn, S. Van Buuren, H. Pan, L. Molinari, R. Martorell, A. W. Onyango, J. C. Martines, and for the WHO Multicentre Growth Reference Study Group. Construction of the World Health Organization child growth standards: selection of methods for attained growth curves. *Statistics in Medicine*, 25(2):247–265, 2006. ISSN 1097-0258. doi: 10.1002/sim.2227. URL <https://onlinelibrary.wiley.com/doi/abs/10.1002/sim.2227>. _eprint: <https://onlinelibrary.wiley.com/doi/pdf/10.1002/sim.2227>.
- Samantha J Broyd, Charmaine Demanuele, Stefan Debener, Suzannah K Helps, Christopher J James, and Edmund JS Sonuga-Barke. Default-mode brain dysfunction in mental disorders: a systematic review. *Neuroscience & biobehavioral reviews*, 33(3):279–296, 2009.
- Randy L Buckner and Fenna M Krienen. The evolution of distributed association networks in the human brain. *Trends in cognitive sciences*, 17(12):648–665, 2013.
- Ed Bullmore and Olaf Sporns. Complex brain networks: graph theoretical analysis of structural and functional systems. *Nature Reviews Neuroscience*, 10(3):186–198, mar 2009. ISSN 1471-003X. doi: 10.1038/nrn2575. URL <http://www.ncbi.nlm.nih.gov/pubmed/19190637><http://www.nature.com/articles/nrn2575>.
- Ed Bullmore and Olaf Sporns. The economy of brain network organization. *Nature reviews neuroscience*, 13(5):336–349, 2012.
- Edward T Bullmore, Jalal Fadili, Voichita Maxim, Levent Şendur, Brandon Whitcher, John Suckling, Michael Brammer, and Michael Breakspear. Wavelets and functional magnetic resonance imaging of the human brain. *NeuroImage*, 23:S234–S249, 2004. ISSN 1053-8119. doi: 10.1016/J.NEUROIMAGE.2004.07.012.
- L Cahill. Why sex matters for neuroscience. *Nat Rev Neurosci*, page 477–484, 2006. ISSN 7. doi: <https://doi.org/10.1038/nrn1909>.
- Jennifer L Carey, Nathalie Nader, Peter R Chai, Stephanie Carreiro, Matthew K Griswold, and Katherine L Boyle. Drugs and medical devices: adverse events and the impact on women’s health. *Clinical therapeutics*, 39(1):10–22, 2017.
- Joshua M. Carlson, Emily Depetro, Joshua Maxwell, Eddie Harmon-Jones, and Greg Hajcak. Gender moderates the association between dorsal medial prefrontal cortex volume and depressive symptoms in a subclinical sample. *Psychiatry Research: Neuroimaging*, 233(2):285–288, aug 2015. ISSN 09254927. doi: 10.1016/j.psychresns.2015.06.005. URL <http://www.ncbi.nlm.nih.gov/pubmed/26166620><https://linkinghub.elsevier.com/retrieve/pii/S0925492715300123>.
- Laura Carruth, Ingrid Reisert, and Arthur Arnold. Sex chromosome genes directly affect brain sexual differentiation. *Nature neuroscience*, 5:933–4, 2002. doi: 10.1038/nn922.

- R Casanova, C T Whitlow, B Wagner, M A Espeland, and J A Maldjian. Combining graph and machine learning methods to analyze differences in functional connectivity across sex. *The open neuroimaging journal*, 6:1–9, 2012. ISSN 1874-4400. doi: 10.2174/1874440001206010001.
- Betty Jo Casey, Tariq Cannonier, May I Conley, Alexandra O Cohen, Deanna M Barch, Mary M Heitzeg, Mary E Soules, Theresa Teslovich, Danielle V Dellarco, Hugh Garavan, et al. The adolescent brain cognitive development (abcd) study: imaging acquisition across 21 sites. *Developmental cognitive neuroscience*, 32:43–54, 2018.
- Adrian Cho. Mri for all. *Science*, 379(6634):748–751, 2023.
- GBD 2019 Mental Disorders Collaborators et al. Global, regional, and national burden of 12 mental disorders in 204 countries and territories, 1990–2019: a systematic analysis for the global burden of disease study 2019. *The Lancet Psychiatry*, 9(2):137–150, 2022.
- Colm G Connolly, Jing Wu, Tiffany C Ho, Fumiko Hoeft, Owen Wolkowitz, Stuart Eisendrath, Guido Frank, Robert Hendren, Jeffrey E Max, Martin P Paulus, Susan F Tapert, Dipavo Banerjee, Alan N Simmons, and Tony T Yang. Resting-State Functional Connectivity of Subgenual Anterior Cingulate Cortex in Depressed Adolescents. *Biological Psychiatry*, 74(12):898–907, 2013. ISSN 0006-3223. doi: 10.1016/J.BIOPSYCH.2013.05.036.
- Colm G. Connolly, Tiffany C. Ho, Eva Henje Blom, Kaja Z. LeWinn, Matthew D. Sacchet, Olga Tymofiyeva, Alan N. Simmons, and Tony T. Yang. Resting-state functional connectivity of the amygdala and longitudinal changes in depression severity in adolescent depression. *Journal of Affective Disorders*, 207:86–94, jan 2017. ISSN 01650327. doi: 10.1016/j.jad.2016.09.026. URL <http://www.ncbi.nlm.nih.gov/pubmed/27716542><http://www.pubmedcentral.nih.gov/articlerender.fcgi?artid=PMC5149416><https://linkinghub.elsevier.com/retrieve/pii/S0165032716310540>.
- ADHD-200 consortium. The adhd-200 consortium: a model to advance the translational potential of neuroimaging in clinical neuroscience. *Frontiers in systems neuroscience*, 6: 62, 2012.
- Christina Corre, Miriam Friedel, Dulcie A Vousden, Ariane Metcalf, Shoshana Spring, Lily R Qiu, Jason P Lerch, and Mark R Palmert. Separate effects of sex hormones and sex chromosomes on brain structure and function revealed by high-resolution magnetic resonance imaging and spatial navigation assessment of the four core genotype mouse model. *Brain Structure and Function*, 221:997–1016, 2016.
- E Jane Costello, Sarah Mustillo, Alaattin Erkanli, Gordon Keeler, and Adrian Angold. Prevalence and development of psychiatric disorders in childhood and adolescence. *Archives of general psychiatry*, 60(8):837–844, 2003.
- Pierrick Coupé, José Vicente Manjón, Enrique Lanuza, and Gwenaëlle Catheline. Lifespan changes of the human brain in alzheimer’s disease. *Scientific reports*, 9(1):3998, 2019.
- Robert W Cox. AFNI: Software for Analysis and Visualization of Functional Magnetic Resonance Neuroimages. *Computers and Biomedical Research*, 29(3):162–173, 1996a. ISSN 0010-4809. doi: 10.1006/CBMR.1996.0014.

- Robert W. Cox. AFNI: Software for Analysis and Visualization of Functional Magnetic Resonance Neuroimages. *Computers and Biomedical Research*, 29(3):162–173, June 1996b. ISSN 0010-4809. doi: 10.1006/cbmr.1996.0014. URL <https://www.sciencedirect.com/science/article/pii/S0010480996900142>.
- Michael M Craig, Anne E Manktelow, Barbara J Sahakian, David K Menon, and Emmanuel A Stamatakis. Spectral diversity in default mode network connectivity reflects behavioral state. *Journal of Cognitive Neuroscience*, 30(4):526–539, 2018.
- Nicolas A Crossley, Andrea Mechelli, Jessica Scott, Francesco Carletti, Peter T Fox, Philip McGuire, and Edward T Bullmore. The hubs of the human connectome are generally implicated in the anatomy of brain disorders. *Brain*, 137(8):2382–2395, 2014.
- Nicolas A. Crossley, Luz María Alliende, Tomas Ossandon, Carmen Paz Castañeda, Alfonso González-Valderrama, Juan Undurraga, Mariana Castro, Salvador Guinjoan, Ana M. Díaz-Zuluaga, Julián A. Pineda-Zapata, Carlos López-Jaramillo, Francisco Reyes-Madrigal, Pablo León-Ortíz, Camilo de la Fuente-Sandoval, Leticia Sanguinetti Czepielewski, Clarissa S. Gama, Andre Zugman, Ary Gadelha, Andrea Jackowski, and Rodrigo Bressan. Imaging social and environmental factors as modulators of brain dysfunction: Time to focus on developing non-western societies. *Biological Psychiatry: Cognitive Neuroscience and Neuroimaging*, 4(1):8–15, 2019. ISSN 2451-9022. doi: <https://doi.org/10.1016/j.bpsc.2018.09.005>. URL <https://www.sciencedirect.com/science/article/pii/S2451902218302441>.
- Kathryn R Cullen, Dylan G Gee, Bonnie Klimes-Dougan, Vilma Gabbay, Leslie Hulvershorn, Bryon A Mueller, Jazmin Camchong, Christopher J Bell, Alaa Houry, Sanjiv Kumra, Kelvin O Lim, F Xavier Castellanos, and Michael P Milham. A preliminary study of functional connectivity in comorbid adolescent depression. *Neuroscience Letters*, 460(3): 227–231, 2009. ISSN 0304-3940. doi: 10.1016/J.NEULET.2009.05.022.
- Jill M Cyranowski, Ellen Frank, Elizabeth Young, and Katherine M Shear. Adolescent Onset of the Gender Difference in Lifetime Rates of Major Depression. *Archives of General Psychiatry*, 57(1):21, 2000. ISSN 0003-990X. doi: 10.1001/archpsyc.57.1.21.
- Ana M Daugherty and Naftali Raz. Accumulation of iron in the putamen predicts its shrinkage in healthy older adults: a multi-occasion longitudinal study. *Neuroimage*, 128: 11–20, 2016.
- Julien Dauguet, Sharon Peled, Vladimir Berezovskii, Thierry Delzescaux, Simon K Warfield, Richard Born, and Carl-Fredrik Westin. Comparison of fiber tracts derived from in-vivo dti tractography with 3d histological neural tract tracer reconstruction on a macaque brain. *Neuroimage*, 37(2):530–538, 2007.
- C. G. Davey, B. J. Harrison, M. Yücel, and N. B. Allen. Regionally specific alterations in functional connectivity of the anterior cingulate cortex in major depressive disorder. *Psychological Medicine*, 42(10):2071–2081, oct 2012. ISSN 0033-2917. doi: 10.1017/S0033291712000323. URL https://www.cambridge.org/core/product/identifier/S0033291712000323/type/journal_{_}article.

- Alex R DeCasien, Elisa Guma, Siyuan Liu, and Armin Raznahan. Sex differences in the human brain: a roadmap for more careful analysis and interpretation of a biological reality. *Biology of Sex Differences*, 13(1):43, 2022.
- Rahul S Desikan, Florent Ségonne, Bruce Fischl, Brian T Quinn, Bradford C Dickerson, Deborah Blacker, Randy L Buckner, Anders M Dale, R Paul Maguire, Bradley T Hyman, et al. An automated labeling system for subdividing the human cerebral cortex on mri scans into gyral based regions of interest. *Neuroimage*, 31(3):968–980, 2006.
- Phoebe Dewing, Tao Shi, Steve Horvath, and Eric Vilain. Sexually dimorphic gene expression in mouse brain precedes gonadal differentiation. *Molecular Brain Research*, 118(1-2): 82–90, 2003.
- Elvisha Dhamala, Leon Qi Rong Ooi, Jianzhong Chen, Ru Kong, Kevin M. Anderson, Rowena Chin, B. T. Thomas Yeo, and Avram J. Holmes. Proportional intracranial volume correction differentially biases behavioral predictions across neuroanatomical features, sexes, and development. *NeuroImage*, 260:119485, 2022. ISSN 1053-8119. doi: 10.1016/j.neuroimage.2022.119485. URL <https://www.sciencedirect.com/science/article/pii/S1053811922006012>.
- Adriana Di Martino, Damien A. Fair, Clare Kelly, Theodore D. Satterthwaite, F. Xavier Castellanos, Moriah E. Thomason, R. Cameron Craddock, Beatriz Luna, Bennett L. Leventhal, Xi-Nian Zuo, and Michael P. Milham. Unraveling the Miswired Connectome: A Developmental Perspective. *Neuron*, 83(6):1335–1353, September 2014a. ISSN 0896-6273. doi: 10.1016/j.neuron.2014.08.050. URL <https://www.sciencedirect.com/science/article/pii/S0896627314007806>.
- Adriana Di Martino, Chao-Gan Yan, Qingyang Li, Erin Denio, Francisco X Castellanos, Kaat Alaerts, Jeffrey S Anderson, Michal Assaf, Susan Y Bookheimer, Mirella Dapretto, et al. The autism brain imaging data exchange: towards a large-scale evaluation of the intrinsic brain architecture in autism. *Molecular psychiatry*, 19(6):659–667, 2014b.
- Adriana Di Martino, David O’connor, Bosi Chen, Kaat Alaerts, Jeffrey S Anderson, Michal Assaf, Joshua H Balsters, Leslie Baxter, Anita Beggato, Sylvie Bernaerts, et al. Enhancing studies of the connectome in autism using the autism brain imaging data exchange ii. *Scientific data*, 4(1):1–15, 2017.
- Danai Dima, Amirhossein Modabbernia, Efstathios Papachristou, Gaelle E. Doucet, Ingrid Agartz, Moji Aghajani, Theophilus N. Akudjedu, Anton Albajes-Eizagirre, Dag Alnæs, Kathryn I. Alpert, Micael Andersson, Nancy C. Andreasen, Ole A. Andreassen, Philip Asherson, Tobias Banaschewski, Nuria Bargallo, Sarah Baumeister, Ramona Baur-Streubel, Alessandro Bertolino, Aurora Bonvino, Dorret I. Boomsma, Stefan Borgwardt, Josiane Bourque, Daniel Brandeis, Alan Breier, Henry Brodaty, Rachel M. Brouwer, Jan K. Buitelaar, Geraldo F. Busatto, Randy L. Buckner, Vincent Calhoun, Erick J. Canales-Rodríguez, Dara M. Cannon, Xavier Caseras, Francisco X. Castellanos, Simon Cervenka, Tiffany M. Chaim-Avancini, Christopher R. K. Ching, Victoria Chubar, Vincent P. Clark, Patricia Conrod, Annette Conzelmann, Benedicto Crespo-Facorro, Fabrice Crivello, Eveline A. Crone, Udo Dannlowski, Anders M. Dale, Christopher Davey, Eco J. C. de Geus, Lieuwe de Haan, Greig I. de Zubicaray, Anouk den Braber, Erin W. Dickie, Annabella Di Giorgio, Nhat Trung Doan, Erlend S. Dørum, Stefan Ehrlich, Susanne Erk, Thomas

- Espeseth, Helena Fatouros-Bergman, Simon E. Fisher, Jean-Paul Fouché, Barbara Franke, Thomas Frodl, Paola Fuentes-Claramonte, David C. Glahn, Ian H. Gotlib, Hans-Jürgen Grabe, Oliver Grimm, Nynke A. Groenewold, Dominik Grotegerd, Oliver Gruber, Patricia Gruner, Rachel E. Gur, Ruben C. Gur, Tim Hahn, Ben J. Harrison, Catharine A. Hartman, Sean N. Hatton, Andreas Heinz, Dirk J. Heslenfeld, Derrek P. Hibar, Ian B. Hickie, Beng-Choon Ho, Pieter J. Hoekstra, Sarah Hohmann, Avram J. Holmes, Martine Hoogman, Norbert Hosten, Fleur M. Howells, Hilleke E. Hulshoff Pol, Chaim Huyser, Neda Jahanshad, Anthony James, Terry L. Jernigan, Jiyang Jiang, Erik G. Jönsson, John A. Joska, Rene Kahn, Andrew Kalnin, Ryota Kanai, Marieke Klein, Tatyana P. Klyushnik, Laura Koenders, Sanne Koops, Bernd Krämer, Jonna Kuntsi, Jim Lagopoulos, Luisa Lázaro, Irina Lebedeva, Won Hee Lee, Klaus-Peter Lesch, Christine Lochner, Marise W. J. Machielsen, Sophie Maingault, Nicholas G. Martin, Ignacio Martínez-Zalacaín, David Mataix-Cols, Bernard Mazoyer, Colm McDonald, Brenna C. McDonald, Andrew M. McIntosh, Katie L. McMahon, Genevieve McPhilemy, Susanne Meinert, José M. Menchón, Sarah E. Medland, Andreas Meyer-Lindenberg, Jilly Naaïjen, Pablo Najt, Tomohiro Nakao, Jan E. Nordvik, Lars Nyberg, Jaap Oosterlaan, Víctor Ortiz-García de la Foz, Yannis Paloyelis, Paul Pauli, Giulio Pergola, Edith Pomarol-Clotet, Maria J. Portella, Steven G. Potkin, Joaquim Radua, Andreas Reif, Daniel A. Rinker, Joshua L. Roffman, Pedro G. P. Rosa, Matthew D. Sacchet, Perminder S. Sachdev, Raymond Salvador, Pascual Sánchez-Juan, Salvador Sarró, Theodore D. Satterthwaite, Andrew J. Saykin, Mauricio H. Serpa, Lianne Schmaal, Knut Schnell, Gunter Schumann, Kang Sim, Jordan W. Smoller, Iris Sommer, Carles Soriano-Mas, Dan J. Stein, Lachlan T. Strike, Suzanne C. Swagerman, Christian K. Tamnes, Henk S. Temmingh, Sophia I. Thomopoulos, Alexander S. Tomyshv, Diana Tordesillas-Gutiérrez, Julian N. Trollor, Jessica A. Turner, Anne Uhlmann, Odile A. van den Heuvel, Dennis van den Meer, Nic J. A. van der Wee, Neeltje E. M. van Haren, Dennis van't Ent, Theo G. M. van Erp, Ilya M. Veer, Dick J. Veltman, Aristotle Voineskos, Henry Völzke, Henrik Walter, Esther Walton, Lei Wang, Yang Wang, Thomas H. Wassink, Bernd Weber, Wei Wen, John D. West, Lars T. Westlye, Heather Whalley, Lara M. Wierenga, Steven C. R. Williams, Katharina Wittfeld, Daniel H. Wolf, Amanda Worker, Margaret J. Wright, Kun Yang, Yulyia Yoncheva, Marcus V. Zanetti, Georg C. Ziegler, Paul M. Thompson, Sophia Frangou, and Karolinska Schizophrenia Project (KaSP). Subcortical volumes across the lifespan: Data from 18,605 healthy individuals aged 3–90 years. *Human Brain Mapping*, 43(1):452–469, 2022. ISSN 1097-0193. doi: 10.1002/hbm.25320. URL <https://onlinelibrary.wiley.com/doi/abs/10.1002/hbm.25320>. _eprint: <https://onlinelibrary.wiley.com/doi/pdf/10.1002/hbm.25320>.
- Christine M Disteche. Dosage compensation of the sex chromosomes and autosomes. In *Seminars in cell & developmental biology*, volume 56, pages 9–18. Elsevier, 2016.
- SM Dombrowski, CC Hilgetag, and H Barbas. Quantitative architecture distinguishes prefrontal cortical systems in the rhesus monkey. *Cerebral cortex*, 11(10):975–988, 2001.
- Chad J Donahue, Stamatios N Sotiropoulos, Saad Jbabdi, Moises Hernandez-Fernandez, Timothy E Behrens, Tim B Dyrby, Timothy Coalson, Henry Kennedy, Kenneth Knoblauch, David C Van Essen, et al. Using diffusion tractography to predict cortical connection strength and distance: a quantitative comparison with tracers in the monkey. *Journal of Neuroscience*, 36(25):6758–6770, 2016.
- Lena Dorfschmidt, Richard A. Bethlehem, Jakob Seidlitz, František Váša, Simon R. White, Rafael Romero-García, Manfred G. Kitzbichler, Athina R. Aruldass, Sarah E. Morgan,

- Ian M. Goodyer, Peter Fonagy, Peter B. Jones, Ray J. Dolan, NSPN Consortium, Neil A. Harrison, Petra E. Vértes, and Edward T. Bullmore. Sexually divergent development of depression-related brain networks during healthy human adolescence. *Science Advances*, 8(21):eabm7825, May 2022. doi: 10.1126/sciadv.abm7825. URL <https://www.science.org/doi/10.1126/sciadv.abm7825>. Publisher: American Association for the Advancement of Science.
- Nico U F Dosenbach, Binyam Nardos, Alexander L Cohen, Damien A Fair, Jonathan D Power, Jessica A Church, Steven M Nelson, Gagan S Wig, Alecia C Vogel, Christina N Lessov-Schlaggar, Kelly Anne Barnes, Joseph W Dubis, Eric Feczko, Rebecca S Coalson, John R Pruett, Deanna M Barch, Steven E Petersen, and Bradley L Schlaggar. Prediction of Individual Brain Maturity Using fMRI. *Science*, 329(5997):1358–1361, 2010. ISSN 0036-8075. doi: 10.1126/science.1194144.
- Joseph D. Dougherty, Eric F. Schmidt, Miho Nakajima, and Nathaniel Heintz. Analytical approaches to RNA profiling data for the identification of genes enriched in specific cells. *Nucleic Acids Research*, 38(13):4218–4230, 2010. ISSN 0305-1048. doi: 10.1093/nar/gkq130. URL <https://doi.org/10.1093/nar/gkq130>.
- Wayne C. Drevets, Joseph L. Price, Joseph R. Simpson, Richard D. Todd, Theodore Reich, Michael Vannier, and Marcus E. Raichle. Subgenual prefrontal cortex abnormalities in mood disorders. *Nature*, 386(6627):824–827, apr 1997. ISSN 0028-0836. doi: 10.1038/386824a0. URL <http://www.nature.com/articles/386824a0>.
- Stacey L Edwards, Jonathan Beesley, Juliet D French, and Alison M Dunning. Beyond gwas: Illuminating the dark road from association to function. *The American Journal of Human Genetics*, 93(5):779–797, 2013. ISSN 0002-9297. doi: <https://doi.org/10.1016/j.ajhg.2013.10.012>.
- Simon Eickhoff, Nathan B Walters, Axel Schleicher, Jillian Kril, Gary F Egan, Karl Zilles, John DG Watson, and Katrin Amunts. High-resolution mri reflects myeloarchitecture and cytoarchitecture of human cerebral cortex. *Human brain mapping*, 24(3):206–215, 2005.
- Live Eikenes, Eelke Visser, Torgil Vangberg, and Asta K Håberg. Both brain size and biological sex contribute to variation in white matter microstructure in middle-aged healthy adults. *Human Brain Mapping*, 2022.
- L Eliot, A Ahmed, H Khan, and J Patel. Dump the “dimorphism”: Comprehensive synthesis of human brain studies reveals few male-female differences beyond size. *Neuroscience & Biobehavioral Reviews*, 2021. ISSN 0149-7634. doi: <https://doi.org/10.1016/j.neubiorev.2021.02.026>.
- ML Elliott, A Romer, AR Knodt, and AR Hariri. A connectome-wide functional signature of transdiagnostic risk for mental illness. *Biol Psychiatry*, 84:452–459, 2018. doi: 10.1016/j.biopsych.2018.03.012.
- Sacha Epskamp, Denny Borsboom, and Eiko I Fried. Estimating psychological networks and their accuracy: A tutorial paper. *Behavior research methods*, 50:195–212, 2018.
- Alan C Evans, Brain Development Cooperative Group, et al. The nih mri study of normal brain development. *Neuroimage*, 30(1):184–202, 2006.

- D A Fair, N U F Dosenbach, J A Church, A L Cohen, S Brahmbhatt, F M Miezin, D M Barch, M E Raichle, S E Petersen, and B L Schlaggar. Development of distinct control networks through segregation and integration. *Proceedings of the National Academy of Sciences*, 104(33):13507–13512, 2007. ISSN 0027-8424. doi: 10.1073/pnas.0705843104.
- Carlo Faravelli, Maria Alessandra Scarpato, Giovanni Castellini, and Carolina Lo Sauro. Gender differences in depression and anxiety: The role of age. *Psychiatry Research*, 210(3):1301–1303, 2013. ISSN 0165-1781. doi: 10.1016/J.PSYCHRES.2013.09.027.
- Daphna Fenchel, Ralica Dimitrova, Jakob Seidlitz, Emma C Robinson, Dafnis Batalle, Jana Hutter, Daan Christiaens, Maximilian Pietsch, Jakki Brandon, Emer J Hughes, et al. Development of microstructural and morphological cortical profiles in the neonatal brain. *Cerebral Cortex*, 30(11):5767–5779, 2020.
- Bart Ferguson, Natalia Petridou, Alessio Fracasso, Martijn P van Den Heuvel, Rachel M Brouwer, Hilleke E Hulshoff Pol, René S Kahn, and René CW Mandl. Detailed t1-weighted profiles from the human cortex measured in vivo at 3 tesla mri. *Neuroinformatics*, 16:181–196, 2018.
- P A Filipek, C Richelme, D N Kennedy, and V S Caviness. The Young Adult Human Brain: An MRI-based Morphometric Analysis. *Cerebral Cortex*, 4(4):344–360, 1994. ISSN 1047-3211. doi: 10.1093/cercor/4.4.344.
- Massimo Filippi, Paola Valsasina, Paolo Misci, Andrea Falini, Giancarlo Comi, and Maria A Rocca. The organization of intrinsic brain activity differs between genders: A resting-state fMRI study in a large cohort of young healthy subjects. *Human Brain Mapping*, 34(6):1330–1343, 2013. ISSN 10659471. doi: 10.1002/hbm.21514.
- Cordelia Fine. *Delusions of gender: The real science behind sex differences*. Icon Books Ltd, 2005.
- Cordelia Fine. Will working mothers’ brains explode? the popular new genre of neurosexism. *Neuroethics*, 1(1):69–72, 2008.
- Cordelia Fine. His brain, her brain? *Science*, 346(6212):915–916, 2014.
- Michael B First. Structured clinical interview for the dsm (scid). *The encyclopedia of clinical psychology*, pages 1–6, 2014.
- B Fischl, D H Salat, E Busa, M Albert, M Dieterich, C Haselgrove, A van der Kouwe, R Killiany, D Kennedy, S Klaveness, A Montillo, N Makris, B Rosen, and A M Dale. Automated labeling of neuroanatomical structures in the human brain. *Cell Press*, 33(3):341–355, 2002. doi: [https://doi.org/10.1016/S0896-6273\(02\)00569-X](https://doi.org/10.1016/S0896-6273(02)00569-X).
- Bruce Fischl. FreeSurfer. *NeuroImage*, 62(2):774–781, August 2012. ISSN 1053-8119. doi: 10.1016/j.neuroimage.2012.01.021. URL <https://www.sciencedirect.com/science/article/pii/S1053811912000389>.
- Bruce Fischl, Martin I. Sereno, and Anders M. Dale. Cortical surface-based analysis: Ii: Inflation, flattening, and a surface-based coordinate system. *NeuroImage*, 9(2):195–207, 1999. ISSN 1053-8119. doi: <https://doi.org/10.1006/nimg.1998.0396>.

- R. A. Fisher. Frequency distribution of the values of the correlation coefficient in samples from an indefinitely large population. *Biometrika*, 10(4):507–521, 1915. ISSN 0006-3444. doi: 10.2307/2331838. URL <https://www.jstor.org/stable/2331838>. Publisher: [Oxford University Press, Biometrika Trust].
- Anders M Fjell, Markus H Sneve, Håkon Grydeland, Andreas B Storsve, Inge K Amlien, Anastasia Yendiki, and Kristine B Walhovd. Relationship between structural and functional connectivity change across the adult lifespan: a longitudinal investigation. *Human brain mapping*, 38(1):561–573, 2017.
- Alex Fornito, Andrew Zalesky, and Edward T Bullmore. *Fundamentals of brain network analysis / Alex Fornito, Andrew Zalesky, Edward T. Bullmore*. Elsevier/Academic Press Amsterdam ; Boston, 2016.
- Jean-Philippe Fortin, Nicholas Cullen, Yvette I Sheline, Warren D Taylor, Irem Aselcioglu, Philip A Cook, Phil Adams, Crystal Cooper, Maurizio Fava, Patrick J McGrath, et al. Harmonization of cortical thickness measurements across scanners and sites. *Neuroimage*, 167:104–120, 2018.
- Thomas Frodl, Markus Jäger, Ivana Smajstrlova, Christine Born, Ronald Bottlender, Tanja Palladino, Maximilian Reiser, Hans-Jürgen Möller, and Eva M. Meisenzahl. Effect of hippocampal and amygdala volumes on clinical outcomes in major depression: a 3-year prospective magnetic resonance imaging study. *Journal of Psychiatry and Neuroscience*, 33(5):423–430, September 2008. ISSN 1180-4882. URL <https://www.jpn.ca/content/33/5/423>. Publisher: Journal of Psychiatry and Neuroscience Section: Research Paper.
- Laura Fusar-Poli, Natascia Brondino, Pierluigi Politi, and Eugenio Aguglia. Missed diagnoses and misdiagnoses of adults with autism spectrum disorder. *European archives of psychiatry and clinical neuroscience*, 272(2):187–198, 2022.
- Paul M Galdas, Francine Cheater, and Paul Marshall. Men and health help-seeking behaviour: literature review. *Journal of advanced nursing*, 49(6):616–623, 2005.
- Paola Galdi, Manuel Blesa, Gemma Sullivan, Gillian J Lamb, David Q Stoye, Alan J Quigley, Michael J Thrippleton, Mark E Bastin, and James P Boardman. Neonatal morphometric similarity networks predict atypical brain development associated with preterm birth. In *Connectomics in NeuroImaging: Second International Workshop, CNI 2018, Held in Conjunction with MICCAI 2018, Granada, Spain, September 20, 2018, Proceedings 2*, pages 47–57. Springer, 2018.
- Paola Galdi, Manuel Blesa, David Q Stoye, Gemma Sullivan, Gillian J Lamb, Alan J Quigley, Michael J Thrippleton, Mark E Bastin, and James P Boardman. Neonatal morphometric similarity mapping for predicting brain age and characterizing neuroanatomic variation associated with preterm birth. *NeuroImage: Clinical*, 25:102195, 2020.
- Michael J. Gandal, Jillian R. Haney, Neelroop N. Parikshak, Virpi Leppä, Gokul Ramaswami, Chris Hartl, Andrew J. Schork, Vivek Appadurai, Alfonso Buil, Thomas M. Werge, Chunyu Liu, Kevin P. White, null null, null null, Steve Horvath, Daniel H. Geschwind, Nenad Sestan, Flora Vaccarino, Mark Gerstein, Sherman Weissman, Sirisha Pochareddy, Matthew State, James Knowles, Peggy Farnham, Schahram Akbarian, Dalila

- Pinto, Harm Van Baekl, Stella Dracheva, Andrew Jaffe, Thomas Hyde, Peter Zandi, Gregory Crawford, Pat Sullivan, Wesley Kurt Thompson, Preben Bo Mortensen, Esben Agerbo, Marianne Giørtz Pedersen, Carsten Bøcker Pedersen, Ole Mors, Anders D. Børghlum, Merete Nordentoft, David M. Hougaard, Jonas Bybjerg-Grauholm, Marie Bækvad-Hansen, Alicia R. Martin, Ashley Dumont, Christine Stevens, Claire Churchhouse, Daniel P. Howrigan, Duncan S. Palmer, Elise B. Robinson, Kyle F. Satterstrom, Felecia Cerrato, Hailiang Huang, Jacqueline Goldstein, Jennifer Moran, Joanna Martin Julian, Maller Kimberly, Chambert Patrick, Patrick Turley, Raymond Walters, Rich Belliveau, Stephan Ripke, Timothy Poterba, Mark J. Daly, Benjamin Neale, Menachem Fromer, Panos Roussos, Jessica S. Johnson, Hardik R. Shah, Milind C. Mahajan, Eric Schadt, Vahram Haroutunian, Douglas M. Ruderfer, Joseph D. Buxbaum, Solveig K. Sieberts, Kristen Dang, Ben Logsdon, Lara M. Mangravite, Mette Peters, Raquel E. Gur, Chang-Gyu Hahn, Bernie Devlin, Lambertus L. Klei, David Lewis, Barbara Lipska, Keisuke Hirai, Hiroyoshi Toyoshiba, and Enrico Domenici. Shared molecular neuropathology across major psychiatric disorders parallels polygenic overlap. *Science*, 359(6376):693–697, 2018. doi: 10.1126/science.aad6469. URL <https://www.science.org/doi/abs/10.1126/science.aad6469>.
- H. Garavan, H. Bartsch, K. Conway, A. Decastro, R. Z. Goldstein, S. Heeringa, T. Jernigan, A. Potter, W. Thompson, and D. Zahs. Recruiting the ABCD sample: Design considerations and procedures. *Developmental Cognitive Neuroscience*, 32:16–22, August 2018. ISSN 1878-9293. doi: 10.1016/j.dcn.2018.04.004. URL <https://www.sciencedirect.com/science/article/pii/S1878929317301809>.
- John H Gilmore, Weili Lin, Marcel W Prastawa, Christopher B Looney, Y Sampath K Vetsa, Rebecca C Knickmeyer, Dianne D Evans, J Keith Smith, Robert M Hamer, Jeffrey A Lieberman, et al. Regional gray matter growth, sexual dimorphism, and cerebral asymmetry in the neonatal brain. *Journal of Neuroscience*, 27(6):1255–1260, 2007.
- John H Gilmore, Feng Shi, Sandra L Woolson, Rebecca C Knickmeyer, Sarah J Short, Weili Lin, Hongtu Zhu, Robert M Hamer, Martin Styner, and Dinggang Shen. Longitudinal development of cortical and subcortical gray matter from birth to 2 years. *Cerebral cortex*, 22(11):2478–2485, 2012.
- John H. Gilmore, Benjamin Langworthy, Jessica B. Girault, Jason Fine, Shaili C. Jha, Sun Hyung Kim, Emil Cornea, and Martin Styner. Individual Variation of Human Cortical Structure Is Established in the First Year of Life. *Biological Psychiatry: Cognitive Neuroscience and Neuroimaging*, 5(10):971–980, October 2020. ISSN 2451-9022. doi: 10.1016/j.bpsc.2020.05.012. URL <https://www.sciencedirect.com/science/article/pii/S2451902220301373>.
- Matthew F Glasser, Stamatiou N Sotiropoulos, J Anthony Wilson, Timothy S Coalson, Bruce Fischl, Jesper L Andersson, Junqian Xu, Saad Jbabdi, Matthew Webster, Jonathan R Polimeni, et al. The minimal preprocessing pipelines for the human connectome project. *Neuroimage*, 80:105–124, 2013.
- Matthew F Glasser, Timothy S Coalson, Emma C Robinson, Carl D Hacker, John Harwell, Essa Yacoub, Kamil Ugurbil, Jesper Andersson, Christian F Beckmann, Mark Jenkinson, Stephen M Smith, and David C Van Essen. A multi-modal parcellation of human cerebral cortex. *Nature*, 536(7615):171–178, 2016a. ISSN 0028-0836. doi: 10.1038/nature18933.

- Matthew F. Glasser, Timothy S. Coalson, Emma C. Robinson, Carl D. Hacker, John Harwell, Essa Yacoub, Kamil Ugurbil, Jesper Andersson, Christian F. Beckmann, Mark Jenkinson, Stephen M. Smith, and David C. Van Essen. A multi-modal parcellation of human cerebral cortex. *Nature*, 536(7615):171–178, August 2016b. ISSN 1476-4687. doi: 10.1038/nature18933. URL <https://www.nature.com/articles/nature18933>. Number: 7615 Publisher: Nature Publishing Group.
- Alexandros Goulas, René Werner, Sarah F Beul, Dennis Säring, Martijn van den Heuvel, Lazaros C Triarhou, and Claus C Hilgetag. Cytoarchitectonic similarity is a wiring principle of the human connectome. *BioRxiv*, page 068254, 2016.
- Alexandros Goulas, Harry B. M. Uylings, and Claus C. Hilgetag. Principles of ipsilateral and contralateral cortico-cortical connectivity in the mouse. *Brain Struct Funct*, 222(3):1281–1295, 2017. ISSN 1863-2661. doi: 10.1007/s00429-016-1277-y. URL <https://doi.org/10.1007/s00429-016-1277-y>.
- Michael D Greicius, Benjamin H Flores, Vinod Menon, Gary H Glover, Hugh B Solvason, Heather Kenna, Allan L Reiss, and Alan F Schatzberg. Resting-state functional connectivity in major depression: abnormally increased contributions from subgenual cingulate cortex and thalamus. *Biological psychiatry*, 62(5):429–437, 2007.
- Hannah Grotzinger, Laura Pritschet, Tyler Santander, and Emily G Jacobs. P684. diurnal fluctuations in testosterone tied to variation in intrinsic functional connectivity in a densely sampled male. *Biological Psychiatry*, 91(9):S367, 2022.
- WHO Multicentre Growth Reference Study Group and Mercedes de Onis. Who child growth standards based on length/height, weight and age. *Acta paediatrica*, 95:76–85, 2006.
- Zijin Gu, Keith Wakefield Jamison, Mert Rory Sabuncu, and Amy Kuceyeski. Heritability and interindividual variability of regional structure-function coupling. *Nat Commun*, 12(1):4894, 2021. ISSN 2041-1723. doi: 10.1038/s41467-021-25184-4. URL <https://www.nature.com/articles/s41467-021-25184-4>. Number: 1 Publisher: Nature Publishing Group.
- Daniel A Hackman, Laura M Betancourt, Nancy L Brodsky, Hallam Hurt, and Martha J Farah. Neighborhood disadvantage and adolescent stress reactivity. *Frontiers in human neuroscience*, 6:277, 2012.
- Patric Hagmann, Lisa Jonasson, Philippe Maeder, Jean-Philippe Thiran, Van J Wedeen, and Reto Meuli. Understanding diffusion mr imaging techniques: from scalar diffusion-weighted imaging to diffusion tensor imaging and beyond. *Radiographics*, 26(suppl_1):S205–S223, 2006.
- Benjamin L Hankin, Lyn Y Abramson, Terrie E Moffitt, Phil A Silva, Rob McGee, and Kathryn E Angell. Development of depression from preadolescence to young adulthood: Emerging gender differences in a 10-year longitudinal study. *Journal of Abnormal Psychology*, 107(1):128–140, 1998. ISSN 1939-1846. doi: 10.1037/0021-843X.107.1.128.
- Michael Hawrylycz, Jeremy A Miller, Vilas Menon, David Feng, Tim Dolbeare, Angela L Guillozet-Bongaarts, Anil G Jegga, Bruce J Aronow, Chang-Kyu Lee, Amy Bernard, et al. Canonical genetic signatures of the adult human brain. *Nature neuroscience*, 18(12):1832–1844, 2015.

- Heather Cody Hazlett, Hongbin Gu, Brent C Munsell, Sun Hyung Kim, Martin Styner, Jason J Wolff, Jed T Elison, Meghan R Swanson, Hongtu Zhu, Kelly N Botteron, et al. Early brain development in infants at high risk for autism spectrum disorder. *Nature*, 542 (7641):348–351, 2017.
- Ningning He, Edmund T Rolls, Wei Zhao, and Shuixia Guo. Predicting human inhibitory control from brain structural mri. *Brain imaging and behavior*, 14:2148–2158, 2020.
- Janet Heinrich, MT Gahart, EJ Rowe, and L Bradley. Drug safety: most drugs withdrawn in recent years had greater health risks for women. *A letter to The Honorable Tom Harkin, The Honorable Olympia J. Snowe, The Honorable Barbara A. Mikulski, United States Senate, The Honorable Henry Waxman, House of Representatives. Washington DC: United States General Accounting Office*, 2001.
- Claus C Hilgetag, Maria Medalla, Sarah F Beul, and Helen Barbas. The primate connectome in context: principles of connections of the cortical visual system. *NeuroImage*, 134: 685–702, 2016a.
- Claus C Hilgetag, Maria Medalla, Sarah F Beul, and Helen Barbas. The primate connectome in context: principles of connections of the cortical visual system. *NeuroImage*, 134: 685–702, 2016b.
- Beng-Choon Ho, Nancy C. Andreasen, Steven Ziebell, Ronald Pierson, and Vincent Magnotta. Long-term Antipsychotic Treatment and Brain Volumes: A Longitudinal Study of First-Episode Schizophrenia. *Archives of General Psychiatry*, 68(2):128–137, February 2011. ISSN 0003-990X. doi: 10.1001/archgenpsychiatry.2010.199. URL <https://doi.org/10.1001/archgenpsychiatry.2010.199>.
- Avram J Holmes, Marisa O Hollinshead, Timothy M O’keefe, Victor I Petrov, Gabriele R Fariello, Lawrence L Wald, Bruce Fischl, Bruce R Rosen, Ross W Mair, Joshua L Roffman, et al. Brain genomics superstruct project initial data release with structural, functional, and behavioral measures. *Scientific data*, 2(1):1–16, 2015.
- Joni Holmes, Annie Bryant, and Susan Elizabeth Gathercole. Protocol for a transdiagnostic study of children with problems of attention, learning and memory (calm). *BMC pediatrics*, 19(1):1–11, 2019.
- Philipp Homan, Miklos Argyelan, Pamela DeRosse, Philip R Szeszko, Juan A Gallego, Lauren Hanna, Delbert G Robinson, John M Kane, Todd Lencz, and Anil K Malhotra. Structural similarity networks predict clinical outcome in early-phase psychosis. *Neuropsychopharmacology*, 44(5):915–922, 2019.
- Brittany R Howell, Martin A Styner, Wei Gao, Pew-Thian Yap, Li Wang, Kristine Baluyot, Essa Yacoub, Geng Chen, Taylor Potts, Andrew Salzwedel, et al. The unc/umn baby connectome project (bcp): An overview of the study design and protocol development. *NeuroImage*, 185:891–905, 2019.
- Kai Hwang, Michael N Hallquist, and Beatriz Luna. The development of hub architecture in the human functional brain network. *Cerebral Cortex*, 23(10):2380–2393, 2013.

- Baohu Ji, Kerin K. Higa, John R. Kelsoe, and Xianjin Zhou. Over-expression of *xist*, the master gene for x chromosome inactivation, in females with major affective disorders. *EBioMedicine*, 2(8):909–918, 2015. ISSN 2352-3964. doi: <https://doi.org/10.1016/j.ebiom.2015.06.012>.
- A N Kaczurkin, A Raznahan, and T D Satterhwaite. Sex differences in the developing brain: insights from multimodal neuroimaging. *Neuropsychopharmacology*, page 71–85, 2019. ISSN 44. doi: <https://doi.org/10.1038/s41386-018-0111-z>.
- Theodor Kaes. *Die Grosshirnrinde des Menschen in ihren Massen und in ihrem Fasergehalt: ein gehirnanatomischer Atlas, mit erläuterndem Text*. fischer, 1907.
- Hyo Jung Kang, Yuka Imamura Kawasawa, Feng Cheng, Ying Zhu, Xuming Xu, Mingfeng Li, André M. M. Sousa, Mihovil Pletikos, Kyle A. Meyer, Goran Sedmak, Tobias Guennel, Yurac Shin, Matthew B. Johnson, Željka Krsnik, Simone Mayer, Sofia Fertuzinhos, Sheila Umlauf, Steven N. Lisgo, Alexander Vortmeyer, Daniel R. Weinberger, Shrikant Mane, Thomas M. Hyde, Anita Huttner, Mark Reimers, Joel E. Kleinman, and Nenad Šestan. Spatiotemporal transcriptome of the human brain. *Nature*, 478(7370):483–489, October 2011. ISSN 0028-0836. doi: [10.1038/nature10523](https://doi.org/10.1038/nature10523). URL <https://www.ncbi.nlm.nih.gov/pmc/articles/PMC3566780/>.
- Linnea Karlsson, Mimmi Tolvanen, Noora M Scheinin, Henna-Maria Uusitupa, Riikka Korja, Eeva Ekholm, Jetro J Tuulari, Marjukka Pajulo, Minna Huotilainen, Tiina Paunio, et al. Cohort profile: the finnbrain birth cohort study (finnbrain). *International journal of epidemiology*, 47(1):15–16j, 2018.
- Matcheri S Keshavan, Stewart Anderson, and Jay W Pettergrew. Is schizophrenia due to excessive synaptic pruning in the prefrontal cortex? the feinberg hypothesis revisited. *Journal of psychiatric research*, 28(3):239–265, 1994.
- Ronald C. Kessler, Patricia Berglund, Olga Demler, Robert Jin, Kathleen R. Merikangas, and Ellen E. Walters. Lifetime Prevalence and Age-of-Onset Distributions of DSM-IV Disorders in the National Comorbidity Survey Replication. *Archives of General Psychiatry*, 62(6):593–602, June 2005. ISSN 0003-990X. doi: [10.1001/archpsyc.62.6.593](https://doi.org/10.1001/archpsyc.62.6.593). URL <https://doi.org/10.1001/archpsyc.62.6.593>.
- Budhachandra S Khundrakpam, Andrew Reid, Jens Brauer, Felix Carbonell, John Lewis, Stephanie Ameis, Sherif Karama, Junki Lee, Zhang Chen, Samir Das, et al. Developmental changes in organization of structural brain networks. *Cerebral Cortex*, 23(9):2072–2085, 2013.
- Beatrix Kiddle, Becky Inkster, Gita Prabhu, Michael Moutoussis, Kirstie J Whitaker, Edward T Bullmore, Raymond J Dolan, Peter Fonagy, Ian M Goodyer, and Peter B Jones. Cohort Profile: The NSPN 2400 Cohort: a developmental sample supporting the Wellcome Trust NeuroScience in Psychiatry Network. *International Journal of Epidemiology*, 47(1):18–19g, 2017. ISSN 0300-5771. doi: [10.1093/ije/dyx117](https://doi.org/10.1093/ije/dyx117).
- L A Kilpatrick, D H Zald, J V Pardo, and L F Cahill. Sex-related differences in amygdala functional connectivity during resting conditions. *NeuroImage*, 30(2):452–461, 2006. ISSN 1053-8119. doi: [10.1016/J.NEUROIMAGE.2005.09.065](https://doi.org/10.1016/J.NEUROIMAGE.2005.09.065).

- Daniel J King and Amanda G Wood. Clinically feasible brain morphometric similarity network construction approaches with restricted magnetic resonance imaging acquisitions. *Network Neuroscience*, 4(1):274–291, 2020.
- Lee T Kissel and Donna M Werling. Neural transcriptomic analysis of sex differences in autism spectrum disorder: current insights and future directions. *Biological Psychiatry*, 91(1):53–60, 2022.
- Manfred G Kitzbichler, Athina R Aruldass, Gareth J Barker, Tobias C Wood, Nicholas G Dowell, Samuel A Hurley, John McLean, Marta Correia, Charlotte Clarke, Linda Pointon, Jonathan Cavanagh, Phil Cowen, Carmine Pariante, NIMA consortium, Mara Cercignani, Edward T Bullmore, and Neil A Harrison. Peripheral inflammation is associated with micro-structural and functional connectivity changes in depression-related brain networks. *medRxiv*s, 2020. doi: 10.1101/2020.09.09.20191262.
- Rebecca C Knickmeyer, Kai Xia, Zhaohua Lu, Mihye Ahn, Shaili C Jha, Fei Zou, Hongtu Zhu, Martin Styner, and John H Gilmore. Impact of demographic and obstetric factors on infant brain volumes: a population neuroscience study. *Cerebral Cortex*, 27(12):5616–5625, 2017.
- Jian Kong, Pei-chi Tu, Carolyn Zyloney, and Tung-ping Su. Intrinsic functional connectivity of the periaqueductal gray, a resting fMRI study. *Behavioural Brain Research*, 211(2):215–219, aug 2010. ISSN 0166-4328. doi: 10.1016/J.BBR.2010.03.042. URL <https://www.sciencedirect.com/science/article/pii/S0166432810002287?via%3Dihub>.
- Xiang-zhen Kong, Zhaoguo Liu, Lijie Huang, Xu Wang, Zetian Yang, Guangfu Zhou, Zonglei Zhen, and Jia Liu. Mapping individual brain networks using statistical similarity in regional morphology from mri. *PloS one*, 10(11):e0141840, 2015.
- Jakub Kopal, Lucina Q Uddin, and Danilo Bzdok. The end game: respecting major sources of population diversity. *Nature Methods*, pages 1–7, 2023.
- Mayuresh S Korgaonkar, Andrea N Goldstein-Piekarski, Alexander Fornito, and Leanne M Williams. Intrinsic connectomes are a predictive biomarker of remission in major depressive disorder. *Molecular psychiatry*, 25(7):1537–1549, 2020.
- Georg S Kranz, Bella BB Zhang, Patricia Handschuh, Vera Ritter, and Rupert Lanzenberger. Gender-affirming hormone treatment—a unique approach to study the effects of sex hormones on brain structure and function. *Cortex*, 129:68–79, 2020.
- Maria Kuklisova-Murgasova, Paul Aljabar, Latha Srinivasan, Serena J Counsell, Valentina Doria, Ahmed Serag, Ioannis S Gousias, James P Boardman, Mary A Rutherford, A David Edwards, et al. A dynamic 4d probabilistic atlas of the developing brain. *NeuroImage*, 54(4):2750–2763, 2011.
- Prantik Kundu, Souheil J Inati, Jennifer W Evans, Wen-Ming Luh, and Peter A Bandettini. Differentiating BOLD and non-BOLD signals in fMRI time series using multi-echo EPI. *NeuroImage*, 60(3):1759–1770, 2012a. ISSN 1053-8119. doi: 10.1016/J.NEUROIMAGE.2011.12.028.

- Prantik Kundu, Souheil J. Inati, Jennifer W. Evans, Wen-Ming Luh, and Peter A. Bandettini. Differentiating BOLD and Non-BOLD Signals in fMRI Time Series Using Multi-Echo EPI. *Neuroimage*, 60(3):1759–1770, April 2012b. ISSN 1053-8119. doi: 10.1016/j.neuroimage.2011.12.028. URL <https://www.ncbi.nlm.nih.gov/pmc/articles/PMC3350785/>.
- Prantik Kundu, Noah D Brenowitz, Valerie Voon, Yulia Worbe, Petra E Vértes, Souheil J Inati, Ziad S Saad, Peter A Bandettini, and Edward T Bullmore. Integrated strategy for improving functional connectivity mapping using multiecho fMRI. *Proceedings of the National Academy of Sciences of the United States of America*, 110(40):16187–92, 2013a. ISSN 1091-6490. doi: 10.1073/pnas.1301725110.
- Prantik Kundu, Noah D. Brenowitz, Valerie Voon, Yulia Worbe, Petra E. Vértes, Souheil J. Inati, Ziad S. Saad, Peter A. Bandettini, and Edward T. Bullmore. Integrated strategy for improving functional connectivity mapping using multiecho fMRI. *Proceedings of the National Academy of Sciences of the United States of America*, 110(40):16187–16192, October 2013b. ISSN 0027-8424. doi: 10.1073/pnas.1301725110. URL <https://www.ncbi.nlm.nih.gov/pmc/articles/PMC3791700/>.
- Prantik Kundu, Brenda E Benson, Dana Rosen, Sophia Frangou, Ellen Leibenluft, Wen-Ming Luh, Peter A Bandettini, Daniel S Pine, and Monique Ernst. The integration of functional brain activity from adolescence to adulthood. *Journal of Neuroscience*, 38(14):3559–3570, 2018.
- Rayus Kuplicki, James Touthang, Obada Al Zoubi, Ahmad Mayeli, Masaya Misaki, NeuroMAP-Investigators, Robin L Aupperle, T Kent Teague, Brett A McKinney, Martin P Paulus, et al. Common data elements, scalable data management infrastructure, and analytics workflows for large-scale neuroimaging studies. *Frontiers in Psychiatry*, 12: 682495, 2021.
- Rebecca Daniels Kush, D Warzel, Maura A Kush, Alexander Sherman, Eileen A Navarro, R Fitzmartin, Frank Pétavy, Jose Galvez, Lauren B Becnel, FL Zhou, et al. Fair data sharing: the roles of common data elements and harmonization. *Journal of Biomedical Informatics*, 107:103421, 2020.
- N Lake, S Chen, B Sos, J Fan, G E Kaeser, Y C Yung, T E Duong, D Gao, J Chun, P V Kharchenko, and K Zhang. Integrative single-cell analysis of transcriptional and epigenetic states in the human adult brain. *Nature Biotechnology*, 36:70–80, 2018. doi: <https://doi.org/10.1038/nbt.4038>.
- Pamela J LaMontagne, Tammie LS Benzinger, John C Morris, Sarah Keefe, Russ Hornbeck, Chengjie Xiong, Elizabeth Grant, Jason Hassenstab, Krista Moulder, Andrei G Vlassenko, et al. Oasis-3: longitudinal neuroimaging, clinical, and cognitive dataset for normal aging and alzheimer disease. *MedRxiv*, pages 2019–12, 2019.
- Wenkun Lei, Qian Xiao, Chun Wang, Weijia Gao, Yiwen Xiao, Yingliang Dai, Guangming Lu, Linyan Su, and Yuan Zhong. Cell-type-specific genes associated with cortical structural abnormalities in pediatric bipolar disorder. *Psychoradiology*, 2(2):56–65, 2022.
- Matthew J Leming, Simon Baron-Cohen, and John Suckling. Single-participant structural similarity matrices lead to greater accuracy in classification of participants than function in autism in mri. *Molecular Autism*, 12(1):1–15, 2021.

- Jason P Lerch, Keith Worsley, W Philip Shaw, Deanna K Greenstein, Rhoshel K Lenroot, Jay Giedd, and Alan C Evans. Mapping anatomical correlations across cerebral cortex (macacc) using cortical thickness from mri. *Neuroimage*, 31(3):993–1003, 2006.
- Jason P. Lerch, André J. W. van der Kouwe, Armin Raznahan, Tomáš Paus, Heidi Johansen-Berg, Karla L. Miller, Stephen M. Smith, Bruce Fischl, and Stamatiou N. Sotiropoulos. Studying neuroanatomy using MRI. *Nature Neuroscience*, 20(3):314–326, March 2017. ISSN 1546-1726. doi: 10.1038/nn.4501. URL <https://www.nature.com/articles/nn.4501>. Number: 3 Publisher: Nature Publishing Group.
- Jiao Li, Jakob Seidlitz, John Suckling, Feiyang Fan, Gong-Jun Ji, Yao Meng, Siqi Yang, Kai Wang, Jiang Qiu, Huafu Chen, et al. Cortical structural differences in major depressive disorder correlate with cell type-specific transcriptional signatures. *Nature communications*, 12(1):1647, 2021.
- Jiao Li, Simon S Keller, Jakob Seidlitz, Huafu Chen, Bing Li, Yifei Weng, Yao Meng, Siqi Yang, Qiang Xu, Qirui Zhang, et al. Cortical morphometric vulnerability to generalised epilepsy reflects chromosome-and cell type-specific transcriptomic signatures. *Neuropathology and applied neurobiology*, page e12857, 2022.
- M Li, G Santpere, Y Imamura Kawasawa, O V Evgrafov, F O Gulden, S Pochareddy, S M Sunkin, Z Li, Y Shin, Y Zhu, A Sousa, D M Werling, R R Kitchenand H J Kang, M Pletikos, J Choi, S Muchnik, X Xu, D Wang, B Lorente-Galdos, . . . , and N Sestan. Integrative functional genomic analysis of human brain development and neuropsychiatric risks. *Science*, 362, 2018a. ISSN 6420. doi: <https://doi.org/10.1126/science.aat7615>.
- Wan Li, Chunlan Yang, Feng Shi, Shuicai Wu, Qun Wang, Yingnan Nie, and Xin Zhang. Construction of individual morphological brain networks with multiple morphometric features. *Frontiers in neuroanatomy*, 11:34, 2017.
- Wan Li, Chunlan Yang, Shuicai Wu, Yingnan Nie, Xin Zhang, Ming Lu, Tongpeng Chu, and Feng Shi. Alterations of graphic properties and related cognitive functioning changes in mild alzheimer’s disease revealed by individual morphological brain network. *Frontiers in Neuroscience*, 12:927, 2018b.
- Siyuan Liu, Jakob Seidlitz, Jonathan D Blumenthal, Liv S Clasen, and Armin Raznahan. Integrative structural, functional, and transcriptomic analyses of sex-biased brain organization in humans. *Proceedings of the National Academy of Sciences*, 117(31):18788–18798, 2020.
- Zhen-Qi Liu, Bertha Vázquez-Rodríguez, R. Nathan Spreng, Boris C. Bernhardt, Richard F. Betzel, and Bratislav Misić. Time-resolved structure-function coupling in brain networks. *Commun Biol*, 5(1):1–10, 2022. ISSN 2399-3642. doi: 10.1038/s42003-022-03466-x. URL <https://www.nature.com/articles/s42003-022-03466-x>. Number: 1 Publisher: Nature Publishing Group.
- Markus Loeffler, Christoph Engel, Peter Ahnert, Dorothee Alfermann, Katrin Arelin, Ronny Baber, Frank Beutner, Hans Binder, Elmar Brähler, Ralph Burkhardt, et al. The life-adult-study: objectives and design of a population-based cohort study with 10,000 deeply phenotyped adults in germany. *BMC public health*, 15(1):1–14, 2015.

- Nikos K. Logothetis and Brian A. Wandell. Interpreting the BOLD Signal. *Annual Review of Physiology*, 66(1):735–769, mar 2004. ISSN 0066-4278. doi: 10.1146/annurev.physiol.66.082602.092845. URL <http://www.annualreviews.org/doi/10.1146/annurev.physiol.66.082602.092845>.
- Martin Lotze, Martin Domin, Florian H Gerlach, Christian Gaser, Eileen Lueders, Carsten O Schmidt, and Nicola Neumann. Novel findings from 2,838 adult brains on sex differences in gray matter brain volume. *Scientific reports*, 9(1):1671, 2019.
- Yuan-Chiao Lu, Kushal Kapse, Nicole Andersen, Jessica Quistorff, Catherine Lopez, Andrea Fry, Jenhao Cheng, Nickie Andescavage, Yao Wu, Kristina Espinosa, et al. Association between socioeconomic status and in utero fetal brain development. *JAMA network open*, 4(3):e213526–e213526, 2021.
- Liyang Ma, Lixia Tian, Tianyu Hu, Tianzi Jiang, and Nianming Zuo. Development of individual variability in brain functional connectivity and capability across the adult lifespan. *Cerebral Cortex*, 31(8):3925–3938, 2021.
- Frank P MacMaster, Yousha Mirza, Philip R Szeszko, Lauren E Kmiecik, Phillip C Easter, S Preeya Taormina, Michelle Lynch, Michelle Rose, Gregory J Moore, and David R Rosenberg. Amygdala and hippocampal volumes in familial early onset major depressive disorder. *Biological psychiatry*, 63(4):385–390, 2008.
- Eleanor A Maguire, Katherine Woollett, and Hugo J Spiers. London taxi drivers and bus drivers: a structural mri and neuropsychological analysis. *Hippocampus*, 16(12):1091–1101, 2006.
- Klaus H Maier-Hein, Peter F Neher, Jean-Christophe Houde, Marc-Alexandre Côté, Eleftherios Garyfallidis, Jidan Zhong, Maxime Chamberland, Fang-Cheng Yeh, Ying-Chia Lin, Qing Ji, et al. The challenge of mapping the human connectome based on diffusion tractography. *Nature communications*, 8(1):1349, 2017.
- Antonios Makropoulos, Emma C Robinson, Andreas Schuh, Robert Wright, Sean Fitzgibbon, Jelena Bozek, Serena J Counsell, Johannes Steinweg, Katy Vecchiato, Jonathan Passerat-Palmbach, et al. The developing human connectome project: A minimal processing pipeline for neonatal cortical surface reconstruction. *Neuroimage*, 173:88–112, 2018.
- Scott Marek, Kai Hwang, William Foran, Michael N Hallquist, and Beatriz Luna. The contribution of network organization and integration to the development of cognitive control. *PLoS biology*, 13(12):e1002328, 2015.
- Scott Marek, Brenden Tervo-Clemmens, Finnegan J Calabro, David F Montez, Benjamin P Kay, Alexander S Hatoum, Meghan Rose Donohue, William Foran, Ryland L Miller, Timothy J Hendrickson, et al. Reproducible brain-wide association studies require thousands of individuals. *Nature*, 603(7902):654–660, 2022.
- Ross D. Markello and Bratislav Misic. Comparing spatial null models for brain maps. *NeuroImage*, 236:118052, 2021. ISSN 1053-8119. doi: <https://doi.org/10.1016/j.neuroimage.2021.118052>. URL <https://www.sciencedirect.com/science/article/pii/S1053811921003293>.

- Julie A Markham and James I Koenig. Prenatal stress: role in psychotic and depressive diseases. *Psychopharmacology*, 214:89–106, 2011.
- Christopher J Markiewicz, Krzysztof J Gorgolewski, Franklin Feingold, Ross Blair, Yaroslav O Halchenko, Eric Miller, Nell Hardcastle, Joe Wexler, Oscar Esteban, Mathias Goncavles, et al. The openneuro resource for sharing of neuroscience data. *Elife*, 10: e71774, 2021.
- Daniel Martins, Ottavia Dipasquale, Mattia Veronese, Federico Turkheimer, Marco L Loggia, Stephen McMahon, Matthew A Howard, and Steven CR Williams. Transcriptional and cellular signatures of cortical morphometric remodelling in chronic pain. *Pain*, 163(6): e759, 2022.
- Margaret M McCarthy and Arthur P Arnold. Reframing sexual differentiation of the brain. *Nature neuroscience*, 14(6):677–83, 2011. doi: doi:10.1038/nn.2834.
- Margaret M McCarthy, Arthur P Arnold, Gregory F Ball, Jeffrey D Blaustein, and Geert J De Vries. Sex differences in the brain: the not so inconvenient truth. *Journal of Neuroscience*, 32(7):2241–2247, 2012.
- Maarten Mennes, Bharat B Biswal, F Xavier Castellanos, and Michael P Milham. Making data sharing work: the fcp/indi experience. *Neuroimage*, 82:683–691, 2013.
- Daniel J Miller, Tetyana Duka, Cheryl D Stimpson, Steven J Schapiro, Wallace B Baze, Mark J McArthur, Archibald J Fobbs, André MM Sousa, Nenad Šestan, Derek E Wildman, et al. Prolonged myelination in human neocortical evolution. *Proceedings of the National Academy of Sciences*, 109(41):16480–16485, 2012.
- Jeremy A Miller, Song-Lin Ding, Susan M Sunkin, Kimberly A Smith, Lydia Ng, Aaron Szafer, Amanda Ebbert, Zackery L Riley, Joshua J Royall, Kaylynn Aiona, James M Arnold, Crissa Bennet, Darren Bertagnolli, Krissy Brouner, Stephanie Butler, Shiella Caldejon, Anita Carey, Christine Cuhaciyar, Rachel A Dalley, Nick Dee, Tim A Dolbeare, Benjamin A C Facer, David Feng, Tim P Fliss, Garrett Gee, Jeff Goldy, Lindsey Gourley, Benjamin W Gregor, Guangyu Gu, Robert E Howard, Jayson M Jochim, Chihchau L Kuan, Christopher Lau, Chang-Kyu Lee, Felix Lee, Tracy A Lemon, Phil Lesnar, Bergen McMurray, Naveed Mastan, Nerick Mosqueda, Theresa Naluai-Cecchini, Nhan-Kiet Ngo, Julie Nyhus, Aaron Oldre, Eric Olson, Jody Parente, Patrick D Parker, Sheana E Parry, Allison Stevens, Mihovil Pletikos, Melissa Reding, Kate Roll, David Sandman, Melaine Sarreal, Sheila Shapouri, Nadiya V Shapovalova, Elaine H Shen, Nathan Sjoquist, Clifford R Slaughterbeck, Michael Smith, Andy J Sodt, Derric Williams, Lilla Zöllei, Bruce Fischl, Mark B Gerstein, Daniel H Geschwind, Ian A Glass, Michael J Hawrylycz, Robert F Hevner, Hao Huang, Allan R Jones, James A Knowles, Pat Levitt, John W Phillips, Nenad Šestan, Paul Wahnoutka, Chinh Dang, Amy Bernard, John G Hohmann, and Ed S Lein. Transcriptional landscape of the prenatal human brain. *Nature*, page 199–206, 2014. ISSN 508. doi: <https://doi.org/10.1038/nature13185>.
- Kathryn L. Mills, Anne-Lise Goddings, Liv S. Clasen, Jay N. Giedd, and Sarah-Jayne Blakemore. The Developmental Mismatch in Structural Brain Maturation during Adolescence. *Developmental Neuroscience*, 36(3-4):147–160, 2014. ISSN 0378-5866. doi: 10.1159/000362328. URL <http://www.ncbi.nlm.nih.gov/pubmed/24993606><https://www.karger.com/Article/FullText/362328>.

- Kathryn L Mills, Anne-Lise Goddings, Megan M Herting, Rosa Meuwese, Sarah-Jayne Blakemore, Eveline A Crone, Ronald E Dahl, Berna Güroğlu, Armin Raznahan, Elizabeth R Sowell, et al. Structural brain development between childhood and adulthood: Convergence across four longitudinal samples. *Neuroimage*, 141:273–281, 2016.
- Derek G.V. Mitchell. The nexus between decision making and emotion regulation: A review of convergent neurocognitive substrates. *Behavioural Brain Research*, 217(1): 215–231, feb 2011. ISSN 0166-4328. doi: 10.1016/J.BBR.2010.10.030. URL <https://www.sciencedirect.com/science/article/pii/S0166432810007151>.
- Sarah E Morgan, Simon R White, Edward T Bullmore, and Petra E Vértes. A network neuroscience approach to typical and atypical brain development. *Biological Psychiatry: Cognitive Neuroscience and Neuroimaging*, 3(9):754–766, 2018.
- Sarah E Morgan, Jakob Seidlitz, Kirstie J Whitaker, Rafael Romero-Garcia, Nicholas E Clifton, Cristina Scarpazza, Therese van Amelsvoort, Machteld Marcelis, Jim van Os, Gary Donohoe, David Mothersill, Aiden Corvin, Andrew Pocklington, Armin Raznahan, Philip McGuire, Petra E Vértes, and Edward T Bullmore. Cortical patterning of abnormal morphometric similarity in psychosis is associated with brain expression of schizophrenia-related genes. *Proceedings of the National Academy of Sciences of the United States of America*, 116(19):9604–9609, 2019. ISSN 1091-6490. doi: 10.1073/pnas.1820754116.
- Sarah E. Morgan, Jonathan Young, Ameera X. Patel, Kirstie J. Whitaker, Cristina Scarpazza, Thérèse van Amelsvoort, Machteld Marcelis, Jim van Os, Gary Donohoe, David Mothersill, Aiden Corvin, Celso Arango, Andrea Mechelli, Martijn van den Heuvel, René S. Kahn, Philip McGuire, Michael Brammer, and Edward T. Bullmore. Functional magnetic resonance imaging connectivity accurately distinguishes cases with psychotic disorders from healthy controls, based on cortical features associated with brain network development. *Biological Psychiatry: Cognitive Neuroscience and Neuroimaging*, 6(12):1125–1134, 2021. ISSN 2451-9022. doi: 10.1016/j.bpsc.2020.05.013. URL <https://www.sciencedirect.com/science/article/pii/S2451902220301385>.
- Lisa Mosconi, Valentina Berti, Jonathan Dyke, Eva Schelbaum, Steven Jett, Lacey Loughlin, Grace Jang, Aneela Rahman, Hollie Hristov, Silky Pahlajani, et al. Menopause impacts human brain structure, connectivity, energy metabolism, and amyloid-beta deposition. *Scientific reports*, 11(1):1–16, 2021.
- Peter C Mulders, Philip F van Eijndhoven, Aart H Schene, Christian F Beckmann, and Indira Tendolkar. Resting-state functional connectivity in major depressive disorder: a review. *Neuroscience & Biobehavioral Reviews*, 56:330–344, 2015.
- Aja Louise Murray, Tom Booth, Manuel Eisner, Bonnie Auyeung, George Murray, and Denis Ribeaud. Sex differences in adhd trajectories across childhood and adolescence. *Developmental science*, 22(1):e12721, 2019.
- Kate Brody Nooner, Stanley J Colcombe, Russell H Tobe, Maarten Mennes, Melissa M Benedict, Alexis L Moreno, Laura J Panek, Shaquanna Brown, Stephen T Zavitz, Qingyang Li, et al. The nki-rockland sample: a model for accelerating the pace of discovery science in psychiatry. *Frontiers in neuroscience*, 6:152, 2012.

- National Institutes of Health et al. Nih guidelines on the inclusion of women and minorities as subjects in clinical research. *Fed Regist*, 59:1408–1413, 1994.
- Stuart Oldham and Alex Fornito. The development of brain network hubs. *Developmental Cognitive Neuroscience*, 36:100607, December 2018. ISSN 1878-9293. doi: 10.1016/j.dcn.2018.12.005. URL <https://www.ncbi.nlm.nih.gov/pmc/articles/PMC6969262/>.
- Meritxell Oliva, Manuel Muñoz-Aguirre, Sarah Kim-Hellmuth, Valentin Wucher, Ariel D. H. Gewirtz, Daniel J. Cotter, Princy Parsana, Silva Kasela, Brunilda Balliu, Ana Viñuela, Stephane E. Castel, Pejman Mohammadi, François Aguet, Yuxin Zou, Ekaterina A. Khramtsova, Andrew D. Skol, Diego Garrido-Martín, Ferran Reverter, Andrew Brown, Patrick Evans, Eric R. Gamazon, Anthony Payne, Rodrigo Bonazzola, Alvaro N. Barbeira, Andrew R. Hamel, Angel Martinez-Perez, José Manuel Soria, GTEx Consortium, Brandon L. Pierce, Matthew Stephens, Eleazar Eskin, Emmanouil T. Dermitzakis, Ayellet V. Segrè, Hae Kyung Im, Barbara E. Engelhardt, Kristin G. Ardlie, Stephen B. Montgomery, Alexis J. Battle, Tuuli Lappalainen, Roderic Guigó, and Barbara E. Stranger. The impact of sex on gene expression across human tissues. *Science*, 369(6509), 2020. ISSN 0036-8075. doi: 10.1126/science.aba3066.
- World Health Organization et al. *WHO child growth standards: length/height-for-age, weight-for-age, weight-for-length, weight-for-height and body mass index-for-age: methods and development*. World Health Organization, 2006.
- Alicia Oshlack and Matthew J Wakefield. Transcript length bias in rna-seq data confounds systems biology. *Biology direct*, 4:1–10, 2009.
- Casey Paquola and Seok-Jun Hong. The potential of myelin-sensitive imaging: Redefining spatiotemporal patterns of myeloarchitecture. *Biological psychiatry*, 2022.
- Casey Paquola, Richard AI Bethlehem, Jakob Seidlitz, Konrad Wagstyl, Rafael Romero-Garcia, Kirstie J Whitaker, Reinder Vos de Wael, Guy B Williams, NSPN Consortium, Petra E Vértes, et al. Shifts in myeloarchitecture characterise adolescent development of cortical gradients. *elife*, 8:e50482, 2019.
- Ameera X Patel, Prantik Kundu, Mikail Rubinov, Peter S Jones, Petra E Vértes, Karen D Ersche, John Suckling, and Edward T Bullmore. A wavelet method for modeling and despiking motion artifacts from resting-state fMRI time series. *NeuroImage*, 95:287–304, 2014. ISSN 1053-8119. doi: 10.1016/J.NEUROIMAGE.2014.03.012.
- Raymond Paternoster, Robert Brame, Paul Mazerolle, and Alex Piquero. Using the Correct Statistical Test for the Equality of Regression Coefficients. *Criminology*, 36(4):859–866, 1998. ISSN 0011-1384. doi: 10.1111/j.1745-9125.1998.tb01268.x.
- George C. Patton, Craig Olsson, Lyndal Bond, John W. Toumbourou, John B. Carlin, Sheryl A. Hemphill, and Richard F. Catalano. Predicting Female Depression Across Puberty: A Two-Nation Longitudinal Study. *Journal of the American Academy of Child & Adolescent Psychiatry*, 47(12):1424–1432, dec 2008. ISSN 0890-8567. doi: 10.1097/CHI.0B013E3181886EBE. URL <https://www.sciencedirect.com/science/article/pii/S0890856708601446?via%3Dihub>.

- Tomáš Paus, Matcheri Keshavan, and Jay N Giedd. Why do many psychiatric disorders emerge during adolescence? *Nature Reviews Neuroscience*, 9(12):947–957, 2008. ISSN 1471-003X. doi: 10.1038/nrn2513.
- Zdravko Petanjek, Miloš Judaš, Goran Šimić, Mladen Roko Rašin, Harry BM Uylings, Pasko Rakic, and Ivica Kostović. Extraordinary neoteny of synaptic spines in the human prefrontal cortex. *Proceedings of the National Academy of Sciences*, 108(32):13281–13286, 2011.
- Ronald Carl Petersen, Paul S Aisen, Laurel A Beckett, Michael C Donohue, Anthony Collins Gamst, Danielle J Harvey, Clifford R Jack, William J Jagust, Leslie M Shaw, Arthur W Toga, et al. Alzheimer’s disease neuroimaging initiative (adni): clinical characterization. *Neurology*, 74(3):201–209, 2010.
- M L Phillips, C D Ladouceur, and W C Drevets. A neural model of voluntary and automatic emotion regulation: implications for understanding the pathophysiology and neurodevelopment of bipolar disorder. *Molecular Psychiatry*, 13(9):833–857, sep 2008. ISSN 1359-4184. doi: 10.1038/mp.2008.65. URL <http://www.nature.com/articles/mp200865>.
- Susan P Phillips. Defining and measuring gender: a social determinant of health whose time has come. *International journal for equity in health*, 4(1):1–4, 2005.
- Charles H Phoenix, Robert W Goy, Arnold A Gerall, and William C Young. Organizing action of prenatally administered testosterone propionate on the tissue mediating mating behavior in the female guinea pig. *Endocrinology*, 65(3):369–382, 1959a. ISSN 0013-7227. doi: 10.1210/endo-65-3-369.
- Charles H Phoenix, Robert W Goy, Arnold A Gerall, and William C Young. Organizing action of prenatally administered testosterone propionate on the tissues mediating mating behavior in the female guinea pig. *Endocrinology*, 65(3):369–382, 1959b.
- Russell A Poldrack, Eliza Congdon, William Triplett, KJ Gorgolewski, KH Karlsgodt, JA Mumford, FW Sabb, NB Freimer, ED London, TD Cannon, et al. A phenome-wide examination of neural and cognitive function. *Scientific data*, 3(1):1–12, 2016.
- Damon Polioudakis, Luis de la Torre-Ubieta, Justin Langerman, Andrew G Elkins, Xu Shi, Jason L Stein, Celine K Vuong, Susanne Nichterwitz, Melinda Gevorgian, Carli K Opland, et al. A single-cell transcriptomic atlas of human neocortical development during mid-gestation. *Neuron*, 103(5):785–801, 2019.
- Raymond Pomponio, Guray Erus, Mohamad Habes, Jimit Doshi, Dhivya Srinivasan, Elizabeth Mamourian, Vishnu Bashyam, Ilya M. Nasrallah, Theodore D. Satterthwaite, Yong Fan, Lenore J. Launer, Colin L. Masters, Paul Maruff, Chuanjun Zhuo, Henry Völzke, Sterling C. Johnson, Jurgen Fripp, Nikolaos Koutsouleris, Daniel H. Wolf, Raquel Gur, Ruben Gur, John Morris, Marilyn S. Albert, Hans J. Grabe, Susan M. Resnick, R. Nick Bryan, David A. Wolk, Russell T. Shinohara, Haochang Shou, and Christos Davatzikos. Harmonization of large MRI datasets for the analysis of brain imaging patterns throughout the lifespan. *NeuroImage*, 208:116450, March 2020. ISSN 1053-8119. doi: 10.1016/j.neuroimage.2019.116450. URL <https://www.sciencedirect.com/science/article/pii/S1053811919310419>.

- Benedikt A Poser, Maarten J Versluis, Johannes M Hoogduin, and David G Norris. Bold contrast sensitivity enhancement and artifact reduction with multiecho epi: Parallel-acquired inhomogeneity-desensitized fmri. *Magnetic Resonance in Medicine*, 55(6): 1227–1235, 2006. doi: <https://doi.org/10.1002/mrm.20900>.
- Jonathan D Power, Kelly A Barnes, Abraham Z Snyder, Bradley L Schlaggar, and Steven E Petersen. Spurious but systematic correlations in functional connectivity MRI networks arise from subject motion. *NeuroImage*, 59(3):2142–54, 2012. ISSN 1095-9572. doi: 10.1016/j.neuroimage.2011.10.018.
- Brian J Prendergast, Kenneth G Onishi, and Irving Zucker. Female mice liberated for inclusion in neuroscience and biomedical research. *Neuroscience & Biobehavioral Reviews*, 40:1–5, 2014.
- Laura Pritschet, Tyler Santander, Caitlin M Taylor, Evan Layher, Shuying Yu, Michael B Miller, Scott T Grafton, and Emily G Jacobs. Functional reorganization of brain networks across the human menstrual cycle. *Neuroimage*, 220:117091, 2020.
- Margaret M Quinn and Peter M Smith. Corrigendum: Gender, work, and health (annals of work exposures and health (2018) 62: 4 (389-392). *Annals of Work Exposures and Health*, 62(4), 2018.
- Divyangana Rakesh and Sarah Whittle. Socioeconomic status and the developing brain—a systematic review of neuroimaging findings in youth. *Neuroscience & Biobehavioral Reviews*, 130:379–407, 2021.
- Harish RaviPrakash, Syed Muhammad Anwar, Nadia M Biassou, and Ulas Bagci. Morphometric and functional brain connectivity differentiates chess masters from amateur players. *Frontiers in Neuroscience*, 15:629478, 2021.
- A Raznahan, J P Lerch, N Lee, D Greenstein, G L Wallace, M Stockman, L Clasen, P W Shaw, and J N Giedd. Patterns of coordinated anatomical change in human cortical development: a longitudinal neuroimaging study of maturational coupling. *Neuron*, 72(5): 873–884, 2011. doi: <https://doi.org/10.1016/j.neuron.2011.09.028>.
- Armin Raznahan and Christine M Disteche. X-chromosome regulation and sex differences in brain anatomy. *Neuroscience & Biobehavioral Reviews*, 120:28–47, 2021.
- PK Reardon, Jakob Seidlitz, Simon Vandekar, Siyuan Liu, Raihaan Patel, Min Tae M Park, Aaron Alexander-Bloch, Liv S Clasen, Jonathan D Blumenthal, Francois M Lalonde, et al. Normative brain size variation and brain shape diversity in humans. *Science*, 360(6394): 1222–1227, 2018.
- Philip Reiss, Lei Huang, Yin-Hsiu Chen, Lan Huo, Thaddeus Tarpey, and Maarten Mennes. Massively parallel nonparametric regression, with an application to developmental brain mapping. *Journal of computational and graphical statistics*, 23:232–248, 02 2014. doi: 10.1080/10618600.2012.733549.
- Jess E Reynolds, Xiangyu Long, Dmitrii Paniukov, Mercedes Bagshawe, and Catherine Lebel. Calgary preschool magnetic resonance imaging (mri) dataset. *Data in brief*, 29: 105224, 2020.

- Hilary Richardson, Grace Lisandrelli, Alexa Riobueno-Naylor, and Rebecca Saxe. Development of the social brain from age three to twelve years. *Nature communications*, 9(1): 1027, 2018.
- Hilary Richardson, Grace Lisandrelli, Alexa Riobueno-Naylor, and Rebecca Saxe. "mri data of 3-12 year old children and adults during viewing of a short animated film", 2019.
- Shannon L Risacher, Andrew J Saykin, John D Wes, Li Shen, Hiram A Firpi, and Brenna C McDonald. Baseline mri predictors of conversion from mci to probable ad in the adni cohort. *Current Alzheimer Research*, 6(4):347–361, 2009.
- José E. Romero, Pierrick Coupe, Enrique Lanuza, Gwenaëlle Catheline, José V. Manjón, and Alzheimer's Disease Neuroimaging Initiative. Toward a unified analysis of cerebellum maturation and aging across the entire lifespan: A MRI analysis. *Human Brain Mapping*, 42(5):1287–1303, 2021. ISSN 1097-0193. doi: 10.1002/hbm.25293. URL <https://onlinelibrary.wiley.com/doi/abs/10.1002/hbm.25293>. _eprint: <https://onlinelibrary.wiley.com/doi/pdf/10.1002/hbm.25293>.
- Adon F. G. Rosen, David R. Roalf, Kosha Ruparel, Jason Blake, Kevin Seelaus, Lakshmi P. Villa, Rastko Ciric, Philip A. Cook, Christos Davatzikos, Mark A. Elliott, Angel Garcia de La Garza, Efstathios D. Gennatas, Megan Quarmley, J. Eric Schmitt, Russell T. Shinohara, M. Dylan Tisdall, R. Cameron Craddock, Raquel E. Gur, Ruben C. Gur, and Theodore D. Satterthwaite. Quantitative Assessment of Structural Image Quality. *NeuroImage*, 169:407–418, April 2018. ISSN 1053-8119. doi: 10.1016/j.neuroimage.2017.12.059. URL <https://www.ncbi.nlm.nih.gov/pmc/articles/PMC5856621/>.
- Amber N. V. Ruigrok, Gholamreza Salimi-Khorshidi, Meng-Chuan Lai, Simon Baron-Cohen, Michael V. Lombardo, Roger J. Tait, and John Suckling. A meta-analysis of sex differences in human brain structure. *Neuroscience & Biobehavioral Reviews*, 39: 34–50, 2014. ISSN 0149-7634. doi: 10.1016/j.neubiorev.2013.12.004. URL <https://www.sciencedirect.com/science/article/pii/S0149763413003011>.
- Saige Rutherford, Seyed Mostafa Kia, Thomas Wolfers, Charlotte Frazza, Mariam Zabihi, Richard Dinga, Pierre Berthet, Amanda Worker, Serena Verdi, Henricus G. Ruhe, Christian F. Beckmann, and Andre F. Marquand. The normative modeling framework for computational psychiatry. *Nature Protocols*, 17(7):1711–1734, July 2022. ISSN 1750-2799. doi: 10.1038/s41596-022-00696-5. URL <https://www.nature.com/articles/s41596-022-00696-5>. Number: 7 Publisher: Nature Publishing Group.
- Ziad S Saad, Daniel R Glen, Gang Chen, Michael S Beauchamp, Rutvik Desai, and Robert W Cox. A new method for improving functional-to-structural mri alignment using local pearson correlation. *NeuroImage*, 44(3):839–848, 2009. ISSN 1053-8119. doi: <https://doi.org/10.1016/j.neuroimage.2008.09.037>.
- Raymond Salvador, John Suckling, Christian Schwarzbauer, and Ed Bullmore. Undirected graphs of frequency-dependent functional connectivity in whole brain networks. *Philosophical Transactions of the Royal Society B: Biological Sciences*, 360(1457):937–946, 2005.
- Carla Sanchis-Segura, Maria Victoria Ibañez-Gual, Naiara Aguirre, Álvaro Javier Cruz-Gómez, and Cristina Forn. Effects of different intracranial volume correction methods on

- univariate sex differences in grey matter volume and multivariate sex prediction. *Scientific Reports*, 10(1):1–15, 2020.
- Theodore . Satterthwaite, Daniel H Wolf, Kosha Ruparel, Guray Erus, Mark A Elliott, Simon B Eickhoff, Efsthios D Gennatas, Chad Jackson, Karthik Prabhakaran, Alex Smith, Hakon Hakonarson, Ragini Verma, Christos Davatzikos, Raquel E Gur, and Ruben C Gur. Heterogeneous impact of motion on fundamental patterns of developmental changes in functional connectivity during youth. *NeuroImage*, 83:45 – 57, 2013. ISSN 1053-8119. doi: <https://doi.org/10.1016/j.neuroimage.2013.06.045>.
- Theodore D Satterthwaite, Daniel H Wolf, James Loughhead, Kosha Ruparel, Mark A Elliott, Hakon Hakonarson, Ruben C Gur, and Raquel E Gur. Impact of in-scanner head motion on multiple measures of functional connectivity: Relevance for studies of neurodevelopment in youth. *NeuroImage*, 60(1):623 – 632, 2012. ISSN 1053-8119. doi: <https://doi.org/10.1016/j.neuroimage.2011.12.063>.
- Theodore D Satterthwaite, John J Connolly, Kosha Ruparel, Monica E Calkins, Chad Jackson, Mark A Elliott, David R Roalf, Ryan Hopson, Karthik Prabhakaran, Meckenzie Behr, et al. The philadelphia neurodevelopmental cohort: A publicly available resource for the study of normal and abnormal brain development in youth. *Neuroimage*, 124:1115–1119, 2016.
- Jenna M Schabdach, James E. Schmitt, Susan Sotardi, Arastoo Vossough, Savvas Andronikou, Timothy Roberts, Hao Huang, Viveknarayanan Padmanabhan, Alfredo Oritz-Rosa, Margaret Gardner, Sydney Covitz, Saashi M Bedford, Barbara Chaiyachati, Simon R. White, Edward T Bullmore, Richard A. I. Bethlehem, Russell Shinohara, Benjamin Billot, Juan E Iglesias, Satrajit S Ghosh, Raquel E. Gur, Theodore D Satterthwaite, David Roalf, Jakob Seidlitz, and Aaron Alexander-Bloch. Brain growth charts of "clinical controls" for quantitative analysis of clinically acquired brain MRI. preprint, *Radiology and Imaging*, 2023. URL <http://medrxiv.org/lookup/doi/10.1101/2023.01.13.23284533>.
- Dustin Scheinost, Emily S Finn, Fuyuze Tokoglu, Xilin Shen, Xenophon Papademetris, Michelle Hampson, and Todd R Constable. Sex differences in normal age trajectories of functional brain networks. *Human Brain Mapping*, 36(4):1524–1535, 2015. ISSN 10659471. doi: 10.1002/hbm.22720.
- Marieke L Schölvinck, Alexander Maier, Frank Q Ye, Jeff H Duyn, and David A Leopold. Neural basis of global resting-state fmri activity. *Proceedings of the National Academy of Sciences*, 107(22):10238–10243, 2010. ISSN 0027-8424. doi: 10.1073/pnas.0913110107.
- Katja Schueler, Jessica Fritz, Lena Dorfschmidt, Anne-Laura Van Harmelen, Eike Stroemer, and Michèle Wessa. Psychological network analysis of general self-efficacy in high vs. low resilient functioning healthy adults. *Frontiers in psychiatry*, page 1979, 2021.
- G Schumann, Eva Loth, T Banaschewski, A Barbot, G Barker, C Büchel, PJ Conrod, JW Dalley, H Flor, J Gallinat, et al. The imagen study: reinforcement-related behaviour in normal brain function and psychopathology. *Molecular psychiatry*, 15(12):1128–1139, 2010.
- Isaac Sebenius, Jakob Seidlitz, Varun Warriar, Richard AI Bethlehem, Aaron Alexander-Bloch, Travis Mallard, Rafael Romero Garcia, Edward T Bullmore, and Sarah E Morgan.

- Mind networks: Robust estimation of structural similarity from brain mri. *bioRxiv*, pages 2022–10, 2022.
- Jakob Seidlitz, František Váša, Maxwell Shinn, Rafael Romero-Garcia, Kirstie J. Whitaker, Petra E. Vértes, Konrad Wagstyl, Paul Kirkpatrick Reardon, Liv Clasen, Siyuan Liu, Adam Messinger, David A. Leopold, Peter Fonagy, Raymond J. Dolan, Peter B. Jones, Ian M. Goodyer, Armin Raznahan, and Edward T. Bullmore. Morphometric Similarity Networks Detect Microscale Cortical Organization and Predict Inter-Individual Cognitive Variation. *Neuron*, 97(1):231–247.e7, January 2018. ISSN 0896-6273. doi: 10.1016/j.neuron.2017.11.039. URL <https://www.sciencedirect.com/science/article/pii/S0896627317310929>.
- Jakob Seidlitz, Ajay Nadig, Siyuan Liu, Richard AI Bethlehem, Petra E Vértes, Sarah E Morgan, František Váša, Rafael Romero-Garcia, François M Lalonde, Liv S Clasen, et al. Transcriptomic and cellular decoding of regional brain vulnerability to neurogenetic disorders. *Nature communications*, 11(1):1–14, 2020.
- LD Selemon and N Zecevic. Schizophrenia: a tale of two critical periods for prefrontal cortical development. *Translational psychiatry*, 5(8):e623–e623, 2015.
- N Y A Sey, B Hu, W Mah, H Fauni, J C McAfee, P Rajarajan, K J Brennand, S Akbarian, and H Won. A computational tool (h-magma) for improved prediction of brain-disorder risk genes by incorporating brain chromatin interaction profiles. *Nature Neuroscience*, page 583–593, 2020. ISSN 23. doi: <https://doi.org/10.1038/s41593-020-0603-0>.
- Meredith A Shafto, Lorraine K Tyler, Marie Dixon, Jason R Taylor, James B Rowe, Rhodri Cusack, Andrew J Calder, William D Marslen-Wilson, John Duncan, Tim Dalgleish, et al. The cambridge centre for ageing and neuroscience (cam-can) study protocol: a cross-sectional, lifespan, multidisciplinary examination of healthy cognitive ageing. *BMC neurology*, 14:1–25, 2014.
- Ziyao Shang, Md Asadullah Turja, Eric Feczko, Audrey Houghton, Amanda Rueter, Lucille A Moore, Kathy Snider, Timothy Hendrickson, Paul Reiners, Sally Stoyell, et al. Learning strategies for contrast-agnostic segmentation via synthseg for infant mri data. In *International Conference on Medical Imaging with Deep Learning*, pages 1075–1084. PMLR, 2022.
- Udaya Shankar Mishra and William Joe. Global gender gap report 2021: Hegemony, level-blind assessments and poor rankings of the global south. *South Asia@ LSE*, 2021.
- Radha R Sharma, Sonam Chawla, and Charlotte M Karam. Global gender gap index: world economic forum perspective. In *Handbook on diversity and inclusion indices*, pages 150–163. Edward Elgar Publishing, 2021.
- Philip Shaw, Nitin Gogtay, and Judith Rapoport. Childhood psychiatric disorders as anomalies in neurodevelopmental trajectories. *Human brain mapping*, 31(6):917–925, 2010.
- Xueyi Shen, David M Howard, Mark J Adams, W David Hill, Toni-Kim Clarke, Ian J Deary, Heather C Whalley, and Andrew M McIntosh. A phenome-wide association and mendelian randomisation study of polygenic risk for depression in uk biobank. *Nature communications*, 11(1):2301, 2020.

- John C Silbereis, Sirisha Pochareddy, Ying Zhu, Mingfeng Li, and Nenad Sestan. The cellular and molecular landscapes of the developing human central nervous system. *Neuron*, 89(2): 248–268, 2016.
- Viviana Simon. Wanted: women in clinical trials, 2005.
- Benjamin Smarr and Lance J Kriegsfeld. Female mice exhibit less overall variance, with a higher proportion of structured variance, than males at multiple timescales of continuous body temperature and locomotive activity records. *Biology of sex differences*, 13(1):41, 2022.
- L Basten Snoek, Mark G Sterken, Rita JM Volkers, Mirre Klatter, Kobus J Bosman, Roel PJ Bevers, Joost AG Riksen, Geert Smant, Andrew R Cossins, and Jan E Kammenga. A rapid and massive gene expression shift marking adolescent transition in *c. elegans*. *Scientific reports*, 4(1):1–5, 2014.
- Lukas Snoek, Maite van der Miesen, Andries van der Leij, Tinka Beemsterboer, Annemarie Eigenhuis, and Steven Scholte. "aomic-id1000", 2020a.
- Lukas Snoek, Maite van der Miesen, Andries van der Leij, Tinka Beemsterboer, Annemarie Eigenhuis, and Steven Scholte. "aomic-piop1", 2020b.
- Lukas Snoek, Maite van der Miesen, Andries van der Leij, Tinka Beemsterboer, Annemarie Eigenhuis, and Steven Scholte. "aomic-piop2", 2020c.
- Lukas Snoek, Maite M van der Miesen, Tinka Beemsterboer, Andries Van Der Leij, Annemarie Eigenhuis, and H Steven Scholte. The amsterdam open mri collection, a set of multimodal mri datasets for individual difference analyses. *Scientific data*, 8(1):85, 2021.
- Marco Solmi, Joaquim Radua, Miriam Olivola, Enrico Croce, Livia Soardo, Gonzalo Salazar de Pablo, Jae Il Shin, James B Kirkbride, Peter Jones, Jae Han Kim, et al. Age at onset of mental disorders worldwide: large-scale meta-analysis of 192 epidemiological studies. *Molecular psychiatry*, 27(1):281–295, 2022.
- Leah H. Somerville, Susan Y. Bookheimer, Randy L. Buckner, Gregory C. Burgess, Sandra W. Curtiss, Mirella Dapretto, Jennifer Stine Elam, Michael S. Gaffrey, Michael P. Harms, Cynthia Hodge, Sridhar Kandala, Erik K. Kastman, Thomas E. Nichols, Bradley L. Schlaggar, Stephen M. Smith, Kathleen M. Thomas, Essa Yacoub, David C. Van Essen, and Deanna M. Barch. The Lifespan Human Connectome Project in Development: A large-scale study of brain connectivity development in 5–21 year olds. *NeuroImage*, 183: 456–468, December 2018a. ISSN 1053-8119. doi: 10.1016/j.neuroimage.2018.08.050. URL <https://www.sciencedirect.com/science/article/pii/S1053811918307481>.
- Leah H Somerville, Susan Y Bookheimer, Randy L Buckner, Gregory C Burgess, Sandra W Curtiss, Mirella Dapretto, Jennifer Stine Elam, Michael S Gaffrey, Michael P Harms, Cynthia Hodge, et al. The lifespan human connectome project in development: A large-scale study of brain connectivity development in 5–21 year olds. *Neuroimage*, 183: 456–468, 2018b.

- Elizabeth R. Sowell, Bradley S. Peterson, Paul M. Thompson, Suzanne E. Welcome, Amy L. Henkenius, and Arthur W. Toga. Mapping cortical change across the human life span. *Nature Neuroscience*, 6(3):309–315, March 2003. ISSN 1546-1726. doi: 10.1038/nn1008. URL <https://www.nature.com/articles/nn1008>. Number: 3 Publisher: Nature Publishing Group.
- Elizabeth R Sowell, Paul M Thompson, and Arthur W Toga. Mapping changes in the human cortex throughout the span of life. *The Neuroscientist*, 10(4):372–392, 2004. doi: 10.1177/1073858404263960.
- Marisa N Spann, Ravi Bansal, Xuejun Hao, Tove S Rosen, and Bradley S Peterson. Prenatal socioeconomic status and social support are associated with neonatal brain morphology, toddler language and psychiatric symptoms. *Child Neuropsychology*, 26(2):170–188, 2020.
- D Mikis Stasinopoulos and Robert A Rigby. Generalized additive models for location scale and shape (gamlss) in r. *Journal of Statistical Software*, 23:1–46, 2008.
- Eva-Maria Stauffer, Richard AI Bethlehem, Varun Warriar, Graham K Murray, Rafael Romero-Garcia, Jakob Seidlitz, and Edward T Bullmore. Grey and white matter microstructure is associated with polygenic risk for schizophrenia. *Molecular Psychiatry*, 26(12):7709–7718, 2021.
- Eva-Maria Stauffer, Richard AI Bethlehem, Lena Dorfschmidt, Hyejung Won, Varun Warriar, and Edward Bullmore. The genetic relationships between brain structure and schizophrenia. *medRxiv*, pages 2023–03, 2023.
- Michael C Stevens. The contributions of resting state and task-based functional connectivity studies to our understanding of adolescent brain network maturation. *Neuroscience & Biobehavioral Reviews*, 70:13–32, 2016.
- Mirjam Stratmann, Carsten Konrad, Harald Kugel, Axel Krug, Sonja Schöning, Patricia Ohrmann, Christina Uhlmann, Christian Postert, Thomas Suslow, Walter Heindel, Volker Arolt, Tilo Kircher, and Udo Dannlowski. Insular and Hippocampal Gray Matter Volume Reductions in Patients with Major Depressive Disorder. *PLOS ONE*, 9(7):e102692, July 2014. ISSN 1932-6203. doi: 10.1371/journal.pone.0102692. URL <https://journals.plos.org/plosone/article?id=10.1371/journal.pone.0102692>. Publisher: Public Library of Science.
- Cathie Sudlow, John Gallacher, Naomi Allen, Valerie Beral, Paul Burton, John Danesh, Paul Downey, Paul Elliott, Jane Green, Martin Landray, Bette Liu, Paul Matthews, Giok Ong, Jill Pell, Alan Silman, Alan Young, Tim Sprosen, Tim Peakman, and Rory Collins. UK Biobank: An Open Access Resource for Identifying the Causes of a Wide Range of Complex Diseases of Middle and Old Age. *PLOS Medicine*, 12(3):e1001779, March 2015. ISSN 1549-1676. doi: 10.1371/journal.pmed.1001779. URL <https://journals.plos.org/plosmedicine/article?id=10.1371/journal.pmed.1001779>. Publisher: Public Library of Science.
- Kaustubh Supekar, Mark Musen, and Vinod Menon. Development of large-scale functional brain networks in children. *PLoS biology*, 7(7):e1000157, 2009.

- Laura E. Suárez, Ross D. Markello, Richard F. Betzel, and Bratislav Misic. Linking structure and function in macroscale brain networks. *Trends Cogn Sci*, 24(4):302–315, 2020. ISSN 1879-307X. doi: 10.1016/j.tics.2020.01.008.
- Valerie J. Sydnor, Bart Larsen, Danielle S. Bassett, Aaron Alexander-Bloch, Damien A. Fair, Conor Liston, Allyson P. Mackey, Michael P. Milham, Adam Pines, David R. Roalf, Jakob Seidlitz, Ting Xu, Armin Raznahan, and Theodore D. Satterthwaite. Neurodevelopment of the association cortices: Patterns, mechanisms, and implications for psychopathology. *Neuron*, 109(18):2820–2846, September 2021. ISSN 0896-6273. doi: 10.1016/j.neuron.2021.06.016. URL <https://www.sciencedirect.com/science/article/pii/S0896627321004578>.
- Damian Szklarczyk, Andrea Franceschini, Stefan Wyder, Kristoffer Forslund, Davide Heller, Jaime Huerta-Cepas, Milan Simonovic, Alexander Roth, Alberto Santos, Kalliopi P Tsafou, et al. String v10: protein–protein interaction networks, integrated over the tree of life. *Nucleic acids research*, 43(D1):D447–D452, 2015.
- Aleksandr Talishinsky, Jonathan Downar, Petra E Vértes, Jakob Seidlitz, Katharine Dunlop, Charles J Lynch, Heather Whalley, Andrew McIntosh, Fidel Vila-Rodriguez, Zafiris J Daskalakis, et al. Regional gene expression signatures are associated with sex-specific functional connectivity changes in depression. *Nature Communications*, 13(1):5692, 2022.
- Carol A Tamminga, Godfrey D Pearlson, Ana D Stan, Robert D Gibbons, Jaya Padmanabhan, Matcheri Keshavan, and Brett A Clementz. Strategies for advancing disease definition using biomarkers and genetics: the bipolar and schizophrenia network for intermediate phenotypes. *Biological Psychiatry: Cognitive Neuroscience and Neuroimaging*, 2(1): 20–27, 2017.
- Christian K Tamnes, Megan M Herting, Anne-Lise Goddings, Rosa Meuwese, Sarah-Jayne Blakemore, Ronald E Dahl, Berna Güroğlu, Armin Raznahan, Elizabeth R Sowell, Eveline A Crone, et al. Development of the cerebral cortex across adolescence: a multisample study of inter-related longitudinal changes in cortical volume, surface area, and thickness. *Journal of Neuroscience*, 37(12):3402–3412, 2017.
- Saori C Tanaka, Ayumu Yamashita, Noriaki Yahata, Takashi Itahashi, Giuseppe Lisi, Takashi Yamada, Naho Ichikawa, Masahiro Takamura, Yujiro Yoshihara, Akira Kunimatsu, et al. A multi-site, multi-disorder resting-state magnetic resonance image database. *Scientific data*, 8(1):227, 2021a.
- Saori C Tanaka, Ayumu Yamashita, Noriaki Yahata, Takashi Itahashi, Giuseppe Lisi, Takashi Yamada, Naho Ichikawa, Masahiro Takamura, Yujiro Yoshihara, Akira Kunimatsu, et al. A multi-site, multi-disorder resting-state magnetic resonance image database. *Scientific data*, 8(1):227, 2021b.
- Maithé Tauber and Charlotte Hoybye. Endocrine disorders in prader-willi syndrome: a model to understand and treat hypothalamic dysfunction. *The Lancet Diabetes & Endocrinology*, 9(4):235–246, 2021.
- Jason R Taylor, Nitin Williams, Rhodri Cusack, Tibor Auer, Meredith A Shafto, Marie Dixon, Lorraine K Tyler, Richard N Henson, et al. The cambridge centre for ageing and neuroscience (cam-can) data repository: Structural and functional mri, meg, and cognitive data from a cross-sectional adult lifespan sample. *neuroimage*, 144:262–269, 2017.

- Cibu Thomas, Frank Q Ye, M Okan Irfanoglu, Pooja Modi, Kadharbatcha S Saleem, David A Leopold, and Carlo Pierpaoli. Anatomical accuracy of brain connections derived from diffusion mri tractography is inherently limited. *Proceedings of the National Academy of Sciences*, 111(46):16574–16579, 2014.
- Tian Tian, Jia Li, Guiling Zhang, Jian Wang, Dong Liu, Changhua Wan, Jicheng Fang, Di Wu, Yiran Zhou, and Wenzhen Zhu. Effects of childhood trauma experience and comt val158met polymorphism on brain connectivity in a multimodal mri study. *Brain and Behavior*, 10(12):e01858, 2020.
- Tian Tian, Jia Li, Guiling Zhang, Jian Wang, Dong Liu, Changhua Wan, Jicheng Fang, Di Wu, Yiran Zhou, and Wenzhen Zhu. Effects of childhood trauma experience and bdnf val66met polymorphism on brain plasticity relate to emotion regulation. *Behavioural brain research*, 398:112949, 2021.
- D Tomasi and N D Volkow. Aging and functional brain networks. *Molecular Psychiatry*, 17(5):549–558, 2012. ISSN 1359-4184. doi: 10.1038/mp.2011.81.
- Ursula A. Tooley, Danielle S. Bassett, and Allyson P. Mackey. Environmental influences on the pace of brain development. *Nature Reviews Neuroscience*, 22(6):372–384, June 2021. ISSN 1471-0048. doi: 10.1038/s41583-021-00457-5. URL <https://doi.org/10.1038/s41583-021-00457-5>.
- Emma K Towlson, Petra E Vértes, Sebastian E Ahnert, William R Schafer, and Edward T Bullmore. The rich club of the c. elegans neuronal connectome. *Journal of Neuroscience*, 33(15):6380–6387, 2013.
- Robert Trampel, Pierre-Louis Bazin, Kerrin Pine, and Nikolaus Weiskopf. In-vivo magnetic resonance imaging (mri) of laminae in the human cortex. *Neuroimage*, 197:707–715, 2019.
- Madhukar H Trivedi, Patrick J McGrath, Maurizio Fava, Ramin V Parsey, Benji T Kurian, Mary L Phillips, Maria A Oquendo, Gerard Bruder, Diego Pizzagalli, Marisa Toups, et al. Establishing moderators and biosignatures of antidepressant response in clinical care (embarc): Rationale and design. *Journal of psychiatric research*, 78:11–23, 2016.
- Vassily Trubetskoy, Antonio F. Pardiñas, Ting Qi, Georgia Panagiotaropoulou, Swapnil Awasthi, Tim B. Bigdeli, Julien Bryois, Chia-Yen Chen, Charlotte A. Dennison, Lynsey S. Hall, Max Lam, Kyoko Watanabe, Oleksandr Frei, Tian Ge, Janet C. Harwood, Frank Koopmans, Sigurdur Magnusson, Alexander L. Richards, Julia Sidorenko, Yang Wu, Jian Zeng, Jakob Grove, Minsoo Kim, Zhiqiang Li, Georgios Voloudakis, Wen Zhang, Mark Adams, Ingrid Agartz, Elizabeth G. Atkinson, Esben Agerbo, Mariam Al Eissa, Margot Albus, Madeline Alexander, Behrooz Z. Alizadeh, Köksal Alptekin, Thomas D. Als, Farooq Amin, Volker Arolt, Manuel Arrojo, Lavinia Athanasiu, Maria Helena Azevedo, Silviu A. Bacanu, Nicholas J. Bass, Martin Begemann, Richard A. Belliveau, Judit Bene, Beben Benyamin, Sarah E. Bergen, Giuseppe Blasi, Julio Bobes, Stefano Bonassi, Alice Braun, Rodrigo Affonseca Bressan, Evelyn J. Bromet, Richard Bruggeman, Peter F. Buckley, Randy L. Buckner, Jonas Bybjerg-Grauholm, Wiepke Cahn, Murray J. Cairns, Monica E. Calkins, Vaughan J. Carr, David Castle, Stanley V. Catts, Kimberley D. Chambert, Raymond C. K. Chan, Boris Chaumette, Wei Cheng, Eric F. C. Cheung, Siow Ann Chong,

David Cohen, Angèle Consoli, Quirino Cordeiro, Javier Costas, Charles Curtis, Michael Davidson, Kenneth L. Davis, Lieuwe de Haan, Franziska Degenhardt, Lynn E. DeLisi, Ditte Demontis, Faith Dickerson, Dimitris Dikeos, Timothy Dinan, Srdjan Djurovic, Jubao Duan, Giuseppe Ducci, Frank Dudbridge, Johan G. Eriksson, Lourdes Fañanás, Stephen V. Faraone, Alessia Fiorentino, Andreas Forstner, Josef Frank, Nelson B. Freimer, Menachem Fromer, Alessandra Frustaci, Ary Gadelha, Giulio Genovese, Elliot S. Gershon, Marianna Giannitelli, Ina Giegling, Paola Giusti-Rodríguez, Stephanie Godard, Jacqueline I. Goldstein, Javier González Peñas, Ana González-Pinto, Srihari Gopal, Jacob Gratten, Michael F. Green, Tiffany A. Greenwood, Olivier Guillin, Sinan Gülöksüz, Raquel E. Gur, Ruben C. Gur, Blanca Gutiérrez, Eric Hahn, Hakon Hakonarson, Vahram Haroutunian, Annette M. Hartmann, Carol Harvey, Caroline Hayward, Frans A. Henskens, Stefan Herms, Per Hoffmann, Daniel P. Howrigan, Masashi Ikeda, Conrad Iyegbe, Inge Joa, Antonio Julià, Anna K. Kähler, Tony Kam-Thong, Yoichiro Kamatani, Sena Karachanak-Yankova, Oussama Kebir, Matthew C. Keller, Brian J. Kelly, Andrey Khrunin, Sung-Wan Kim, Janis Klovinis, Nikolay Kondratiev, Bettina Konte, Julia Kraft, Michiaki Kubo, Vaidutis Kučinskis, Zita Ausrele Kučinskiene, Agung Kusumawardhani, Hana Kuzelova-Ptackova, Stefano Landi, Laura C. Lazzeroni, Phil H. Lee, Sophie E. Legge, Douglas S. Lehrer, Rebecca Lencer, Bernard Lerer, Miaoxin Li, Jeffrey Lieberman, Gregory A. Light, Svetlana Limborska, Chih-Min Liu, Jouko Lönnqvist, Carmel M. Loughland, Jan Lubinski, Jurjen J. Luykx, Amy Lynham, Milan Macek, Andrew Mackinnon, Patrik K. E. Magnusson, Brion S. Maher, Wolfgang Maier, Dolores Malaspina, Jacques Mallet, Stephen R. Marder, Sara Marsal, Alicia R. Martin, Lourdes Martorell, Manuel Mattheisen, Robert W. McCarley, Colm McDonald, John J. McGrath, Helena Medeiros, Sandra Meier, Bela Melegh, Ingrid Melle, Raquelle I. Meshulam-Gately, Andres Metspalu, Patricia T. Michie, Lili Milani, Vihra Milanova, Marina Mitjans, Espen Molden, Esther Molina, María Dolores Molto, Valeria Mondelli, Carmen Moreno, Christopher P. Morley, Gerard Muntané, Kieran C. Murphy, Inez Myin-Germeys, Igor Nenadić, Gerald Nestadt, Liene Nikitina-Zake, Cristiano Noto, Keith H. Nuechterlein, Niamh Louise O'Brien, F. Anthony O'Neill, Sang-Yun Oh, Ann Olincy, Vanessa Kiyomi Ota, Christos Pantelis, George N. Papadimitriou, Mara Parellada, Tiina Paunio, Renata Pellegrino, Sathish Periyasamy, Diana O. Perkins, Bruno Pfulmann, Olli Pietiläinen, Jonathan Pimm, David Porteous, John Powell, Diego Quattrone, Digby Quested, Allen D. Radant, Antonio Rampino, Mark H. Rapaport, Anna Rautanen, Abraham Reichenberg, Cheryl Roe, Joshua L. Roffman, Julian Roth, Matthias Rothermundt, Bart P. F. Rutten, Safaa Saker-Delye, Veikko Salomaa, Julio Sanjuan, Marcos Leite Santoro, Adam Savitz, Ulrich Schall, Rodney J. Scott, Larry J. Seidman, Sally Isabel Sharp, Jianxin Shi, Larry J. Siever, Engilbert Sigurdsson, Kang Sim, Nora Skarabis, Petr Slominsky, Hon-Cheong So, Janet L. Sobell, Erik Söderman, Helen J. Stain, Nils Eiel Steen, Agnes A. Steixner-Kumar, Elisabeth Stögmänn, William S. Stone, Richard E. Straub, Fabian Streit, Eric Strengman, T. Scott Stroup, Mythily Subramaniam, Catherine A. Sugar, Jaana Suvisaari, Dragan M. Svrakic, Neal R. Swerdlow, Jin P. Szaatkiewicz, Thi Minh Tam Ta, Atsushi Takahashi, Chikashi Terao, Florence Thibaut, Draga Toncheva, Paul A. Tooney, Silvia Torretta, Sarah Tosato, Gian Battista Tura, Bruce I. Turetsky, Alp Üçok, Arne Vaaler, Therese van Amelsvoort, Ruud van Winkel, Juha Veijola, John Waddington, Henrik Walter, Anna Waterreus, Bradley T. Webb, Mark Weiser, Nigel M. Williams, Stephanie H. Witt, Brandon K. Wormley, Jing Qin Wu, Zhida Xu, Robert Yolken, Clement C. Zai, Wei Zhou, Feng Zhu, Fritz Zimprich, Eşref Cem Atbaşoğlu, Muhammad Ayub, Christian Benner, Alessandro Bertolino, Donald W. Black, Nicholas J. Bray, Gerome Breen, Nancy G. Buccola, William F. Byerley, Wei J. Chen, C. Robert

- Cloninger, Benedicto Crespo-Facorro, Gary Donohoe, Robert Freedman, Cherrie Galletly, Michael J. Gandal, Massimo Gennarelli, David M. Hougaard, Hai-Gwo Hwu, Assen V. Jablensky, Steven A. McCarroll, Jennifer L. Moran, Ole Mors, Preben B. Mortensen, Bertram Müller-Myhsok, Amanda L. Neil, Merete Nordentoft, Michele T. Pato, Tracey L. Petryshen, Matti Pirinen, Ann E. Pulver, Thomas G. Schulze, Jeremy M. Silverman, Jordan W. Smoller, Eli A. Stahl, Debby W. Tsuang, Elisabet Vilella, Shi-Heng Wang, Shuhua Xu, Rolf Adolfsson, Celso Arango, Bernhard T. Baune, Sintia Iole Belangero, Anders D. Børghlum, David Braff, Elvira Bramon, Joseph D. Buxbaum, Dominique Campion, Jorge A. Cervilla, Sven Cichon, David A. Collier, Aiden Corvin, David Curtis, Marta Di Forti, Enrico Domenici, Hannelore Ehrenreich, Valentina Escott-Price, Tõnu Esko, Ayman H. Fanous, Anna Gareeva, Micha Gawlik, Pablo V. Gejman, Michael Gill, Stephen J. Glatt, Vera Golimbet, Kyung Sue Hong, Christina M. Hultman, Steven E. Hyman, Nakao Iwata, Erik G. Jönsson, René S. Kahn, James L. Kennedy, Elza Khusnutdinova, George Kirov, James A. Knowles, Marie-Odile Krebs, Claudine Laurent-Levinson, Jimmy Lee, Todd Lencz, Douglas F. Levinson, Qingqin S. Li, Jianjun Liu, Anil K. Malhotra, Dheeraj Malhotra, Andrew McIntosh, Andrew McQuillin, Paulo R. Menezes, Vera A. Morgan, Derek W. Morris, Bryan J. Mowry, Robin M. Murray, Vishwajit Nimgaonkar, Markus M. Nöthen, Roel A. Ophoff, Sara A. Paciga, Aarno Palotie, Carlos N. Pato, Shengying Qin, Marcella Rietschel, Brien P. Riley, Margarita Rivera, Dan Rujescu, Meram C. Saka, Alan R. Sanders, Sibylle G. Schwab, Alessandro Serretti, Pak C. Sham, Yongyong Shi, David St Clair, Hreinn Stefánsson, Kari Stefansson, Ming T. Tsuang, Jim van Os, Marquis P. Vawter, Daniel R. Weinberger, Thomas Werge, Dieter B. Wildenauer, Xin Yu, Weihua Yue, Peter A. Holmans, Andrew J. Pocklington, Panos Roussos, Evangelos Vassos, Matthijs Verhage, Peter M. Visscher, Jian Yang, Danielle Posthuma, Ole A. Andreassen, Kenneth S. Kendler, Michael J. Owen, Naomi R. Wray, Mark J. Daly, Hailiang Huang, Benjamin M. Neale, Patrick F. Sullivan, Stephan Ripke, James T. R. Walters, and Michael C. O'Donovan. Mapping genomic loci implicates genes and synaptic biology in schizophrenia. *Nature*, 604(7906):502–508, 2022. ISSN 1476-4687. doi: 10.1038/s41586-022-04434-5. URL <https://www.nature.com/articles/s41586-022-04434-5>. Number: 7906 Publisher: Nature Publishing Group.
- Scientific United Nations Educational and Cultural Organization *UNESCO*. *Global education monitoring report 2022: gender report: deepening the debate on those still left behind*. UNESCO, Paris, France, 2022.
- Martijn P. van den Heuvel and Hilleke E. Hulshoff Pol. Exploring the brain network: A review on resting-state fMRI functional connectivity. *European Neuropsychopharmacology*, 20(8):519–534, aug 2010. ISSN 0924977X. doi: 10.1016/j.euroneuro.2010.03.008. URL <https://linkinghub.elsevier.com/retrieve/pii/S0924977X10000684>.
- E Van Diessen, T Numan, E Van Dellen, AW Van Der Kooi, M Boersma, D Hofman, R Van Lutterveld, BW Van Dijk, ECW Van Straaten, A Hillebrand, et al. Opportunities and methodological challenges in eeg and meg resting state functional brain network research. *Clinical Neurophysiology*, 126(8):1468–1481, 2015.
- Anna CK van Duijvenvoorde, M Achterberg, Barbara R Braams, Sabine Peters, and Eveline A Crone. Testing a dual-systems model of adolescent brain development using resting-state connectivity analyses. *Neuroimage*, 124:409–420, 2016.

- Anna CK Van Duijvenvoorde, Bianca Westhoff, Frank de Vos, Lara M Wierenga, and Eveline A Crone. A three-wave longitudinal study of subcortical–cortical resting-state connectivity in adolescence: Testing age- and puberty-related changes. *Human Brain Mapping*, 40(13):3769–3783, 2019.
- Theo GM Van Erp, Derrek P Hibar, Jerod M Rasmussen, David C Glahn, Godfrey D Pearlson, Ole A Andreassen, Ingrid Agartz, Lars T Westlye, Unn K Haukvik, Anders M Dale, et al. Subcortical brain volume abnormalities in 2028 individuals with schizophrenia and 2540 healthy controls via the ENIGMA consortium. *Molecular Psychiatry*, 21(4):547–553, 2016.
- D. C. Van Essen, K. Ugurbil, E. Auerbach, D. Barch, T. E. J. Behrens, R. Bucholz, A. Chang, L. Chen, M. Corbetta, S. W. Curtiss, S. Della Penna, D. Feinberg, M. F. Glasser, N. Harel, A. C. Heath, L. Larson-Prior, D. Marcus, G. Michalareas, S. Moeller, R. Oostenveld, S. E. Petersen, F. Prior, B. L. Schlaggar, S. M. Smith, A. Z. Snyder, J. Xu, and E. Yacoub. The Human Connectome Project: A data acquisition perspective. *NeuroImage*, 62(4):2222–2231, October 2012. ISSN 1053-8119. doi: 10.1016/j.neuroimage.2012.02.018. URL <https://www.sciencedirect.com/science/article/pii/S1053811912001954>.
- David C Van Essen, Stephen M Smith, Deanna M Barch, Timothy EJ Behrens, Essa Yacoub, Kamil Ugurbil, Wu-Minn HCP Consortium, et al. The wu-minn human connectome project: an overview. *Neuroimage*, 80:62–79, 2013.
- František Váša, Jakob Seidlitz, Rafael Romero-Garcia, Kirstie J Whitaker, Gideon Rosenthal, Petra E Vértes, Maxwell Shinn, Aaron Alexander-Bloch, Peter Fonagy, Raymond J Dolan, Peter B Jones, Ian M Goodyer, Olaf Sporns, and Edward T Bullmore. Adolescent Tuning of Association Cortex in Human Structural Brain Networks. *Cerebral Cortex*, 28(1):281–294, 2018. ISSN 1047-3211. doi: 10.1093/cercor/bhx249.
- František Váša, Rafael Romero-Garcia, Manfred G Kitzbichler, Jakob Seidlitz, Kirstie J Whitaker, Matilde M Vaghi, Prantik Kundu, Ameera X Patel, Peter Fonagy, Raymond J Dolan, Peter B Jones, Ian M Goodyer, Petra E Vértes, and Edward T Bullmore. Conservative and disruptive modes of adolescent change in human brain functional connectivity. *Proceedings of the National Academy of Sciences*, 117(6):3248–3253, 2020. ISSN 0027-8424. doi: 10.1073/pnas.1906144117.
- Dennis Velakoulis, Stephen J. Wood, Michael T. H. Wong, Patrick D. McGorry, Alison Yung, Lisa Phillips, De Smith, Warrick Brewer, Tina Proffitt, Patricia Desmond, and Christos Pantelis. Hippocampal and Amygdala Volumes According to Psychosis Stage and Diagnosis: A Magnetic Resonance Imaging Study of Chronic Schizophrenia, First-Episode Psychosis, and Ultra-High-Risk Individuals. *Archives of General Psychiatry*, 63(2):139–149, February 2006. ISSN 0003-990X. doi: 10.1001/archpsyc.63.2.139. URL <https://doi.org/10.1001/archpsyc.63.2.139>.
- Petra E Vértes, Timothy Rittman, Kirstie J Whitaker, Rafael Romero-García, František Váša, Manfred G Kitzbichler, Konrad Wagstyl, Peter Fonagy, Raymond J Dolan, Peter B Jones, Ian M Goodyer, and Edward T Bullmore. Gene transcription profiles associated with inter-modular hubs and connection distance in human functional magnetic resonance imaging networks. *Philosophical Transactions of the Royal Society B: Biological Sciences*, 371(1705):20150362, 2016. doi: 10.1098/rstb.2015.0362.

- Oskar Vogt. Die myeloarchitektonische felderung des menschlichen. *Journal für Psychologie und Neurologie*, 15(4/5):221–232, 1910.
- Aristotle N Voineskos, Benoit H Mulsant, Erin W Dickie, Nicholas H Neufeld, Anthony J Rothschild, Ellen M Whyte, Barnett S Meyers, George S Alexopoulos, Matthew J Hoptman, Jason P Lerch, et al. Effects of antipsychotic medication on brain structure in patients with major depressive disorder and psychotic features: neuroimaging findings in the context of a randomized placebo-controlled clinical trial. *JAMA psychiatry*, 77(7):674–683, 2020.
- Constantin Freiherr von Economo and Georg N Koskinas. *Die cytoarchitektonik der hirnrinde des erwachsenen menschen*. J. Springer, 1925.
- Vesna Vuksanović. Brain morphometric similarity and flexibility. *Cerebral Cortex Communications*, 3(3):tgac024, 2022.
- František Váša, Jakob Seidlitz, Rafael Romero-Garcia, Kirstie J Whitaker, Gideon Rosenthal, Petra E Vértes, Maxwell Shinn, Aaron Alexander-Bloch, Peter Fonagy, Raymond J Dolan, Peter B Jones, Ian M Goodyer, the NSPN consortium, Olaf Sporns, and Edward T Bullmore. Adolescent tuning of association cortex in human structural brain networks. *Cerebral Cortex*, 28(1):281–294, 2018. ISSN 1047-3211. doi: 10.1093/cercor/bhx249. URL <https://doi.org/10.1093/cercor/bhx249>.
- František Váša, Rafael Romero-Garcia, Manfred G. Kitzbichler, Jakob Seidlitz, Kirstie J. Whitaker, Matilde M. Vaghi, Prantik Kundu, Ameera X. Patel, Peter Fonagy, Raymond J. Dolan, Peter B. Jones, Ian M. Goodyer, the NSPN Consortium, Petra E. Vértes, Edward T. Bullmore, Edward Bullmore, Raymond Dolan, Ian Goodyer, Peter Fonagy, Peter Jones, Michael Moutoussis, Tobias Hauser, Sharon Neufeld, Rafael Romero-Garcia, Michelle St Clair, Petra Vértes, Kirstie Whitaker, Becky Inkster, Gita Prabhu, Cinly Ooi, Umar Toseeb, Barry Widmer, Junaid Bhatti, Laura Villis, Ayesha Alrumaithi, Sarah Birt, Aislinn Bowler, Kalia Cleridou, Hina Dadabhoy, Emma Davies, Ashlyn Firkins, Sian Granville, Elizabeth Harding, Alexandra Hopkins, Daniel Isaacs, Janchai King, Danae Kokorikou, Christina Maurice, Cleo McIntosh, Jessica Memarzia, Harriet Mills, Ciara O’Donnell, Sara Pantaleone, Jenny Scott, Pasco Fearon, John Suckling, Anne-Laura van Harmelen, and Rogier Kievit. Conservative and disruptive modes of adolescent change in human brain functional connectivity. *Proceedings of the National Academy of Sciences*, 117(6): 3248–3253, February 2020. ISSN 0027-8424, 1091-6490. doi: 10.1073/pnas.1906144117. URL <https://pnas.org/doi/full/10.1073/pnas.1906144117>.
- Lindsay Walker, Marta Gozzi, Rhoshel Lenroot, Audrey Thurm, Babak Behseta, Susan Swedo, and Carlo Pierpaoli. Diffusion tensor imaging in young children with autism: biological effects and potential confounds. *Biological psychiatry*, 72(12):1043–1051, 2012.
- Lubin Wang, Longfei Su, Hui Shen, and Dewen Hu. Decoding lifespan changes of the human brain using resting-state functional connectivity mri. *PLoS One*, 2012.
- Yulin Wang, Debo Dong, Ximei Chen, Xiao Gao, Yong Liu, Mingyue Xiao, Cheng Guo, and Hong Chen. Individualized morphometric similarity predicts body mass index and food approach behavior in school-age children. *Cerebral Cortex*, 2022.

- Allysa Warling, Cassidy L McDermott, Siyuan Liu, Jakob Seidlitz, Amanda L Rodrigue, Ajay Nadig, Ruben C Gur, Raquel E Gur, David Roalf, Tyler M Moore, et al. Regional white matter scaling in the human brain. *Journal of Neuroscience*, 41(33):7015–7028, 2021.
- Varun Warriar, Eva-Maria Stauffer, Qin Qin Huang, Emilie M Wigdor, Eric AW Slob, Jakob Seidlitz, Lisa Ronan, Sofie L Valk, Travis T Mallard, Andrew D Grotzinger, et al. The genetics of cortical organisation and development: a study of 2,347 neuroimaging phenotypes. *bioRxiv*, pages 2022–09, 2022.
- Lei Wei, Xu Han, Xuchen Yu, Yawen Sun, Ming Ding, Yasong Du, Wenqing Jiang, Yan Zhou, and He Wang. Brain controllability and morphometry similarity of internet gaming addiction. *Methods*, 192:93–102, 2021.
- Nikolaus Weiskopf, John Suckling, Guy Williams, Marta M. Correia, Becky Inkster, Roger Tait, Cinly Ooi, Edward T. Bullmore, and Antoine Lutti. Quantitative multi-parameter mapping of R1, PD*, MT, and R2* at 3T: a multi-center validation. *Frontiers in Neuroscience*, 7:95, June 2013. ISSN 1662-4548. doi: 10.3389/fnins.2013.00095. URL <https://www.ncbi.nlm.nih.gov/pmc/articles/PMC3677134/>.
- Irit Weissman-Fogel, Massieh Moayedi, Keri S Taylor, Geoff Pope, and Karen D Davis. Cognitive and default-mode resting state networks: Do male and female brains “rest” differently? *Human Brain Mapping*, 31(11):n/a–n/a, 2010. ISSN 10659471. doi: 10.1002/hbm.20968.
- Kirstie J Whitaker, Petra E Vértes, Rafael Romero-Garcia, František Váša, Michael Moutoussis, Gita Prabhu, Nikolaus Weiskopf, Martina F Callaghan, Konrad Wagstyl, Timothy Rittman, Roger Tait, Cinly Ooi, John Suckling, Becky Inkster, Peter Fonagy, Raymond J Dolan, Peter B Jones, Ian M Goodyer, the NSPN Consortium, and Edward T Bullmore. Adolescence is associated with genomically patterned consolidation of the hubs of the human brain connectome. *Proceedings of the National Academy of Sciences of the United States of America*, 113(32):9105–10, 2016a. ISSN 1091-6490. doi: 10.1073/pnas.1601745113.
- Kirstie J. Whitaker, Petra E. Vértes, Rafael Romero-Garcia, František Váša, Michael Moutoussis, Gita Prabhu, Nikolaus Weiskopf, Martina F. Callaghan, Konrad Wagstyl, Timothy Rittman, Roger Tait, Cinly Ooi, John Suckling, Becky Inkster, Peter Fonagy, Raymond J. Dolan, Peter B. Jones, Ian M. Goodyer, the NSPN Consortium, and Edward T. Bullmore. Adolescence is associated with genomically patterned consolidation of the hubs of the human brain connectome. *Proceedings of the National Academy of Sciences*, 113(32):9105–9110, August 2016b. doi: 10.1073/pnas.1601745113. URL <https://www.pnas.org/doi/10.1073/pnas.1601745113>. Publisher: Proceedings of the National Academy of Sciences.
- John G White, Eileen Southgate, J Nichol Thomson, Sydney Brenner, et al. The structure of the nervous system of the nematode *Caenorhabditis elegans*. *Philos Trans R Soc Lond B Biol Sci*, 314(1165):1–340, 1986.
- Tonya White, Elisabet Blok, and Vince D Calhoun. Data sharing and privacy issues in neuroimaging research: Opportunities, obstacles, challenges, and monsters under the bed. *Human Brain Mapping*, 43(1):278–291, 2022.

- Sarah Whittle, Nandita Vijayakumar, Julian G Simmons, Meg Dennison, Orli Schwartz, Christos Pantelis, Lisa Sheeber, Michelle L Byrne, and Nicholas B Allen. Role of positive parenting in the association between neighborhood social disadvantage and brain development across adolescence. *JAMA psychiatry*, 74(8):824–832, 2017.
- Jennifer L. Whitwell, Scott A. Przybelski, Stephen D. Weigand, David S. Knopman, Bradley F. Boeve, Ronald C. Petersen, and Clifford R. Jack, Jr. 3D maps from multiple MRI illustrate changing atrophy patterns as subjects progress from mild cognitive impairment to Alzheimer’s disease. *Brain*, 130(7):1777–1786, July 2007. ISSN 0006-8950. doi: 10.1093/brain/awm112. URL <https://doi.org/10.1093/brain/awm112>.
- Lara M Wierenga, Gaelle E Doucet, Danai Dima, Ingrid Agartz, Moji Aghajani, Theophilus N Akudjedu, Anton Albajes-Eizagirre, Dag Alnæs, Kathryn I Alpert, Ole A Andreassen, Alan Anticevic, Philip Asherson, Tobias Banaschewski, Nuria Bargallo, Sarah Baumeister, Ramona Baur-Streubel, Alessandro Bertolino, Aurora Bonvino, Dorret I Boomsma, Stefan Borgwardt, Josiane Bourque, Anouk den Braber, Daniel Brandeis, Alan Breier, Henry Brodaty, Rachel M Brouwer, Jan K Buitelaar, Geraldo F Busatto, Vince D Calhoun, Erick J Canales-Rodríguez, Dara M Cannon, Xavier Caseras, Francisco X Castellanos, Tiffany M Chaim-Avancini, Christopher RK Ching, Vincent P Clark, Patricia J Conrod, Annette Conzelmann, Fabrice Crivello, Christopher G Davey, Erin W Dickie, Stefan Ehrlich, Dennis van’t Ent, Simon E Fisher, Jean-Paul Fouche, Barbara Franke, Paola Fuentes-Claramonte, Eco JC de Geus, Annabella Di Giorgio, David C Glahn, Ian H Gotlib, Hans J Grabe, Oliver Gruber, Patricia Gruner, Raquel E Gur, Ruben C Gur, Tiril P Gurholt, Lieuwe de Haan, Beathe Haatveit, Ben J Harrison, Catharina A Hartman, Sean N Hatton, Dirk J Heslenfeld, Odile A van den Heuvel, Ian B Hickie, Pieter J Hoekstra, Sarah Hohmann, Avram J Holmes, Martine Hoogman, Norbert Hosten, Fleur M Howells, Hilleke E Hulshoff Pol, Chaim Huyser, Neda Jahanshad, Anthony C James, Jiyang Jiang, Erik G Jönsson, John A Joska, Andrew J Kalnin, Karolinska Schizophrenia Project (KaSP) Consortium, Marieke Klein, Laura Koenders, Knut K Kolskår, Bernd Krämer, Jonna Kuntsi, Jim Lagopoulos, Luisa Lazaro, Irina S Lebedeva, Phil H Lee, Christine Lochner, Marise WJ Machielsen, Sophie Maingault, Nicholas G Martin, Ignacio Martínez-Zalacaín, David Mataix-Cols, Bernard Mazoyer, Brenna C McDonald, Colm McDonald, Andrew M McIntosh, Katie L McMahan, Genevieve McPhilemy, Dennis van der Meer, José M Menchón, Jilly Naaijen, Lars Nyberg, Jaap Oosterlaan, Yannis Paloyelis, Paul Pauli, Giulio Pergola, Edith Pomarol-Clotet, Maria J Portella, Joaquim Radua, Andreas Reif, Geneviève Richard, Joshua L Roffman, Pedro GP Rosa, Matthew D Sacchet, Perminder S Sachdev, Raymond Salvador, Salvador Sarró, Theodore D Satterthwaite, Andrew J Saykin, Mauricio H Serpa, Kang Sim, Andrew Simmons, Jordan W Smoller, Iris E Sommer, Carles Soriano-Mas, Dan J Stein, Lachlan T Strike, Philip R Szeszko, Henk S Temmingh, Sophia I Thomopoulos, Alexander S Tomyshev, Julian N Trollor, Anne Uhlmann, Ilya M Veer, Dick J Veltman, Aristotle Voineskos, Henry Völzke, Henrik Walter, Lei Wang, Yang Wang, Bernd Weber, Wei Wen, John D West, Lars T Westlye, Heather C Whalley, Steven CR Williams, Katharina Wittfeld, Daniel H Wolf, Margaret J Wright, Yuliya N Yoncheva, Marcus V Zanetti, Georg C Ziegler, Greig I de Zubicaray, Paul M Thompson, Eveline A Crone, Sophia Frangou, and Christian K Tamnes. Greater male than female variability in regional brain structure across the lifespan. *Human Brain Mapping*, 43(1):470–499, 2022. ISSN 1097-0193. doi: 10.1002/hbm.25204. URL <https://onlinelibrary.wiley.com/doi/abs/10.1002/hbm.25204>. _eprint: <https://onlinelibrary.wiley.com/doi/pdf/10.1002/hbm.25204>.

- Camille Michèle Williams, Hugo Peyre, Roberto Toro, and Franck Ramus. Sex differences in the brain are not reduced to differences in body size. *Neuroscience & Biobehavioral Reviews*, 130:509–511, 2021.
- Daniel Witvliet, Ben Mulcahy, James K. Mitchell, Yaron Meirovitch, Daniel R. Berger, Yuelong Wu, Yufang Liu, Wan Xian Koh, Rajeev Parvathala, Douglas Holmyard, Richard L. Schalek, Nir Shavit, Andrew D. Chisholm, Jeff W. Lichtman, Aravinthan D. T. Samuel, and Mei Zhen. Connectomes across development reveal principles of brain maturation. *Nature*, 596(7871):257–261, 2021. ISSN 1476-4687. doi: 10.1038/s41586-021-03778-8. URL <https://www.nature.com/articles/s41586-021-03778-8>. Number: 7871 Publisher: Nature Publishing Group.
- N R Wray, S Ripke, M Mattheisen, and et al. Genome-wide association analyses identify 44 risk variants and refine the genetic architecture of major depression. *Nature Genetics*, page 668–681, 2018. ISSN 50. doi: <https://doi.org/10.1038/s41588-018-0090-3>.
- Xinran Wu, Lena Palaniyappan, Gechang Yu, Kai Zhang, Jakob Seidlitz, Zhaowen Liu, Xiangzhen Kong, Gunter Schumann, Jianfeng Feng, Barbara J Sahakian, et al. Morphometric dis-similarity between cortical and subcortical areas underlies cognitive function and psychiatric symptomatology: a preadolescence study from abcd. *Molecular Psychiatry*, pages 1–13, 2022.
- Xiaoxiao Xu, Alan B Wells, David R O’Brien, Arye Nehorai, and Joseph D Dougherty. Cell type-specific expression analysis to identify putative cellular mechanisms for neurogenetic disorders. *Journal of Neuroscience*, 34(4):1420–1431, 2014. ISSN 0270-6474. doi: 10.1523/JNEUROSCI.4488-13.2014.
- Kaizhong Xue, Lining Guo, Wenshuang Zhu, Sixiang Liang, Qiang Xu, Lin Ma, Mengge Liu, Yong Zhang, and Feng Liu. Transcriptional signatures of the cortical morphometric similarity network gradient in first-episode, treatment-naive major depressive disorder. *Neuropsychopharmacology*, 48(3):518–528, 2023.
- Siqi Yang, Konrad Wagstyl, Yao Meng, Xiaopeng Zhao, Jiao Li, Peng Zhong, Bing Li, Yun-Shuang Fan, Huafu Chen, and Wei Liao. Cortical patterning of morphometric similarity gradient reveals diverged hierarchical organization in sensory-motor cortices. *Cell Reports*, 36(8):109582, 2021.
- Zhijian Yao, Rui Yan, Maobin Wei, Hao Tang, Jiaolong Qin, and Qing Lu. Gender differences in brain activity and the relationship between brain activity and differences in prevalence rates between male and female major depressive disorder patients: A resting-state fMRI study. *Clinical Neurophysiology*, 125(11):2232–2239, nov 2014. ISSN 1388-2457. doi: 10.1016/J.CLINPH.2014.03.006. URL <https://www.sciencedirect.com/science/article/pii/S138824571400131X?via%3Dihub>.
- T Yarkoni, R A Poldrack, T E Nichols, D C Van Essen, and T D Wager. Large-scale automated synthesis of human functional neuroimaging data. *Nature methods*, 8(8):665–670, 2011. doi: <https://doi.org/10.1038/nmeth.1635>.
- B T Yeo, F M Krienen, J Sepulcre, M R Sabuncu, D Lashkari, M Hollinshead, J L Roffman, J W Smoller, L Zöllei, J R Polimeni, B Fischl, H Liu, and R L Buckner. The organization

- of the human cerebral cortex estimated by intrinsic functional connectivity. *Journal of neurophysiology*, 106(3):1125–1165, 2011. doi: <https://doi.org/10.1152/jn.00338.2011>.
- BT Thomas Yeo, Fenna M Krienen, Simon B Eickhoff, Siti N Yaakub, Peter T Fox, Randy L Buckner, Christopher L Asplund, and Michael WL Chee. Functional specialization and flexibility in human association cortex. *Cerebral cortex*, 25(10):3654–3672, 2015.
- Shoukai Yu. Uncovering the hidden impacts of inequality on mental health: a global study. *Translational Psychiatry*, 8(1):98, May 2018. ISSN 2158-3188. doi: 10.1038/s41398-018-0148-0. URL <https://doi.org/10.1038/s41398-018-0148-0>.
- Farnaz Zamani Esfahlani, Joshua Faskowitz, Jonah Slack, Bratislav Mišić, and Richard F. Betzel. Local structure-function relationships in human brain networks across the lifespan. *Nat Commun*, 13(1):2053, 2022. ISSN 2041-1723. doi: 10.1038/s41467-022-29770-y. URL <https://www.nature.com/articles/s41467-022-29770-y>. Number: 1 Publisher: Nature Publishing Group.
- Bin Zhang and Steve Horvath. A general framework for weighted gene co-expression network analysis. *Statistical applications in genetics and molecular biology*, 4(1), 2005.
- Chao Zhang, Nathan D Cahill, Mohammad R Arbabshirani, Tonya White, Stefi A Baum, and Andrew M Michael. Sex and Age Effects of Functional Connectivity in Early Adulthood. *Brain Connectivity*, 6(9):700–713, 2016. ISSN 2158-0014. doi: 10.1089/brain.2016.0429.
- Chao Zhang, Chase C Dougherty, Stefi A Baum, Tonya White, and Andrew M Michael. Functional connectivity predicts gender: Evidence for gender differences in resting brain connectivity. *Human Brain Mapping*, 39(4):1765–1776, 2018. ISSN 1065-9471. doi: 10.1002/hbm.23950.
- Yang Zhang, Min Ma, Zhonghua Xie, Heng Wu, Nan Zhang, and Junlin Shen. Bridging the gap between morphometric similarity mapping and gene transcription in alzheimer’s disease. *Frontiers in Neuroscience*, 15:731292, 2021a.
- Yi Zhang, Qiang Luo, Chu-Chung Huang, Chun-Yi Zac Lo, Christelle Langley, Sylvane Desrivières, Erin Burke Quinlan, Tobias Banaschewski, Sabina Millenet, Arun LW Bokde, et al. The human brain is best described as being on a female/male continuum: evidence from a neuroimaging connectivity study. *Cerebral Cortex*, 31(6):3021–3033, 2021b.
- Dongming Zhou, Catherine Lebel, Sarah Treit, Alan Evans, and Christian Beaulieu. Accelerated longitudinal cortical thinning in adolescence. *Neuroimage*, 104:138–145, 2015.
- Yan-Ling Zhou, Feng-Chun Wu, Wei-Jian Liu, Wei Zheng, Cheng-Yu Wang, Yan-Ni Zhan, Xiao-Feng Lan, and Yu-Ping Ning. Volumetric changes in subcortical structures following repeated ketamine treatment in patients with major depressive disorder: a longitudinal analysis. *Translational Psychiatry*, 10:264, August 2020. ISSN 2158-3188. doi: 10.1038/s41398-020-00945-9. URL <https://www.ncbi.nlm.nih.gov/pmc/articles/PMC7400625/>.
- Peter Zhukovsky, George Savulich, Sarah Morgan, Jeffrey W Dalley, Guy B Williams, and Karen D Ersche. Morphometric similarity deviations in stimulant use disorder point towards abnormal brain ageing. *Brain Communications*, 4(3):fcac079, 2022.

- Xiaofen Zong, Jiangbo Zhang, Lei Li, Tao Yao, Simeng Ma, Lijun Kang, Nan Zhang, Zhaowen Nie, Zhongchun Liu, Junjie Zheng, et al. Virtual histology of morphometric similarity network after risperidone monotherapy and imaging-epigenetic biomarkers for treatment response in first-episode schizophrenia. *Asian Journal of Psychiatry*, 80:103406, 2023.
- Mustafa S. Çetin, Fletcher Christensen, Christopher C. Abbott, Julia M. Stephen, Andrew R. Mayer, José M. Cañive, Juan R. Bustillo, Godfrey D. Pearlson, and Vince D. Calhoun. Thalamus and posterior temporal lobe show greater inter-network connectivity at rest and across sensory paradigms in schizophrenia. *NeuroImage*, 97:117–126, 2014. ISSN 1053-8119. doi: 10.1016/j.neuroimage.2014.04.009. URL <https://www.sciencedirect.com/science/article/pii/S105381191400264X>.

Appendix A

Supplementary Tables

Paper	Data	#Subj	age(y)	CS	rsfMRI	ROI	BL	Age	Inter.	Summary
Alarcon 2018	in house	49	15-18	CS	rsfMRI & flanker task	DMN, FPN	Yes	NA	NA	FC female > male in DMN and FPN during cognitive control in a self referential context Mediated by higher co-rumination in females
Zhang 2018	HCP	820	22-37	CS	rsfMRI	WB	NA	NA	NA	PLS classification of gender (87%) based on whole brain FC Most contributing ROIs in DMN, fronto-parietal and sensorimotor networks Regressing out age had no effect
Mao 2017	1000 FC	148	18-26	CS	rsfMRI	Yes	Yes	NA	NA	12 ROIs with gender differences in dynamic FC Flex. female < male in amy., hipp. and parah. Flex. male < female in TL, prec., MCG, SOC, IOG
Peterson 2017	1000 FC	250	18-49	CS	rsfMRI	VTA, SNc to WB	Yes	in men	Yes	FC VTA/SNc to left posterior orbital gyrus male > women Age effect in FC VTA/SNc to cortical and cerebellar ROIs in men only

Continued ...

Paper	Data	#Subj	age(y)	CS	rsfMRI	ROI	BL	Age	Inter.	Summary
Zhang 2016	HCP	494	22-36	CS	rsfMRI	WB	Yes	Yes	Yes	Edgeswise FC male>female in 1025 ROIs Sex differences mostly in frontal, parietal and temporal lobes Age effects in 29 ROIs Interaction did not survive; greater decline in FC with age in females
Alarcon 2015	Dataset	122	10-16	CS	rsfMRI	amy. /w WB	Yes.	Yes	Yes	increased FC amygdala and mPFC SFA. and parieto-occipital ROIs FC decrease with age female > male BLA and parieto-occipital ROIs FC decrease with age female > male
Scheinost 2015	Dataset	103	18-65	CS	task	WB	Yes	Yes	Yes	Used intrinsic connectivity distribution, ICD Age by sex interaction in several networks, including DMN, FPN, visual, auditory Age effect in several ROIs including putamen, caudate, amygdala, orbito frontal cortex (all pos.) and default mode (neg.) Sex effect female > male in subcortex and limbic areas Sex effect male > female in sensorimotor areas

Continued ...

Paper	Data	#Subj	age(y)	CS	rsfMRI	ROI	BL	Age	Inter.	Summary
Satterthwaite 2014	PNDC	674	9-22	CS	rsfMRI	Yes	Yes	NA	NA	Between module connectivity males >females Within-module connectivity females >males SVM classification of sex based on FC 71% accuracy
Filippi 2013	Dataset	100	20-29	CS	rsfMRI	Network rsfMRI	Yes	NA	NA	Marginal sex effect in sensory networks FC parietal-occipital ROIs male > female FC frontal, temporal ROIs and cerebellum female > male FNC cognitive, sensory male > female FNC attention, right working memory female > male
Casanova 2012	1000 FC	148	21	CS	rsfMRI	WB	Yes	NA	NA	Lasso (62.3%) and Random Forest (65.4%) to classify sex female discriminative edges: cingulate gyrus, left frontal lobe, basal ganglia, thalamus, right cerebellum male discriminative edges: cingulate gyrus, sensory motor cortex, cerebellum, left frontal lobe
Tian 2011	in-house	86	18-25	CS	rsfMRI	within-hemi-sphere	Yes	NA	NA	Right hemisphere's clustering coefficient male >female Left hemisphere's clustering coefficient female >male

Continued ...

Paper	Data	#Subj	age(y)	CS	rsfMRI	ROI	BL	Age	Inter.	Summary
Biswal 2010	1000 FC	1,414	μ =age < 60	CS	rsfMRI	WB	Yes	Yes	NA	FC female > male in frontal ROIs FC male > female in occipital and parietal ROIs Delta Age positive in association cortex
Kong 2010	Dataset	100	age	CS	task	PAG to WB	Yes	NA	NA	FC PAG to mid cingulate cortex female > male FC PAG to left medial orbital prefrontal cortex, uncus, right insula und prefrontal cortex male > female
Weissm.- F. 2010	in-house	49	21-50	CS	rsfMRI	ECN, SN, DMN	No	NA	NA	No within-network differences in ECN,SN;DMN
Liu 2009	in-house	300	μ =22	CS	rsfMRI	WB	Yes	NA	NA	Men showed stronger intrinsic laterality
Kilpatrick 2005	in-house	72	??	CS	rsfMRI	amy. to WB	Yes	NA	NA	Right amy. FC male > female Left amy. FC female > male

Table A.1 Sex differences in fMRI literature: We reviewed literature on sex differences in functional connectivity development.

ROI	ΔMI	Z-Value	P-Value	Trend	Yeo-Network
R FOP5	-0.79	10.57	0.00	female more disruptive	Ventral Attention
R s32	-0.71	11.70	0.00	female more disruptive	Default Mode
L s32	-0.71	12.05	0.00	female more disruptive	Default Mode
L VMV2	-0.71	11.59	0.00	female more disruptive	Visual
L 47s	-0.67	12.00	0.00	female more disruptive	Default Mode
R PGI	-0.64	9.04	0.00	female more disruptive	Default Mode
L MI	-0.63	9.42	0.00	female more disruptive	Ventral Attention
L VMV3	-0.63	13.16	0.00	female more disruptive	Visual
R IFSa	-0.60	9.39	0.00	female more disruptive	Frontoparietal
R Pir	-0.59	6.98	0.00	female more disruptive	Subcortex
L accumbens	-0.57	6.79	0.00	female more disruptive	Subcortex
L p32	-0.56	10.30	0.00	female more disruptive	Default Mode
L a24	-0.50	9.44	0.00	female more disruptive	Default Mode
R STSvp	-0.50	7.07	0.00	female more disruptive	Default Mode
R STSda	-0.49	7.62	0.00	female more disruptive	Default Mode
R accumbens	-0.49	5.13	0.00	female more disruptive	Subcortex
R A5	-0.48	5.98	0.00	female more disruptive	Somatomotor
L A5	-0.47	6.47	0.00	female more disruptive	Somatomotor
R 47l	-0.47	5.54	0.00	female more disruptive	Default Mode
L p24	-0.46	8.45	0.00	female more disruptive	Default Mode
L 10r	-0.46	6.29	0.00	female more disruptive	Default Mode
R 47s	-0.45	7.63	0.00	female more disruptive	Default Mode
R FOP4	-0.45	6.86	0.00	female more disruptive	Ventral Attention
R a32pr	-0.44	5.85	0.00	female more disruptive	Frontoparietal
L PoI1	-0.44	6.61	0.00	female less conservative	Ventral Attention
R AAIC	-0.44	5.37	0.00	female more disruptive	Default Mode
L 45	-0.43	7.17	0.00	female more disruptive	Default Mode
L 31pd	-0.43	4.97	0.00	female more disruptive	Default Mode
R STSdp	-0.43	5.61	0.00	female more disruptive	Default Mode
R p24	-0.42	7.54	0.00	female more disruptive	Default Mode
L FOP4	-0.41	6.32	0.00	female more disruptive	Ventral Attention
L FOP5	-0.41	5.78	0.00	female more disruptive	Ventral Attention
L d32	-0.40	6.34	0.00	female more disruptive	Default Mode
R a24	-0.40	7.02	0.00	female more disruptive	Default Mode

Continued on next page

ROI	ΔMI	Z-Value	P-Value	Trend	Yeo-Network
L SFL	-0.40	5.93	0.00	female more disruptive	Frontoparietal
L IFSa	-0.40	5.10	0.00	female more disruptive	Frontoparietal
L STSda	-0.40	5.90	0.00	female more disruptive	Default Mode
L AAIC	-0.39	6.20	0.00	female more disruptive	Default Mode
R p32pr	-0.38	5.08	0.00	female more disruptive	Ventral Attention
L 8BL	-0.38	5.32	0.00	female more disruptive	Default Mode
R p32	-0.38	6.19	0.00	female more disruptive	Default Mode
L Pir	-0.38	3.81	0.00	female more disruptive	Subcortex
L 25	-0.38	5.11	0.00	female more disruptive	Limbic
L pallidum	-0.37	5.35	0.00	female more disruptive	Subcortex
R 9m	-0.36	6.81	0.00	female more disruptive	Default Mode
L 9p	-0.36	5.32	0.00	female more disruptive	Default Mode
L STGa	-0.36	4.59	0.00	female more disruptive	Default Mode
R 8BL	-0.36	3.76	0.00	female more disruptive	Default Mode
R POS1	-0.35	4.39	0.00	female more disruptive	Default Mode
L IFSp	-0.35	5.05	0.00	female more disruptive	Frontoparietal
L 47l	-0.35	6.28	0.00	female more disruptive	Default Mode
L AVI	-0.34	4.25	0.00	female more disruptive	Frontoparietal
L STSdp	-0.34	5.28	0.00	female more disruptive	Default Mode
R 10r	-0.34	4.50	0.00	female more disruptive	Default Mode
L STSvp	-0.34	5.94	0.00	female more disruptive	Default Mode
L putamen	-0.34	6.28	0.00	female more disruptive	Subcortex
L POS1	-0.33	3.94	0.00	female more disruptive	Default Mode
L PoI2	-0.33	4.84	0.00	female less conservative	Ventral Attention
R VMV2	-0.33	6.42	0.00	female less conservative	Visual
L 31pv	-0.33	3.30	0.00	female more disruptive	Default Mode
L 7m	-0.32	3.98	0.00	female more disruptive	Default Mode
L 10v	-0.32	5.02	0.00	female more disruptive	Limbic
R 46	-0.32	4.93	0.00	female more disruptive	Frontoparietal
L v23ab	-0.31	4.14	0.00	female more disruptive	Default Mode
L VMV1	-0.31	5.16	0.00	female less conservative	Visual
R 25	-0.31	4.42	0.00	female more disruptive	Limbic
R 9p	-0.31	3.09	0.00	female more disruptive	Default Mode
R STV	-0.31	4.27	0.00	female less conservative	Default Mode

Continued on next page

ROI	ΔMI	Z-Value	P-Value	Trend	Yeo-Network
L 43	-0.30	4.87	0.00	female less conservative	Somatomotor
R TE1a	-0.30	5.33	0.00	female more disruptive	Default Mode
R PoI1	-0.30	4.72	0.00	female less conservative	Ventral Attention
L OP4	-0.30	4.45	0.00	female less conservative	Somatomotor
R p47r	-0.29	4.87	0.00	female more disruptive	Frontoparietal
L VVC	-0.29	5.25	0.00	female more disruptive	Visual
R 23d	-0.29	4.01	0.00	female more disruptive	Default Mode
R MI	-0.29	4.74	0.00	female more disruptive	Ventral Attention
R PHA2	-0.29	2.47	0.02	female more disruptive	Visual
L 52	-0.29	3.54	0.00	female less conservative	Somatomotor
R IFSp	-0.29	4.16	0.00	female more disruptive	Frontoparietal
R 31pd	-0.29	3.57	0.00	female more disruptive	Default Mode
R pallidum	-0.28	4.42	0.00	female more disruptive	Subcortex
L 9-46d	-0.28	4.79	0.00	female more disruptive	Frontoparietal
R 10d	-0.28	4.24	0.00	female more disruptive	Default Mode
L TPOJ1	-0.27	3.99	0.00	female less conservative	Ventral Attention
L PF	-0.26	3.52	0.00	female more disruptive	Ventral Attention
R AVI	-0.25	2.90	0.01	female more disruptive	Frontoparietal
L STSva	-0.25	4.51	0.00	female more disruptive	Default Mode
L p24pr	-0.25	4.04	0.00	female less conservative	Ventral Attention
R RSC	-0.25	2.60	0.02	female more disruptive	Default Mode
R 10v	-0.25	3.24	0.00	female more disruptive	Limbic
R VMV3	-0.24	7.13	0.00	female more disruptive	Visual
R STGa	-0.24	3.65	0.00	female more disruptive	Default Mode
L 23d	-0.24	3.65	0.00	female more disruptive	Default Mode
L a32pr	-0.24	3.25	0.00	female more disruptive	Frontoparietal
L RSC	-0.24	2.87	0.01	female more disruptive	Default Mode
L 24dd	-0.23	2.57	0.02	female less conservative	Somatomotor
R 33pr	-0.23	3.22	0.00	female more disruptive	Ventral Attention
R STSva	-0.23	3.33	0.00	female more disruptive	Default Mode
R VVC	-0.23	4.14	0.00	female more disruptive	Visual
L STV	-0.23	3.54	0.00	female more disruptive	Default Mode
R OP2-3	-0.23	4.41	0.00	female less conservative	Somatomotor
L a47r	-0.23	3.93	0.00	female more disruptive	Frontoparietal

Continued on next page

ROI	ΔMI	Z-Value	P-Value	Trend	Yeo-Network
L a10p	-0.22	4.17	0.00	female more disruptive	Frontoparietal
L 10d	-0.22	3.86	0.00	female more disruptive	Default Mode
L MBelt	-0.22	3.54	0.00	female less conservative	Somatomotor
L A4	-0.22	4.45	0.00	female less conservative	Somatomotor
R putamen	-0.22	4.63	0.00	female more disruptive	Subcortex
L thalamus	-0.22	3.16	0.00	female more disruptive	Subcortex
R 47m	-0.21	2.78	0.01	female more disruptive	Default Mode
R a47r	-0.21	4.18	0.00	female more disruptive	Frontoparietal
L PGi	-0.21	2.17	0.05	female more disruptive	Default Mode
R v23ab	-0.21	2.79	0.01	female more disruptive	Default Mode
R FOP2	-0.19	3.39	0.00	female less conservative	Somatomotor
L 44	-0.19	3.25	0.00	female more disruptive	Frontoparietal
L p10p	-0.18	3.87	0.00	female more disruptive	Frontoparietal
R 44	-0.18	2.82	0.01	female more disruptive	Frontoparietal
R p24pr	-0.18	3.27	0.00	female less conservative	Ventral Attention
L OP2-3	-0.17	2.90	0.01	female less conservative	Somatomotor
L 9m	-0.17	4.29	0.00	female more disruptive	Default Mode
L a24pr	-0.17	2.66	0.01	female less conservative	Ventral Attention
R V8	-0.16	4.44	0.00	female less conservative	Visual
R SCEF	-0.16	2.42	0.02	female less conservative	Ventral Attention
R IFJa	-0.16	2.34	0.03	female more disruptive	Frontoparietal
L caudate	-0.15	2.31	0.03	female more disruptive	Subcortex
L 23c	-0.15	2.29	0.03	female less conservative	Ventral Attention
R IFJp	-0.15	2.54	0.02	female more disruptive	Dorsal Attention
L LO2	-0.14	2.30	0.03	female less conservative	Visual
L FOP3	-0.14	2.38	0.03	female less conservative	Ventral Attention
R A1	-0.13	2.43	0.02	female less conservative	Somatomotor
R 9-46d	-0.12	2.15	0.05	female more disruptive	Frontoparietal
R 7m	-0.12	2.24	0.04	female more disruptive	Default Mode
R V6	-0.11	2.73	0.01	female less conservative	Visual
R LO2	-0.10	3.42	0.00	female less conservative	Visual
L PBelt	-0.09	2.21	0.04	female less conservative	Somatomotor
R 11l	-0.09	2.70	0.01	female more disruptive	Frontoparietal
R V4	-0.08	3.56	0.00	female less conservative	Visual

Continued on next page

ROI	ΔMI	Z-Value	P-Value	Trend	Yeo-Network
R VMV1	-0.06	3.41	0.00	female less conservative	Visual
L V4	-0.01	2.50	0.02	female less conservative	Visual
R V3CD	0.02	3.42	0.00	female more conservative	Visual
L hippocampus	0.09	-2.20	0.04	female less disruptive	Subcortex
R a9-46v	0.10	-2.46	0.02	female less disruptive	Frontoparietal
L FEF	0.15	-2.14	0.05	female more conservative	Dorsal Attention
L PreS	0.15	-3.29	0.00	female less disruptive	Visual
R 2	0.15	-2.35	0.03	female more conservative	Somatomotor
L 6v	0.16	-3.16	0.00	female more conservative	Somatomotor
L 1	0.16	-3.09	0.00	female more conservative	Somatomotor
R 1	0.16	-3.04	0.00	female more conservative	Somatomotor
R PFt	0.16	-2.30	0.03	female more conservative	Dorsal Attention
L 6d	0.17	-2.54	0.02	female more conservative	Somatomotor
R 52	0.17	-2.84	0.01	female more conservative	Somatomotor
L 31a	0.18	-3.39	0.00	female less disruptive	Frontoparietal
L PGs	0.18	-3.36	0.00	female less disruptive	Default Mode
R 8Ad	0.18	-3.62	0.00	female less disruptive	Default Mode
R TPOJ3	0.19	-2.21	0.04	female more conservative	Dorsal Attention
R 8BM	0.19	-2.23	0.04	female less disruptive	Frontoparietal
R PSL	0.19	-3.14	0.00	female more conservative	Default Mode
L a9-46v	0.19	-3.58	0.00	female less disruptive	Frontoparietal
L V6A	0.20	-2.60	0.02	female more conservative	Visual
R PGs	0.21	-3.24	0.00	female less disruptive	Default Mode
L s6-8	0.21	-3.06	0.00	female less disruptive	Frontoparietal
R FFC	0.21	-2.95	0.01	female more conservative	Visual
R FST	0.22	-3.82	0.00	female more conservative	Dorsal Attention
L 8BM	0.22	-2.66	0.01	female less disruptive	Frontoparietal
R PreS	0.23	-5.01	0.00	female less disruptive	Visual
R MT	0.23	-2.60	0.02	female more conservative	Visual
L 2	0.23	-2.48	0.02	female more conservative	Somatomotor
R 6d	0.24	-3.44	0.00	female more conservative	Somatomotor
L 8C	0.27	-4.09	0.00	female less disruptive	Frontoparietal
R PFm	0.27	-3.22	0.00	female less disruptive	Frontoparietal
L 5L	0.28	-3.46	0.00	female more conservative	Somatomotor

Continued on next page

ROI	ΔMI	Z-Value	P-Value	Trend	Yeo-Network
R d23ab	0.28	-4.89	0.00	female less disruptive	Default Mode
R p9-46v	0.29	-2.83	0.01	female less disruptive	Frontoparietal
L 6r	0.29	-4.24	0.00	female more conservative	Ventral Attention
L 8Av	0.29	-4.25	0.00	female less disruptive	Frontoparietal
L 7PC	0.29	-3.00	0.00	female more conservative	Dorsal Attention
R 6r	0.30	-4.07	0.00	female more conservative	Ventral Attention
L PH	0.31	-3.70	0.00	female more conservative	Dorsal Attention
L 7AL	0.31	-2.80	0.01	female more conservative	Dorsal Attention
L IP1	0.32	-3.47	0.00	female less disruptive	Frontoparietal
R PCV	0.32	-4.11	0.00	female less disruptive	Default Mode
L MT	0.32	-2.67	0.01	female more conservative	Visual
L V4t	0.32	-3.46	0.00	female more conservative	Visual
R 6ma	0.34	-4.23	0.00	female more conservative	Ventral Attention
L MST	0.34	-4.28	0.00	female more conservative	Visual
R IP0	0.34	-4.71	0.00	female more conservative	Dorsal Attention
L 8Ad	0.34	-5.79	0.00	female less disruptive	Default Mode
R VIP	0.36	-4.71	0.00	female more conservative	Dorsal Attention
R V7	0.36	-3.02	0.00	female more conservative	Visual
L PFt	0.36	-4.11	0.00	female more conservative	Dorsal Attention
R 6a	0.37	-3.96	0.00	female more conservative	Dorsal Attention
L PHT	0.38	-4.75	0.00	female more conservative	Dorsal Attention
R LIPv	0.38	-5.10	0.00	female more conservative	Dorsal Attention
L LIPv	0.38	-4.90	0.00	female more conservative	Dorsal Attention
R 7PC	0.38	-3.75	0.00	female more conservative	Dorsal Attention
R s6-8	0.39	-4.74	0.00	female less disruptive	Frontoparietal
L 7Pm	0.39	-5.65	0.00	female less disruptive	Frontoparietal
L TPOJ2	0.39	-4.71	0.00	female more conservative	Dorsal Attention
R PH	0.39	-5.95	0.00	female more conservative	Dorsal Attention
R i6-8	0.40	-5.28	0.00	female less disruptive	Frontoparietal
L FFC	0.40	-6.81	0.00	female more conservative	Visual
R PGp	0.41	-6.37	0.00	female less disruptive	Dorsal Attention
R 8Av	0.41	-5.67	0.00	female less disruptive	Frontoparietal
L 6a	0.42	-4.92	0.00	female more conservative	Dorsal Attention
L V7	0.42	-3.74	0.00	female more conservative	Visual

Continued on next page

ROI	ΔMI	Z-Value	P-Value	Trend	Yeo-Network
R MST	0.43	-4.44	0.00	female more conservative	Visual
L PGp	0.43	-5.79	0.00	female less disruptive	Dorsal Attention
L 7Am	0.44	-6.34	0.00	female less disruptive	Dorsal Attention
L 6ma	0.44	-5.45	0.00	female more conservative	Ventral Attention
L PFm	0.46	-7.15	0.00	female less disruptive	Frontoparietal
R 7Am	0.47	-6.02	0.00	female more conservative	Dorsal Attention
R 8C	0.48	-6.24	0.00	female less disruptive	Frontoparietal
L AIP	0.48	-4.87	0.00	female more conservative	Dorsal Attention
L 7PL	0.49	-6.72	0.00	female more conservative	Dorsal Attention
L VIP	0.49	-6.28	0.00	female more conservative	Dorsal Attention
R 7Pm	0.50	-7.75	0.00	female less disruptive	Frontoparietal
L i6-8	0.52	-7.12	0.00	female less disruptive	Frontoparietal
R IPS1	0.52	-7.42	0.00	female more conservative	Dorsal Attention
L p9-46v	0.54	-5.07	0.00	female more conservative	Frontoparietal
R 7PL	0.54	-7.60	0.00	female more conservative	Dorsal Attention
R AIP	0.57	-6.30	0.00	female more conservative	Dorsal Attention
R MIP	0.58	-8.11	0.00	female more conservative	Dorsal Attention
R IP1	0.59	-7.40	0.00	female less disruptive	Frontoparietal
R V1	0.60	-8.27	0.00	female more conservative	Visual
L V1	0.62	-7.60	0.00	female more conservative	Visual
L MIP	0.63	-8.23	0.00	female more conservative	Dorsal Attention
L IPS1	0.63	-8.53	0.00	female more conservative	Dorsal Attention
R TPOJ2	0.68	-9.32	0.00	female more conservative	Dorsal Attention
R PEF	0.76	-10.03	0.00	female more conservative	Dorsal Attention
L IPO	0.77	-10.83	0.00	female more conservative	Dorsal Attention
L FST	0.80	-11.75	0.00	female more conservative	Dorsal Attention

Table A.3 **ROIs with significantly different ΔMI** : We tested for sex differences in maturational index (MI). Here we show all 230 regions displaying a significant sex difference in MI ($P(\Delta MI = 0) < 0.05$). We show the regions name in the HCP parcellation; it's ΔMI value, the p-value and Z-value from the parametric test of the sex difference in MI; the functional network they are located in ('Yeo-Network') Yeo et al. (2011); as well as which one of four trends they display: (1) 'female more conservative', (2) 'female more disruptive', (3) 'female less conservative', (4) 'female less disruptive'.

	region	t	P_{FDR}	network
1	L POS2	-3.02	0.04	2
2	L p24pr	3.02	0.04	6
3	L a24pr	3.10	0.03	6
4	L a24	3.20	0.03	6
5	L 6r	-3.27	0.03	1
6	L 47s	2.96	0.04	4
7	L PoI2	4.34	0.00	7
8	L MI	3.49	0.02	7
9	L PeEc	2.90	0.05	3
10	L STGa	-3.07	0.04	3
11	L IP2	-3.38	0.02	3
12	L VVC	3.94	0.00	4
13	L pOFC	3.09	0.03	7
14	L a32pr	4.57	0.00	6
15	R V8	-2.93	0.04	1
16	R RSC	-4.02	0.00	2
17	R 7PC	-4.09	0.00	2
18	R 1	-3.02	0.04	5
19	R 33pr	3.74	0.01	6
20	R p32pr	3.69	0.01	6
21	R IFJp	-2.93	0.04	2
22	R 46	-2.94	0.04	3
23	R 10v	-3.13	0.03	3
24	R PFcm	4.29	0.00	7
25	R FOP4	5.04	0.00	7
26	R PFt	-4.00	0.00	2
27	R H	3.27	0.03	6
28	R TPOJ2	-3.15	0.03	2
29	R DVT	-3.15	0.03	3
30	R 31a	3.93	0.00	4
31	R s32	3.45	0.02	7
32	R TE1m	4.52	0.00	2
33	R PI	3.17	0.03	6

Table A.4 Significant regional effects of age on morphometric similarity: We estimated the linear effect of age on morphometric similarity using linear mixed effects models with a fixed effect of age, sex and site, and a random effect of subject. We find that 33 regions show significant effects of age after FDR-correction. Above, we list the t and P -values for these regions, together with their von Economo class assignment.

study	pipeline	sites	country	N	Age_{min}	Age_{max}
ABCD	FS6_T1	22	USA	377 (156)	9	11
ABCD	FS6_T1T2	23	USA	10206 (4925)	9	11
ABIDE	FS6_T1	35	USA	2085 (393)	5	64
ADHD200	FS6_T1	10	USA	951 (368)	7	26
ADHD200	FS6_T1	10	China	951 (368)	7	26
ADNI	FS6_T1	62	USA	1733 (776)	54	93
BCP-old	FS6_T1	1	USA	28 (NA)	3	5
BCP-young	FSInfant	1	USA	212 (NA)	0	3
BGSP	FS6_T1	1	USA	1570 (905)	18	34
Calgary	FS6_T1	1	Canada	84 (39)	3	7
CALM	FS6_T1	1	UK	37 (17)	6	13
CALM	FS6_T1T2	1	UK	367 (122)	6	16
Cam-CAN	FS53	1	UK	650 (329)	18	88
dHCP	Custom	1	UK	487 (213)	-0	0
DLBS	FS6_T1	1	USA	314 (197)	21	89
FinnBrain	Custom	1	Finland	248 (120)	0	6
HBN	Custom	3	USA	1085 (428)	5	22
HCP	FS53	1	USA	1113 (606)	22	37
HCP-A	FS6_T1T2	1	USA	689 (395)	35	99
HCP-D	FS6_T1T2	1	USA	655 (332)	7	21
IMAGEN	FS6_T1	8	UK	1770 (904)	12	25
IMAGEN	FS6_T1	8	Germany	1770 (904)	12	25
IMAGEN	FS6_T1	8	France	1770 (904)	12	25
IMAGEN	FS6_T1	8	Ireland	1770 (904)	12	25
IMAGEN	FS6_T1T2	7	UK	355 (180)	13	25
IMAGEN	FS6_T1T2	7	Germany	355 (180)	13	25
IMAGEN	FS6_T1T2	7	Ireland	355 (180)	13	25
IMAGEN	FS6_T1T2	7	France	355 (180)	13	25
IXI	FS6_T1	1	UK	4 (0)	23	62
IXI	FS6_T1T2	1	UK	557 (313)	19	86
LIFE	FS53	1	Germany	2633 (1231)	18	81
NDAR_BSNIP	FS6_T1	6	USA	1077 (613)	9	65
NDAR_EMBARC	FS6_T1	4	USA	323 (214)	17	65
NDAR_FemaleASD	FS6_T1	3	USA	666 (337)	6	17

Continued on next page

study	pipeline	sites	country	N	Age_{min}	Age_{max}
NDAR_IBIS	FSInfant	4	USA	605 (192)	0	3
NDAR_UCSD	FS6_T1	1	USA	93 (38)	3	18
NDAR_UCSD	FSInfant	1	USA	299 (164)	1	3
NIHPD-old	FS6_T1	1	USA	846 (436)	4	22
NIHPD-young	FSInfant	1	USA	192 (84)	0	3
NKI	FS6_T1	1	USA	731 (444)	6	85
NSPN	FS53	3	UK	304 (151)	14	26
OASIS	FS6_T1	1	USA	82 (46)	42	91
OASIS	FS6_T1T2	1	USA	2548 (1453)	41	94
OpenNeuro_ID1000	FS6_T1	1	Netherlands	2755 (1439)	19	26
OpenNeuro_LA5c	FS6_T1	2	USA	265 (112)	21	50
OpenNeuro_PIOP1	FS6_T1T2	1	Netherlands	73 (44)	18	26
OpenNeuro_PIOP2	FS6_T1	1	Netherlands	224 (128)	17	25
OpenNeuro_Pixar	FS6_T1	1	USA	155 (84)	4	39
Oulu	FS6_T1	1	Finland	102 (65)	20	23
POND	FS6_T1	1	Canada	635 (177)	2	24
RDB	Custom	1		492 (126)	1	55
SRPBS1600	FS7_T1	13	Japan	1562 (644)	16	83
UKB	FS6_T1	3	UK	975 (500)	44	80
UKB	FS6_T1T2	3	UK	35419 (18754)	45	81
WAYNE	FS6_T1	1	USA	199 (133)	18	79

Table A.5 **Processing pipelines by dataset:** Overview of processing pipelines and sites by dataset. We further show the number of unique subjects (N) and the number of females in brackets, as well as the age range (Age_{min} and Age_{min})

	Area.Name	Area.Description
1	V1	Primary Visual Cortex
2	MST	Medial Superior Temporal Area
3	V6	Sixth Visual Area
4	V2	Second Visual Area
5	V3	Third Visual Area
6	V4	Fourth Visual Area
7	V8	Eighth Visual Area
8	4	Primary Motor Cortex
9	3b	Primary Sensory Cortex
10	FEF	Frontal Eye Fields
11	PEF	Premotor Eye Field
12	55b	Area 55b
13	V3A	Area V3A
14	RSC	RetroSplenial Complex
15	POS2	Parieto-Occipital Sulcus Area 2
16	V7	Seventh Visual Area
17	IPS1	IntraParietal Sulcus Area 1
18	FFC	Fusiform Face Complex
19	V3B	Area V3B
20	LO1	Area Lateral Occipital 1
21	LO2	Area Lateral Occipital 2
22	PIT	Posterior InferoTemporal complex
23	MT	Middle Temporal Area
24	A1	Primary Auditory Cortex
25	PSL	PeriSylvian Language Area
26	SFL	Superior Frontal Language Area
27	PCV	PreCuneus Visual Area
28	STV	Superior Temporal Visual Area
29	7Pm	Medial Area 7P
30	7m	Area 7m
31	POS1	Parieto-Occipital Sulcus Area 1
32	23d	Area 23d
33	v23ab	Area ventral 23 a+b
34	d23ab	Area dorsal 23 a+b
35	31pv	Area 31p ventral
36	5m	Area 5m
37	5mv	Area 5m ventral
38	23c	Area 23c
39	5L	Area 5L
40	24dd	Dorsal Area 24d
41	24dv	Ventral Area 24d
42	7AL	Lateral Area 7A
43	SCEF	Supplementary and Cingulate Eye Field
44	6ma	Area 6m anterior
45	7Am	Medial Area 7A
46	7Pl	Lateral Area 7P
47	7PC	Area 7PC
48	LIPv	Area Lateral IntraParietal ventral
49	VIP	Ventral IntraParietal Complex
50	MIP	Medial IntraParietal Area

Appendix B

Supplementary Figures

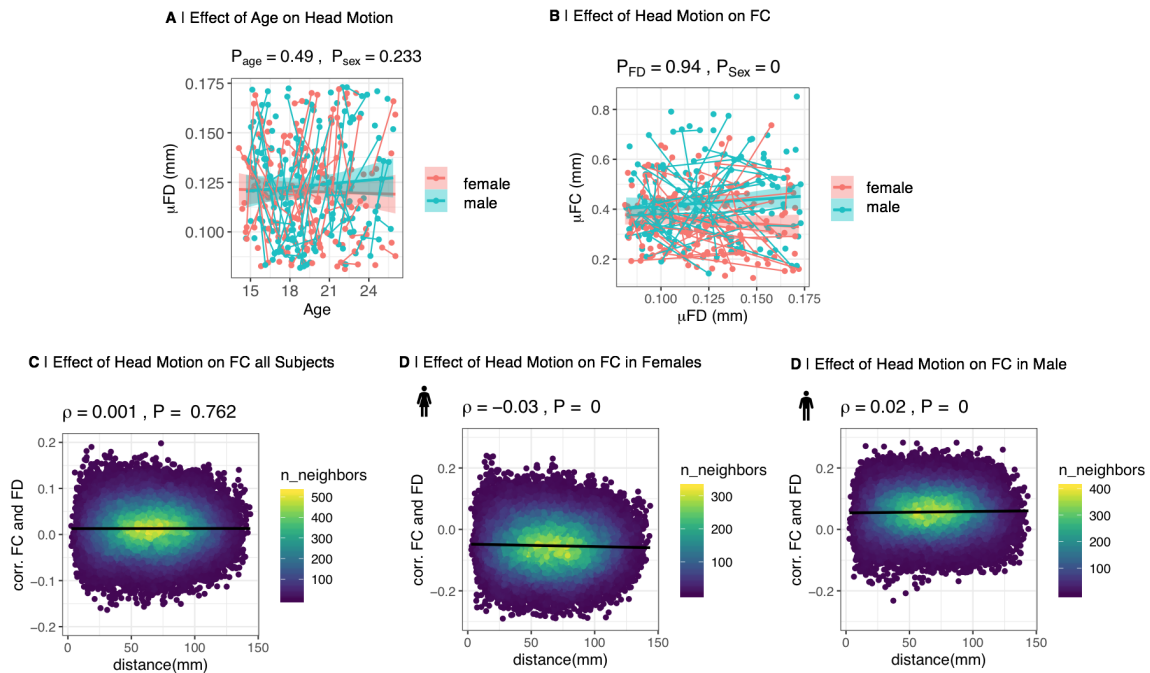


Fig. B.1 Effect of head motion (FD) on functional connectivity (FC) in the motion-matched sample: The motion-matched sample is a subsample of the full data set, in which we removed the dependence of FC on motion in our sample by regressing FD from each edge; the residuals constitute participant-specific FD-corrected FC, with intercepts retained to maintain the relative importance of edges across the group as well as the interpretability of FC values. (A) In this subsample, average head motion, quantified as mean frame-wise displacement (FD), did not change with age ($P_{age} = 0.49$). And there was no effect of sex on FD ($P_{sex} = 0.23$). (B) The effect of participants' motion (across participants) on global FC was not significant ($P_{FD} = 0.94$). (C) There was no effect of distance on the correlation between FC and motion ($\rho = 0.001, P = 0.76$), and the average edge-wise correlation between FC and motion was almost zero (intercept = 0.01). (D) However, since our motion correction was performed across all subjects in the full sample, we still observed weak, but significant effects of distance on the correlation of FC and FD for females ($\rho = -0.03, P < 0.001$) (D) and males ($\rho = 0.02, P < 0.001$) (E) separately, and the average edge-wise correlation between FC and motion was non-zero ($intercept_{females} = -0.050.02, intercept_{males} = 0.05$).

Appendix C

Supplementary Text

C.1 Primary datasets

ABCD - Adolescent Brain and Cognitive Development

The ABCD study (Casey et al., 2018) is the largest longitudinal study of pediatric brain development in the USA. It includes data from children aged 9-12 years, scanned between one and three times at 21 sites. It further includes a range of questionnaire data on social, emotional and cognitive development, as well as a variety of health and environmental outcomes. We downloaded minimally processed T1 and T2 weighted imaging for 10,588 individuals through the NIMH Data Archive (NDAR) and processed using FreeSurfer 6.0.1 using the combined T1-T2 processing pipeline whenever both T1 and T2 scans were available. When only T1 scans were available, we processed the data using the 'standard' pipeline. Individuals were included in the reference model as healthy controls (CN) based on the parental response to the ABCD screening and risk questionnaire (https://nda.nih.gov/data_structure.html?short_name=abcd_screen01) indicating the individual had never been diagnosed with a mental health disorder. Data access information can be found here: <https://abcdstudy.org/scientists/data-sharing/>.

ABIDE - Autism Brain Imaging Data Exchange

The Autism Brain Imaging Data Exchange (ABIDE) (Di Martino et al., 2014b, 2017) is an aggregated dataset of functional and structural neuroimaging data collected from various international sites. It aims to investigate the neural bases of ASD. T1-weighted structural

data was processed using recon-all as implemented in FreeSurfer 6.0.1. The data can be accessed here: https://fcon_1000.projects.nitrc.org/indi/abide/.

ADNI - Alzheimer's Disease Neuroimaging Initiative

The Alzheimer's Disease Neuroimaging Initiative (ADNI) (Petersen et al., 2010) includes MRI data from healthy controls and patients with Alzheimer's disease and mild cognitive impairment (MCI). The study aim was to investigate whether MRI, PET and biological markers could explain the progression from MCI to Alzheimer's disease. Further information is available at: www.adni-info.org.

ADHD200

The ADHD-200 Sample (consortium, 2012) is a grassroots initiative. With the unrestricted public release of 776 anatomical datasets of children and young adults aged seven to 21 years, acquired at 8 independent imaging sites (491 healthy controls and 285 children and adolescents with ADHD), it aims to accelerate the scientific community's understanding of the neural basis of ADHD through the implementation of open data-sharing and discovery-based science. T1-weighted structural data was processed using recon-all as implemented in FreeSurfer 6.0.1. The data can be accessed here: http://fcon_1000.projects.nitrc.org/indi/adhd200/.

Baby Connectome Project

The Lifespan Baby Connectome Project (BCP) data (Howell et al., 2019) forms part the "Human Connectome Projects", a series of public research data which aims to map the human structural and functional connectome. BCP is part of the HCP Lifespan Projects which includes multimodal imaging data acquired across the lifespan, in four age groups (prenatal, 0-5, 6-21, and 36-100+), all of which have scanning protocols similar to the first "HCP" dataset, except they are shorter in duration. This dataset includes 500 subjects, aged 0-4 years. Data access can be requested here: <https://www.humanconnectome.org>

BGSP - Brain Genomics Superstruct Project

The Brain Genomics Superstruct Project Open Access Data Release (Holmes et al., 2015) includes behaviour, cognitive, and personality data for over 1,500 subjects, as well as structural and functional MRI data.

BSNIP - Bipolar & Schizophrenia Consortium for Parsing Intermediate Phenotypes

Bipolar & Schizophrenia Consortium for Parsing Intermediate Phenotypes (BSNIP) data (Tamminga et al., 2017) is available on NDAR and includes neuroimaging data for healthy controls, subjects with psychosis, bipolar disorder and first degree relatives of patients.

Calgary

The Calgary Preschool MRI Dataset (Reynolds et al., 2020) was provided by the Developmental Neuroimaging Lab at the University of Calgary and consists of MRI data from healthy children, aged two to eight years.

CALM – Centre for Attention Learning and Memory

The children with problems of attention, learning and memory (CALM) cohort (Holmes et al., 2019) includes data from typically developing children and children with difficulties in attention, learning and memory that were recruited from the same schools. A subset of the cohort completed MRI scanning at the MRC CBU www.mrc-cbu.cam.ac.uk in Cambridge, UK. The children were introduced to the scanning environment with the help of a mock MRI scanner. The study was approved by the Cambridgeshire Research Ethics Committee and participants or their legal guardians provided informed consent. The data was collected on a 3T Siemens Prisma with a 32-channel quadrature head coil.

Cam-CAN – Cambridge Centre for Aging and Neuroscience

The Cambridge Centre for Aging and Neuroscience (Cam-CAN; www.cam-can.org) study (Shafto et al., 2014; Taylor et al., 2017) includes data from healthy adults ages 18-88 years, recruited locally. Ethical approval was obtained from the Cambridgeshire Research Ethics Committee and participants gave written informed consent. The data was collected on a 3T Siemens Prisma with a 32-channel quadrature head coil.

dHCP

The developing Human Connectome Project (dHCP) data forms part the “Human Connectome Projects”, a series of public research data which aims to map the human structural and functional connectome (Makropoulos et al., 2018). dHCP is part of the HCP Lifespan Projects which includes multimodal imaging data acquired across the lifespan, in four age groups (prenatal, 0-5, 6-21, and 36-100+), all of which have scanning protocols similar to the first “HCP” dataset, except they are shorter in duration. This dataset includes 1500 subjects, aged 20-44 weeks post partum, acquired at King’s College London, Imperial College London, and Oxford University. Data access can be requested here: <https://www.humanconnectome.org>

DLBS - Dallas Lifespan Brain Study

The Dallas Lifespan Brain Study (DLBS) includes data from healthy adults, aged 20-89 years. It was acquired to study the decline of cognitive function at different stages of the adult lifespan, in particular with respect to healthy subjects approaching the development of Alzheimer’s disease. Structural MRI, DTI, three task-based functional MRI scans, and a resting state scan were acquired on a Philips 3T Philips Achieva scanner equipped with an 8-channel head coil. Here, raw structural T1-weighted scans were processed with FreeSurfer 6.0.1.

EMBARC – Establishing Moderators and Biosignatures Of Antidepressant Response for Clinical Care

The Establishing Moderators and Biosignatures Of Antidepressant Response for Clinical Care (EMBARC) study (Trivedi et al., 2016) was established to compare the effectiveness of three mechanistically distinct treatments for major depressive disorder (MDD) (citalopram, bupropion, and cognitive behavioural therapy). The study collected neuroimaging data, together with clinical (i.e., anxious depression, early life trauma) and biological (i.e., genetic, neuroimaging, serum, epigenetic) outcome moderators. Here, raw structural T1-weighted scans were processed with FreeSurfer 6.0.1.

Female ASD

The NDAR dataset ‘Multimodal Developmental Neurogenetics of Females with ASD’ (NDAR ID 2021; here referred to as “Female ASD”) includes participants with and with-

out attention deficit hyperactivity disorder (ADHD), in a sex-balanced cohort acquired at George Washington University. Here, raw structural T1-weighted scans were processed with FreeSurfer 6.0.1.

FinnBrain

The FinnBrain Birth Cohort Study (Karlsson et al., 2018) is a population-based cohort from Southwestern Finland (Turku region and Åland islands). The study includes data from infants and their mothers. The study was approved by the Ethics Committee of the Hospital District of Southwest Finland (ETMK:31/180/2011).

HBN - Healthy Brain Network

The Healthy Brain Network (HBN) is an ongoing study by the Child Mind Institute that aims to create a biobank of data from 10,000 New York area participants between the ages of five and 21 (Alexander et al., 2017). It collects psychiatric, behavioural, cognitive, and lifestyle phenotypes, as well as multimodal brain imaging (resting and naturalistic viewing fMRI, diffusion MRI, morphometric MRI), electroencephalography, eye-tracking, voice and video recordings, genetics and actigraphy. Here, we use data from release 7.

HCP-A

The Human Connectome Project Ageing (HCP-A) data (Bookheimer et al., 2019) forms part the “Human Connectome Projects”, a series of public research data which aims to map the human structural and functional connectome. HCP-A is part of the HCP Lifespan Projects which includes multimodal imaging data acquired across the lifespan, in four age groups (prenatal, 0-5, 6-21, and 36-100+), all of which have scanning protocols similar to the first “HCP” dataset, except they are shorter in duration. This dataset includes 1200 subjects, aged 36-100+, acquired at Washington University, University of Minnesota, Massachusetts General Hospital, Harvard University, University of California Los Angeles, Oxford University. Data access can be requested here: <https://www.humanconnectome.org>.

Human Connectome Project

The Human Connectome Project (HCP) forms part the “Human Connectome Projects” (Glasser et al., 2013; Van Essen et al., 2013), a series of public research data which aims

to map the human structural and functional connectome. The HCP data is the young adult healthy cohort. It includes 1200 Subjects, aged 22-35, acquired at Washington U. in Saint Louis, University of Minnesota, University of Oxford, Saint Louis University, Indiana University, University d'Annunzio, Ernst Strungmann Institute, Warwick University, Radboud U. Nijmegen, and University of California at Berkeley. Data access can be requested here: <https://www.humanconnectome.org>.

HCP-D

The Human Connectome Project Development (HCP-D) study (Somerville et al., 2018b) forms part the “Human Connectome Projects”, a series of public research data which aims to map the human structural and functional connectome. HCP-D is part of the HCP Lifespan Projects which includes multimodal imaging data acquired across the lifespan, in four age groups (prenatal, 0-5, 6-21, and 36-100+), all of which have scanning protocols similar to the first “HCP” dataset, except they are shorter in duration. This dataset includes 1350 subjects, aged 5-21, acquired at Washington University, University of Minnesota, University of California at Los Angeles, Harvard University, and Oxford University. Data access can be requested here: <https://www.humanconnectome.org>.

IBIS

The IBIS dataset is an aggregated dataset including data from several NDAR projects: Longitudinal MRI Study of Infants at Risk for Autism (19), Biomarkers of Developmental Trajectories and Treatment in autism spectrum disorder (ASD) (2026). We used Infant FreeSurfer to process data for individuals younger than 36 months, while individuals older than 36 months were processed with FreeSurfer 6.0.1.

IMAGEN

IMAGEN (Schumann et al., 2010) is a European research project that was established to study biological, psychological, and environmental factors that influence brain development and mental health during adolescence. It includes longitudinal neuroimaging data. Here, raw structural T1-weighted scans were processed with FreeSurfer 6.0.1.

IXI

The IXI dataset (Kuklisova-Murgasova et al., 2011) includes scans from healthy subjects. MRI data were acquired on three different scanners: A 3T Philips Intera scanner and two 1.5T Philips Gyroscan Intera scanners. Further information is available at: <https://brain-development.org/ixi-dataset/>. All scans were processed with FreeSurfer 6.0.1.

LIFE – Leipzig Research Centre for Civilization Diseases Study

The Leipzig Research Centre for Civilization Diseases Study (LIFE) study (Loeffler et al., 2015) is a population-based cohort from Leipzig, Germany, that aimed to investigate the development of major modern diseases. The study included 10,000 participants who randomly drawn from the local population, 2,667 of whom underwent MRI scanning. The MRI cohort was selected to include mostly participants older than 60 years to allow studying age-associated diseases such as mild and major neurocognitive disorder.

NIHPD

The NIH study of pediatric development (NIHPD) is a multi-site, combined cross-sectional and longitudinal study of normal, healthy developing children from early childhood through young adulthood (Evans et al., 2006). The data were acquired to be representative of the US Census 2000 statistics for gender, family income, race/ethnicity. Detailed information on sites and scanning procedures can be found here: https://www.nitrc.org/docman/view.php/98/288/MRI_Manual_Nov06.pdf.

NKI

The Nathan Kline Institute (NKI) Rockland Sample (Nooner et al., 2012) is an ongoing study that aims to generate a deeply phenotyped and community based lifespan sample, including neuroimaging and genetic data. Here, we downloaded multi-modal imaging data from the 1000-functional connectomes project for 532 quality controlled T1 images. The data were processed using FreeSurfer 5.3.

NSPN

The Neuroscience in Psychiatry Network (NSPN) sample (Kiddle et al., 2017) is a longitudinal study of healthy adolescents, using a population-representative sample from Cambridgeshire and Peterborough, UK. It includes neuroimaging data from roughly 300 adolescents, scanned between 1 and 3 times. The sample has been described in depth in **Chapter 2-4**. The raw data can be accessed here: <https://nspn.org.uk>.

OASIS – Open Access Series of Imaging Studies

The Open Access Series of Imaging Studies (OASIS) is a freely available, multimodal aggregated dataset (LaMontagne et al., 2019) containing three individual studies acquired at the Charles F. and Joanne Knight Alzheimer Disease Research Center (Knight ADRC) at Washington University in St. Louis. The individual studies were acquired over the time of 15 years and are: Memory and Aging Project, Adult Children Study, and Healthy Aging and Senile Dementia. OASIS-3 aims to study healthy aging and Alzheimer's disease (AD). The study includes 1,098 participants healthy controls and individuals with early-stage AD aged 42 to 95. Exclusion criteria included medical conditions that precluded longitudinal participation or conditions that would not allow participants to be scanned safely (e.g., end-stage renal disease requiring dialysis, pacemakers, anticoagulant use for lumbar puncture).

OpenNeuro ID1000

The ID1000 dataset (Snoek et al., 2020a) is available on OpenNeuro (ds003097) at: <https://openneuro.org/datasets/ds003097/versions/1.2.1>. It is one of three datasets that jointly form the Amsterdam Open MRI Collection (AOMIC) collection of multimodal (3T) MRI datasets (<https://nilab-uva.github.io/AOMIC.github.io/>; Snoek et al. (2021)). The dataset includes healthy participants that underwent structural and task-based fMRI.

OpenNeuro LA5c - UCLA Consortium for Neuropsychiatric Phenomics LA5c Study

The UCLA Consortium for Neuropsychiatric Phenomics LA5c (LA5c) study (Bilder et al., 2018; Poldrack et al., 2016) is available on OpenNeuro (ds000030) at: <https://openneuro.org/datasets/ds000030/versions/00016>. The study includes 272 subjects with and without psychiatric diagnoses. We processed the T1-weighted scans using FreeSurfer 6.0.1.

OpenNeuro PIOP1

The PIOP1 dataset (Snoek et al., 2020b) is available on OpenNeuro (ds002785) at: <https://openneuro.org/datasets/ds002785/versions/2.0.0>. It is one of three datasets that jointly form the Amsterdam Open MRI Collection (AOMIC) collection of multimodal (3T) MRI datasets (<https://nilab-uva.github.io/AOMIC.github.io/>; Snoek et al. (2021)). The dataset includes healthy participants that underwent structural and task-based fMRI during a number of paradigms (emotion matching, gender-stroop, resting state, working memory, face perception, anticipation).

OpenNeuro PIOP2

The PIOP2 dataset (Snoek et al., 2020c) is available on OpenNeuro (ds002790) at: <https://openneuro.org/datasets/ds003097/versions/1.2.1>. It is one of three datasets that jointly form the Amsterdam Open MRI Collection (AOMIC) collection of multimodal (3T) MRI datasets (<https://nilab-uva.github.io/AOMIC.github.io/>; Snoek et al. (2021)). The dataset includes healthy participants that underwent structural and task-based fMRI during a number of paradigms (emotion matching, resting state, working memory, stop signal).

OpenNeuro Pixar

Pixar is an OpenNeuro dataset (ds000228) of 155 children who watched Disney Pixar’s “Partly Cloudy” during scanning without a specific task (Richardson et al., 2018, 2019). The movie began after 10s of rest (black screen; TRs 1-5). The first 10s of the movie are the opening credits (disney castle, pixar logo; TRs 6-10). The data can be accessed here: <https://openneuro.org/datasets/ds000228/versions/1.1.0>. Here, we processed the T1-weighted scans using FreeSurfer 6.0.1.

Oulu

The Oulu dataset is part of the International Neuroimaging Datasharing Initiative (INDI; Mennes et al. (2013)). It includes data from healthy subjects aged 20 to 23. Here, raw structural T1-weighted scans were processed with FreeSurfer 6.0.1.

POND – Province of Ontario Neurodevelopmental Disorders

The Province of Ontario Neurodevelopmental Disorders (POND) study is a multi-site study that includes healthy participants and participants with a diagnosis of ADHD, obsessive compulsive disorder (OCD) or ASD. Subjects were aged under 18 years. The data collected at Centers in Ontario, Canada (Holland Bloorview Kids Rehabilitation Hospital, Toronto; The Hospital for Sick Children, Toronto; McMaster Children’s Hospital, Hamilton; Queen’s University, and Lawson Health Research Institute, London). We processed the T1-weighted scans using FreeSurfer 6.0.1.

SRPBS1600 – SRPBS Multidisorder MRI Dataset

The SRPBS Multidisorder MRI Dataset (Tanaka et al., 2021a) is a multi-site study that collected neuroimaging data from 1600 subjects, both healthy controls and of patients with psychiatric disorders, collected in Japan. Further information is available at: <https://bicr-resource.atr.jp/srpbs1600/>.

UKB

The UK BioBank (UKB) (Alfaro-Almagro et al., 2018) aims to collect phenotypic information (demographic, genetic) from 100,000 subjects. A subset of about 40,000 subjects have undergone neuroimaging. We downloaded minimally processed T1- and T2-FLAIR weighted data (application 20904) and further preprocessed with FreeSurfer 6.0.1 using the T2-FLAIR weighted image to improve pial surface reconstruction. We determined controls to be subjects who never had mental health problems as diagnosed by a mental health professional (data-field 20544).

WAYNE

The Wayne State longitudinal data set for the Brain Aging in Detroit Longitudinal Study (Daugherty and Raz, 2016) collected longitudinal neuroimaging data from 114 healthy participants. The study aimed to study changes in the brain during adulthood, and to understand the relationships between changes in brain properties and cognitive performance. More information is available here: http://fcon_1000.projects.nitrc.org/indi/retro/wayne_10.html.

C.2 GAMLSS models

Thalamus:

$GMV_{Thalamus} \sim \text{GeneralisedGamma}(\mu, \sigma, \nu)$ with

$$\log(\mu) = \alpha_{\mu} + \alpha_{\mu,sex} + \alpha_{\mu,ver} + \beta_{\mu,1}(age)^{-2} + \beta_{\mu,2}(age)^{-3} + \beta_{\mu,3}(age)^{-2}\log(age) + \varepsilon_{\mu,study}$$

$$\log(\sigma) = \alpha_{\mu} + \alpha_{\mu,sex} + \alpha_{\mu,ver} + \beta_{\mu,1}(age)^{-2} + \beta_{\mu,2}(age)^{-2}\log(age) + \beta_{\mu,3}(age)^{-2}\log(age)^2 + \varepsilon_{\mu,study}$$

$$\nu = \alpha_{\nu}$$

Caudate:

$GMV_{Caudate} \sim \text{GeneralisedGamma}(\mu, \sigma, \nu)$ with

$$\log(\mu) = \alpha_{\mu} + \alpha_{\mu,sex} + \alpha_{\mu,ver} + \beta_{\mu,1}(age)^3 + \beta_{\mu,2}(age)^3\log(age) + \beta_{\mu,3}(age)^3\log(age)^2 + \varepsilon_{\mu,study}$$

$$\log(\sigma) = \alpha_{\mu} + \alpha_{\mu,sex} + \alpha_{\mu,ver} + \beta_{\mu,1}(age)^3 + \beta_{\mu,2}(age)^3\log(age) + \beta_{\mu,3}(age)^3\log(age)^2 + \varepsilon_{\mu,study}$$

$$\nu = \alpha_{\nu}$$

Putamen:

$GMV_{Putamen} \sim \text{GeneralisedGamma}(\mu, \sigma, \nu)$ with

$$\log(\mu) = \alpha_{\mu} + \alpha_{\mu,sex} + \alpha_{\mu,ver} + \beta_{\mu,1}(age)^{-2} + \beta_{\mu,2}(age)^{-2}\log(age) + \beta_{\mu,3}(age)^3 + \varepsilon_{\mu,study}$$

$$\log(\sigma) = \alpha_{\mu} + \alpha_{\mu,sex} + \alpha_{\mu,ver} + \beta_{\mu,1}(age)^3 + \beta_{\mu,2}(age)^3\log(age) + \beta_{\mu,3}(age)^3\log(age)^2 + \varepsilon_{\mu,study}$$

$$\nu = \alpha_{\nu}$$

Pallidum:

$GMV_{Pallidum} \sim \text{GeneralisedGamma}(\mu, \sigma, \nu)$ with

$$\log(\mu) = \alpha_{\mu} + \alpha_{\mu,sex} + \alpha_{\mu,ver} + \beta_{\mu,1}(age)^{-2} + \beta_{\mu,2}(age)^{-2}\log(age) + \beta_{\mu,3}(age)^3 + \varepsilon_{\mu,study}$$

$$\log(\sigma) = \alpha_{\mu} + \alpha_{\mu,sex} + \alpha_{\mu,ver} + \beta_{\mu,1}(age)^3 + \beta_{\mu,2}(age)^3 \log(age) + \epsilon_{\mu,study}$$

$$\nu = \alpha_{\nu}$$

Hippocampus:

$GMV_{Hippocampus} \sim \text{GeneralisedGamma}(\mu, \sigma, \nu)$ with

$$\log(\mu) = \alpha_{\mu} + \alpha_{\mu,sex} + \alpha_{\mu,ver} + \beta_{\mu,1}(age)^{-2} + \beta_{\mu,2}(age)^3 + \epsilon_{\mu,study}$$

$$\log(\sigma) = \alpha_{\mu} + \alpha_{\mu,sex} + \alpha_{\mu,ver} + \beta_{\mu,1}(age)^3 + \beta_{\mu,2}(age)^2 + \epsilon_{\mu,study}$$

$$\nu = \alpha_{\nu}$$

Amygdala:

$GMV_{Amygdala} \sim \text{GeneralisedGamma}(\mu, \sigma, \nu)$ with

$$\log(\mu) = \alpha_{\mu} + \alpha_{\mu,sex} + \alpha_{\mu,ver} + \beta_{\mu,1}(age)^{-2} + \beta_{\mu,2}(age)^3 + \epsilon_{\mu,study}$$

$$\log(\sigma) = \alpha_{\mu} + \alpha_{\mu,sex} + \alpha_{\mu,ver} + \beta_{\mu,1}(age)^{-2} + \beta_{\mu,2}(age)^{-2} \log(age) + \epsilon_{\mu,study}$$

$$\nu = \alpha_{\nu}$$

Accumbens:

$GMV_{Accumbens} \sim \text{GeneralisedGamma}(\mu, \sigma, \nu)$ with

$$\log(\mu) = \alpha_{\mu} + \alpha_{\mu,sex} + \alpha_{\mu,ver} + \beta_{\mu,1}(age)^3 + \beta_{\mu,2}(age)^3 \log(age) + \beta_{\mu,3}(age)^3 \log(age)^2 + \epsilon_{\mu,study}$$

$$\log(\sigma) = \alpha_{\mu} + \alpha_{\mu,sex} + \alpha_{\mu,ver} + \beta_{\mu,1}(age)^{-2} + \beta_{\mu,2}(age)^{-2} \log(age) + \epsilon_{\mu,study}$$

$$\nu = \alpha_{\nu}$$

Ventral DC:

$GMV_{VentralDC} \sim \text{GeneralisedGamma}(\mu, \sigma, \nu)$ with

$$\log(\mu) = \alpha_{\mu} + \alpha_{\mu,sex} + \alpha_{\mu,ver} + \beta_{\mu,1}(age)^3 + \beta_{\mu,2}(age)^3 \log(age) + \beta_{\mu,3}(age)^3 \log(age)^2 + \epsilon_{\mu,study}$$

$$\log(\sigma) = \alpha_{\mu} + \alpha_{\mu,sex} + \alpha_{\mu,ver} + \beta_{\mu,1}(age)^3 + \beta_{\mu,2}(age)^3 \log(age) + \beta_{\mu,3}(age)^3 \log(age)^2 + \varepsilon_{\mu,study}$$

$$\nu = \alpha_{\nu}$$

Corpus Callosum Posterior:

$WM_{PosteriorCC} \sim GeneralisedGamma(\mu, \sigma, \nu)$ with

$$\log(\mu) = \alpha_{\mu} + \alpha_{\mu,sex} + \alpha_{\mu,ver} + \beta_{\mu,1}(age)^{-1} + \beta_{\mu,2}(age)^1 + \beta_{\mu,3}(age)^3 + \varepsilon_{\mu,study}$$

$$\log(\sigma) = \alpha_{\mu} + \alpha_{\mu,sex} + \alpha_{\mu,ver} + \beta_{\mu,1}(age)^3 + \beta_{\mu,2}(age)^3 \log(age) + \beta_{\mu,3}(age)^3 \log(age)^2 + \varepsilon_{\mu,study}$$

$$\nu = \alpha_{\nu}$$

Corpus Callosum Mid Posterior:

$WM_{MidPosteriorCC} \sim GeneralisedGamma(\mu, \sigma, \nu)$ with

$$\log(\mu) = \alpha_{\mu} + \alpha_{\mu,sex} + \alpha_{\mu,ver} + \beta_{\mu,1}(age)^3 + \beta_{\mu,2}(age)^3 \log(age) + \beta_{\mu,3}(age)^3 \log(3)^2 + \varepsilon_{\mu,study}$$

$$\log(\sigma) = \alpha_{\mu} + \alpha_{\mu,sex} + \alpha_{\mu,ver} + \beta_{\mu,1}(age)^{-2} + \beta_{\mu,2}(age)^3 + \varepsilon_{\mu,study}$$

$$\nu = \alpha_{\nu}$$

Corpus Callosum Central:

$WM_{CentralCC} \sim GeneralisedGamma(\mu, \sigma, \nu)$ with

$$\log(\mu) = \alpha_{\mu} + \alpha_{\mu,sex} + \alpha_{\mu,ver} + \beta_{\mu,1}(age)^3 + \beta_{\mu,2}(age)^3 \log(age) + \beta_{\mu,3}(age)^3 \log(age)^2 + \varepsilon_{\mu,study}$$

$$\log(\sigma) = \alpha_{\mu} + \alpha_{\mu,sex} + \alpha_{\mu,ver} + \beta_{\mu,1}(age)^3 + \beta_{\mu,2}(age)^3 \log(age) + \beta_{\mu,3}(age)^3 \log(age)^2 + \varepsilon_{\mu,study}$$

$$\nu = \alpha_{\nu}$$

Corpus Callosum Mid Anterior:

$WM_{MidAnteriorCC} \sim GeneralisedGamma(\mu, \sigma, \nu)$ with

$$\log(\mu) = \alpha_{\mu} + \alpha_{\mu,sex} + \alpha_{\mu,ver} + \beta_{\mu,1}(age)^3 + \beta_{\mu,2}(age)^3 \log(age) + \beta_{\mu,3}(age)^3 \log(age)^2 + \epsilon_{\mu,study}$$

$$\log(\sigma) = \alpha_{\mu} + \alpha_{\mu,sex} + \alpha_{\mu,ver} + \beta_{\mu,1}(age)^3 + \beta_{\mu,2}(age)^3 \log(age) + \epsilon_{\mu,study}$$

$$\nu = \alpha_{\nu}$$

Corpus Callosum Anterior:

$WM_{AnteriorCC} \sim GeneralisedGamma(\mu, \sigma, \nu)$ with

$$\log(\mu) = \alpha_{\mu} + \alpha_{\mu,sex} + \alpha_{\mu,ver} + \beta_{\mu,1}(age)^3 + \beta_{\mu,2}(age)^3 \log(age) + \beta_{\mu,3}(age)^3 \log(age)^2 + \epsilon_{\mu,study}$$

$$\log(\sigma) = \alpha_{\mu} + \alpha_{\mu,sex} + \alpha_{\mu,ver} + \beta_{\mu,1}(age)^3 + \epsilon_{\mu,study}$$

$$\nu = \alpha_{\nu}$$

Cerebellum White Matter:

$WM_{Cerebellum} \sim GeneralisedGamma(\mu, \sigma, \nu)$ with

$$\log(\mu) = \alpha_{\mu} + \alpha_{\mu,sex} + \alpha_{\mu,ver} + \beta_{\mu,1}(age)^3 + \beta_{\mu,2}(age)^3 \log(age) + \beta_{\mu,3}(age)^3 \log(age)^2 + \epsilon_{\mu,study}$$

$$\log(\sigma) = \alpha_{\mu} + \alpha_{\mu,sex} + \alpha_{\mu,ver} + \beta_{\mu,1}(age)^3 + \beta_{\mu,2}(age)^3 \log(age) + \epsilon_{\mu,study}$$

$$\nu = \alpha_{\nu}$$

Cerebellum Grey Matter:

$GM_{Cerebellum} \sim GeneralisedGamma(\mu, \sigma, \nu)$ with

$$\log(\mu) = \alpha_{\mu} + \alpha_{\mu,sex} + \alpha_{\mu,ver} + \beta_{\mu,1}(age)^{-2} + \beta_{\mu,2}(age)^0 + \epsilon_{\mu,study}$$

$$\log(\sigma) = \alpha_{\mu} + \alpha_{\mu,sex} + \alpha_{\mu,ver} + \beta_{\mu,1}(age)^3 + \epsilon_{\mu,study}$$

$$\nu = \alpha_{\nu}$$

C.3 Data, code, and image availability

Access to the raw scans for the Neuroscience in Psychiatry Network (NSPN) sample used in **Chapter 2-3** and **Chapter 5** can be applied for at <https://nspn.org.uk>.

The pre-processed functional magnetic resonance imaging (fMRI) data, as well as all replication datasets, and the MDD and schizophrenia case-control maps, used in **Chapter 2 and 3**, are archived at [10.5281/zenodo.6390851](https://zenodo.org/record/6390851). The external gene lists used for the gene enrichment analyses are available in the cited manuscripts. The code required to replicate the analyses can be found on GitHub (https://github.com/LenaDorfschmidt/sex_differences_adolescence), with a version also archived at [10.5281/zenodo.6390752](https://zenodo.org/record/6390752).

The code used in **Chapter 5** and the processed structural imaging data will be made available on publication of these results in a peer-reviewed journal.

I used the code published with Bethlehem et al. (2022) to estimate the normative trajectories derived in **Chapter 6**, which is available on GitHub <https://github.com/brainchart/Lifespan>. The fitted models will be made available on publication of these results in a peer-reviewed journal.

Vector files of figures created for **Chapter 1** are free to use under a **CC BY 4.0** licence and available at [10.5281/zenodo.7782905](https://zenodo.org/record/7782905).